


January 2015

# Genomic Aberrations at the 3q and 14q loci: Investigation of Key Players in Ovarian and Renal Cancer Biology

Punashi Dutta

*University of South Florida*, [punashidutta@mail.usf.edu](mailto:punashidutta@mail.usf.edu)

Follow this and additional works at: <http://scholarcommons.usf.edu/etd>

 Part of the [Cell Biology Commons](#), and the [Molecular Biology Commons](#)

## Scholar Commons Citation

Dutta, Punashi, "Genomic Aberrations at the 3q and 14q loci: Investigation of Key Players in Ovarian and Renal Cancer Biology" (2015). *Graduate Theses and Dissertations*.  
<http://scholarcommons.usf.edu/etd/5679>

This Dissertation is brought to you for free and open access by the Graduate School at Scholar Commons. It has been accepted for inclusion in Graduate Theses and Dissertations by an authorized administrator of Scholar Commons. For more information, please contact [scholarcommons@usf.edu](mailto:scholarcommons@usf.edu).

Genomic Aberrations at the 3q and 14q loci: Investigation of Key Players in Ovarian and Renal  
Cancer Biology

by

Punashi Dutta

A dissertation submitted in partial fulfillment  
of the requirements for the degree of  
Doctor of Philosophy in Cell and Molecular Biology  
Department of Cell Biology, Microbiology and Molecular Biology  
College of Arts and Sciences  
University of South Florida

Major Professor: Meera Nanjundan, Ph.D.  
Patrick Bradshaw, Ph.D.  
Younghoon Kee, Ph.D.  
Sandy Westerheide, Ph.D.

Date of Approval:  
June 18, 2015

Keywords: Chemotherapeutics, EVI1, SnoN/SkiL, miR-494, lipid droplets

Copyright © 2015, Punashi Dutta

## Dedication

I dedicate this work to my parents, Dr. Sharad Datta and Dr. Shailaja Datta who taught me to believe in myself and gave me the confidence to embark upon this journey. Everything that I have and will accomplish is because of their struggles and sacrifices. I also dedicate this work to my friend and husband, Dr. Madhav Karthik Kodigepalli for being there with me at every step of this journey.

## Acknowledgments

I would like to express my deepest appreciation for my mentor, Dr. Meera Nanjundan, whose expert guidance has been instrumental in my graduate education. I cannot adequately express my gratitude towards her for her wisdom, enthusiasm, constant motivation, and understanding without which this dissertation would not have been possible. I will always be grateful to her for all her encouragement and advice.

I would like to sincerely acknowledge my committee members, Dr. Patrick Bradshaw, Dr. Younghoon Kee, and Dr. Sandy Westerheide for their valuable inputs and scientific discussions which has contributed to this dissertation.

I want to express my sincere appreciation to all my lab colleagues and undergraduate students for all their help and support and for creating a wonderful working environment.

Finally, I am thankful also to my family and all my friends for their unwavering support and encouragement always. I am blessed to have you all in my life.

## Table of Contents

List of Tables.....	v
List of Figures .....	vi
Abbreviations .....	viii
Abstract.....	x
Chapter 1: Introduction .....	1
Ovarian Cancer .....	1
Breast Cancer .....	2
Renal Cancer .....	2
Genomic Aberrations .....	3
Chromosomal Aberrations at 3q: Serous EOC and BRCA1 Positive Basal Breast Cancers.....	4
Ecotropic viral integration site 1 (EVI1) .....	5
Gene structure .....	5
Splice variants .....	6
Interacting partners.....	7
Functions .....	9
Ski-related novel protein N/Ski-like protein (SnoN/SkiL) .....	9
Chromosomal Aberrations at 14q: Renal Cancer .....	11
The DLK1-DIO3 cluster and microRNAs (miRNAs) .....	11
miR-494 .....	13
Pathways that Alter the Hallmarks of Cancer.....	15
Transforming growth factor beta (TGF $\beta$ ) pathway.....	15
Epithelial-mesenchymal transition (EMT).....	16
Programmed cell death (PCD) .....	17
Apoptosis .....	18
Autophagy .....	18
Cross-talk between autophagy and apoptosis.....	20
Hypothesis and Aims .....	21
Specific aim 1 .....	21
Specific aim 2 .....	21
Specific aim 3 .....	21
Overall Impact and Significance.....	21
Chapter 2: Materials and Methods.....	23
Cell Culture, Maintenance, and Propagation .....	23
Cloning of Bcl-2 into <i>pBABE-puro</i> and <i>pQCXIN</i> Plasmids .....	24
Generation of Retroviral Stable Cell Lines .....	25
Treatment with Drugs.....	26

miRNA Mimic/Inhibitor Transfection .....	27
siRNA Transfection Strategies .....	27
Dual Transfection with siRNA and Mimic .....	29
Indirect Immunofluorescence .....	29
EGFP-LC3B Immunofluorescence Studies .....	31
Assessing Transfection Efficiency Using <i>pEGFP-C1</i> .....	32
mCherry-GFP-LC3B Flux Assay and Macro Image J Analysis .....	32
Total RNA Isolation and Quantitative Real-Time PCR .....	33
miRNA Isolation and Quantitative Real-Time PCR .....	33
Protein Isolation and Western Blotting Analysis .....	35
Reverse Phase Protein Array (RPPA) .....	36
Cell Viability Assay Using Crystal Violet .....	37
Lactate Dehydrogenase (LDH) Cytotoxicity Assay (Necrosis Assay) .....	37
Migration Assay Using Boyden Chambers .....	38
Apoptosis Assay .....	38
Cell Cycle Analysis .....	39
Colony Formation Assay .....	39
Cholesterol Measurements .....	40
LipidTOX Neutral Lipid Staining .....	40
MitoSOX Assay .....	41
3'UTR Luciferase Assay .....	41
Luciferase Promoter Assay .....	42
RT <sup>2</sup> -PCR Pathway Focused PCR Array (Lipoprotein Signaling and Cholesterol Metabolism, Autophagy, and Apoptosis) .....	42
Transmission Electron Microscopy (TEM) .....	43
Bioinformatic Analyses .....	44
Statistical Analyses .....	44
 Chapter 3: EVI1 Splice Variants Modulate Epithelial-Mesenchymal Transition in Ovarian and Breast Cancer Cells .....	 45
Introduction .....	45
Results .....	46
siRNA targeting the splice junction between exon 2 of MDS1 to exon 2 of EVI1 elevates claudin-1 protein .....	46
siRNA targeting the splice junction between exon 2 of MDS1 to exon 2 of EVI1 alters the RNA expression of key EMT markers .....	49
siRNA targeting the splice junction between exon 2 of MDS1 to exon 2 of EVI1 reduces the migratory potential of HEY and MDA-MB-231 cells .....	52
Specific EVI1 splice variants modulate claudin-1 promoter activity .....	53
siRNA targeting the splice junction between exon 2 of MDS1 to exon 2 of EVI1 does not alter the levels of miR-200 family of miRNAs .....	54
Reverse phase protein array (RPPA) analysis on cell lines overexpressing EVI1 splice variants .....	55
Cyclin E1 levels are altered upon TGF $\beta$ treatment in OVCAR8 ovarian cancer cells following overexpression of EVI1 splice variants .....	57
Discussion .....	59
Acknowledgments .....	62
 Chapter 4: miR-494 Modulates SnoN/SkiL Expression and Cell Death Response upon As <sub>2</sub> O <sub>3</sub> Treatment in Ovarian Cancer Cells .....	 63

Introduction .....	63
Results .....	65
Bioinformatic analyses reveal miR-216b, miR-410, miR-494, and miR-495 putative binding sites in the 3'UTR of <i>SnoN</i> .....	65
miR-494 modulates SnoN protein and mRNA expression .....	67
miR-494 leads to the formation of diffused EGFP-LC3B expression upon As <sub>2</sub> O <sub>3</sub> treatment .....	69
miR-494 sensitizes the cellular response of HEY ovarian cancer cells to As <sub>2</sub> O <sub>3</sub> treatment .....	70
Discussion .....	72
Acknowledgments .....	75
 Chapter 5: miR-494 Modulates Cell Survival and Induces Lipid Droplet Formation in Renal Cancer Cells .....	76
Introduction .....	76
Results .....	78
miR-494 modulates the protein levels of LC3B and cleaved PARP in normal and renal cancer cells.....	78
miR-494 antagomir and Ago2 siRNA-mediated knockdown reverse the induction of LC3B-I/II and cleaved PARP protein levels in 769-P renal cancer cells upon miR-494 mimic transfection .....	82
miR-494-mediated apoptotic induction occurs in the absence of change in protein levels of pro-caspases or nuclear localization of AIF.....	84
miR-494 reduces Bcl-2 protein levels and knockdown of Bcl-2 mimics effects elicited by miR-494 expression .....	86
Investigation of miR-494 targets via RT <sup>2</sup> -PCR arrays identify LC3B as a potential target.....	88
Increase in LC3B mRNA and protein levels upon miR-494 transfection occur in the absence of autophagic flux changes.....	89
miR-494 expression leads to accumulation of LDs, an event mediated via LC3B.....	91
Mitochondrial structural organization is altered upon miR-494 expression in 769-P cells .....	98
Discussion .....	101
Acknowledgments .....	105
 Chapter 6: Future Directions and Significance of the Study .....	106
Overview of the Major Findings.....	106
Chapters 3 and 4: Limitations of the Studies .....	108
Chapter 5: Potential Mechanisms Underlying Altered Mitochondrial Organization and Accumulation of LDs with miR-494 Expression .....	108
miR-494 expression increases LC3B levels: implications in lipid metabolism .....	108
Contribution of miR-494 in lipid metabolism.....	110
Involvement of miR-494 in mitochondrial dynamics and mitophagy.....	111
Accumulation of LDs in miR-494 expressing cells: mitochondrial involvement .....	113
Cross-talk between miR-494 and the pro-survival Bcl-2 molecule.....	116
Contribution of the miRNA Cluster at 14q32 in Renal Cancer Pathophysiology.....	118
Renal Cancer Specimens: Cellular Changes with Altered miR-494 Expression.....	119
Renal Cancer Mouse Models: Effects of miR-494 on Tumor Growth .....	120

Acknowledgments .....	122
References.....	124
Appendices .....	142
Appendix A: Copyright Permissions .....	142



## List of Tables

Table 1: List of miR-494 targets identified according to published reports .....	14
Table 2: List of cell lines utilized for dissertation .....	23
Table 3: List of siRNA target genes utilized for dissertation .....	29
Table 4: List of primary antibodies utilized for immunofluorescence analyses .....	31
Table 5: List of primary antibodies utilized for western blotting analyses .....	36
Table 6: A summary of a subset of genes involved in lipid metabolism harboring miR-494 binding sites.....	112

## List of Figures

Figure 1: Human chromosome 3q .....	4
Figure 2: EVI1 gene structure .....	5
Figure 3: Mechanism of splicing and formation of the MDS1/EVI1 splice variant.....	7
Figure 4: miRNA biogenesis and mode of action.....	12
Figure 5: Mechanism of EMT .....	16
Figure 6: Schematic model of the autophagy pathway .....	19
Figure 7: Specific regions on the EVI1 splice variants targeted by the tested siRNA constructs.....	47
Figure 8: Knockdown of EVI1 splice variants via siRNAs in HEY cells modulate protein levels of EMT markers .....	48
Figure 9: Knockdown of EVI1 splice variants via siRNAs in MDA-MB-231 cells modulate protein levels of EMT markers.....	49
Figure 10: Knockdown of EVI1 splice variants via siRNAs in HEY and MDA-MB-231 cells modulate mRNA expression of EMT markers.....	50
Figure 11: Effect of knockdown of EVI1 splice variants on the migratory potential of HEY and MDA-MB-231 cells.....	52
Figure 12: Effect of knockdown of EVI1 splice variants on the promoter activity of claudin-1.....	53
Figure 13: Effect of knockdown of EVI1 splice variants on the expression of miR-200a, miR-200b, and miR-200c .....	55
Figure 14: Protein analyses of EVI1 splice forms in T29 and OVCAR8 cells .....	56
Figure 15: Reverse phase protein array analysis (RPPA) in cells overexpressing EVI1 splice forms .....	57
Figure 16: Modulation of Cyclin E1 protein levels following EVI1 splice variants overexpression in OVCAR8 cells .....	58

Figure 17: Cell cycle analysis following EVI1 splice variants overexpression in OVCAR8 cells .....	59
Figure 18: miR-494 modulates SnoN protein levels .....	65
Figure 19: miR-494 modulates SnoN mRNA expression.....	68
Figure 20: Pattern of EGFP-LC3B expression in miR-494 overexpressing cells in the presence of As <sub>2</sub> O <sub>3</sub> treatment .....	69
Figure 21: miR-494 sensitizes HEY ovarian cancer cells to As <sub>2</sub> O <sub>3</sub> treatment.....	70
Figure 22: The DLK1-DIO3 genomic cluster harbors a set of 54 miRNAs.....	77
Figure 23: miR-494 modulates cell death in renal cancer cells.....	79
Figure 24: miR-494 reduces 769-P viability and colony forming ability .....	81
Figure 25: Validation of miR-494-mediated cellular responses .....	83
Figure 26: Mechanism of miR-494-induced apoptosis.....	85
Figure 27: miR-494 reduces Bcl-2 protein levels .....	86
Figure 28: LC3B, a potential direct target of miR-494.....	88
Figure 29: miR-494 expressing cells exhibit increased LC3B punctae without changes in autophagic flux .....	89
Figure 30: Accumulation of LDs in miR-494 expressing cells occurs in an LC3B-dependent mechanism.....	92
Figure 31: miR-494 induces disorganized structural mitochondrial patterns .....	99
Figure 32: Schematic of miR-494 functional responses in 769-P renal cancer cells .....	102
Figure 33: miR-494 leads to increased LC3B levels - implications in lipid metabolism .....	109
Figure 34: Mfn1/Mfn2 - potential targets of miR-494 .....	114
Figure 35: Potential contribution of miR-494 to the mitochondrial fission/fusion events.....	115
Figure 36: Potential cross-talk between Bcl-2 and miR-494 .....	116
Figure 37: Overall model of proposed cellular effects mediating the cell death response elicited by miR-494.....	117
Figure 38: Proposed experimental outline to investigate the effects of miR-494 on tumor growth in mouse model.....	121

## Abbreviations

aCGH: Array comparative genomic hybridization  
Ago2: Argonaute 2  
AIF: Apoptosis-inducing factor  
AMPK $\alpha$ : AMP-activated protein kinase alpha  
AP-1: Activator protein-1  
APL: Acute promyelocytic leukemia  
As<sub>2</sub>O<sub>3</sub>: Arsenic trioxide  
ATG: Autophagy-related  
Bcl-2: B-cell lymphoma 2  
BSA: Bovine serum albumin  
DAPI: 4',6-diamino-2-phenylindole  
DIO3: Deiodinase, iodothyronine type III  
DLK1: Delta-like 1 homolog  
Drp1: Dynamin-related protein 1  
EDTA: Ethylenediaminetetraacetic acid  
EGFP: Enhanced green fluorescent protein  
EGFR: Epidermal growth factor receptor  
EMEM: Eagle's minimal essential medium  
ER: Estrogen receptor  
EOC: Epithelial ovarian cancer  
EVI1: Ecotropic viral integration site 1  
FBS: Fetal bovine serum  
GFP: Green fluorescent protein  
HAD: Human autophagy database  
HER2: Human epidermal growth factor receptor 2  
IHC: Immunohistochemistry  
KIRC: Kidney renal clear cell carcinoma  
LAMP-2A: Lysosomal-associated membrane protein-2A  
LC3B: Microtubule-associated protein 1 light chain 3 alpha  
LDs: Lipid droplets  
MDS1: Myelodysplastic syndrome 1  
MECOM: MDS1 and EVI1 complex locus  
Mfn: Mitofusin  
miRNA: microRNA  
mRNA: messenger RNA  
mTOR: mammalian Target of rapamycin  
MTT: 3-(4,5-dimethylthiazol-2-yl)-2,5-diphenyltetrazolium bromide  
NaOH: Sodium hydroxide  
PARP: Poly ADP ribose polymerase  
PBS: Phosphate-buffered saline  
PCR: Polymerase chain reaction

PE: Phosphatidylethanolamine  
PI: Propidium iodide  
PI3K: Phosphoinositide 3-kinase  
PIK3CA: Phosphoinositide 3-kinase catalytic subunit alpha  
PINK1: PTEN-induced putative kinase 1  
PKC $\iota$ : Protein kinase C iota  
PR: Progesterone receptor  
RPMI: Roswell Park Memorial Institute  
RPPA: Reverse phase protein array  
SDS-PAGE: Sodium dodecyl sulphate-polyacrylamide gel electrophoresis  
SFM: Serum free media  
SNALPs: Stable nucleic acid lipid particles  
SnoN/SkiL: Ski-related novel protein N/Ski-like protein  
TCGA: The cancer genome atlas  
TBST: Tris-buffered saline with Tween-20  
TEM: Transmission electron microscopy  
TGF $\beta$ : Transforming growth factor beta  
UTR: Untranslated region  
VHL: von Hippel-Lindau  
ZEB1/2: Zinc finger E-box binding homeobox 1

## Abstract

Genomic aberrations are primary contributors to the pathophysiology of cancer [11]. Dysregulated expression of genes located within these aberrations are important predictors of chemoresistance, disease prognosis, and patient outcome [12]. This dissertation is focused on understanding the regulation and/or functions of specific genes located at dysregulated genomic regions such as 3q26 and 14q32 in the biology of ovarian and renal cancer, respectively.

Serous epithelial ovarian cancer (EOC) manifest amplification at the 3q26.2 locus [2], an observation consistent with the cancer genome atlas (TCGA) [13]. The most amplified gene in this region is EVI1 which has been extensively studied in hematological malignancies [2]. However, its contribution to the pathophysiology of solid cancers remains unknown. We hypothesized that dysregulated EVI1 and SnoN/SkiL expression (located at the 3q26.2 amplicon) leads to the altered cellular functional response, thereby contributing to the pathophysiology of ovarian cancer. Our group has previously shown that EVI1 splice forms may exhibit altered subcellular localization and functional properties relative to the wild type form [14]. In Chapter 3 of this dissertation, we identified that EVI1 splice forms could modulate epithelial-mesenchymal transition. Our findings indicate that siRNA construct targeting the splice junction between exon 2 of MDS1 to exon 2 of EVI1, (reduces the expression of MDS1/EVI1 and EVI1<sup>Del190-515</sup> splice forms) increases epithelial cell markers while decreasing mesenchymal markers and reducing migratory potential of ovarian and breast cancer cells.

SnoN/SkiL, another gene overexpressed at the 3q26 is reported by our group to be induced upon As<sub>2</sub>O<sub>3</sub> treatment in ovarian cancer cells via unknown mechanisms [15]. This induction of SnoN opposes the apoptotic cell death pathway induced by the drug treatment [15].

We have previously identified that the PI3K/AKT pathway (also dysregulated in ovarian cancer [16]) contributes to the up-regulation of SnoN upon treatment with As<sub>2</sub>O<sub>3</sub> [17]. However, SnoN is regulated via multiple mechanisms including post-translational modifications [18]. Additionally, c-Ski (a homolog of SnoN) is regulated post-transcriptionally by numerous miRNAs in cancer cells [19-22]. In Chapter 4, we attempted to identify potential miRNAs that could regulate SnoN expression post-transcriptionally. We discovered that miR-494 reduces both SnoN mRNA and protein levels. Our experimental outcomes also demonstrate that miR-494 further sensitizes ovarian cancer cells to drug treatment.

Interestingly, miR-494 is located at the 14q32 region which has been shown to be down-regulated in renal cancers [23]. Several reports indicate miR-494 to be involved in tumor suppressive responses including apoptosis and cell cycle arrest in various cancers [24-26]. However, its role in renal cancer biology remains unknown. We hypothesized that miR-494 elicits a tumor suppressive response in renal cancer cells. Through our studies in Chapter 5, we demonstrate that miR-494 reduces cell viability and increases apoptotic response in renal cancer cells. We also show that miR-494 increases LC3B mRNA and protein levels. A 3'UTR luciferase assay indicated that LC3B may be a potential target of miR-494. Intracellular lipid droplets (LDs) increased in miR-494 expressing in a LC3B-dependent manner. This was accompanied with reduced intracellular cholesterol content, increased mitochondrial structural disorganization, and altered Drp1 localization.

The outcome of our findings have improved our understanding of the regulation and functional response of these genes/miRNAs (EVI1, SnoN, and miR-494) in ovarian and renal cancers. The studies reported in Chapter 5 identified a novel function of miR-494 in increasing LDs and reducing renal cell survival. However, additional studies are warranted to fully understand the underlying mechanism of increased LDs formation in miR-494 expressing cells and the implication of miR-494 and other miRNAs at the 14q32 region in renal cancer biology. In

future, these studies will aid in the development of better treatment strategies which will contribute towards the management of cancer.



## Chapter 1

### Introduction

#### Ovarian Cancer

According to the American Cancer Society, ovarian cancer is the fifth most common cause of deaths due to cancer in women (<http://www.cancer.org/cancer/ovariancancer/detailedguide/ovarian-cancer-key-statistics>). The National Cancer Institute (NCI) predicts an estimated 21,290 new cases and 14,180 deaths in 2015, due to ovarian cancer (<http://seer.cancer.gov/statfacts/html/ovary.html>). The high mortality rate of ovarian cancer is attributed to the lack of early stage detection methods [27]. Ovarian cancer is a heterogenous disease that can be classified into three major subtypes: (1) clear cell, (2) endometrioid, and (3) high grade serous [28]. The latter is the most common, accounting for ~70% of the cases, whereas endometrioid and clear cell account for a total of ~20% of the cases [29]. Rarer forms account for the remaining ~10%. The origin and pathogenesis of ovarian cancer is complex.

Due to the asymptomatic nature of this disease, diagnosis of ovarian cancer remains a significant problem. Therefore, identification of better prognostic markers is needed for early detection of this deadly disease. A common treatment strategy for epithelial ovarian cancer (EOC) involves a combination of surgery, followed by treatment with taxanes and platinum-based chemotherapeutic drugs [30]. Cisplatin is the most common first-line treatment regime, although patients develop resistance to the drug over time [31]. Other first-line treatment options include anti-angiogenic drugs such as bevacizumab [32] and pegylated liposomal doxorubicin

[33]. Recent reports have also shown PARP (poly (ADP-ribose) polymerase) inhibitors as promising therapeutic tools for the treatment of epithelial ovarian cancer [34]. However, after completion of primary therapy, the risk for recurrence is around 60-70% [35]. Therefore, improved treatment strategies are direly needed to better treat patients with ovarian cancer.

## **Breast Cancer**

Breast cancer is the most common form of cancer among women in the United States and the second most common cause of cancer related mortality in women (<http://www.cancer.org/cancer/breastcancer/detailedguide/breast-cancer-key-statistics>). It is estimated that there will be 231,840 new cases and 40,290 deaths in 2015 due to this disease (<http://seer.cancer.gov/statfacts/html/breast.html>). Breast cancers can be classified into three broad categories based on *HER2* and ER/PR status. These are (1) luminal A (ER and /or PR<sup>+</sup>, *HER2*<sup>-</sup>), (2) luminal B (ER and /or PR<sup>+</sup>, *HER2*<sup>+</sup>), (3) triple negative/basal-like (ER and /or PR<sup>-</sup>, *HER2*<sup>-</sup>), and (4) *HER2* type (ER and /or PR<sup>-</sup>, *HER2*<sup>+</sup>) [36] [37] [38]. The luminal A cancers are the most prevalent (~40%), followed by luminal B (~20%), triple negative (~15-20%), and *HER2* (~10-15%) [37]. The treatment strategies for breast cancers include tyrosine kinase and angiogenic inhibitors [39]. Hormone therapy is the most favorable line of treatment for hormone positive breast cancers [40]. The use of taxanes with other chemotherapeutic drugs is an effective combinatorial strategy; however, there is a high incidence of toxic effects with this strategy [40]. Therefore, better treatment strategies are needed to combat breast cancer.

## **Renal Cancer**

Renal cell carcinoma can be subdivided into various categories which are (1) clear cell, (2) papillary, (3) chromophobe, (4) oncocytic, and (5) collecting duct. The clear cell renal cancer is the most frequent subtype, which affects ~70% of patients with renal cancer. According to NCI, the estimated new cases and deaths from kidney (and renal pelvis) cancer in the USA in

2015 are 61,560 and 14,080, respectively (<http://seer.cancer.gov/statfacts/html/kidrp.html>). Renal cancer can be acquired in a sporadic or hereditary manner. The gene associated with the hereditary form of this cancer is von Hippel-Lindau (VHL), which is located at 3p25. Renal cancer is a metabolic disease and the VHL/HIF pathway dysregulation is crucial in renal cancer progression [41]. VHL deletion is also associated with sporadic forms of renal carcinoma [42] [43]. This protein is an E3 ubiquitin ligase and its primary function is in the regulation of the hypoxia response pathway, which is a metabolic pathway critical for tumor survival under hypoxic conditions [44]. Under normoxia, VHL ubiquitinates and targets HIF1 $\alpha$  (hypoxia inducible factor 1 alpha) for degradation, thereby inhibiting the expression of HIF1 $\alpha$ -regulated genes [45].

The current treatment strategies for renal cancer can be grouped into four categories: (1) surgery, (2) radiation therapy, (3) immunotherapy, and (4) molecular-targeted therapy. The surgical and radiation approaches are dependent on the stage of the disease. Immunotherapeutic treatment may include IL-2 and IFN- $\alpha$  [46]. Targeted therapy involves kinase inhibitors of VEGF, PDGF, TGF $\beta$ , and mTOR, such as sunitinib, pazopanib, axitinib, sorafenib, tivozanib, and temsirolimus [46]. Identification of predictive biomarkers will aid in improving treatment outcomes.

### **Genomic Aberrations**

Genetic instability is a hallmark of cancer and a major cause of genomic alterations involving DNA copy number changes and/or mutations [47]. Gain-of-function mutations or DNA copy number gains can activate proto-oncogenes. In a similar manner, loss-of-function mutations or DNA copy number losses can inactivate a tumor suppressor gene, thus disrupting normal gene functions [48]. The common genomic alterations associated with serous EOC include copy number gains at 1q, 3q, 7q, and 8q; whereas losses occur at 17p, 19q and 22q [13] [49]. The most common genes mutated in serous EOC include *TP53*, *BRCA1*, *BRCA2* [50],

and additional *PTEN* mutations which are correlated with a worsened patient outcome [51]. Mutations in *BRCA1/2*, *TP53*, *PTEN*, *STK11*, and *CDH1* are associated with a high risk for development of breast cancers [52]. It is interesting that serous EOC and basal-like breast tumors exhibit similar molecular characteristics, suggesting that analogous therapeutic opportunities can be investigated for treatment [53]. The most common deletion in the 3p region in renal cancers involves mutations/deletions in four major genes: *VHL*, *PBRM1*, *BAP1*, and *SETD2* [43]. The loss of 14q chromosomal region harboring *HIF1 $\alpha$*  is also a frequent event leading to an aggressive phenotype [23, 45]. There is also a gain at the 5q chromosomal region, which leads to an increase in *SQSTM1*, associated with development of renal cancer [43] [54].

### Chromosomal Aberrations at 3q: Serous EOC and BRCA1 Positive Basal Breast Cancers

In particular, amplification of the 3q26 chromosomal region is an early and common event in epithelial cancers, including basal *BRCA1* positive breast [55] [56] and serous EOC [2]. The genes that are amplified at this regions include catalytic subunit of phosphoinositide-3-

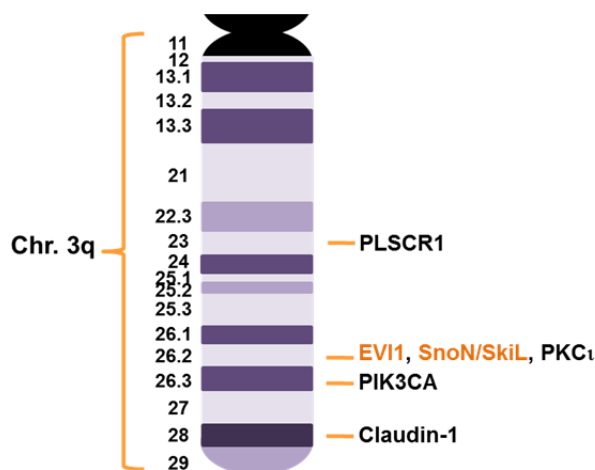


**Figure 1: Human chromosome 3q**

The q arm of human chromosome 3 showing the genes that are amplified in several solid cancers [1, 2]. These include (1) *EVI1*, *SnoN/SkiL*, and *PKC $\iota$*  at 3q26.2, (2) *PIK3CA* at 3q26.3, (3) *Claudin-1* at 3q28, and (4) *PLSCR1* (Phospholipid scramblase 1) at 3q23. (Adapted from Dr. Nanjundan's grant proposal). (\*Figure created by Punashi Dutta)

kinase (PI3K) (PIK3CA), Protein Kinase C, Iota (PKC $\iota$ ), EVI1 [2], and SnoN [1] (Figure 1). Our studies reported in Chapter 4 focus on the contribution of EVI1 and SnoN in ovarian and/or breast cancer biology.

### Ecotropic viral integration site-1 (EVI1)

#### Gene structure:

Transcripts of EVI1 are encoded by the MECOM (MDS1-EVI1 complex locus) locus [57]. As depicted in Figure 2, the EVI1 gene is composed of 16 exons [57] and is over 100 kb long [58]. The start and the stop codon for EVI1 are located at exon 3 and 16, respectively [59]. The EVI1 nuclear protein consists of 1051 amino acids and is ~145 kDa [58]. The EVI1 protein contains two Zinc (Zn) finger domains (7 and 3 Zn finger motifs, respectively from the N- to the C-terminal region) and an acidic C-terminal region [60]. The intervening region (IR) and

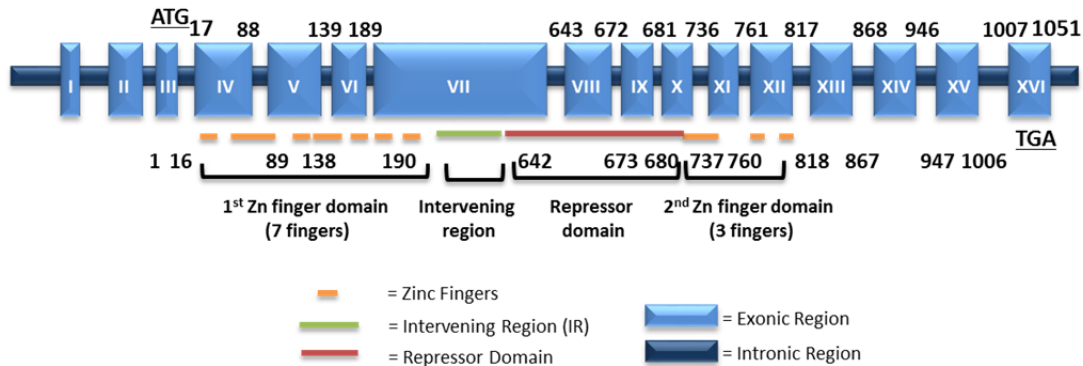


**Figure 2: EVI1 gene structure**

Schematic representation of EVI1 gene structure including exonic regions and important functional domains. The first Zinc (Zn) finger domain contains 7 Zn fingers, which is followed by the intervening region and the repressor domain. The second Zn finger domain, containing 3 Zn fingers follows the repressor domain. The EVI1 gene consists of 16 exons; the mRNA product of which translates into a protein with 1051 amino acids. (Adapted from Dr. Nanjundan's grant proposal). (\*Figure created by Punashi Dutta)

repressor domain are located in between the two Zn finger domains. EVI1 has been shown to bind to the GATA2 promoter via its first Zn finger domain and enhance its transcription to control hematopoietic stem cell proliferation [61]. The first Zn finger domain is also required for the repression of the transforming growth factor beta 1 (TGF $\beta$ ) pathway via interaction with Smad3 [62]. EVI1 is known to interact with other Smad family members (i.e., Smad1, 2, and 4) [63]. EVI1 inhibits JNK via direct interaction [64], antagonizing stress induced apoptosis, and thus contributing to leukemogenesis. The first Zn finger domain is also required for transformation of Rat1 fibroblasts [65].

#### Splice variants:

The MDS1/EVI1 splice variant is generated by the splicing of the second exon of myelodysplastic syndrome 1 (MDS1) to the second exon of EVI1, as indicated in Figure 3. This splice variant of EVI1 has an additional 188 codons: 125 of these arising from the exon 1 and 2 of MDS1 and 63 codons arising from the exon 2 and 3 of EVI1 [4]. MDS1/EVI1 exhibits a novel PR domain with 40% homology to the PR domain of the histone methyltransferase, PRDM2 [4, 66].

Another splice variant of EVI1 lacking 324 amino acids within exon 7 has been identified in human endometrial carcinoma cells [67, 68]. This variant contains the 6<sup>th</sup> and 7<sup>th</sup> Zn finger motifs of the 1<sup>st</sup> Zn finger domain but lacks the intervening region and a portion of the repressor domain and is designated as EVI1s [3] or Del324 [67]. EVI1  $\Delta$ 105, a variant of EVI1 identified in murine leukemia cells, lacks the C-terminal 105 amino acids which are located in exon 15 [59]. On occasion, variants of EVI1 that contain an insertion of 9 amino acids in the repressor domain (exon 9) have been reported; it does not appear to alter the activity of EVI1, as reported thus far [59]. Six different 5' alternative EVI1 mRNA transcripts have been reported; these appear to be the result of altered initiation transcription start sites within the first exonic region leading to the

different fragments of the first exon spliced to the exon 2 [69]. The detailed functional response of these different splice variants of EVI1 is presently unclear.

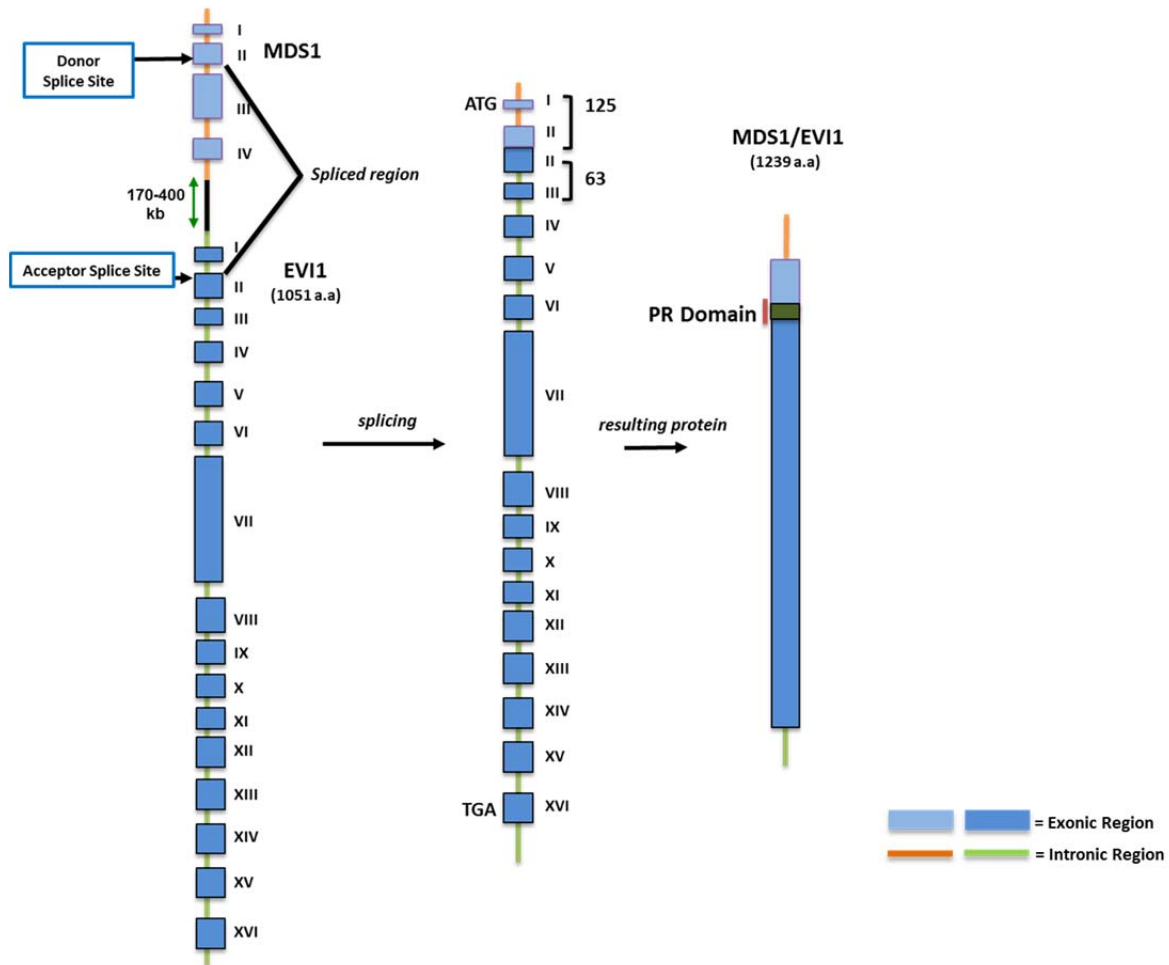


**Figure 3: Mechanism of splicing and formation of the MDS1/EVI1 splice variant**

The MDS1/EVI1 splice variant arises due to a splicing event between the exon 2 of MDS1 and exon 2 of EVI1, giving rise to a novel PR domain and a resultant protein with 1239 amino acids [4]. (\*Figure created by Punashi Dutta)

Interacting partners:

The intervening region (amino acids 239-514), located after the first Zn finger domain, is required for the repressor activity of EVI1; this was demonstrated using a splice variant of EVI1 lacking this region which was unable to transform Rat1 fibroblasts [65]. The repressor activity of EVI1 is also dependent on the proline-rich repressor domain which is required for its interaction

with C-terminal binding protein1 (CtBP1) [70] and for inhibiting the TGF $\beta$  pathway. However, this proline-rich region does not directly interact with Smads [62]. GATA2 up-regulation and inhibition of TGF $\beta$  signaling by EVI1 are required for the hematopoietic development [71]. The C-terminus of EVI1 interacts with BRG1 (SWI/SNF ATPase subunit factor involved in chromatin remodeling) and stimulates E2F1 activity and proliferation [72]. The second Zn finger domain is required for the interaction with c-FOS and activating AP-1 transcription [73]. The 8<sup>th</sup> Zn finger motif of this domain binds to RUNX1 which facilitates its DNA binding activity [74]. EVI1 also exhibits “non-DNA binding” properties and can act as a scaffold protein mediating transcriptional repression/activation [75, 76].

EVI1 interacts with HDACs histone deacetylase (HDACs) [77] and histone acetylase (HATs) such as CREB-binding protein (CBP) (at amino acids 283-514) and p300/CBP-associated factor (P/CAF) (at amino acids 1-283) [78]. These HATs acetylate EVI1 and promote its localization to nuclear speckle domains [78]. In contrast, HDACs and CtBP1 promote EVI1 localization to the nuclear compartment, which has a diffused pattern of expression [78]. Acetylation of EVI1 at lysine residue 564 is required for the transcriptional activation of GATA2 [79]. Interestingly, HDAC inhibitors can only partially relieve EVI1-mediated repression of target genes, indicating that other chromosomal modifications are required for EVI1-mediated repression [75]. Consistent with this notion, it has been reported that histone methyltransferases, SUV39H1 and G9a, interact with the N-terminal region of EVI1 and contribute to its repressor property [75, 76]. In addition, EVI1 can also bind to DNMT3a/3b and repress the transcription of miR-124-3 [80]. EVI1 binds to the promoter of the stress responsive gene, SIRT1 and induces its transcription [81]. However, SIRT1 is also shown to deacetylate and degrade EVI1 [81]. Moreover, EVI1 can bind to PTEN and repress its expression via binding to polycomb group of proteins (PcG), thus modulating the AKT/mTOR pathway [82].



### Functions:

Two decades ago, EVI1 was reported to be increased at the mRNA levels up to 40-fold in ovarian cancers via an RNase protection assay [83]. This was supported by a similar study conducted in 2006, demonstrating increased EVI1 expression in advanced stage ovarian cancers, relative to normal via the use of expression profiling microarray [84]. The DNA copy number of EVI1 was found to be elevated in 43% of ovarian cancers [84]. Both MDS1/EVI1 have been shown to contribute to the pathophysiology of ovarian cancer [2]. Increase in EVI1 transcript levels are associated with worsened patient outcome while increase in EVI1 DNA copy number and MDS1/EVI1 transcripts have been associated with good patient outcome [2]. Transient transfection of EVI1 and MDS1/EVI1 in both normal ovarian cells stimulates cell proliferation, migration and decreases TGF $\beta$ -mediated PAI-1 promoter activity [2]. There is evidence supporting that MDS1/EVI1 is an antagonist of EVI1 [85]; MDS1/EVI1 has also been reported to act cooperatively with EVI1 [86] [87]. However, the function of MDS1 is presently unclear [4]. A recent study by Bard-Chapeau and group identified 78 interacting partners of EVI1/EVI1 splice variants via SILAC-based quantitative proteomics approach, and was further validated some of these targets by yeast-2-hybrid and co-immunoprecipitation studies, identifying EVI1 as a modulator of transcription, recombination, and mitosis [88]. EVI1 has not been widely studied in solid cancers other than that of the ovary. However, EVI1 gene copy number has been shown to be increased in colon and colorectal cancers [89, 90].

### Ski-related novel protein N/ Ski-like protein (SnoN/SkiL)

SnoN/SkiL (Ski-related novel protein-1/Ski-like oncogene) belongs to the Ski family of proto-oncogenes. SnoN transcription is induced by the TGF $\beta$  signaling pathway [91]. It negatively regulates the TGF $\beta$  pathway by binding to both R-Smads (Smad2/3) and the co-Smad (Smad4), thus inhibiting their DNA binding ability and blocking the transcription of TGF $\beta$ -

regulated genes [92]. SnoN binds to a number of transcriptional regulators such as N-CoR [93], and members of the HDAC family [94], thus inhibiting the activity of Smads. This inhibitory role in the TGF $\beta$  signaling pathway is required for the transforming ability and proliferative potential of SnoN and its related oncoprotein, Ski [95] [96]. The role of SnoN as an oncogene or a tumor suppressor gene in cancer is complex and dependent on the cancer type [18]. SnoN positively regulates cell cycle arrest and senescence in ovarian epithelial cells and also leads to enhanced cellular proliferation in ovarian cancer cells [1]. SnoN expression has been reported to be elevated in a number of cancers, including melanoma [97], esophageal squamous cell carcinoma [98], colorectal carcinoma [99], leukemia [100], and estrogen receptor-positive breast carcinoma [96]. On the contrary, it has also been reported that knockdown of SnoN in lung and breast cancer cells does not alter the transforming ability of these cells [101]. SnoN can also increase PML transcription via direct binding, leading to the localization of SnoN to PML nuclear bodies and thus inducing premature senescence via stabilization of p53 [18]. Furthermore, knockdown of SnoN via shRNA constructs can promote EMT and invasion of breast cancer cells *in vitro* as well as enhance tumor metastasis *in vivo* [101] [102].

SnoN subcellular localization is primarily nuclear (in malignant cells); however, studies have also shown SnoN to be localized to the cytoplasm (in normal tissues) [103]. The regulation of function and expression of SnoN is altered via post translational modifications [18]. Several E3 ubiquitin ligases have been identified to ubiquitinate and degrade SnoN upon TGF $\beta$  treatment, such as Smurf2 [104] and APC/C [105]. SnoN is rapidly degraded when it becomes phosphorylated by TAK1, a kinase that is activated by TGF $\beta$  treatment [106]. Prior studies performed in our laboratory have shown that SnoN expression is induced upon As<sub>2</sub>O<sub>3</sub> treatment in ovarian cancer cells, leading to induction of a beclin-1-independent autophagic response in these cells [15]. The PI3K pathway is involved in this process; however, the exact mechanism underlying this event remains to be investigated [17].

## Chromosomal Aberrations at 14q: Renal Cancer

Loss of the 14q chromosomal locus is observed in various cancer types including kidney [107] [23, 108] [109, 110], breast [111], colorectal [112] [113, 114] ovarian [115], and gastrointestinal [116]. Anomalies in miRNAs at 14q32 locus have also been studied in ovarian [117] and bladder [118] cancer. Loss of key genes within this region has been shown to contribute to disease pathophysiology; thus, understanding the precise role of these genes that are lost will aid in a better understanding of this disease. In renal cancer, the 14q deletion is associated with worsened patient outcome and increased cancer recurrence [23]. As described earlier, VHL is deleted at the 3p locus and HIF1 $\alpha$  is deleted at the 14q region; these events contribute to renal cancer biology [45].

### The DLK1-DIO3 cluster and microRNAs (miRNAs)

The DLK1-DIO3 region harbors the largest miRNA cluster in the human genome. In particular, the 14q32 miRNA cluster, contains 54 non-coding miRNAs, some of which are dysregulated in specific cancer types [119]. miRNAs are key regulators of gene expression involved in a spectrum of cellular processes and signaling pathways that impact cellular fate. Some miRNAs in this region shown to be altered in renal cancer include miR-127, miR-323a, miR-369, miR-376c, miR-379, miR-382, miR-485, and miR-493 [119]. In a separate study conducted by Juan and group, 5 miRNAs down-regulated in clear cell renal cell carcinoma (ccRCC) were identified namely miR-136, miR-154, miR-337, miR-377, and miR-411 [120].

miRNAs are small non-coding RNAs involved in a plethora of biological processes and modulate a number of cancer-related pathways, such as apoptosis, cell cycle control, proliferation, migration, and metabolism [121]. The first identified miRNA was lin-4 in *C.elegans* and was shown to modulate the development timing of the nematode via targeting lin-14 [122]. Since then miRNAs have been widely studied with respect to their mRNA targets and functional outcome in disease pathogenesis. The contribution of miRNAs to cancer development was first

identified by a study conducted more than a decade ago in chronic lymphocytic leukemia [123] [124]. miRNAs are transcribed by RNA polymerase II from exonic sequences or from introns of protein coding genes [121] (Figure 4). After transcription, these long primary RNA (pri-miRNA) are cleaved by RNase III enzyme, Drosha and its co-factor, DGCR8 to generate 60-100 small

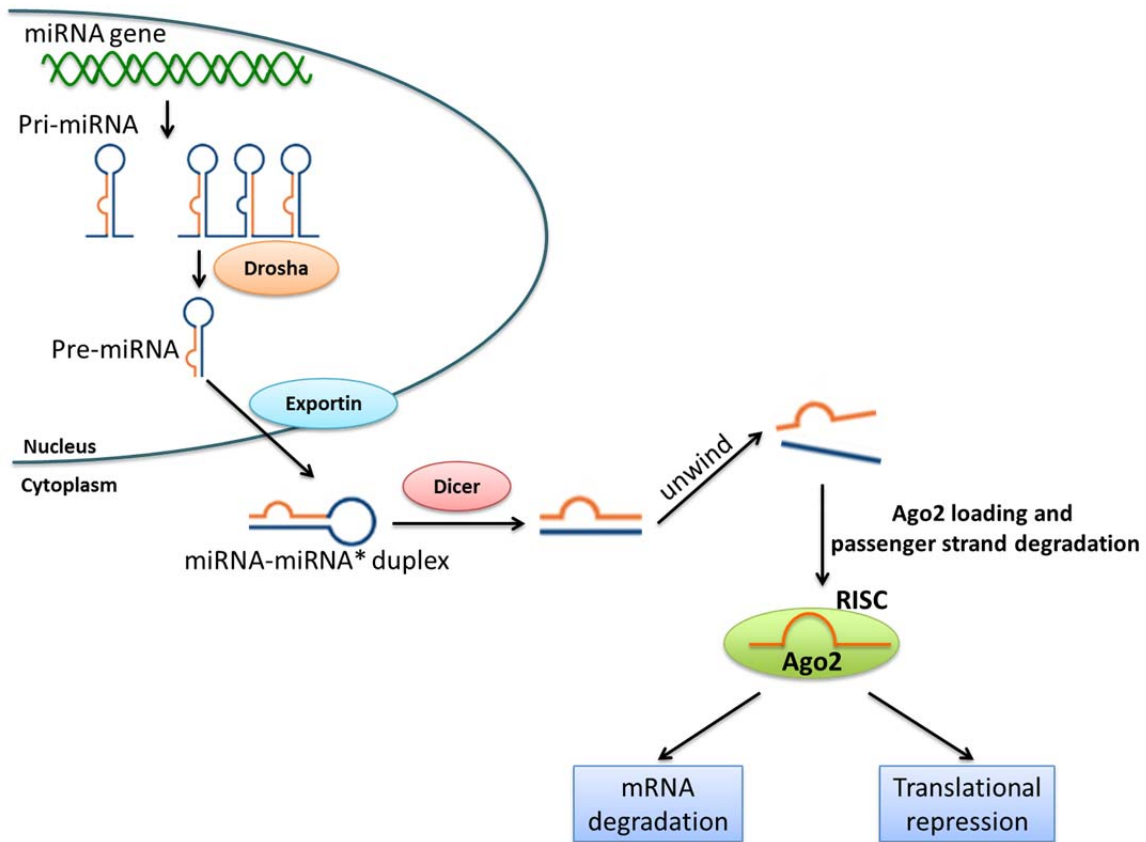


**Figure 4: miRNA biogenesis and mode of action**

The figure depicts the mechanism of miRNA biogenesis. Following transcription in the nucleus, pri-miRNA is cleaved by nuclear enzyme Drosha giving rise to pre-miRNA. This pre-miRNA is exported into the cytoplasm via exportin and further cleaved by Dicer to generate mature miRNA. Ago2 then loads the guide strand to the RISC complex and reduces target mRNA expression by translational inhibition or mRNA degradation [7]. (\*Figure created by Punashi Dutta)

RNA hairpins (pre-miRNA), which are then transported out of the nucleus into the cytoplasm by the action of Ran-GTP and Exportin 5. Once in the cytoplasm, RNase III enzyme, DICER further trims the pre-miRNA to form 21-24 nucleotide duplex, facilitated by TRBP and PACT

proteins [7]. This gives rise to the miRNA-miRNA\* duplex wherein the miRNA is the antisense or guide strand and the miRNA\* is the sense or passenger strand [125]. This miRNA duplex is then loaded to the RISC (RNA-inducing silencing complex) complex along with argonaute 2 (Ago2) protein which is involved in the dissociation of the passenger strand leading to the activated RISC complex [126]. This active RISC complex then binds to the target mRNA and based on the complementarity match can either inhibit translation (imperfect match) or lead to deadenylation and degradation of target mRNA (perfect match) [127]. However, recent evidence indicates that miRNAs may also induce transcriptional activation [128, 129]. The miRNA-mediated increase in gene expression depends on a number of factors such as (1) the context of the RNA sequence, (2) the presence or absence of RNP (ribonucleoprotein), and (3) cellular conditions [130].

#### miR-494:

miR-494 is located within the DLK1-DIO3 cluster at the chromosomal locus, chr14:101029634-chr14:101029714 [131]. miR-494 elicits contrasting responses in tumor cells. For example it targets both anti- and pro-apoptotic proteins [132]; indeed miRNAs can function both as oncogenic miRNAs (oncomirs [133]) or tumor suppressors in different cellular settings. miR-494 has been reported to be reduced in ovarian tumors [134]. miR-494 induces senescence in lung cancer cells [135] and inhibits proliferation via targeting c-KIT and HOXA10 expression in gastrointestinal [24] and oral cancer [136], respectively. miR-494 also suppresses cell growth in prostate cancer cells [137] and causes G2/M cell cycle arrest in cholangiocarcinoma cells [138]. miR-494 expression has also been reported to increase with treatment of chemotherapeutic drugs such as cinobufacin, used in gastric cancer cells [139]. miR-494 also suppresses invasion, migration, proliferation, and induces apoptosis in nasopharyngeal carcinoma [140]. The oncogenic functions of miR-494, in contrast include its

**Table 1: List of miR-494 targets identified according to published reports**

Target	Gene Name	Type of Cancer	PMID
BAG-1	Bcl-2-associated Athanogene	Gastric cancer	24606447
Bmal1	Brain and Muscle Arnt-like protein-1	NA	24928439
CaMKIId	Calcium/Calmodulin-Dependent Protein Kinase II Delta	NA	20837890
CDK16	Cyclin-Dependent Kinase 16	Nasopharyngeal carcinoma	25809707
CFTR	Cystic Fibrosis Transmembrane conductance Regulator	NA	22028919
C-KIT	V-Kit Hardy-Zuckerman 4 Feline Sarcoma Viral Oncogene Homolog	Gastrointestinal stromal tumor	22042971
CLPTM1L	Cleft-Lip and Palate Transmembrane 1-Like	Esophageal squamous cell carcinoma	25480402
c-myc	V-Myc Avian Myelocytomatosis Viral Oncogene Homolog	Gastric carcinoma, Pancreatic cancer	24612089, 25965392
CXCR4	Chemokine (C-X-C Motif) Receptor4	Prostate cancer, Breast cancer	24644030, 25955111
DDHD2	DDHD Domain Containing 2	NA	25653011
DJ-1	Parkinson Protein 7	NA	24269020
DYPD	Dihydrothymine Dehydrogenase	Colon cancer	25873402
FGFR2	Fibroblast Growth Factor Receptor 2	NA, Mouse pre-osteoblastic cells	20837890, 25795570
Foxj3	Forkhead box j3	NA	23047984
GALNT7	Polypeptide N-Acetylgalactosaminyltransferase 7	Nasopharyngeal carcinoma	25809707
HOXA10	Homeobox A 10	Oral cancer	25500095
IGF2BP1	Insulin-like Growth Factor 2 mRNA-Binding Protein 1	Lung cancer	22151897
JunD	Transcription factor JunD	NA	25906693
LIF	Leukemia Inhibitory Factor	NA	20837890
mtTFA	Mitochondrial transcription factor A	NA	23047984
PROS1	Protein S 1	NA	23789915
PTEN	Phosphate and Tensin homolog	NA	20837890,20006626
PTTG1	Pituitary Tumor-Transforming 1	Human cholangiocarcinoma, Cervical cancer	22785131, 25877755
P190B RhoGAP	Rho GTPase Activating Protein 35	Glioblastoma	24316134
ROCK1	Rho-Associated, Coiled-Coil Containing Protein Kinase 1	NA, Mouse pre-osteoblastic cells	20837890, 25795570
SCGN	Secretagonin	Small cell lung cancer	25226615
SDC-1	Syndecan-1	Medulloblastoma	23728345
SIRT1	Sirtuin 1	Pancreatic cancer	25965392
SLC26A3	Solute Carrier Family 26 (Anion Exchanger), Member 3	NA	24177028
TET-1	Ten Eleven Translocation-1	Hepatocellular carcinoma	25820676
TOP2A	Topoisomerase (DNA) II Alpha 170kDa	Hunman cholangiocarcinoma	22785131
VEGF	Vascular Endothelial Growth Factor	NA	25660325

up-regulation in certain cancers such as colorectal [141] and non-small cell lung cancer [142]. In addition, miR-494 inhibits expression of PTEN, a tumor suppressor [143, 144]. In hepatocellular carcinoma, miR-494 is up-regulated and plays a critical role in tumor progression [145, 146]. A summary of miR-494 targets is presented in Table 1.

The role of miR-494 (located within the 14q32 cluster) in clear cell renal carcinoma has not yet been investigated. Therefore, analysis of its expression and functional responses in normal and renal cancer cells may provide useful insight into understanding molecular mechanisms underlying renal cancer biology.

### **Pathways that Alter the Hallmarks of Cancer**

#### Transforming growth factor beta (TGF $\beta$ ) pathway

The TGF $\beta$  pathway regulates multiple cellular processes, including differentiation, proliferation, and apoptosis; dysregulation of this pathway is reported in various cancer types [147]. The signaling cascade is initiated by the TGF $\beta$  ligand binding to the TGF $\beta$  type-II receptor (TGF $\beta$ RII), resulting in the heterodimerization of TGF $\beta$ RII and TGF $\beta$  type-I receptor (TGF $\beta$ RI) followed by the phosphorylation of the R-Smads (Smad2/3) [148]. Phosphorylated Smad2/3 interact with Smad4, translocate to the nucleus, and activate the transcription of TGF $\beta$ -responsive genes [148]. TGF $\beta$  signaling can be negatively regulated by EVI1, SnoN/SkiL, and Smad7 [147]. The cellular responses elicited by the TGF $\beta$  pathway are cell type specific and moreover, the pathway elicits both tumor suppressive and oncogenic functions [149]. Of interest, ovarian cancer is characterized by dysregulated TGF $\beta$  signaling as a result of EVI1 and SnoN which are TGF $\beta$  corepressors, as well as TGF $\beta$ RII [150]. These changes lead to resistance towards the growth inhibition by TGF $\beta$ . TGF $\beta$  can also induce EMT and invasion in

borderline ovarian serous cancers and promote apoptosis in low-grade ovarian tumors, supporting its dual role [151].

### Epithelial-mesenchymal transition (EMT)

During development, cells frequently undergo epithelial-mesenchymal transition in addition to mesenchymal-epithelial transition (MET) [152] (Figure 5). These pathways are crucial for basic cellular processes including implantation, embryogenesis, organ development,

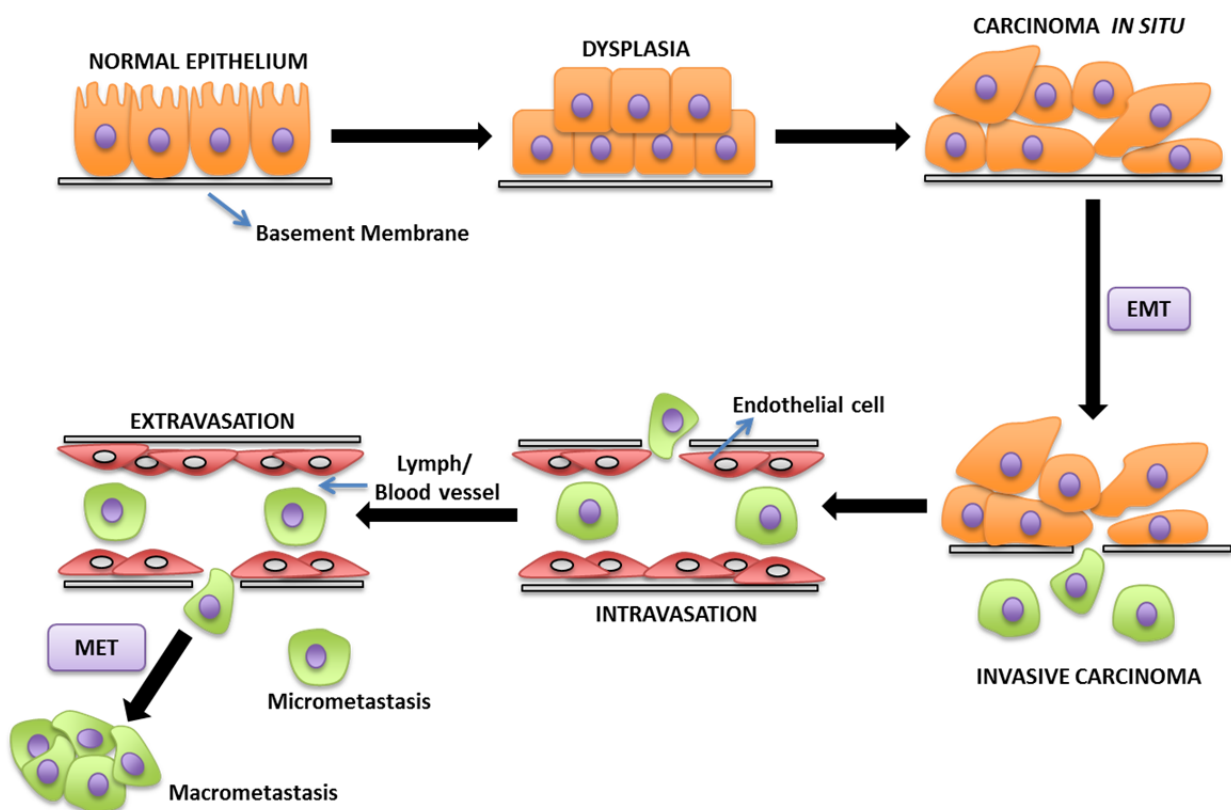


**Figure 5: Mechanism of EMT**

The multi-step process of EMT begins with dysplasia, a phenotype which confers abnormal morphology to epithelial cells. This is followed by disruption of cell-cell and cell-ECM (extracellular matrix) connections. These cells then infiltrate the bloodstream and undergo metastases to distant organs, following which they undergo MET (mesenchymal-epithelial transition) [6]. (Adapted from “The Biology of Cancer”, Garland Science 2007). (\*Figure created by Punashi Dutta)



and tissue regeneration [6]. In addition, EMT plays an important role in cancer biology since this pathway allows cancer cells to disseminate into the bloodstream and implant/grow at secondary metastases sites. [153].

The process of EMT is characterized by well-defined steps and involves specific markers that dictate the epithelial versus mesenchymal phenotype of cells. The epithelial phenotype is characterized by cell-cell connections, which are maintained by the tight junction proteins [154]. When cancer cells transition from an epithelial to mesenchymal morphology, the cell junctions disintegrate and the basement membrane degrades [152]. The primary epithelial marker, E-Cadherin is replaced by N-Cadherin, a mesenchymal marker. These changes promote a mesenchymal phenotype as well as resistance to anoikis (a cell death pathway promoted by detachment from the extracellular matrix [155]); the acquisition of this cellular characteristic will promote cellular migration and invasion [152] [156]. Claudin-1 is a tight junction protein, important in maintaining cell-cell connections. Interestingly, claudin-1 is located at chromosome 3q28, in close proximity to the frequently dysregulated 3q26 region. Our laboratory findings have shown that genes located at neighboring chromosomal regions may regulate each other [157]; for example, PLSCR1 (located at 3q23) is regulated by SnoN/SkiL (located at 3q26.2). It is presently unknown whether genes such as EVI1, located at 3q26 may regulate claudin-1.

#### Programmed cell death (PCD)

The imbalance between cell division and cell death is an important feature of cancer cells [158]. PCD is characterized by a defined and regulated set of cellular events [159]. The two major types of PCDs are apoptosis and autophagy. There exist other cell death mechanisms including necrosis, as well as other pathway such as necroptosis, pyroptosis, entosis, and ferroptosis [160] [161].

### Apoptosis:

Apoptosis is characterized by cell shrinkage, nuclear fragmentation, followed by sequestration of intracellular components into apoptotic bodies, a process referred to as “budding” [162]. These cells are then phagocytosed by macrophages. Apoptosis occurs as a normal cellular process to maintain cellular homeostasis [162]; however, cancer cells evade apoptosis [163]. There are two major apoptotic pathways: intrinsic and extrinsic pathways. The extrinsic pathway is activated, for example, by the binding of the ligand Fas L to its cognate receptor; this results in the recruitment of FADD and procaspase-8, which form the death-inducing signaling complex (DISC) [164]. Pro-caspase-8 is then activated leading to activation of the executioner caspase-3. The intrinsic pathway is triggered by DNA damage and is dependent on the release of cytochrome c from the mitochondria, which recruits Apaf-1 and procaspase 9 to form the apoptosome [164]. The Bcl-2 family of proteins includes both anti- and pro-apoptotic members. The pro-apoptotic proteins such as Bax and Bak aid in the release of cytochrome c from the mitochondria [165]. However, the anti-apoptotic proteins such as Bcl-2 and Bcl-xL antagonize apoptosis by inhibiting the release of cytochrome c from the mitochondria by directly binding Bax and/or Bak [166].

### Autophagy:

Autophagy refers to a process in which damaged organelles and proteins are recycled in double-membrane vesicles called autophagosomes to obtain energy during conditions of stress, including starvation [167]. The autophagy related genes (ATG) were identified in the yeast in 1993 [168]; the molecular basis of autophagy is conserved among yeast, plants, and mammals [169]. Autophagy can be divided into the following stages: (1) induction, (2) nucleation, (3) elongation and completion, (4) docking and fusion, and (5) degradation and recycling [170]. A schematic representation of this process including the proteins involved is depicted in Figure 6. Autophagy can be induced by a number of stimuli such as nutrient deprivation, stress, and

inhibition of mTORC1 (mammalian target of rapamycin) [5]. In all of these events, ULK1/ATG1 becomes phosphorylated by AMPK [171]. mTORC1 (GβL, mTOR, Raptor) is regulated by

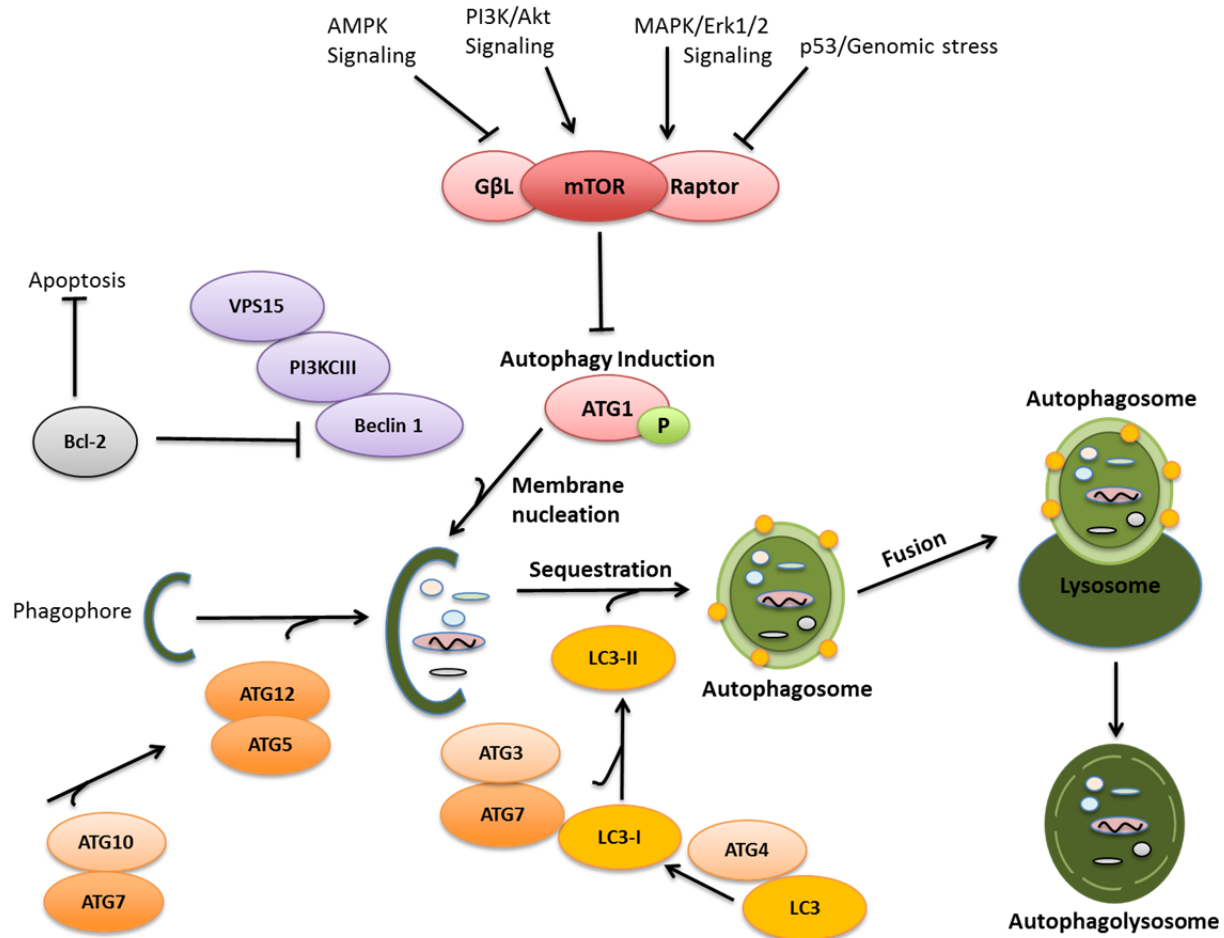


**Figure 6: Schematic model of the autophagy pathway**

The induction of autophagy can be regulated via several mediators, for example active mTOR inhibits autophagy [5]. mTOR itself is regulated via various signaling pathways [8]. Bcl-2 inhibits autophagy by binding beclin-1 [9] and inhibiting the formation of the initiation complex. The autophagy pathway progresses via two ubiquitin-like conjugation steps that involve the conjugation of ATG12 and ATG5 via ATG7 and ATG10 [10]. In the second step, ATG4 cleaves LC3 exposing the cysteine residue where PE attaches via activation of ATG7 and ATG3. The conjugated ATG5-ATG12 act as the E3 ubiquitin ligase for this reaction. This lipidated form of LC3 (LC3-II) is bound to the autophagosomal membrane. Following this, the autophagosome fuses with the lysosome leading to degradation of the damaged cellular components [10]. (Adapted from <http://www.cellsignal.com/>). (\*Figure created by Punashi Dutta).

signaling pathways such as AMPK, PI3K/AKT, and MAPK [8]. Following induction, vesicle

nucleation or formation of the phagophore membrane occurs, which is dependent on the complex formation between hVps34 or PI3KCIII, Vps15, and beclin-1 (pre-initiation complex) [172]. The vesicle elongation step is facilitated by two ubiquitin-like proteins involved in two ubiquitin-like pathways. The first ubiquitin-like pathway involves the conjugation of ATG12 to ATG5 via the E1-like protein, ATG7, and the E2-like protein, ATG10 [173, 174]. In the second ubiquitin-like pathway, ATG4 cleaves LC3, following which the E1 (ATG7) and E2 (ATG3)-like proteins conjugate PE (phosphatidylethanolamine) to LC3-I, leading to the formation of LC3-II [175, 176]. The conjugated ATG5-ATG12 act as the E3 ubiquitin ligase for this reaction. This lipidated form of LC3 (LC3-II) is then recruited to the autophagosomal membrane. When the autophagosome is fully formed, LC3 detaches from the autophagosomal membrane via the action of ATG4 and is thus released into the cytosol [176]. This pathway may be inhibited by Bcl-2, an anti-apoptotic protein which binds to beclin-1, thus inhibiting the formation of the pre-initiation complex [9]. Autophagy is a protective mechanism employed by the cell; however, its role in cancers is complex. Indeed, the autophagic pathway may exhibit both oncogenic or tumor suppressive roles based on the context [177].

#### *Cross-talk between autophagy and apoptosis:*

Autophagic and apoptotic pathways share multiple common mediators and these pathways are not independent of each other [178]. The interplay of these pathways is important in deciding the fate of the cancer cell. In one scenario, autophagy and apoptosis can cooperatively induce cell death. In another situation, autophagy can antagonize apoptotic cell death or in some cases facilitate apoptotic cell death [178]. Several cancer therapeutic strategies are designed for targeting or modulating these pathways; however, the impact of one pathway over the other should be an important consideration when designing therapeutic targets.

## Hypothesis and Aims

It is well established that the 3q26 region contains amplified genes such as EVI1 and SnoN in a variety of epithelial cancers, including ovarian and breast cancer. The functional role of these TGF $\beta$  transcriptional repressors in modulating specific hallmarks of ovarian and breast cancers, specifically EMT and migration have not yet been investigated. The mechanism by which SnoN is induced following As<sub>2</sub>O<sub>3</sub> treatment in ovarian cancer cells is unclear. It is unknown whether miRNAs are involved in this pathway. Additionally, we propose that loss of miRNAs at the 14q32 genomic cluster in renal cancer may modulate the biology of this disease. Thus our overall hypothesis is that “genes located at 3q26 and 14q32 contribute to the pathophysiology of ovarian and renal cancer, respectively.” We will address the hypothesis via the following specific aims:

Specific aim 1 (presented in Chapter 3): We will test whether EVI1 splice variants modulate epithelial-mesenchymal transition by assessing expression of EMT markers and the cellular migratory potential.

Specific aim 2 (presented in Chapter 4): We will test whether As<sub>2</sub>O<sub>3</sub> modulates SnoN levels in a miRNA-dependent manner.

Specific aim 3 (presented in Chapter 5): We will test whether the expression of miR-494 (located at 14q32 locus, which is lost in renal cancer) alters renal cancer cell survival.

## Overall Impact and Significance

At the end of this work, our findings will allow us to better understand the contribution of EVI1 and its splice variants in EMT. Further, an understanding of the mechanism by which SnoN becomes induced upon As<sub>2</sub>O<sub>3</sub> treatment, will allow us to understand chemotherapeutic

resistance in ovarian cancer cells, which is presently unclear. Since renal cancers are characterized by 14q loss and miR-494 is one of 54 miRNAs located at this region, this will provide an incentive to further investigate this locus and understand its role in the biology of renal cancer.

## Chapter 2

### Materials and Methods

#### Cell Culture, Maintenance, and Propagation

**Table 2: List of cell lines utilized for dissertation**

Name of Cell Line	Tissue of Origin	Media	Passage Number	Obtained From
T29	Large T antigen/hTERT immortalized normal ovarian surface epithelial cells	RPMI	p=n+8	Dr. Gordon B Mills, MD Anderson Cancer Center
T80	Large T antigen/hTERT immortalized normal ovarian surface epithelial cells	RPMI	p=n+17	Dr. Gordon B Mills, MD Anderson Cancer Center
OVCAR8	Ovarian serous epithelial carcinoma	RPMI	p=n+5	Dr. Gordon B Mills, MD Anderson Cancer Center
HEY	Ovarian serous epithelial carcinoma	RPMI	p=n+9- n+30	Dr. Gordon B Mills, MD Anderson Cancer Center
MDA-MB-231	Mammary epithelial adenocarcinoma cells	RPMI	p=n+6- n+12	ATCC
HEK293T	Human embryonic kidney epithelial cells	RPMI	p=n+4- n+12	Dr. Gordon B Mills, MD Anderson Cancer Center
HK-2	HPV-16 transformed normal kidney cortex/proximal tubule cells	K-SFM (supplemented with BPE and EGF)	p=n+2- n+5	ATCC
769-P	Epithelial renal adenocarcinoma cells	RPMI	p=31-42	ATCC
786-0	Epithelial renal adenocarcinoma cells	RPMI	p=111-114	ATCC
A-498	Epithelial renal adenocarcinoma cells	EMEM	p=36-38	ATCC

A summary of the cell lines used in this dissertation is presented in Table 2 along with information regarding media conditions, passage numbers, and source. All the cell lines reported in this study were maintained in an incubator at 37°C with 5% CO<sub>2</sub>. With the exception of HK-2 and A-498 cells, all other cell lines were cultured in RPMI 1640 media (HyClone, Fisher Scientific, Pittsburg, PA), supplemented with 8% fetal bovine serum (FBS) and 5% penicillin/streptomycin. HK-2 cells were maintained in bovine pituitary extract and epidermal growth factor containing keratinocyte media (Gibco, Life Technologies, Grand Island, NY), supplemented with 5% penicillin/streptomycin. A-498 cells were grown in EMEM media (ATCC, Manassas, VA) supplemented with 8% fetal bovine serum (FBS) and 5% penicillin/streptomycin. For the purpose of sub-culturing, seeding or passaging cells, cells were trypsinized using 1 ml (T25 flask) or 2 mls (T75 flask) Trypsin/EDTA, followed by neutralization in the respective media. Cells were then centrifuged at 1000 rpm for 5 minutes at room temperature. The supernatant was discarded and the pellet re-suspended in the appropriate amount of fresh media. For sub-culturing of HK-2 cells, 1:5 Trypsin/EDTA solution was utilized and neutralized in 5% FBS in PBS solution. 769-P cells were passaged at a ratio of 1:3. All other cell lines were passaged at a ratio of 1:4.

### **Cloning of Bcl-2 into *pBABE-puro* and *pQCXIN* Plasmids**

Bcl-2 sequence was excised using EcoRI from *pcDNA3* plasmid (Addgene Plasmid #19279, Cambridge, MA, deposited by Dr. Philip Leder) [179] and cloned into *pBABE-puro* and *pQCXIN* plasmids using the following cloning strategy. The excised sequence of Bcl-2 was run on a 1% agarose gel, following which gel purification (QIAquick Gel Extraction Kit, Qiagen, #28706) was carried out to retrieve the insert in 30 µl of EB buffer. Heat inactivation and vector dephosphorylation step for each of the plasmid was performed. Ligation was carried out using 10 µl of the insert, 1 µl of the dephosphorylated vectors, 1 µl enzyme and 10 µl ligation buffer.



The mixture was incubated at room temperature for 5 minutes and at 4°C for 1 hour. Following ligation, transformation was performed in Top10F' bacteria. Bacterial colonies were selected and the positive transformants were subjected to restriction digestion by Sac II to determine correct orientation. The constructs were then sent for sequencing at the Molecular Genomics Core, Moffitt Cancer center, Tampa, FL.

### **Generation of Retroviral Stable Cell Lines**

T29 and OVCAR8 cells were utilized for the generation of retroviral cell lines stably expressing either control, EVI1 wild-type (WT), EVI1<sup>Del427-515</sup>, or EVI1<sup>Del190-515</sup> sequence cloned into *pLEGFP-C1* plasmid [14]. HEK 293T cells were used as the packaging cell line and were seeded in 6-well plates at 1.5 million cells/well. Following 24 hour overnight adherence of the cells to the culture dish, the media in the wells was replaced with 2 mls of serum-free media. The transfection mixture (per transfection) was prepared by adding 100 µl serum-free media to cryovials, following which, 1 µg of plasmids (*pCGP*, *pVSVG*, and the *pLEGFP-C1* plasmids in the ratio 1:1:1) and 3 µl Fugene HD (Promega, Madison, WI) were added. This transfection mixture was allowed to incubate at room temperature for 15 minutes, following which it was added dropwise onto the cells. The cells were then overlaid with 2 mls of complete media 6 hours post-transfection. The following day, media from the wells was replaced with 2 mls of complete media. On the same day, T29 and OVCAR8 cells were seeded at 250,000 cells/well. Twenty-four hours after seeding, the first round of infection was performed by replacing the media in the wells with supernatant containing viruses from HEK293T cells along with polybrene (8 µg/ml) (the viral media was filtered using a 0.45 µm filter before application). Two mls of complete media was added to the HEK293T cells plate. The following day, a second round of infection was performed as described above. Twenty-four hours post the second infection, media in the wells was replaced by 2 mls of complete media and the following day G418

containing media was added to the wells (the concentration of G418 utilized for T29 cells was 1 mg/ml and OVCAR8 cells was 0.1 mg/ml) in order to apply selection pressure. The cells were monitored for growth and viability. Media was replaced periodically, as required. Once confluent, they were expanded to a T25 or T75 flask, as appropriate and subsequently frozen.

The *pBABE-puro-mCherry-GFP-LC3B* plasmid was obtained from Addgene (Plasmid #22418, Addgene, Cambridge, MA, deposited by Dr. Jayanta Debnath) [180]. For the purpose of generating 769-P cells stably expressing mCherry-GFP-LC3B (two independent retroviral pools), a similar protocol was followed, with some changes. One million 769-P cells were seeded for the infection and only one round of infection was performed. Cells were recovered with 2 mls of complete media 24 hours post-infection; 3 hours post-recovery, cells were trypsinized and expanded to a T25 flask. The next day, 0.75 µg/ml puromycin containing media was added to the wells and cells were monitored for growth and viability. Once cells were confluent, they were expanded and subsequently frozen down for storage.

769-P parental and 769-P mCherry-GFP-LC3B cells stably expressing Bcl-2 were also established utilizing *pBABE-puro-Bcl-2* and *pQCXIN-Bcl2* plasmids, respectively. The protocol for retroviral stable cell line generation was identical to the one described above for 769-P cells. For the selection with *pQCXIN* plasmid, G418 was utilized at a concentration of 0.5 mg/ml in addition to puromycin at 0.75 µg/ml (since it was double gene overexpressing cell line – mCherry-GFP-LC3B and Bcl-2).

### **Treatment with Drugs**

As<sub>2</sub>O<sub>3</sub> and TGFβ were used in the present study. NaOH and nanopure water were used to dissolve As<sub>2</sub>O<sub>3</sub> (Sigma-Aldrich, St. Louis, MO) to prepare a working stock of 5 mM, which was further also filter sterilized using a 0.2 µm filter. TGFβ (Calbiochem, Rockland, MA) was used at a concentration of 50 pM and was prepared in 500 µl of 0.1% BSA and 4 mM HCl.

### **miRNA Mimic/Inhibitor Transfection**

For transfection with miRNA mimic or inhibitor, 250,000 cells were seeded in 6-well plates. Following 24 hours adherence, cells were transfected with either mimic (Negative control miRNA mimic, #4464058; hsa-miR-216b, #4464066, MC12302; hsa-miR-410, #4464066, MC11119; hsa-miR-494, #4464066, MC12409; and/or hsa-miR-495, #4464066, MC11526 mimic) or inhibitor (Negative control miRNA inhibitor, #4464076; hsa-miR-494 inhibitor, #4464084, MH12409), or both, at a concentration of 200 pmol. The mimics and inhibitors utilized in the study were obtained from Life Technologies, Grand Island, NY. For transfection (per well), 100  $\mu$ l serum-free media was added to cryovials following 200 pmol (4  $\mu$ l) mimic/inhibitor and 3  $\mu$ l Fugene HD (Promega, Madison, WI). This transfection mixture was allowed to incubate at room temperature for 15 minutes, following which it was added dropwise in a spiral manner onto the wells. Cells were overlaid with complete media, 6 hours post-transfection. Following 24 hours post-transfection, cells were trypsinized, counted, and re-seeded at 250,000 cells/well. They were processed at 24, 48, 72, or 96 hours post-transfection with or without drug/inhibitor treatment (indicated in a separate section). Mimic/inhibitor transfection was also performed in 24-well plates with an initial cell seeding number of 50,000 cells/well. The procedure was similar as described above; however, all the volumes were reduced 5 times and the re-seeding step was omitted.

### **siRNA Transfection Strategies**

Cells were seeded in complete media at different densities depending on the cell type (as described below, in detail) in 6-well plates or 35 mm dishes for siRNA-mediated knockdown experiments. After overnight adherence, complete media from the wells was replaced with 37<sup>0</sup>C pre-warmed serum-free media. Transfection mixture (per transfection) was prepared in eppendorf tubes by adding 100  $\mu$ l serum-free media and 4  $\mu$ l Dharmafect transfection reagent

(Dharmacon, GE Healthcare, Lafayette, CO). This mixture was allowed to incubate at room temperature for 10 minutes following which 5  $\mu$ l (50 nM) of the respective siRNA (obtained from Dharmacon GE Healthcare, Lafayette, CO) was added to the tubes and incubated at room temperature for 20 minutes. This transfection mixture was then added dropwise onto the cells followed by overlaying with complete media after 3 hours. Twenty-four hours post the first siRNA transfection, media from the wells was removed and replaced with complete media. Following a 3 hour recovery period, another round of siRNA transfection was performed as described above. Twenty-four hours post the second round of siRNA transfection, cells were recovered by replacing the media in the wells with complete media. The cells were then either re-seeded 24 hours or harvested 48 hours post the second transfection (depending on experiment type). siRNA knockdown with minor variations across various experiments are indicated as follows:

1. For the purpose of miRNA isolation in order to quantify miR-200a/b/c members, 2 million MDA-MB-231 and 650,000 HEY cells were seeded in 60 mm dishes. siRNA transfection was performed (non-targeting ON-TARGETplus control siRNA and siME) as described above except the quantities were doubled for the 60 mm dishes.
2. In order to isolate total RNA for quantification of relative mRNA levels or protein analysis, 1 million MDA-MB-231 and 325,000 HEY cells were seeded in 6-well plates. siRNA transfection (mock, non-targeting ON-TARGETplus control siRNA, siB, si2Kb, si04, and siME) was performed as described above.
3. 769-P cells were seeded at 750,000 cells/well. siRNA transfection (non-targeting ON-TARGETplus control siRNA, *Ago2*, *ATG7*, *Bcl-2*, or *LC3B*) was performed as described above. For transfection involving *Bcl-2* siRNA, a concentration of 100 nM was utilized, instead of 50 nM.

A list of siRNAs utilized in the present study obtained from Dharmacon (GE Healthcare, Lafayette, CO) are summarized in Table 3 along with their catalog numbers.

**Table 3: List of siRNA target genes utilized for dissertation**

siRNA	Catalog number
<i>Ago2</i>	L-004639-00
<i>ATG7</i>	L-020112-00
<i>Bcl-2</i>	L-003307-00
Non-targeting ON-TARGETPlus control	D-001810-10
<i>LC3B</i>	L-012846-00

siRNA targeting various splice variants of EVI1 (siB, si2Kb, si04, siME) were custom designed by Dharmacon (GE Healthcare, Lafayette, CO), according to a study conducted by Jazaeri and colleagues [3]. EVI1 siB reduced the protein expression of WT EVI1, MDS1/EVI1, and EVI1<sup>Del190-515</sup>; EVI1 si2Kb reduced the protein expression of EVI1<sup>Del190-515</sup>; EVI1 si04 reduced the protein expression of MDS1/EVI1; and EVI1 siME reduced the protein expression of MDS1/EVI1 and EVI1<sup>Del190-515</sup>.

### Dual Transfection with siRNA and Mimic

For co-transfection experiments with siRNA and mimic, cells were seeded and siRNA transfection conducted as described above. Following 24 hours of a second round of siRNA transfection, cells were recovered for 3 hours and then trypsinized, counted, and re-seeded at 250,000 cells/well. Twenty-four hours post re-seeding, cells were transfected with mimic, as described above. Cells were processed at 72 hours post-mimic transfection.

### Indirect Immunofluorescence

769-P cells were seeded at 250,000 cells/well. Cells were transfected using control or miR-494 mimic, as described above. Twenty-four hours post-transfection, 150,000 cells were re-seeded onto glass coverslips. Ninety-six hours post-transfection, the cells were rinsed in PBS and fixed using 4% paraformaldehyde (in PBS) for 30 minutes at room temperature (for

experiments involving co-staining with LC3B and another antibody, fixation was performed for 15 minutes with 4% paraformaldehyde at room temperature, followed by 15 minutes in ice-cold 100% methanol at -20°C). Following fixation, two PBS washes were conducted for 5 minutes each, after which the cells were blocked for 1 hour at room temperature in PBS solution with 5% goat serum and 0.1% Triton X-100. After the blocking step, two PBS washes were performed (5 minutes each). Now, primary antibody application was performed by placing the coverslips in petri dishes onto 50 µl primary antibody (prepared in PBS solution with 1% goat serum, 0.1% Triton X-100, and the appropriate primary antibody dilution). These petri dishes were then placed in a humidified chamber and left overnight at 4°C.

The next day, coverslips were placed into 6-well plates with fresh PBS solution, followed by two 5 minute PBS washes. Five hundred µl/well of secondary antibody was applied to the wells and incubated at room temperature for 1 hour. The secondary antibody solution was prepared in PBS solution with 1% goat serum, 0.1% Triton X-100, and 1:500 dilution of goat anti-rabbit Alexa Fluor-546 (#A11035, Life Technologies, Grand Island, NY) or goat anti-mouse Alexa Fluor-488 (#A11029, Invitrogen, Life Technologies, Grand Island, NY) secondary antibody. Following secondary antibody application, three 5 minute PBS washes were performed. Following this, for experiments involving co-staining utilizing two different antibodies, the second primary antibody was applied as described above. If not, the coverslips were mounted on glass slides onto mounting media containing DAPI for staining the nucleus. Images were captured using a Perkin Elmer Confocal Spinning Disc Microscope (CMMB Core Facility, University of South Florida, Tampa, FL). (For immunofluorescence experiments involving both siRNA and mimic transfection, 250,000 cells were re-seeded per well on glass coverslips after the co-transfection and an identical protocol was followed as described in the above section). A list of antibodies and related information utilized for this section is summarized in Table 4.

**Table 4: List of primary antibodies utilized for immunofluorescence analyses**

Antibody	Dilution	Category	Company	Catalog number
AIF	1:400	Rabbit monoclonal	Cell Signaling Technology	#5318
Cytochrome c	1:250	Mouse monoclonal	Cell Signaling Technology	#12963
Drp1	1:50	Rabbit monoclonal	Cell Signaling Technology	#8570
LC3B	1:400	Rabbit polyclonal	Cell Signaling Technology	#2775

### **EGFP-LC3B Immunofluorescence Studies**

HEY cells were seeded at 250,000 cells/well in 6-well plates. After 24 hours, cells were transfected with control or miR-494 mimic, as described above. Twenty-four hours post-transfection, cells were re-seeded onto glass coverslips. Following a 24 hour period of adherence, cells were transfected with 1  $\mu$ g/well *pEGFP-LC3B* plasmid (Addgene Plasmid #24920, Cambridge, MA, deposited by Dr. Toren Finkel) [181], using Fugene HD as transfection reagent. At 72 hours post mimic transfection, cells were treated with 10  $\mu$ M  $As_2O_3$  for 18 hours following which they were fixed, blocked, and mounted onto glass slides with DAPI at 96 hours post-mimic transfection. Images were captured using a Zeiss inverted fluorescent microscope (Analytic Microscopy Core, Moffitt Cancer Center, Tampa, FL).

769-P cells, seeded on glass coverslips were transfected with miR-494 mimic, as described above. Forty-eight hours post-transfection, cells were transfected with *pEGFP-LC3B* plasmid, as described. Cells were then treated with 25  $\mu$ M CQ (for 18 hours) at 72 hours post-mimic transfection. At 96 hours post-mimic transfection, cells were processed as mentioned above and images were captured using a Perkin Elmer Confocal Spinning Disc Microscope (CMMB Core Facility, University of South Florida, Tampa, FL).

For studies involving *Bcl-2* siRNA, 769-P cells were seeded at 500,000 cells/well on glass coverslips. After 24 hour overnight adherence, *Bcl-2* siRNA transfection was performed as described above (only one round of transfection performed at a concentration of 100 nM).

*EGFP-LC3B* plasmid transfection was then performed at 24 hours post-transfection. The next day, cells were processed as described above and imaged using a Perkin Elmer Confocal Spinning Disc Microscope (CMMB Core Facility, University of South Florida, Tampa, FL).

### **Assessing Transfection Efficiency Using *pEGFP-C1***

Following seeding of HK-2, 769-P, 786-O, and A-498 cells at 250,000 cells/well on glass coverslips, they were transfected with 1  $\mu$ g *pEGFP-C1* plasmid (Clontech, CA), using Fugene HD as transfection reagent, as described above. Forty-eight hours post-transfection, cells were fixed, blocked, and coverslips were mounted on glass slides with DAPI mounting media. Images were captured using the Perkin Elmer Confocal Spinning Disc Microscope (CMMB Core Facility, University of South Florida, Tampa, FL).

### **mCherry-GFP-LC3B Flux Assay and Macro Image J Analysis**

769-P cells stably expressing mCherry-GFP-LC3B fusion protein, (both retroviral cell lines 1 and 2) were seeded at 250,000 cells/well in a 6-well plate. Control and miR-494 mimic transfection were performed, as stated above. Twenty-four hours post-transfection, cells were recovered and re-seeded at 250,000 cells/well for protein harvest (western blot validation analysis) and 150,000 cells/well on glass coverslips for immunofluorescence analysis. Ninety-six hours post-transfection, cells were fixed, blocked, and coverslips were then mounted on glass slides in mounting media containing DAPI. Images were captured using the Perkin Elmer Confocal Spinning Disc Microscope (CMMB Core Facility, University of South Florida, Tampa, FL). Ten images per sample were captured for a total of 30 images for the control mimic and 30 images for miR-494 mimic transfected cells for each retroviral cell line (1 and 2). The images were subjected to Image J macro analysis, a program that automatically divides the merged figure into separate green, red, and merged images and quantifies the number and area of



punctae [182]. The macro data was then further analyzed to obtain average values as well as number of punctae/cell and punctae area/cell for the green, red, and merged punctae.

### **Total RNA Isolation and Quantitative Real-Time PCR**

For isolating total RNA, RNeasy mini kit was utilized from Qiagen (Valencia, CA) and RNA isolation was carried out according to the manufacturer's instructions. RNA concentration and purity was quantified using Nanodrop (Thermo Scientific, Hudson, New Hampshire). Quantitative real-time PCR analysis was performed using One-step TaqMan master mix and probes/primers obtained from Applied Biosystems (Grand Island, NY). The following probes/primers were obtained from Applied Biosystems Assays-on-Demand: E-Cadherin (Hs01023894); Claudin 1 (Hs00221623); LC3B (Hs00797944\_s1); N-Cadherin (Hs00983056); PRKAG2 (Hs00211903\_m1); Snail (Hs00195591); SnoN (Hs00180524\_m1); Slug ((Hs00950344); Twist (Hs00361186); ZEB1 (Hs00232783); and ZEB2 (Hs00207691). The correlative method was utilized to calculate RNA-fold changes from  $C_T$  of genes using  $\beta$ -actin as the endogenous control.

### **miRNA Isolation and Quantitative Real-Time PCR**

Total RNA isolation was carried out according to the manufacturer's protocol provided with the mirVana miRNA isolation kit from Ambion (NY, USA). Briefly, cells were washed with PBS and then an appropriate volume of the lysis/binding solution was added. Lysates were collected and one tenth the volume of miRNA homogenate additive was added followed by an incubation on ice for 10 minutes. Acid-phenol:chloroform, equal to the amount of lysis/binding buffer was then added and the mixture was vortexed for 30–60 seconds. The samples were then centrifuged for 10 minutes at 10,000 g at room temperature in order to separate the aqueous and organic phases. An appropriate volume of the aqueous (upper) phase was carefully collected. The volume was recorded and then 1.25 times this amount of room

temperature 100% ethanol was added to the aqueous phase, recovered from the previous organic extraction step. For each sample, a filter cartridge was placed into the collection tubes and the lysate/ethanol mixture (from the previous step) was added onto the filter cartridge. The mixture was centrifuged for ~15 seconds at 10,000 g and the flow-through was discarded. Seven hundred  $\mu$ l miRNA wash solution 1 was added and centrifuge for ~5–10 seconds at the same speed. The flow-through was discarded. Now, 500  $\mu$ l of wash solution 2/3 was added and centrifuged for ~15 seconds for 10,000 g. This step was repeated and after discarding the flow-through from the last wash, the filter cartridge was replaced and the assembly was centrifuged for 1 minute (twice) to remove residual fluid from the filter. Now the filter cartridge was transferred into a fresh collection tube and RNA eluted in 25  $\mu$ l of pre-heated (95<sup>0</sup>C) nuclease-free water and quantified using Nanodrop.

The reverse transcription reaction and PCR was performed according to the manufacturer's protocol (TaqMan MicroRNA Assays, Applied Biosystems, NY, USA). The probes/primers for both the reverse transcription and PCR reaction were obtained from Applied Biosystems Assays-on-Demand: hsa-miR-200a, RT:000502, TM:000502; hsa-miR-200b, RT:002251, TM:002251; hsa-miR-200c, RT:002300, TM:002300; hsa-miR-494, RT:002365, TM:002365; and RNU6B, RT:001093, TM:001093. The "RT" stands for probes/primers for the reverse transcription reaction and "TM" stands for those used for the PCR reaction. The RT reaction cycle conditions were as follows: 30 minutes at 16<sup>0</sup>C, 30 minutes at 42<sup>0</sup>C, and 5 minutes at 85<sup>0</sup>C. The cycle conditions for PCR were as follows: 95<sup>0</sup>C for 10 minutes, followed by 50 cycles of 15 seconds at 95<sup>0</sup>C and 1 minute at 60<sup>0</sup>C. Correlative method was utilized to calculate RNA-fold changes as C<sub>T</sub> of genes using RNU6B as the endogenous control.

## Protein Isolation and Western Blotting Analysis

In order to isolate protein, cells were lysed for 1 hour in the appropriate volume (depending on cell density at the time of harvest) of lysis buffer. The lysis buffer solution was prepared in Nanopure water and is composed of 150 mM NaCl, 1 mM MgCl<sub>2</sub>, 1 mM EGTA, 50 mM HEPES, 1% Triton X-100, 10% glycerol, and protease inhibitor tablet (Roche, Madison, WI). Following 1 hour lysis, cells were gently scraped, collected into eppendorf tubes and centrifuged at 14,000 rpm for 10 minutes at 4<sup>o</sup>C. Supernatant was collected and protein concentration was calculated using the Bicinchoninic Assay (BCA) Kit (Pierce, Fischer Scientific, Pittsburgh, PA). Protein concentration was normalized to the lowest sample. A total of 10 µl 6X SDS dye was added to 50 µl sample (diluted in lysis buffer) and 20 µl was loaded into the wells. Samples were run on appropriate percent (8, 10, or 12%) of SDS-PAGE (sodium dodecyl sulphate – polyacrylamide gel electrophoresis) gel. The gel was run typically for 2 hours at a constant voltage of 100 Volts following which gels were transferred to PVDF (polyvinylidene difluoride) membrane using a semi-dry transfer apparatus (Bio-Rad, Hercules, CA). The transfer settings for 1 gel utilized were at 0.11 Amps (or 0.15 Amps for 2 gels) for 2 hours. The membranes were then washed for 10 minutes in TBST (Tris-buffered saline containing 0.1% Tween-20, Bio-Rad, Hercules, CA) buffer on an orbital shaker (Thermo Scientific, Hudson, New Hampshire). Next, membranes were blocked for 1 hour in 5% milk prepared in TBST. After blocking, they were rinsed in TBST and primary antibody solution was applied (prepared in 5% bovine serum albumin (Fraction V heat-shock treated, #BP1600-100, Fisher Scientific, Waltham, MA) in TBST) and incubated overnight on an orbital shaker at 4<sup>o</sup>C. The next day, the primary antibody was collected and 15 minute washes in TBST were performed for 1 hour, following which HRP-conjugated secondary antibody in 5% milk (prepared in TBST) was applied. The secondary antibody was either goat anti-rabbit (#107-5046, Immun-Star, Biorad, Hercules, CA), goat anti-mouse (#107-5047, Immun-Star, Biorad, Hercules, CA), or donkey anti-goat (sc-2020, Santa

Cruz Biotechnology, Santa Cruz, CA) as appropriate. After the 1 hour secondary antibody incubation, 15 minute washes were performed for 1 hour and 30 minutes. Enhanced chemiluminescence solution (Immun-Star, Bio-Rad, Hercules, CA or LumiGLO, Cell Signaling, Danvers, MA) was then applied on the membranes prior to exposure of the membrane to X-ray film in order to detect bound antibodies. A list of antibodies utilized in the current study are summarized in Table 5.

**Table 5: List of primary antibodies utilized for western blotting analyses**

<b>Antibody</b>	<b>Dilution</b>	<b>Category</b>	<b>Company</b>	<b>Catalog number</b>
Ago2	1:500	Rabbit monoclonal	Cell Signaling Technology	#2897
ATG7	1:1000	Rabbit polyclonal	MBL International	PM039
Bcl-2	1:500	Rabbit monoclonal	Cell Signaling Technology	#2870
Bcl-2	1:1000	Rabbit monoclonal	Cell Signaling Technology	#4223
Caspase 2	1:1000	Mouse monoclonal	Cell Signaling Technology	#12675
Caspase 3	1:1000	Rabbit monoclonal	Cell Signaling Technology	#12675
Caspase 8	1:1000	Mouse monoclonal	Cell Signaling Technology	#12675
Caspase 9	1:1000	Mouse monoclonal	Cell Signaling Technology	#12675
Claudin-1	1:4000	Rabbit polyclonal	Life Technologies	187362
Cyclin E1	1:500	Mouse monoclonal	Santa Cruz Biotechnology	sc-247
Drp1	1:1000	Rabbit monoclonal	Cell Signaling Technology	#8570
EVI1	1:1000	Rabbit monoclonal	Cell Signaling Technology	#2593
GAPDH	1:4000	Rabbit polyclonal	Cell Signaling Technology	#2118
GFP	1:1000	Mouse monoclonal	Santa Cruz Biotechnology	sc-9996
LC3B	1:1000	Rabbit polyclonal	Cell Signaling Technology	#2775
N-Cadherin	1:500	Rabbit polyclonal	Cell Signaling Technology	#4061
Pan Actin	1:1000	Rabbit polyclonal	Cell Signaling Technology	#4968
PARP	1:1000	Rabbit polyclonal	Cell Signaling Technology	#9542
PINK1	1:500	Rabbit monoclonal	Cell Signaling Technology	#6946
SnoN	1:1000	Rabbit polyclonal	Santa Cruz Biotechnology	sc-914

### **Reverse Phase Protein Array (RPPA)**

T29 and OVCAR8 retroviral stable cells overexpressing EVI1 splice variants were seeded at 500,000 and 1 million cells, respectively, and treated with TGF $\beta$  at a concentration of 50 pM for various time points (0 hour, 5 minutes, 1, 3, 6, and 24 hours). Cell protein lysates were harvested as described above and samples were sent to MD Anderson Cancer Center

(Houston, Texas) for analysis. RPPA analysis was performed as described by Nanjundan and colleagues [183]. Briefly, Aushon arrayer was utilized to print protein lysate arrays on nitrocellulose-coated glass FAST slides. An automated DAKO autostainer was utilized to perform staining of the validated primary antibodies and data was quantified using the Supercurve method [183].

### **Cell Viability Assay Using Crystal Violet**

HEY or 769-P cells were seeded at 250,000 cells/well in a 6-well plate. Following 24 hour adherence, they were transfected with control or miR-494 mimic. Twenty-four hours post-transfection, cells were re-seeded at 5,000 cells/well in a transparent 96-well plate. At 96 hours post-transfection, (with or without 25  $\mu$ M As<sub>2</sub>O<sub>3</sub> treatment for 18 hours), media was removed from the plates and 100  $\mu$ l crystal violet staining solution was added and washed with Nanopure water after 15-20 minutes. Following overnight drying, 200  $\mu$ l of Sorenson's buffer was added to the wells and the viability was assessed by reading the absorbance at 570 nm on a Biotek plate reader [184].

### **Lactate Dehydrogenase (LDH) Cytotoxicity Assay (Necrosis Assay)**

769-P cells were seeded at 250,000 cells/well in a 6-well plate. Following 24 hour adherence, they were transfected with control or miR-494 mimic. Twenty-four hours post-transfection, cells were re-seeded at 25,000 cells/well in a 96-well plate. Following overnight adherence, the media in the wells was replaced with 200  $\mu$ l of 1% FBS-media. Ninety-six hours post-transfection, the plate was pulse centrifuged to bring the contents to the bottom of the well. Following this, 100  $\mu$ l of media was removed from the wells and transferred to a new opaque plate. One-hundred  $\mu$ l aliquot of the catalyst and dye (Roche, CA, USA) was added to the wells.

The plate was then shaken for 1 hour in the dark. The plate was incubated in the dark for 30 minutes and absorbance read at 490 nm on a Biotek plate reader.

### **Migration Assay Using Boyden Chambers**

HEY and MDA-MB-231 cells were seeded at 325,000 and 1 million cells/well in a 6-well plate. Following two rounds of siRNA transfections (as described above), cells were trypsinized and re-seeded at 25,000 cells/well in 500  $\mu$ l serum-free media in the top insert of a 24-well Boyden chamber insert plate. The bottom chamber was filled with 750  $\mu$ l of complete media (containing serum as chemoattractant). Twenty-four hours post re-seeding, media was removed from the inserts and a cotton swab was used to wipe away the cells from the inside of the insert membrane. One ml crystal violet staining solution was then added to the inserts. Following 20 minutes incubation, the inserts were washed with Nanopure water. A cotton swab was used to carefully dry out the inserts after which they were transferred to a fresh 24-well plate and the cells were counted under a bright field light microscope.

### **Apoptosis Assay**

The apoptosis assay was performed using the annexin V-FITC Apoptosis Detection Kit (#PF032) from Millipore, Billerica, MA. Following appropriate treatments and transfection, both floating and adherent (released by trypsinization) cells were collected from each well of a 6-well plate. The cells were centrifuged at a speed of 1,000 rpm for 5 minutes. After removing the supernatant, the pellet was re-suspended in 500  $\mu$ l of PBS. Ten  $\mu$ l media-binding buffer was added to the tubes along with 1.25  $\mu$ l annexin-V/FITC. The samples were incubated for 15 minutes at room temperature in the dark. The samples were then centrifuged at 1,000 g for 5 minutes. The supernatant was discarded and 500  $\mu$ l of binding buffer was added along with 10  $\mu$ l PI (propidium iodide). The samples were then incubated for 30 minutes in the dark at which

time they were transferred to flow cytometry tubes for analysis (Karoly Szekeres, College of Medicine, Flow cytometry core, University of South Florida, Tampa, FL).

### **Cell Cycle Analysis**

HEY cells were seeded at 250,000 cells/well in a 6-well plate. Following 24 hour adherence, they were transfected with control or miR-494 mimic. Twenty-four hours post-transfection, cells were re-seeded at 25,000 cells/well in a 6-well plate. Ninety-six hours post-mimic transfection, floating cells were collected and the adherent cells were trypsinized and collected in the same tube that had the floating cells. The cells were centrifuged at 1,000 rpm for 5 minutes. The supernatant was removed and pellet re-suspended in 1 ml PBS. In a separate set of tubes, 9 mls of 70% ethanol (prepared in PBS) was added. The cells resuspended in PBS were added to the 9 mls of 70% ethanol dropwise with gentle vortexing. The tubes were then placed at -20°C overnight. The next day, the samples were centrifuged at 1,000 rpm at 4°C for 10 minutes. The supernatant was discarded and the pellet was re-suspended in 3 mls of ice cold PBS. The centrifugation was repeated and the pellet was re-suspended in 500 µl of PI staining solution, containing 500 µg/ml PI, 0.5% Triton X-100, and DNAase-free RNAase A (prepared in PBS). The samples were placed for 30 minutes at room temperature and then analyzed (Karoly Szekeres, College of Medicine, Flow cytometry core, University of South Florida, Tampa, FL).

### **Colony Formation Assay**

769-P cells were seeded at 250,000 cells/well in a 6-well plate. Following 24 hour adherence, they were transfected with control or miR-494 mimic. Twenty-four hours post-transfection, cells were re-seeded at 5,000 cells/well in a 6-well plate. Following 2 weeks, cells were stained with crystal violet.

## **Cholesterol Measurements**

Cholesterol was measured using the Amplex Red Cholesterol Assay Kit (#A12216, Life Technologies, Grand Island, NY) and the assay was performed according to the manufacturer's instructions. Briefly, 769-P cells were seeded, transfected, and protein harvested as described above. Protein samples were all normalized to the sample with the lowest concentration. The samples were added to the wells of a black opaque 96-well plate in a 2:3 ratio with 1X reaction buffer, provided with the kit (total 50  $\mu$ l). Cholesterol standards used for the assay were 0, 0.5, 1.0, 2.5, 5.0, 7.5, and 10  $\mu$ g/ml. Fifty  $\mu$ l of each of these standards was added to the 96-well plate. Lysis buffer and 1X reaction buffer in the ratio 2:3 was used as a negative control. Fifty  $\mu$ l of 10  $\mu$ M H<sub>2</sub>O<sub>2</sub> (hydrogen peroxide) was used as a positive control. Then, 50  $\mu$ l of the Amplex Red working solution was added to each well and the plate was incubated in the dark at 37<sup>0</sup>C for 30 minutes, following which fluorescent readings were measured at 528/20 (excitation), 590/35 (emission) on a Biotek plate reader.

## **LipidTOX Neutral Lipid Staining**

769-P cells were seeded into 6-well plates followed by siRNA and/or miRNA mimic transfections which were performed as described above. Cells were re-seeded at 150,000 cells/well (if transfected with mimic only) or 250,000 cells/well (if transfected with both siRNA and mimic) on glass coverslips. Seventy-two (if transfected with siRNA and mimic) or 96 hours (if transfected with mimic only) post-mimic transfection, cells were rinsed with PBS and fixed using 4% paraformaldehyde for 30 minutes at room temperature. Two PBS washes (5 minutes each) were performed, following which a 1:200 dilution of the LipidTOX green neutral lipid stain (#H34475, Life Technologies, Grand Island, NY) in PBS was added to the wells. Coverslips were mounted onto glass slides with DAPI and images were captured using the Perkin Elmer



Confocal Spinning Disc Microscope (CMMB Core Facility, University of South Florida, Tampa, FL).

### **MitoSOX Assay**

Control or miR-494 mimic expressing 769-P cells were re-seeded at 150,000 cells/well on glass coverslips following transfection. Ninety-six hours post-transfection, complete media from the well was replaced with 1 ml of 5  $\mu$ M MitoSOX red reagent (#M36008, Life Technologies, Grand Island, NY) prepared in Hank's Balanced Salt Solution (HBSS) containing calcium and magnesium. The cells were incubated in the above solution for 10 minutes at 37°C, following which 3 washes (2 minutes each) were performed in HBSS. After the washes, cells were rinsed in PBS, followed by fixation, and blocking. Cells were further processed and imaged as described above.

### **3'UTR Luciferase Assay**

Twenty-four hours post-seeding of T80 cells at 250,000 cells/well, they were transfected with control or miR-494 mimic and 1  $\mu$ g of *pEZX-MT01* 3'UTR luciferase plasmid (control, CmiT000001-MT01; Bcl-2a, HmiT016211a-MT01; Bcl-2b, HmiT016211b-MT01; LC3B, HmiT019948-MT01, (GeneCopoeia, Rockville, MD)) in serum-free media using Fugene HD as transfection reagent, as described above. Twenty-four hours post-transfection, cells were recovered in complete media and following a 3 hour recovery, the assay was performed according to the manufacturer's instructions provided with the Luc-Pair miR Luciferase Assay Kit (LPFR-M010, Genecopoeia, Rockville, MD). Briefly, cells were rinsed in PBS and 100  $\mu$ l of solution I was added. The wells were scraped lightly and 50  $\mu$ l was added to 1 well of an opaque 96-well plate, already containing 50  $\mu$ l of solution I. Following a 10 minute incubation at room temperature in the dark, firefly luminescence readings were taken using the Biotek plate

reader. Then, 100  $\mu$ l of solution II was added and following a 10 minute incubation, renilla luminescence readings were measured. A ratio of luminescence was calculated from the firefly to the renilla luciferase in order to determine transfection efficiency since the 3'UTR target is downstream of the firefly luciferase and the renilla luciferase is for assessing efficacy of transfection.

### **Luciferase Promoter Assay**

OVCAR8 cells stably expressing EVI1 constructs were seeded at 250,000 cells/well in G418 containing media. Twenty-four hours post seeding, cells were transfected with *pGL3* plasmid harboring claudin-1 promoter (the claudin-1 promoter was a kind gift from Dr. Yoshiaki Ito, Institute of Molecular and Cell Biology, Proteos, Singapore) downstream of the luciferase gene, following standard plasmid transfection protocol as described above. Forty-eight hours post transfection, protein lysates were collected and luciferase assay was performed according to instructions provided with the kit (Luciferase assay, #E151A, Promega, Madison, WI). Luminescence readings were recorded using a Biotek plate reader.

### **RT<sup>2</sup>-PCR Pathway Focused PCR Array (Lipoprotein Signaling and Cholesterol Metabolism, Autophagy, and Apoptosis)**

Total RNA was isolated from 769-P cells expressing control or miR-494 mimic, as described above. Overall, cDNA was prepared, following which the PCR array was performed as per manufacturer's instructions (Lipoprotein signaling and cholesterol metabolism, PAHS-080Z; Autophagy, PAHS-084Z; or Apoptosis, PAHS-012Z). Each array consisted of probes/primers for 84 different genes, 6 housekeeping genes, 3 positive PCR controls, 3 reverse-transcription controls, and 1 genomic DNA control. For the cDNA synthesis, two separate mixtures were prepared. The genomic DNA elimination mixture was prepared by adding 0.5  $\mu$ g of RNA, 2  $\mu$ l of Buffer GE, and the volume was made up to 10  $\mu$ l by adding

RNase-free water. Ten  $\mu\text{l}$  of the reverse-transcription mixture was then prepared by mixing 4  $\mu\text{l}$  of 5X buffer BC3, 1  $\mu\text{l}$  Control P2, 2 $\mu\text{l}$  RE3 reverse transcriptase mix, and 3  $\mu\text{l}$  RNase-free water. The genomic DNA elimination mixture was incubated at 42 $^{\circ}\text{C}$  for 5 minutes and placed immediately on ice for 1 minute, after which it was added to the reverse-transcription mixture and incubated at 42 $^{\circ}\text{C}$  for 15 minutes. Ninety-one  $\mu\text{l}$  of RNase-free water was then added to this combined mixture. For the array, the PCR component mixture was prepared by adding 1350  $\mu\text{l}$  2X RT<sup>2</sup> SYBR green master mix, 102  $\mu\text{l}$  cDNA synthesis reaction (as prepared above) and 1248  $\mu\text{l}$  RNase-free water. Twenty-five  $\mu\text{l}$  of this mixture was added to each well of the 96-well array plate. The cycling conditions used were as follows: 10 minutes at 95 $^{\circ}\text{C}$  followed by 40 cycles of 15 seconds at 95 $^{\circ}\text{C}$  and 1 minute 60 $^{\circ}\text{C}$ . Additionally, melt curves were acquired to generate first derivative dissociation curves for each well necessary for verifying PCR specificity. The results from the array were analyzed using the online Qiagen analysis web tool (<https://www.qiagen.com/us/products/genes%20and%20pathways/data-analysis-center-overview-page/>).

### **Transmission Electron Microscopy (TEM)**

769-P cells transfected with control or miR-494 mimic in 100 mm culture dishes were provided to Edward Haller (Department of Integrative Biology, University of South Florida, Tampa, FL) at ninety-six hours post mimic transfection. The control and experimental samples were fixed overnight in 2.5% glutaraldehyde (with 0.1 M phosphate buffer). The next day, another fixation was performed for 1 hour in 1% buffered osmium tetroxide that was dehydrated in acetone. This was followed by embedding the samples in LX 112 epoxy resin. Thereafter, thin section from the blocks were subsequently stained with 8% aqueous uranyl acetate and Reynold's lead citrate. Images were captured using a FEI Morgagni 268D (FEI Company, Inc, Hillsboro, OR) transmission electron microscope.

## Bioinformatic Analyses

The following programs were used to identify miRNA targets in the 3'-UTR of SnoN: PicTar, TargetScan, MicroCosm, PITA, miRANDA, and miRDB. In order to identify miR-494 binding sites in the 3'UTR of HAD database genes, Human TargetScan program was used. The following bioinformatics programs (along with the weblinks) were utilized in the current study:

cBioPortal for Cancer Genomics: <http://www.cbioportal.org/public-portal/>

PITA: [http://genie.weizmann.ac.il/pubs/mir07/mir07\\_prediction.html](http://genie.weizmann.ac.il/pubs/mir07/mir07_prediction.html)

MicroCosm: <http://www.ebi.ac.uk/enright-srv/microcosm/cgi-bin/targets/v5/search.pl>

TargetScanHuman: <http://www.targetscan.org/>

miRanda: <http://www.microrna.org/microrna/home.do>

miRDB: <http://mirdb.org/miRDB/>

PicTar: <http://pictar.mdc-berlin.de/>

Human Autophagy Database (HAD): <http://autophagy.lu/> [\[185\]](#)

## Statistical Analyses

Statistics were generated using the Student two tail t-test using Prism Graphpad. Representation of p values is as follows:  $p > 0.05$  (ns),  $p < 0.05$  (\*),  $p < 0.01$  (\*\*),  $p < 0.001$  (\*\*\*),  $p < 0.0001$  (\*\*\*\*). The number of replicates performed for every experiment is indicated in the figure legend of the respective experiment.

## Chapter 3

### **EVI1 Splice Variants Modulate Epithelial Mesenchymal Transition in Ovarian and Breast Cancer Cells**

#### **Introduction**

MDS1 and EVI1 complex locus (MECOM), located at the 3q chromosomal region (3q26.2) is amplified at the DNA level in serous EOC [2]. The DNA copy number increase at this locus in this subtype of ovarian cancer is associated with increased MDS1, EVI1, and MDS1/EVI1 splice transcripts and protein [2]. Increased EVI1 transcripts are linked to worsened patient outcome [2]. In contrast, increased MDS1/EVI1 transcripts are associated with good patient outcome [2], suggesting that these transcript variants may have opposing functions. A study conducted by our laboratory identified novel splice forms of EVI1 (using primers targeting the start and stop codons of MDS and EVI1) from normal epithelial ovarian and breast cells, ovarian cancer cell lines, and stage III/IV serous EOC specimens [14]. The major novel splice forms that were identified included EVI1<sup>Del190-515</sup> and EVI1<sup>Del427-515</sup> along with some rarer variants [14]. The EVI1<sup>Del190-515</sup> splice variant (identical to the EVI1s or Del324 form earlier described in Chapter 1) likely arises as a result of splicing between the donor splice site at the end of exon 6 and a cryptic acceptor splice site within exon 7. The EVI1<sup>Del427-515</sup> splice form is generated by a splicing event from an internal donor and acceptor site within exon 7 [14]. The EVI1<sup>Del190-515</sup> form exhibited increased localization to PML nuclear bodies and a marked loss of transcriptional repressor activity with the TGFβ-mediated plasminogen activator inhibitor-1 (PAI-1) and activator protein-1 (AP-1) promoters relative to WT EVI1 and EVI1<sup>Del427-515</sup> [14]. Further

investigation is necessary to elucidate the function of EVI1 and its splice variants in ovarian cancer biology.

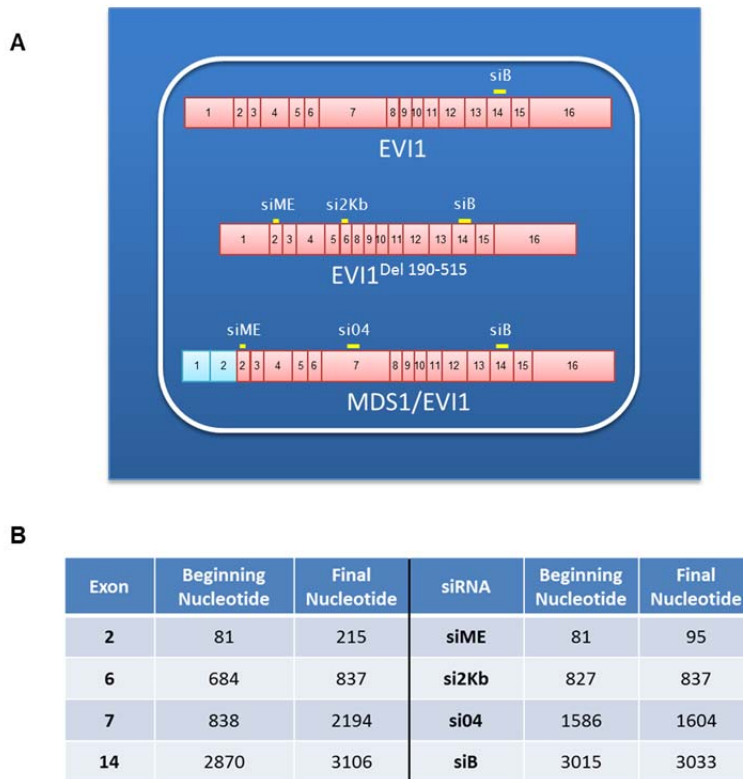
Previous reports described the contribution of EVI1 in mouse development and embryogenesis [186]. In addition, the *C.elegans* EVI1 homolog, egl-43, is reported to be involved in migratory and invasion events important in nematode development [187] [188]. Specifically, egl-43 induces breakdown of the basement membrane thereby promoting cell invasion. This event is mediated by the AP-1 (activator protein-1) pathway [189] which is also associated with the metastatic phenotype of solid tumors; AP-1 is a heterodimer comprised of c-FOS and c-JUN [187]. EVI1 binds directly to the promoters of both AP-1 and c-FOS leading to cellular regulation of proliferation, cell adhesion, and colony formation [190]. It is presently unknown whether EVI1 splice forms regulate expression of genes involved in altering EMT, an important hallmark of cancer. Herein, we assessed whether EVI1 splice variants could regulate expression of molecules involved in EMT. We addressed this question using both ovarian and breast cancer cells since the molecular characteristics (amplification of 3q26.2 and high level EVI1 expression) of both of these cancer types are very similar [53]. In this chapter, we demonstrate that knockdown of certain EVI1 splice variants increases the expression of epithelial cell markers while inhibiting the cellular migratory potential of these two cancer cell types.

## Results

### siRNA targeting the splice junction between exon 2 of MDS1 to exon 2 of EVI1 elevates claudin-1 protein

In order to determine whether EVI1 splice variants modulate EMT, we decreased the protein expression of EVI1 splice forms using a siRNA knockdown strategy followed by an assessment of the protein expression of specific epithelial and mesenchymal markers in the

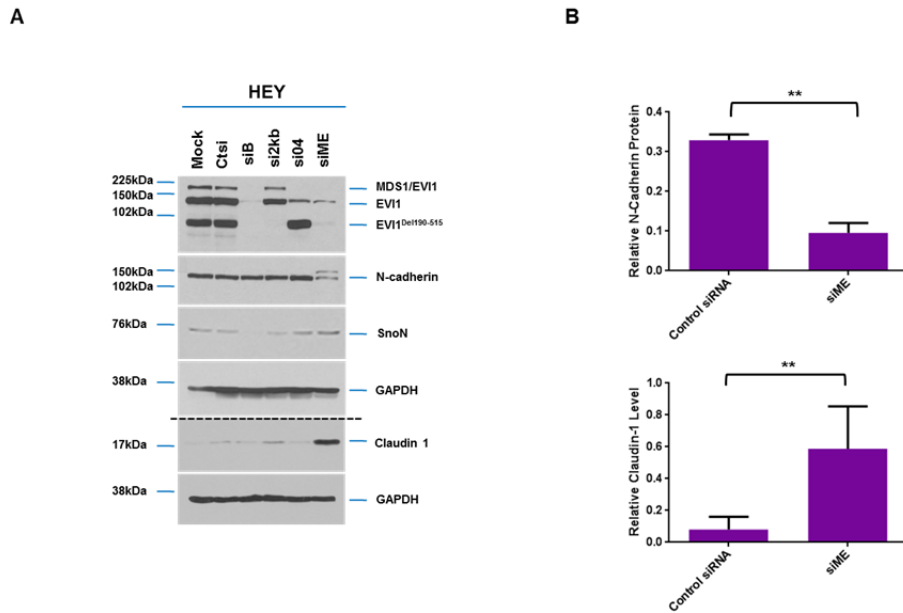
ovarian HEY and breast MDA-MB-231 cancer cell lines. Sequences for designing siRNA targeting specific splice variants were developed and validated by Jazaeri and colleagues [3]. As shown in Figure 7A and 7B, siRNA which targets exon 14 of WT EVI1 (siB) reduced WT EVI1, MDS1/EVI1, and the EVI1<sup>Del190-515</sup> protein. siRNA which targets exon 6-7 junction (si2Kb) reduced EVI1<sup>Del190-515</sup> protein. siRNA which targets exon 7 (si04) reduced MDS1/EVI1 protein. siRNA targeting the splice junction between exon 2 of MDS1 to exon 2 of EVI1 (siME) reduced both MDS1/EVI1 and the EVI1<sup>Del190-515</sup> protein. Following knockdown in the two cancer cell lines using the above-described siRNA, we collected protein lysates and performed western analyses in these cell lines.



**Figure 7: Specific regions on the EVI1 splice variants targeted by the tested siRNA constructs**

(A) Schematic representation of EVI1 splice variants and the exonic regions targeted by the different siRNA constructs [3]. (B) The exact nucleotide position targeted by EVI1 siRNA knockdown constructs are indicated in a tabular format [3]. (\*Figure created by Punashi Dutta)

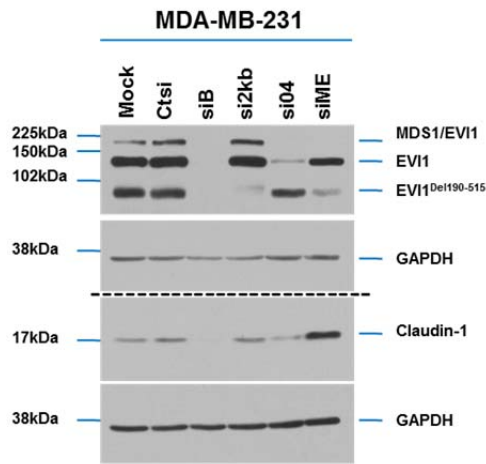
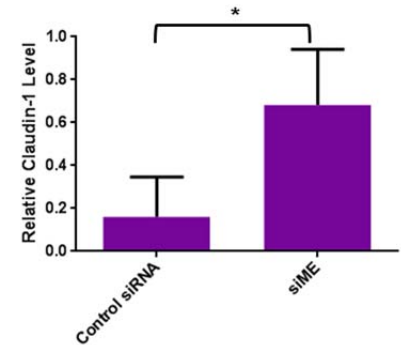
As shown in Figure 8A and 9A, we first ascertained successful knockdown of the different splice variants. We then measured protein expression of claudin-1, an epithelial marker whose gene is located at 3q28 (close to the 3q26.2 region where EVI1 is amplified in epithelial cancers). We observed a massive increase in the protein level of claudin-1 with siME in both HEY and MDA-MB-231 cells (Figure 8A and 9A). Additionally, we also assessed N-Cadherin, a mesenchymal cell marker, was decreased with siME in HEY cells. Densitometric analyses demonstrated that these changes were statistically significant (Figure 8B and 9B). In HEY cells, we also noted a reduction in SnoN protein with siB; SnoN (as described in Chapter 1) is also located at 3q26.2 (Figure 8A).



**Figure 8: Knockdown of EVI1 splice variants via siRNAs in HEY cells modulate protein levels of EMT markers**

(A) HEY cells were transfected with mock, control, siB, si2Kb, si04, and siME. Protein lysates were collected 48 hours post the second round of transfection. Samples were run on 8 or 12% SDS-PAGE gel and analyzed using the indicated antibodies. Western results shown above the dotted line are from samples run on 8% gel. Western results shown above the dotted line are from the same samples run on 12% gel. The data shown is representative of three different experiments. (B) Densitometric analyses performed on the western blotting results (presented in A) for N-Cadherin and claudin-1 protein levels in control or siME transfected HEY cells are presented in a graphical format along with p-values.



**A****B**

### Figure 9: Knockdown of EVI1 splice variants via siRNAs in MDA-MB-231 cells modulate protein levels of EMT markers

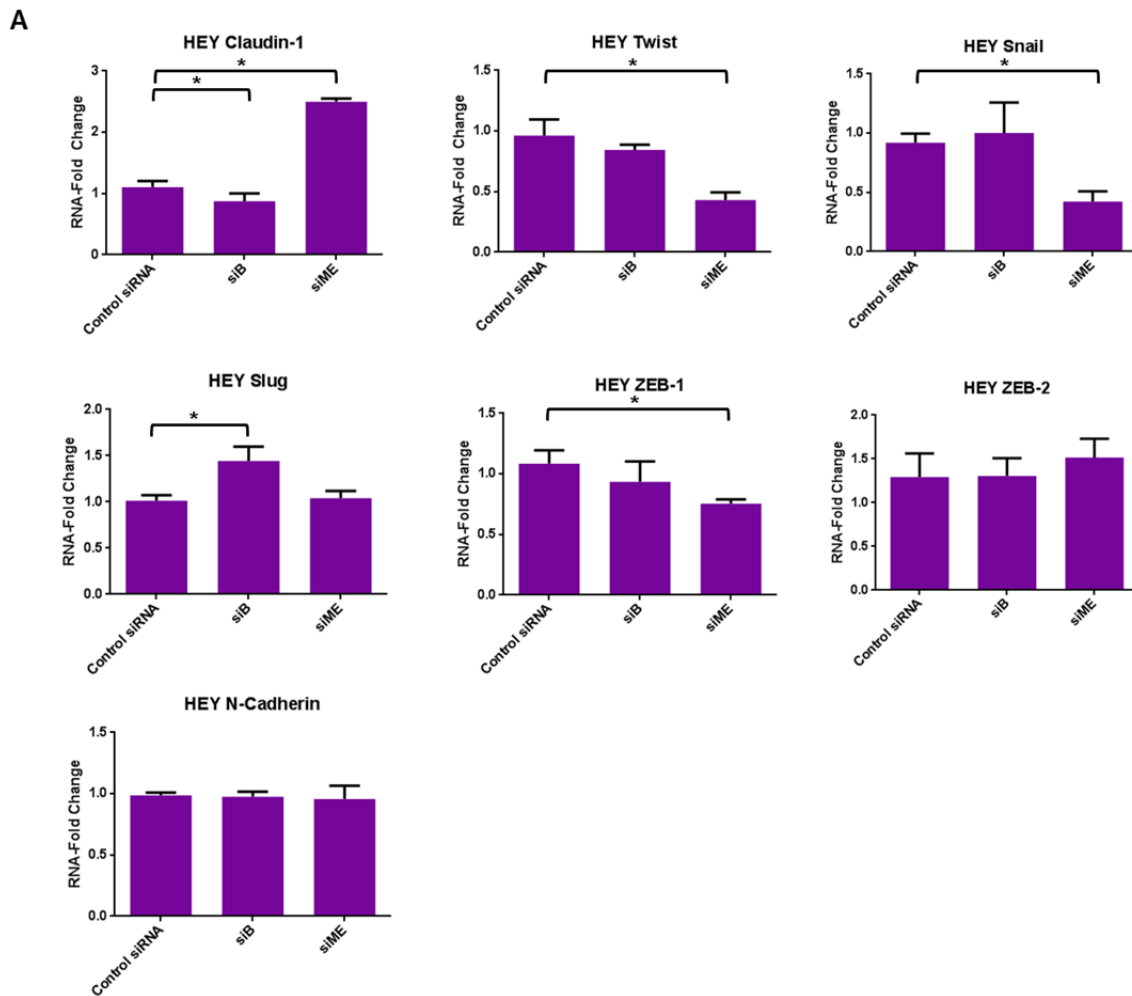
(A) MDA-MB-231 cells were transfected with mock, control, siB, si2Kb, si04, and siME. Protein lysates were collected 48 hours post the second round of transfection. Samples were run on 8 or 12% SDS-PAGE gel and analyzed using the indicated antibodies. Western results shown above the dotted line are from samples run on 8% gel. Western results shown above the dotted line are from the same samples run on 12% gel. The data shown is representative of three different experiments. (B) Densitometric analyses performed on the western blotting results (presented in A) for claudin-1 protein levels in control or siME transfected MDA-MB-231 cells are presented in a graphical format along with p-values.

### siRNA targeting the splice junction between exon 2 of MDS1 to exon 2 of EVI1 alters the RNA expression of key EMT markers

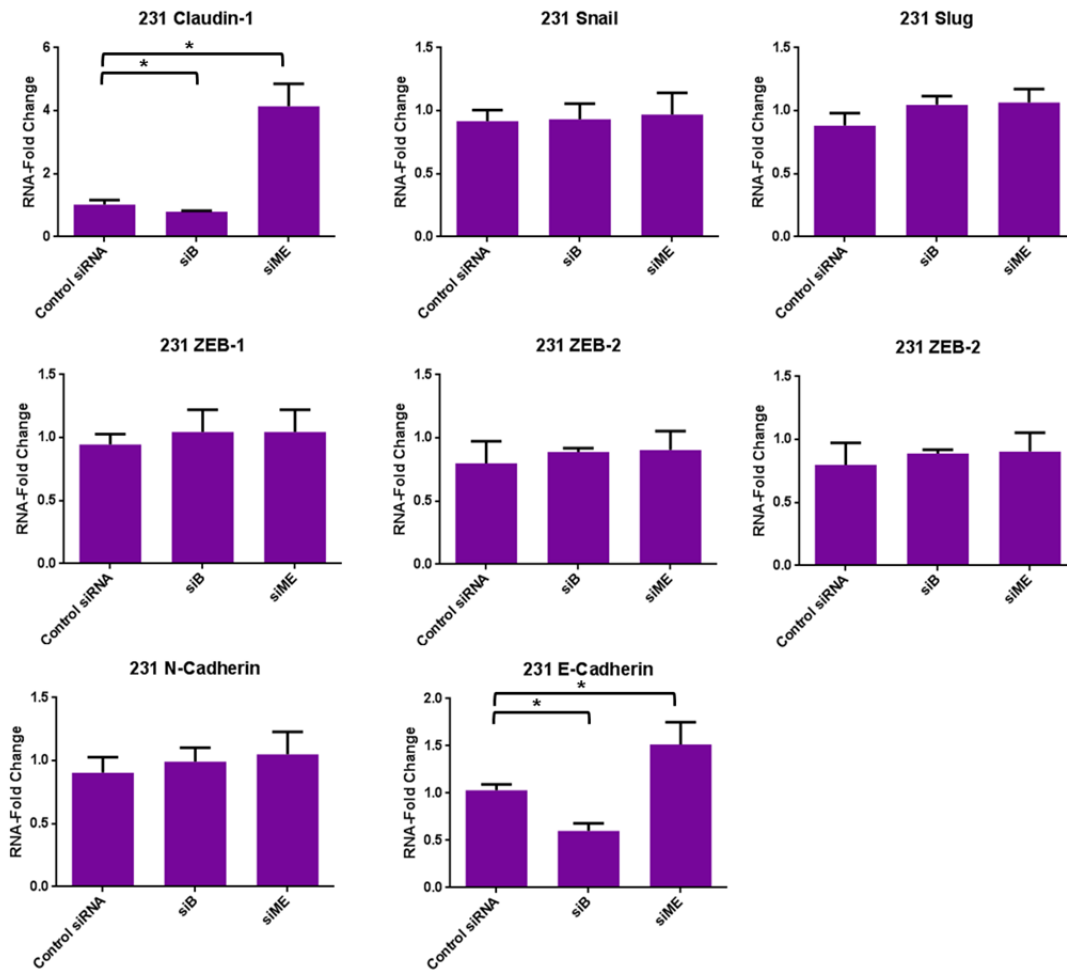
Since we noticed changes in the protein levels of claudin-1 and N-Cadherin (markers of epithelial and mesenchymal phenotype, respectively), we next examined transcript level changes in these and other EMT markers via real-time PCR analyses. Consistent with the protein changes, the mRNA levels of claudin-1 were increased in both HEY and MDA-MB-231 cells with siME. In contrast, siB reduced claudin-1 mRNA levels (Figure 10A and 10B).

We next tested the effect of the above described siRNA (siB, siME) on other EMT markers including snail, slug, and twist (which all transcriptionally repress the expression of E-

Cadherin (an epithelial cell marker [191]) [192] [193, 194] [195]. We also included ZEB1/2 in our investigation since these proteins transcriptionally repress E-Cadherin expression [156, 196]. Upon cellular treatment with siME, we observed reduced mRNA transcripts for twist, snail, and ZEB-1 in HEY cells and an increase in E-Cadherin in the MDA-MB-231 cells. Knockdown with siB increased slug and decreased claudin-1 levels in HEY cells also in addition to reducing E-Cadherin levels in MDA-MB-231 cells (Figure 10A and 10B). These results demonstrate that



**Figure 10: Knockdown of EVI1 splice variants via siRNAs in HEY and MDA-MB-231 cells modulate mRNA expression of EMT markers (\*Continued on next page)**

**B**

**Figure 10: Knockdown of EVI1 splice variants via siRNAs in HEY and MDA-MB-231 cells modulate mRNA expression of EMT markers**

(A) RNA was isolated from HEY cells transfected with control, siB, or siME and real-time PCR analysis was performed for claudin-1, twist, snail, slug, ZEB-1, ZEB-2, and N-Cadherin. The correlative method was used for the real-time PCR analysis and  $\beta$ -actin was used as the endogenous control. The data shown is compiled from three different experiments. (B) RNA was isolated from MDA-MB-231 cells transfected with control, siB, or siME and real-time PCR analysis was performed for claudin-1, twist, snail, slug, ZEB-1, ZEB-2, and N-Cadherin. The correlative method was used for the real-time PCR analysis and  $\beta$ -actin was used as the endogenous control. The data shown is compiled from three different experiments.

knockdown with siRNA targeted towards the splice junction between exon 2 of MDS1 to exon 2 of EVI1 (siME) led to increase in epithelial markers as opposed to siRNA targeting exon 14 of EVI1 (siB), which caused an increase in mesenchymal markers.

siRNA targeting the splice junction between exon 2 of MDS1 to exon 2 of EVI1 reduces the migratory potential of HEY and MDA-MB-231 cells

Since we observed an increase in claudin-1 and other EMT markers with siME and changes in EMT markers can alter migration [6], we performed a directional migration assay using the Boyden chamber using siME in HEY and MDA-MB-231 cancer cells. Since we observed an increase in epithelial markers upon siRNA knockdown targeting the splice junction between exon 2 of MDS1 to exon 2 of EVI1 (siME), we utilized this siRNA for this assay. HEY and MDA-MB-231 cells were transfected with non-targeting control or siME and the assay was conducted as described in Chapter 2.

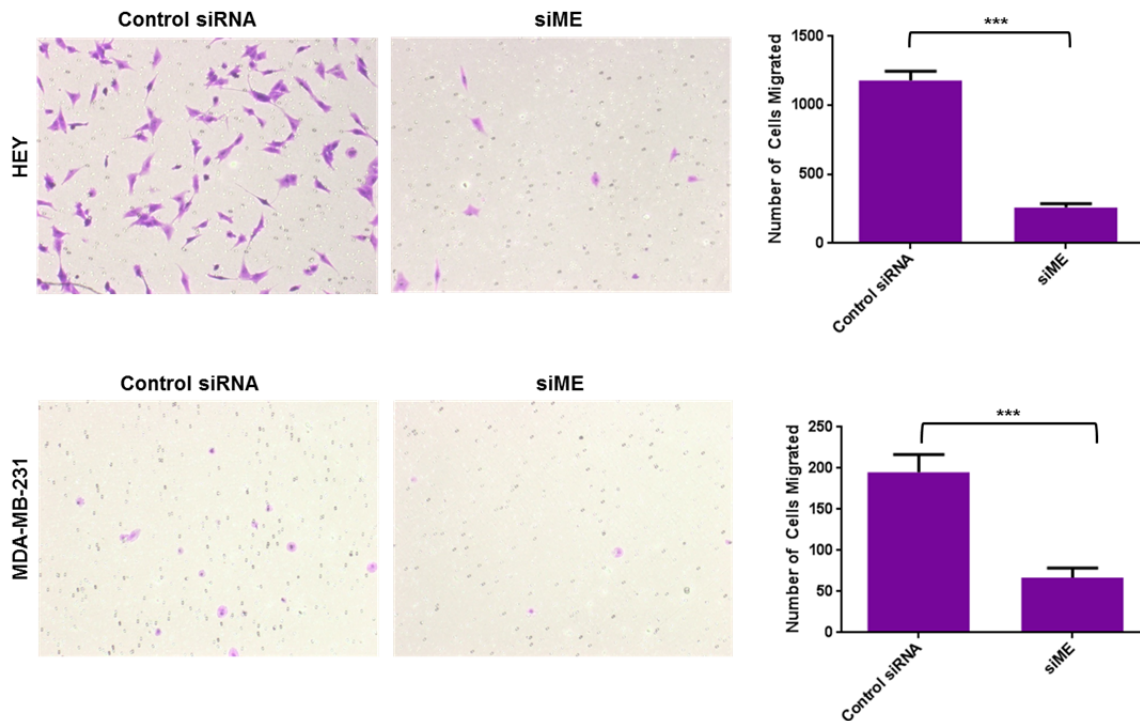


**Figure 11: Effect of knockdown of EVI1 splice variants on the migratory potential of HEY and MDA-MB-231 cells**

Control or siME transfected HEY or MDA-MB-231 cells were re-seeded at 25,000 cells/well into 24 well plate inserts. Directional migration assay was performed and cells were stained using crystal violet dye, following which images were captured using a bright field light microscope. Representative images are presented along with quantitative analyses in a graphical format with p-values. The data shown are compiled from two different experiments.

As indicated in Figure 11, we observed a significant reduction in the cellular migratory potential in both HEY and MDA-MB-231 cells transfected with siME, compared to control transfected cells. These findings indicate that EVI1 splice variants alter cellular migration of HEY and MDA-MB-231 cancer cells.

### Specific EVI1 splice variants modulate claudin-1 promoter activity

EVI1 is a transcriptional regulator and has the ability to bind DNA sequences via its Zn finger domains [197], thus regulating gene expression of a variety of genes (as mentioned in Chapter 1). As shown in Figures 8-10, siME increased mRNA and protein levels of claudin-1. To determine whether EVI1 splice variants can alter claudin-1 promoter activity, we used OVCAR8 cells stably overexpressing specific EVI1 splice variants (WT EVI1, EVI1<sup>Del190-515</sup>, and EVI1<sup>Del427-515</sup>). OVCAR8 cells have a deletion at the EVI1 chromosomal locus and therefore served as an appropriate model for overexpression studies [14].

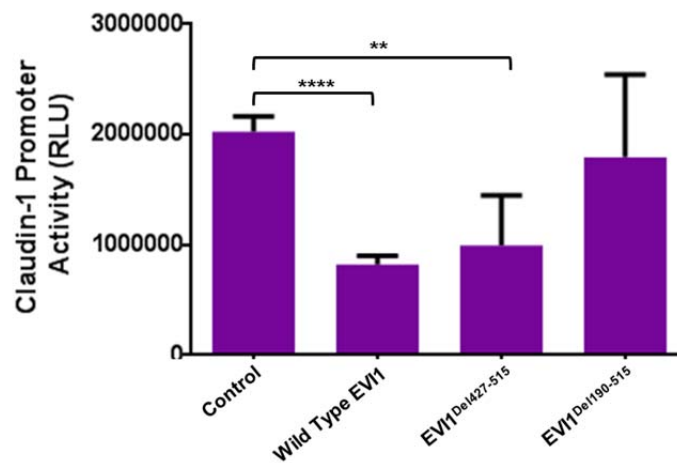


**Figure 12: Effect of knockdown of EVI1 splice variants on the promoter activity of claudin-1**

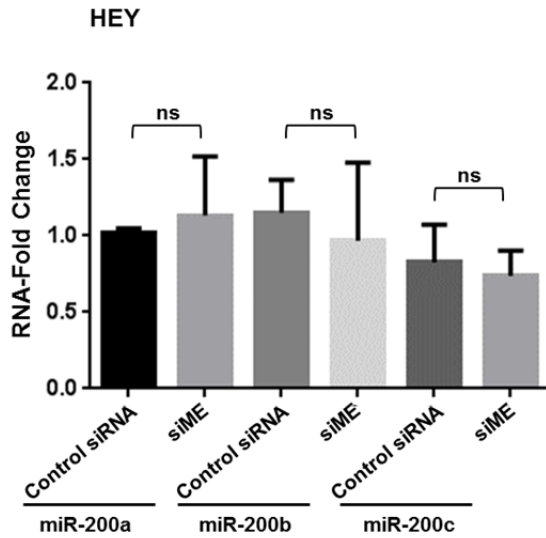
OVCAR8 retroviral stable cells overexpressing control, WT EVI1, EVI1<sup>Del190-515</sup>, or EVI1<sup>Del427-515</sup> forms were transfected with *pGL3* claudin-1 promoter plasmid. Luminescence was analyzed and data presented as a graph along with p-values. The data shown are compiled from two different experiments.

Luciferase-based reporter assay using *pGL3* claudin-1 promoter construct was performed by transfecting this construct in the OVCAR8 overexpression cell lines. The results indicated a significant reduction in the relative light units with overexpression of WT EVI1 and EVI1<sup>Del427-515</sup> form, but not with overexpression of the EVI1<sup>Del190-515</sup> form, as compared to control transfected cells (Figure 12). These findings suggest that WT EVI1 and/or EVI1<sup>Del427-515</sup> may bind to claudin-1 promoter to regulate its activity and thus modulate claudin-1 expression.

siRNA targeting the splice junction between exon 2 of MDS1 to exon 2 of EVI1 does not alter the expression levels of the miR-200 family of miRNAs

miRNAs affect multiple cellular processes, including gene regulatory networks involved in EMT [198]. With respect to EMT, the miR-200 family are well-described to be important regulators of this cellular process [199]. The miR-200 family of miRNAs is down-regulated during EMT [156]; overexpression of these miRNAs induce E-Cadherin expression, silence ZEB1/2 expression [17], enhance epithelial cell phenotype, and inhibit cellular motility [156]. Since EVI1 can regulate expression of specific miRNAs such as miR-143 [200], miR-124 [201], miR-96 [202], and miR-449A [203], we assessed whether the miR-200 family may be regulated via EVI1 splice variants. For this purpose, we transfected HEY and MDA-MB-231 cells with non-targeting control siRNA or siME followed by miRNA isolation and quantification of miRNA-200 family members (miR-200a, miR-200b, and miR-200c). As shown in Figure 13A and 13B, the knockdown of EVI1 splice variants did not alter the levels of these miR-200 family members. However, the present analysis was conducted only in 2 experimental replicates and variation was observed among the control transfected cells.

A



B

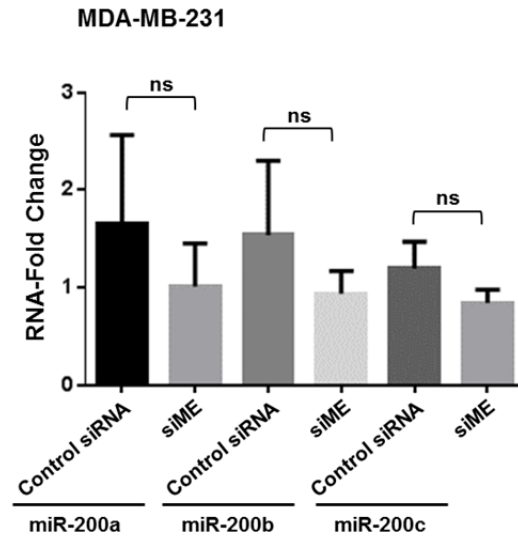


**Figure 13: Effect of knockdown of EVI1 splice variants on the expression of miR-200a, miR-200b, and miR-200c**

HEY or MDA-MB-231 cells were transfected with control or siME and miRNA was isolated. Relative levels of miR-200a, miR-200b, and miR-200c were quantified by real-time PCR using the correlative method and RNU6B as the endogenous control. The data shown are derived from two different experiments.

#### Reverse phase protein array (RPPA) analysis on cell lines overexpressing EVI1 splice variants

In order to further assess cellular changes mediated by specific EVI1 forms, we stably overexpressed WT EVI1, EVI1<sup>Del190-515</sup>, and EVI1<sup>Del427-515</sup> *EGFP* plasmids into appropriate ovarian cell lines. We selected the T29 normal immortalized ovarian and OVCAR8 ovarian cancer cells. Since T29 cells have low endogenous expression of EVI1, and the OVCAR8 cells have a deletion in the EVI1 locus, these cell lines served as a good overexpression model [14]. Two independent retroviral parental stable cell lines were generated for each of these cell lines. As shown in Figure 14, we validated the expression level of WT EVI1, EVI1<sup>Del190-515</sup>, and EVI1<sup>Del427-515</sup> forms via western analysis using the cell signaling antibody towards the N terminal region of the protein. Additionally, we detected multiple other bands of lower molecular weights

which are likely to be proteolytic degradation products of the overexpressed forms or other splice variants of EVI1.

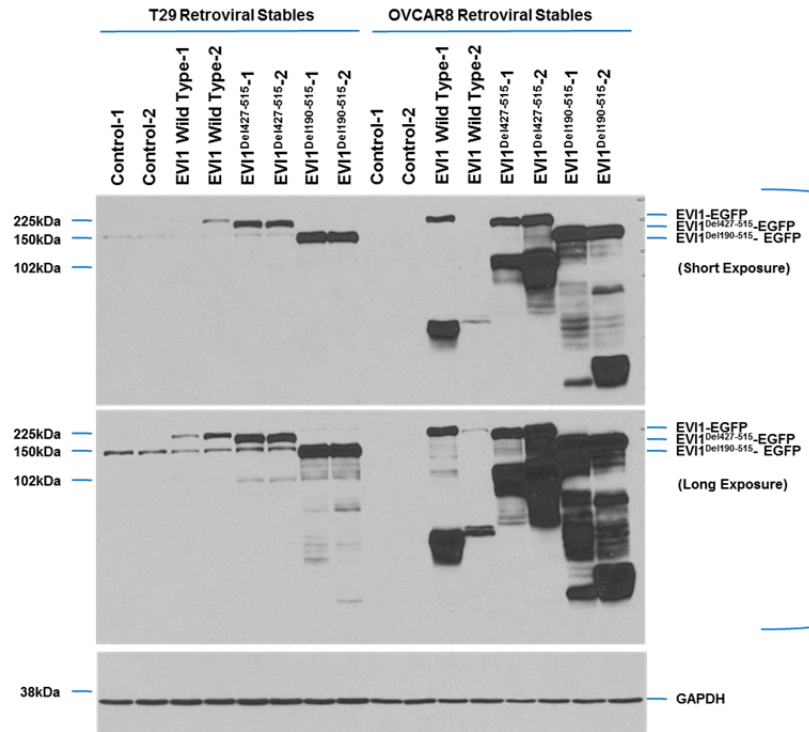


**Figure 14: Protein analyses of EVI1 splice forms in T29 and OVCAR8 cells**

T29 or OVCAR8 cells overexpressing control, WT EVI1, EVI1<sup>Del190-515</sup>, or EVI1<sup>Del427-515</sup> cells (retroviral pools 1 and 2) were run on an 8% SDS-PAGE gel and western analyses performed for the indicated antibodies (EVI1 and GAPDH).

We next assessed whether EVI1 splice variants (WT EVI1, EVI1<sup>Del190-515</sup>, and EVI1<sup>Del427-515</sup>) altered the activation status and expression level of key signaling molecules in important signaling pathways (such as cell cycle, MAPK pathway, TGF $\beta$  pathway) via RPPA. This method assesses changes in protein expression using 154 validated antibodies (as described in Chapter 2) in a high-throughput manner. Since EVI1 negatively regulates the TGF $\beta$  pathway, an important signaling pathway dysregulated in ovarian cancer [204], we assessed the cellular response to EVI1 splice variant expression in the absence or presence of TGF $\beta$  treatment. We



treated the overexpression cell lines with 50 pmol TGF $\beta$  for 5 minutes, 1 hour, 3 hours, 6 hours, and 24 hours. We noted a similarity in the expression of various mediators between the WT EVI1 and the EVI1<sup>Del427-515</sup> form and between the control and the EVI1<sup>Del190-515</sup> form, as shown in the heat map (Figure 15). A few targets assessed by RPPA appeared altered from the heat map presented in Figure 15 upon overexpression of WT EVI1 and EVI1<sup>Del427-515</sup> including Cyclin E1.

Cyclin E1 levels are altered upon TGF $\beta$  treatment in OVCAR8 ovarian cancer cells following overexpression of EVI1 splice variants

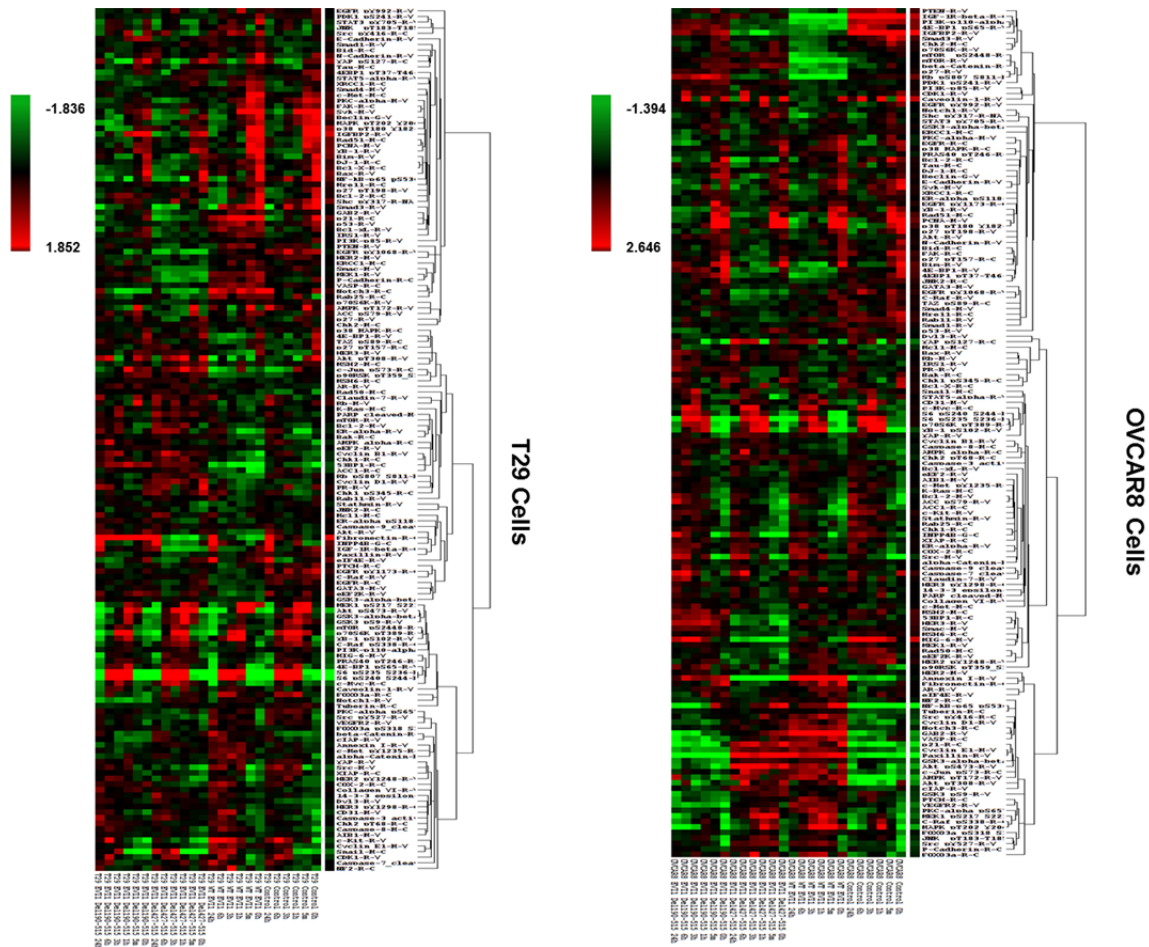


**Figure 15: Reverse phase protein array analysis (RPPA) in cells overexpressing EVI1 splice forms**

Heat maps displaying the results obtained from RPPA analysis in T29 and OVCAR8 cells expressing EVI1 splice variants upon TGF $\beta$  treatment are shown.

Since RPPA analyses identified changes in Cyclin E1 protein following expression with WT EVI1 and EVI1<sup>Del427-515</sup> form but not with the EVI1<sup>Del190-515</sup> form, we next validated the change in cyclin E1 via western blotting. We observed an increase in the low molecular weight (LMW)

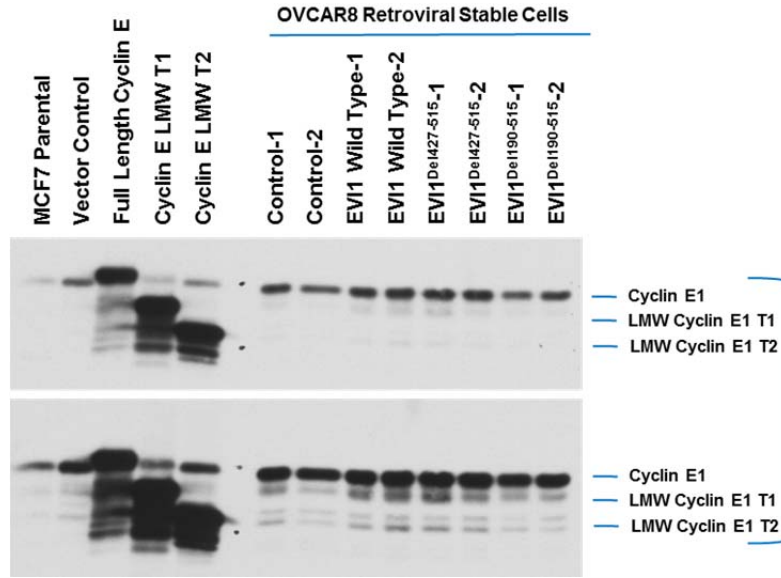


**Figure 16: Modulation of Cyclin E1 protein levels following EVI1 splice variants overexpression in OVCAR8 cells**

OVCAR8 cells overexpressing control, WT EVI1, EVI1<sup>Del190-515</sup>, or EVI1<sup>Del427-515</sup> cells (retroviral pools 1 and 2) and MCF7 cells overexpressing full length and LMW Cyclin E1 forms were ran on an SDS-PAGE gel and western analysis was performed using the indicated antibodies.

forms of Cyclin E1. Cyclin E1 regulates the G1 phase of the cell cycle. Cyclin E1 and Cdk2 together control the transition from the G1 to the S phase of the cell cycle [205]. Interestingly, LMW Cyclin E1 has been reported to stimulate the G1/S transition more efficiently as compared to the full length form [206]. In breast cancers, LMW Cyclin E1 is a potent predictor of breast cancer mortality, owing to their effect on genetic instability and cellular proliferation [207]. As a positive control, we used MCF7 cells overexpressing the full length and the LMW form of Cyclin

E1, run together with the OVCAR8 overexpressing cells on the same SDS-PAGE gel (Figure 16).

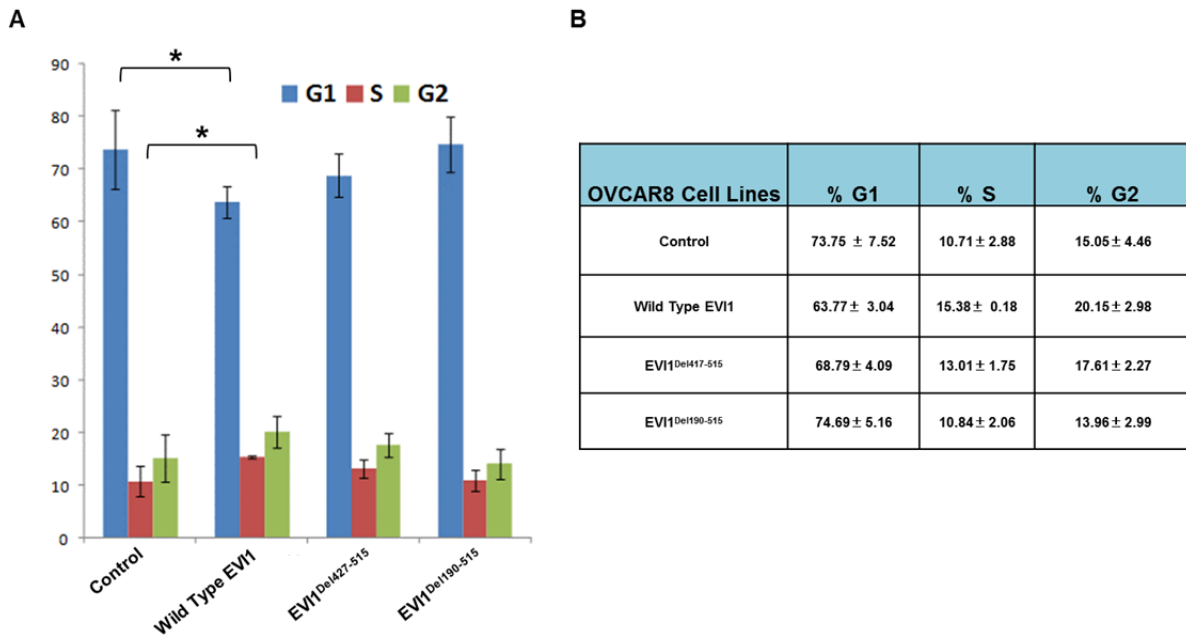


**Figure 17: Cell cycle analysis following EVI1 splice variants overexpression in OVCAR8 cells.**

(A) Graphical representation of cell cycle stages in OVCAR8 cells expressing EVI1 splice forms. The data shown is compiled from two different experiments. (B) Tabular representation of results presented in (A) are shown.

To next assess the functional implications of the altered Cyclin E1 expression in OVCAR8 cells, we performed cell cycle analysis. As shown in Figure 17A and 17B, the WT EVI1 and the EVI1<sup>Del427-515</sup> overexpressing OVCAR8 cells showed a subtle increase in the percentage of cells in the S phase and a decrease in percentage of cells in the G1 phase of the cell cycle. However, we did not identify any change in the percentage of cells in the different cell cycle phases with either the control or the EVI1<sup>Del190-515</sup> form.

## Discussion

Our findings reported in this chapter demonstrate that EVI1 splice variants modulate the mRNA and/or protein levels of specific EMT markers. Alterations in these EMT mediators using

siME were associated with reduced migratory potential of HEY and MDA-MB-231 cancer cells. Our studies suggest that EVI1 splice variants elevate claudin-1 and reduce migration which may contribute to the pathophysiology of ovarian and breast cancers. We did not observe any change in the expression levels of miR-200 family with the siME knockdown. However, it is possible that the miRNAs are unable to bind to the 3'UTR of the respective genes due to the presence of RNA binding proteins such as HuR [208]. It would therefore be necessary to investigate the mechanism by which EVI1 variants may modulate miRNA:mRNA target binding affinity. Since our findings implicate a role of EVI1 splice variants in modulating EMT markers, it would be worthwhile to investigate and analyze the expression levels of EVI1 splice variants in patient specimens and their association to the expression of EMT markers.

Of interest, we saw a significant increase in both protein and mRNA levels of claudin-1, an epithelial marker in both HEY and MDA-MB-231 cells upon knockdown of MDS1/EVI1 and EVI1<sup>Del190-515</sup> form. Claudin-1 is located very close to the 3q26 region (where EVI1 is located), at 3q28. Our group has previously demonstrated that SnoN/SkiL, located at 3q26.2, can regulate the expression of PLSCR1, a gene present in close proximity at 3q23 [157]. Therefore, genes located in close proximity to each are likely to regulate each other's expression levels. Since EVI1 functions as a transcriptional regulator, EVI1 and/or its splice variants may regulate the expression of these EMT mediators by directly binding to the DNA sequence of these genes. We observed notable differences in the claudin-1 promoter activity upon overexpression with specific EVI1 splice variants. Interestingly, the WT EVI1 and EVI1<sup>Del427-515</sup> form behaved similarly (both down-regulated the promoter activity of claudin-1) and in contrast to the EVI1<sup>Del190-515</sup> form (which was similar to control) a trend also observed in the RPPA analysis. It is established that altered ratios of splice variants can modulate cellular responses [209]. These altered ratios rather than the reduction in a particular splice variant may be contributing to the observed changes in EMT and migratory potential. Moreover, the EVI1<sup>Del190-515</sup> form showed altered nuclear localization and binding to interacting partners of WT EVI1 [14]. Therefore, we believe

that the EVI1<sup>Del190-515</sup> splice form may be exhibiting a dominant-negative effect on the cellular functions of WT EVI1.

It is presently unclear how EVI1 splicing events are regulated. Since a balance between expression levels of splice variants can elicit diverse cellular responses [209], it would be necessary to investigate the mechanism of EVI1 splicing. Several signaling pathways regulate splicing events by directly modulating SR (serine/arginine-rich) proteins which are major splicing factors [210]. Some of these signaling pathway mediators such as Ras and PI3K/AKT are dysregulated in ovarian cancers and thus may modulate the alternative splicing [211, 212]. Other factors that may regulate splicing are the presence of mutations; however, our research group did not identify any mutations upon sequencing EVI1 from serous EOC patient specimens [2]; however, there could be mutations deep within the introns, resulting in a cryptic acceptor/donor splice site.

Our results suggest that EVI1 splice variants may behave differently from the WT EVI1 and since the splice variants have altered exonic regions, their binding affinity to interacting partners is affected. Indeed, a study by Copeland and colleagues identified 78 EVI1 interacting partners via SILAC, and further validated 22 of these targets via co-immunoprecipitation studies, followed by yeast-two-hybrid experiments which validated five EVI1 binding partners [88]. In order to understand the functions of the splice variants in ovarian and breast cancers, it is necessary to determine differential binding of these to known EVI1 binding partners and further identify new binding partners and the implications in ovarian/breast cancer biology. Additionally, although EVI1 is a nuclear protein [78], whether EVI1 localizes to other subcellular regions is presently unknown. Since subcellular localization can affect protein function [213] it would be worthwhile to study this in detail. Our RPPA and western data indicated elevated protein levels of LMW Cyclin E1 in cells overexpressing WT EVI1 or EVI1<sup>Del427-515</sup> form, which was consistent with an increase in cells in the S phase of the cell cycle. However, Cdk2 and Cyclin E1 kinase activity remained unaltered with the overexpression of the splice variants, therefore, it is

possible that the altered Cyclin E1 expression via the overexpression of splice variants in OVCAR8 cells is independent of the dysregulation in the cell cycle.

### **Acknowledgments**

I would like to thank my mentor, Dr. Meera Nanjundan for the identification of EVI1 splice variants, cloning/generation of EVI1 splice variant constructs, and for all the studies described in the introduction section of this chapter. I would also like to extend my gratitude to Dr. Khandan Keyomarsi (Professor, Department of Experimental Radiation Oncology, Division of Radiation Oncology, The University of Texas MD Anderson Cancer Center, Houston, TX) for assistance with the Cyclin E1 western study and Dr. Gordon B Mills (Department Chair, Department of Systems Biology, Division of Cancer Medicine, The University of Texas MD Anderson Cancer Center, Houston, TX) for conducting the RPPA studies and providing the ovarian cells.

## Chapter 4

### miR-494 Modulates SnoN/SkiL Expression and Cell Death Response upon As<sub>2</sub>O<sub>3</sub> Treatment in Ovarian Cancer Cells

#### Introduction

Serous EOC accounts for 70% of the deaths due to ovarian cancer, which is the fifth most common cause of mortality due to cancer in women in the United States [29]. As mentioned in Chapter 1, the high mortality rate in this cancer is due to the absence of early detection biomarkers and methods. Serous EOC exhibits amplification of genes at the 3q26 chromosomal region, including MECOM [214] and SnoN/SkiL [215]. There is substantial evidence suggesting that aberrant genomic regions contribute to ovarian cancer biology [216, 217]. Therefore, an in-depth understanding of the regulation of genes that are highly amplified and aberrantly expressed in epithelial EOC may aid in development of tools for early diagnosis and better therapeutic treatment strategies. SnoN/SkiL, located at the 3q26.2 locus is elevated in a variety of cancers (such as colorectal cancer, esophageal squamous cell cancer, and melanoma) at the DNA level in addition to being overexpressed at the mRNA and protein levels [1, 91, 99, 101, 218, 219]. SnoN negatively regulates the TGF $\beta$  pathway (a pathway dysregulated in ovarian cancer [220]), by binding Smads and inhibiting the transcription of TGF $\beta$  regulated genes [92]. However, SnoN can also bind to transcriptional inhibitors such as HDACs and inhibit the activity of Smads [94]. Interestingly, SnoN exhibits both pro- and anti-tumorigenic properties at different stages of malignant progression in epithelial cancers [101].

Previous studies from our group demonstrated that SnoN expression is elevated following treatment with chemotherapeutic drugs such as As<sub>2</sub>O<sub>3</sub> in ovarian cancer cells [15]. As<sub>2</sub>O<sub>3</sub>, a chemotherapeutic agent that has been FDA approved for the treatment of acute promyelocytic leukemia (APL) [221] reduces cell proliferation in solid cancers including ovarian cancer [222-224]. This increase in SnoN levels was at the mRNA and protein levels; its levels were associated with increased LC3B-II (an autophagy marker) and the presence of double membrane autophagosomes assessed by TEM [15]. LC3 becomes conjugated with PE to form LC3-II and translocates from the cytosol to the autophagosome membrane, a hallmark event in the induction of autophagy [225]. Further, the induction of autophagic flux was demonstrated by EGFP-LC3 punctae formation and assessment of LC3-II protein levels upon the use of early and late stage autophagy inhibitors such as 3-methyladenine (3-MA) and bafilomycin A1 (BAF) [15]. Importantly, siRNA mediated knockdown of SnoN reduced LC3-II protein levels, decreased EGFP-LC3 punctae, and led to increased apoptosis by As<sub>2</sub>O<sub>3</sub> treatment [15]. In a recent study, we demonstrated that SnoN induction is mediated by the activation of PI3K/AKT pathway upon As<sub>2</sub>O<sub>3</sub> treatment [17]. As<sub>2</sub>O<sub>3</sub>-mediated increase in SnoN expression was antagonized by inhibitors of PI3K or by knockdown of PIK3CA [17]. However, the detailed mechanism underlying the induction of SnoN expression upon treatment with As<sub>2</sub>O<sub>3</sub> is unclear and requires further investigation.

Gene regulatory pathways mediated by miRNAs are critical in post-transcriptional regulation of gene expression [127]. miRNAs bind the target mRNA at the 3'UTR and inhibit gene expression via mRNA degradation or inhibition of translation [124]. However, it has recently been reported that miRNAs may bind to the 5'UTR [226] or coding region [227] within the mRNA target sequence. Interestingly, c-Ski (a homolog of SnoN/SkiL [228]) is a target of miR-155 in human melanoma cells; its down-regulation by miR-155 leads to reduced melanoma cell proliferation [19]. Additionally, miR-29a, miR-127, and miR-21 also target c-Ski in AML [20], glioblastoma [21], and rat vascular smooth muscle cells [22], respectively. Whether SnoN



expression is regulated by miRNAs is presently unknown. Our findings reported in this chapter demonstrate that miR-494 overexpression in HEY ovarian cancer cells reduces both mRNA and protein levels of SnoN. Of interest, we identified a perfect miR-494 binding site in the 3'-UTR region of *SnoN* via *in silico* analysis. Further, miR-494 sensitized HEY ovarian cancer cells to As<sub>2</sub>O<sub>3</sub> treatment, increasing cell death due to apoptosis. Additionally, miR-494 reversed the formation of EGFP-LC3B punctae mediated by SnoN upon treatment with As<sub>2</sub>O<sub>3</sub>. Collectively, these findings implicate miR-494 in modulating drug-induced cell death response via reducing SnoN mRNA and protein levels.

## Results

Bioinformatic analyses reveal miR-216b, miR-410, miR-494, and miR-495 putative binding sites in the 3'UTR of *SnoN*

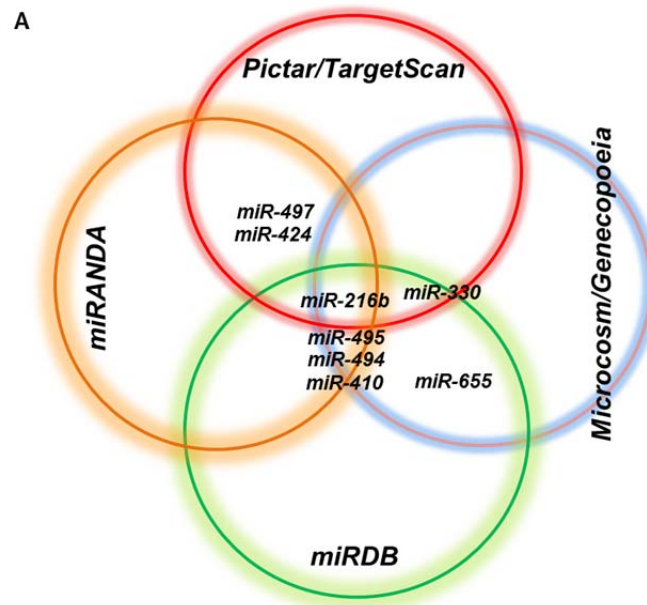
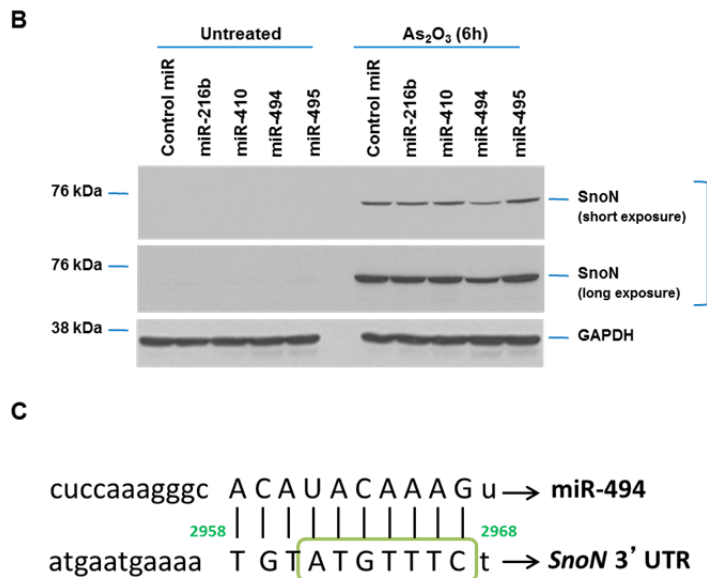


Figure 18: miR-494 modulates SnoN protein levels (\*Continued on next page)

Since SnoN is a homolog of c-Ski, which is regulated via miRNAs in several cancer types [19-22], we investigated whether SnoN levels are modulated via the action of miRNAs. Therefore, in order to identify putative miRNA binding sites in the 3'UTR of *SnoN*, we conducted bioinformatics analyses using six different bioinformatics programs including Pictar, GeneCopoeia, Microcosm, miRDB, TargetScanHuman, and miRANDA. Four miRNAs (miR-216b, miR-410, miR-494, and miR-495) were identified in four or more of these above stated bioinformatics programs to have potential binding regions in the 3'UTR of *SnoN*. A Venn diagram summarizing the results obtained from the *in silico* analysis is presented in Figure 18A.



**Figure 18: miR-494 modulates SnoN protein levels**

(A) A Venn diagram is presented which summarizes the top hits from miRNA analysis performed using six different bioinformatics programs (PicTar, Microcosm, miRANDA, TargetScanHuman, miRDB, and GeneCopoeia) showing miRNA putative binding sites in the 3'-UTR of *SnoN/SkiL*. (\*Figure created by Dr. Nanjundan). (B) HEY cells expressing negative control miR, miR-216b, miR-410, miR-494 or miR-495 mimic (200 pmol) for 96 hours were treated with 25  $\mu$ M As<sub>2</sub>O<sub>3</sub> for 6 hours. Protein lysates were harvested and subjected to western analyses using the indicated antibodies. The data shown is representative of two different experiments. (C) Schematic representation of miR-494 binding sites in the *SnoN* 3'UTR. Green boxes indicate the binding region on the SnoN transcript.

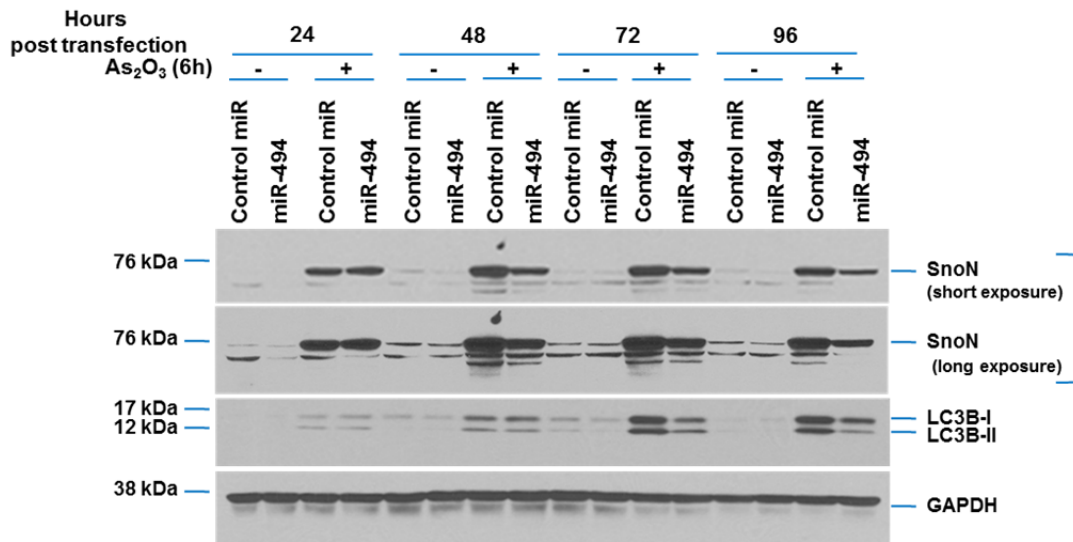
In order to validate the results obtained from the bioinformatics study, we performed western blotting analysis to examine SnoN protein levels upon exogenous transfection of these miRNAs. For this purpose, we transfected HEY ovarian cancer cells with 200 pmol of the above mentioned miRNAs (presented as mimics) for 96 hours, a time point used in previous studies [229]. We performed this analysis with or without 6 hour As<sub>2</sub>O<sub>3</sub> treatment, since SnoN levels are induced with As<sub>2</sub>O<sub>3</sub> treatment at this time point in HEY cells [15]. As shown in Figure 18B, we identified a reduction in the protein levels of SnoN upon transfection with miR-494 mimic in the presence of As<sub>2</sub>O<sub>3</sub> treatment, but not with the other miRNAs (miR-216b, miR-410, and miR-495). A schematic of the 3'UTR of *SnoN* with the binding site for miR-494 is presented in Figure 18C.

#### miR-494 modulates SnoN protein and mRNA expression

To determine whether the reduction in SnoN protein with miR-494 mimic transfection (Figure 18B) was dependent on the duration of mimic transfection, we harvested protein lysates from HEY cells at 24, 48, 72, and 96 hours post-transfection with or without 6 hours As<sub>2</sub>O<sub>3</sub> treatment. As shown in the western blots presented in Figure 19A, protein levels of SnoN were down-regulated in a time-dependent fashion with a maximum reduction at 72 and 96 hours post-mimic transfection with As<sub>2</sub>O<sub>3</sub> treatment. We also assessed the levels of LC3B (an autophagic marker) in our western analysis since the induction of SnoN upon As<sub>2</sub>O<sub>3</sub> treatment leads to an increase in LC3-II [15]. Interestingly, we observed a reduction in LC3B-II with miR-494 transfection supporting a previous report by our group which demonstrated a reduction in LC3B-II upon siRNA-mediated knockdown of SnoN [15]. Since the reduction in SnoN protein levels reached a peak at 96 hours post-transfection, we used this time point for further studies described in this chapter.

The base-pairing complementarity between the miR-494 and the target mRNA sequence will determine the mechanism of gene repression via miRNAs [230]. miRNAs repress gene

A



B

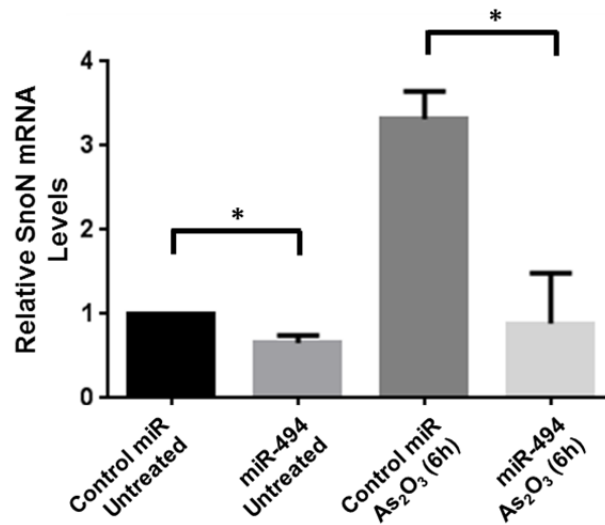


**Figure 19: miR-494 modulates SnoN mRNA expression**

(A) HEY cells expressing miR-494 or negative control miR mimic for 24 to 96 hours were treated with 25  $\mu$ M As<sub>2</sub>O<sub>3</sub> for 6 hours. Protein lysates were harvested and subjected to western analyses using the indicated antibodies. The data shown is representative of two different experiments. (B) HEY cells expressing miR-494 or negative control miR were treated with 25  $\mu$ M As<sub>2</sub>O<sub>3</sub> for 6 hours. Total RNA was isolated and used for real-time PCR. Relative RNA-fold changes are presented for SnoN. The data shown is derived from two different experiments.

expression via mRNA degradation (perfect complementarity base pairing between miRNA and mRNA) or translational inhibition (imperfect complementarity base pairing between miRNA and mRNA) [230]. Since the 3'UTR of *SnoN* harbors a perfect complementary site for miR-494, we next examined whether miR-494 affected the mRNA expression of *SnoN*, in addition to protein level changes. Therefore, we transfected HEY cells with miR-494 mimic in the presence or absence of  $As_2O_3$  treatment for 6 hours and isolated mRNA. Real-time PCR analysis revealed a significant reduction in *SnoN* mRNA levels (as shown in Figure 19B) both in the presence and absence of  $As_2O_3$  treatment.

#### miR-494 leads to the formation of diffused EGFP-LC3B expression upon $As_2O_3$ treatment

As shown in Figure 19A, miR-494 overexpression reduced LC3B-II protein levels. Our group has previously shown that  $As_2O_3$  treatment led to increase in LC3B-II protein levels which

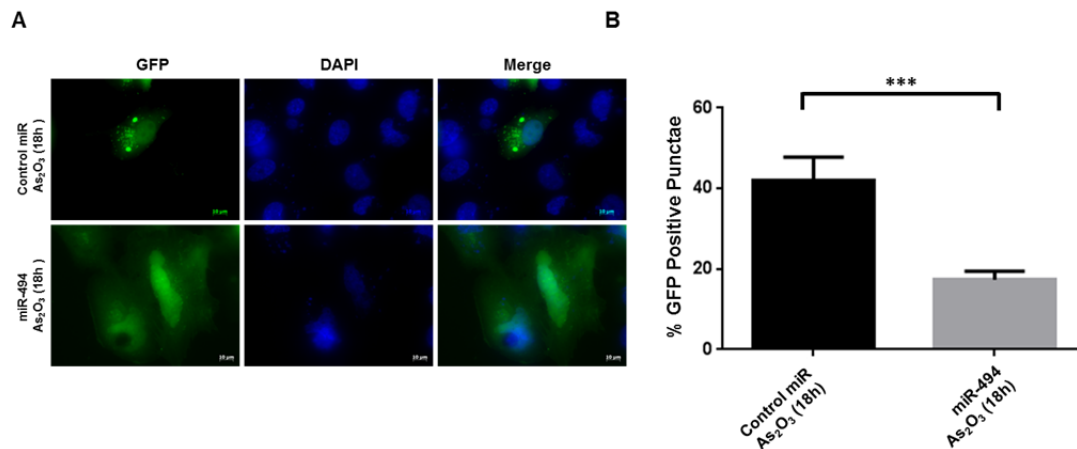


**Figure 20: Pattern of EGFP-LC3B expression in miR-494 overexpressing cells in the presence of  $As_2O_3$  treatment**

(A) HEY cells expressing miR-494 or negative control miR were transfected with *pEGFP-LC3*. At 72 hours post-transfection, cells were treated with 10  $\mu M$   $As_2O_3$  for 18 hours. Representative immunofluorescence images are shown; EGFP-LC3 punctae were quantified by counting the number of cells positive for EGFP-LC3 punctae. The data shown is representative of two different experiments. (B) The graph presents the results from (A) as the percentage of cells with positive GFP-punctae. The data shown is compiled from two different experiments.

were associated with the formation of distinct EGFP-LC3B punctae [15]. Therefore, we next investigated whether miR-494 can alter the formation of EGFP-LC3B punctae upon treatment with  $As_2O_3$ , mediated by SnoN. For this purpose, we transfected HEY cells with control or miR-494 mimic as well as *EGFP-LC3B* plasmid in the presence of  $As_2O_3$ . As expected, we observed an increase in distinct EGFP-LC3 punctae with drug treatment in the control cells. However, miR-494 overexpression altered the LC3B pattern to a diffuse expression in the presence of  $As_2O_3$  (Figure 20A). Indeed, we noted a significant reduction in the percentage of GFP positive punctae with miR-494 expression (Figure 20B).

miR-494 sensitizes the cellular response of HEY ovarian cancer cells to  $As_2O_3$  treatment

Since  $As_2O_3$  treatment reduces HEY cell viability [15], we next assessed whether miR-494 could modulate this cellular response. Thus, we transfected these cells with miR-494 mimic in the absence or presence of  $As_2O_3$  for 18 hours (a time point previously shown to induce cells death in these cells [15]).

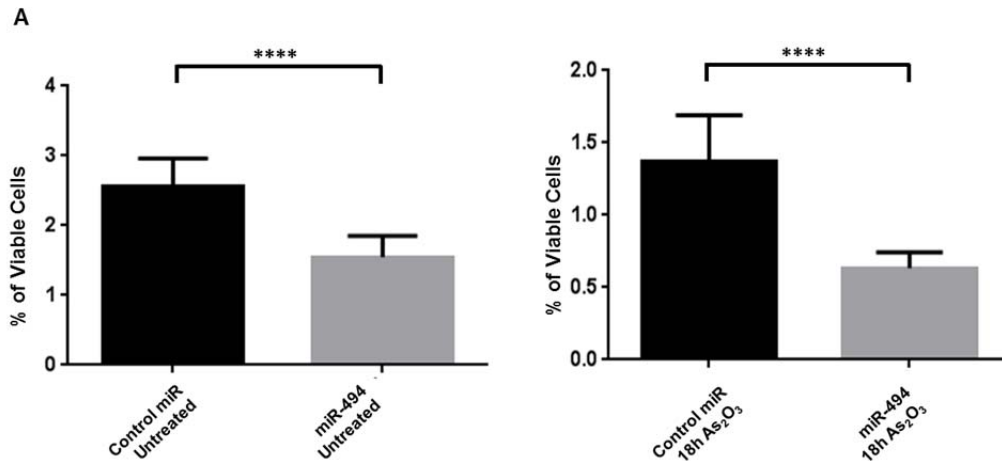


**Figure 21: miR-494 sensitizes HEY ovarian cancer cells to  $As_2O_3$  treatment (\*Continued on next page)**

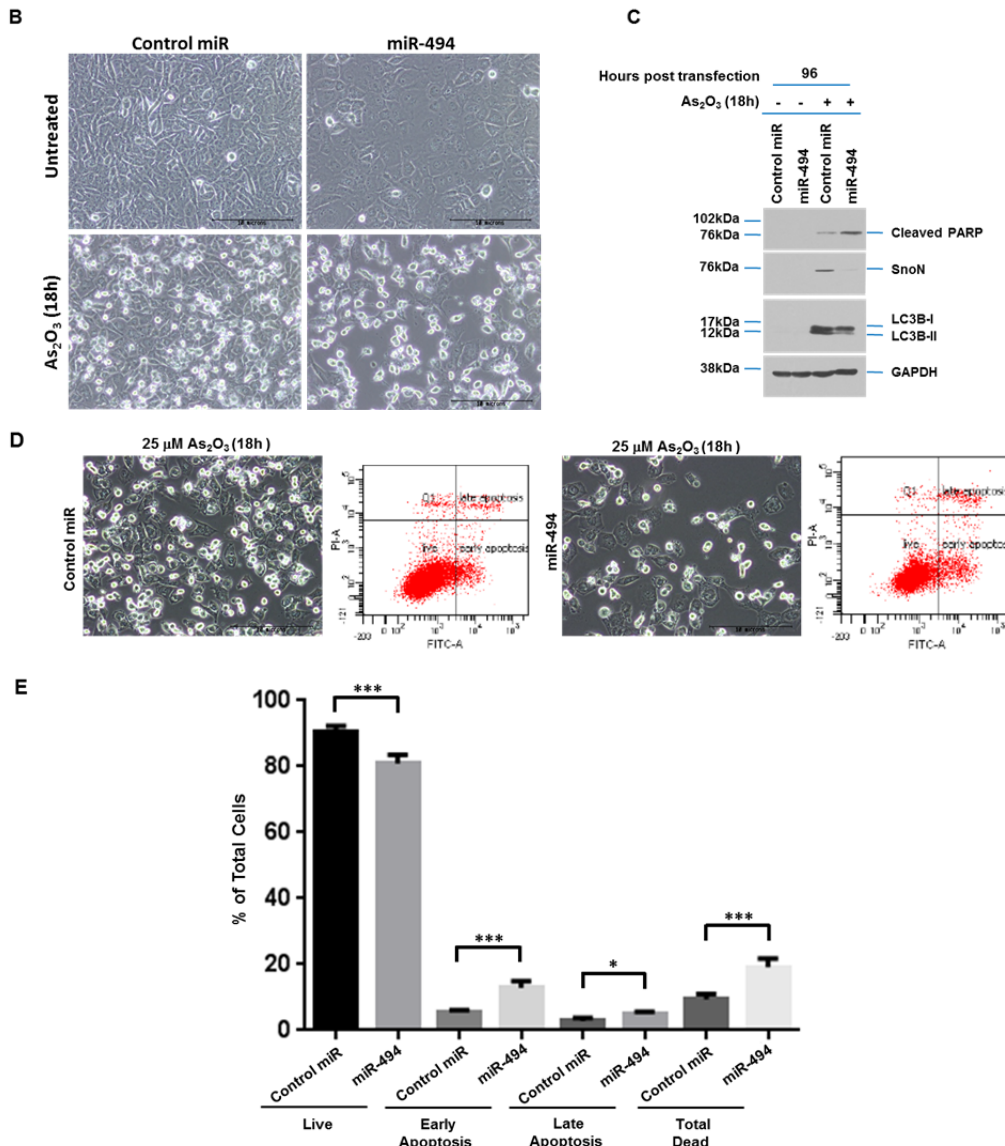


**Figure 21: miR-494 sensitizes HEY ovarian cancer cells to As<sub>2</sub>O<sub>3</sub> treatment**

(A) HEY cells expressing miR-494 or negative control miR were assessed for changes in cell viability by crystal violet staining, both in the presence and absence of 25 μM As<sub>2</sub>O<sub>3</sub> for 18 hours. The data shown is compiled from two different experiments. (B) Light microscope images of HEY cells expressing miR-494 or negative control miR in the presence or absence of 25 μM As<sub>2</sub>O<sub>3</sub> for 18 hours. (C) HEY cells expressing miR-494 or negative control miR mimic for 96 hours were treated with 25 μM As<sub>2</sub>O<sub>3</sub> for 18 hours. Protein lysates were harvested and subjected to western analyses using the indicated antibodies. The data shown is representative of three different experiments. (D) HEY cells expressing miR-494 or negative control miR were treated with 25 μM As<sub>2</sub>O<sub>3</sub> for 18 hours. Ninety-six hours post-transfection, both adherent and floating cells were collected and processed, as indicated in the materials. Cells were then stained with annexin V-FITC and propidium iodide (PI) followed by flow cytometry. Raw data plots and light microscopic images are presented. The data shown is representative of two different experiments. (E) The percentage of viable, early apoptotic, and late apoptotic/necrotic cells from (D) is presented in a graphical format. The data shown is compiled from two different experiments.

We performed cell viability analysis using crystal violet staining and observed that miR-494 decreased cellular survival both with and without drug treatment. (Figure 21A). Interestingly, the morphology of the cells was altered dramatically upon miR-494 expression; in particular, the cells exhibited increased cytoplasmic area with a phenotype similar to that observed in senescent cells (Figure 21B). As mentioned above, our group previously demonstrated that the inhibition of SnoN expression (via siRNA-mediated knockdown) in HEY ovarian cancer cells upon As<sub>2</sub>O<sub>3</sub> treatment increases cell death via apoptosis [15]. Therefore, in order to determine whether the reduction in SnoN levels by miR-494 mimic increases cell death by apoptosis in HEY cells, we performed western blotting analysis to assess the levels of cleaved PARP (a marker for apoptotic cell death [231]), in HEY cells following miR-494 mimic transfection and As<sub>2</sub>O<sub>3</sub> treatment. Indeed, miR-494 overexpression elevated cleaved PARP levels in response to As<sub>2</sub>O<sub>3</sub> treatment (Figure 21C). A reduction in both SnoN and LC3B was also observed, as reported earlier (Figure 19A).

Furthermore, in order to validate whether apoptosis was involved in the cell death mechanism, we conducted annexin V/PI staining in these cells followed by flow cytometry. The apoptotic response with miR-494 expression (early and late apoptotic cell populations) was significantly increased with miR-494 mimic in the presence of As<sub>2</sub>O<sub>3</sub> (Figure 21D and 21E), demonstrating that miR-494 sensitized the cells to As<sub>2</sub>O<sub>3</sub>-mediated apoptotic cell death response.

## Discussion

As<sub>2</sub>O<sub>3</sub> modulates SnoN expression and consequent autophagic response in ovarian cancer cells [15]. In this chapter, we demonstrate that miR-494 mimic overexpression antagonizes SnoN induction in the presence of As<sub>2</sub>O<sub>3</sub> and sensitizes the cells, increasing the cell death response via apoptosis. We also show that miR-494 overexpression leads to reduced LC3-II protein levels and diffused EGFP-LC3 punctae. Additional experiments will need to be



performed in order to determine whether this reduction in LC3-II and altered EGFP-LC3 punctae is also associated with modulation in autophagic flux. It would also be necessary to validate the outcomes observed upon miR-494 mimic overexpression by using miR-494 antagomir in order to determine whether endogenous miR-494 activity is abrogated with the antagomir in the presence of As<sub>2</sub>O<sub>3</sub>. Although we attempted to determine whether the miR-494 effects could be reversed using Ago2 (the slicer activity of which is required for the establishment of RNA inducing silencing complex (RISC) [232]) siRNA, the results obtained were unexpected. We did not observe reduction in SnoN protein level with miR-494 in the presence of control siRNA (results not shown). Since the combination of control siRNA and miR-494 mimic did not elicit the response (reduction in SnoN protein) as observed by the transfection of miR-494 mimic alone, it was difficult to interpret the results. Other experimental technical modifications need to be implemented to study this further.

Several reports have identified a subset of miRNAs that are altered upon As<sub>2</sub>O<sub>3</sub> treatment [233, 234]. We attempted to measure endogenous miR-494 levels upon treatment with As<sub>2</sub>O<sub>3</sub>, in order to determine whether the levels of miR-494 are altered. However, due to technical shortcomings associated with real-time PCR quantification analysis, we were unable to derive conclusions. Additionally, similar to our findings, miR-494 appears to be involved in cinobufacin [139] and fluorouracil [235] (anti-cancer agents) mediated cell death. We have previously reported that SnoN is induced upon drug treatment via the activation of the EGFR/PI3K/AKT pathway [17]. Interestingly, several studies have indicated that miR-494 is involved in the modulation of the PI3K/AKT pathway, thereby affecting cell proliferation and apoptosis [236, 237]. However, the detailed mechanism by which SnoN is induced upon As<sub>2</sub>O<sub>3</sub> treatment and whether cross-talk occurs between EGFR pathway and miR-494 is involved in this mechanism remains to be identified.

miRNA expression patterns are dysregulated in a variety of cancer types [238]. Analysis of miRNA expression profiles may provide better insight into the dysregulated molecular

mechanisms that are critical in tumorigenesis [238]. We have identified miRNAs that may target the 3'-UTR of *SnoN* (Figure 18A). Several of these miRNAs are associated with ovarian cancer biology including miR-497 [239-242], miR-655 [240], miR-424 [243, 244] and miR-410 [245]. In this regard, it would be interesting to assess their contribution in altering *SnoN* expression. Interestingly, Cheng and colleagues demonstrated a ~2-fold reduction in miR-494 expression in primary ovarian tumors relative to the normal ovary [134]. More recently, it was noted that miR-494 was markedly down-regulated in ovarian cancer cells (SKOV3, KF, KFr-, Tx, TUOS3, and TUOS-4) relative to normal ovarian cells (IOSC397 and IOSC386) [246]. Further, several *in silico* approaches have been applied to identify miRNAs that are altered in ovarian cancer development that could potentially regulate expression of mediators of the autophagic pathway [247]; additional experimental work is needed to validate these observations. In this regard, it would be worthwhile to examine miR-494 expression levels in serous EOC patient specimens compared to normal ovarian cells and correlate these to the presence/absence of autophagic markers, since *SnoN* modulates the autophagic pathway induced upon  $As_2O_3$  treatment in ovarian cancer cells [15]. miR-494 has been reported to suppress cell proliferation in prostate [137], lung [248] and gastric cancers [24, 139, 249]. Similar to our studies in ovarian cancer cells, miR-494 also induces cell death responses, including apoptosis [250] in a variety of other cancers such as glioblastoma [251] and small cell lung cancers [252].

miR-494 is located at the 14q chromosomal region (14q32) [253]. A study conducted by Bandera and colleagues to determine loss of heterozygosity at the 14q arm in ovarian cancer demonstrated 14q32.1-14q32.2 to be one of the regions deleted at this arm [115]. Strikingly, another study also indicated the deletion at 14q32.1-14q32.2 to have a possible contribution in the progression of bladder cancer [254]. More importantly, this 14q region is also frequently deleted in renal cancer [23]. This observation is supported by the TCGA research network [43]. The 14q32 chromosomal region harbors a 54 miRNA cluster, which includes miR-494 [253].

Therefore, in the next chapter (Chapter 5) we attempted to study the functional consequences of miR-494 expression in renal cancer cells.

### **Acknowledgments**

I would like to thank my mentor, Dr. Meera Nanjundan for her kind contribution in the *in silico* analysis performed in order to identify putative miRNAs that harbor binding sites in the *SnoN* 3'UTR. I would also like to thank Karoly Szekeres, Ph.D. (Scientific Researcher, College of Medicine, Flow cytometry core, University of South Florida, Tampa, FL) for his assistance with flow cytometric analyses.

## Chapter 5

### miR-494 Modulates Cell Survival and Induces Lipid Droplet Formation in Renal Cancer Cells

#### Introduction

The loss of heterozygosity associated with the 14q chromosomal region has been reported in several cancers such as renal [23] [43], ovarian [115], bladder [254], colorectal [255], endometrial [256], and neuroblastoma [257]. As discussed in Chapter 4, the 14q32 chromosomal region, in particular contains the DLK1-DIO3 genomic cluster. This cluster harbors a set of 54 miRNAs (among other important imprinted genes) that are dysregulated in various solid and blood cancers, including renal cancer (Figure 22) [253]. miRNAs are a class of non-coding RNA molecules that do not translate into a functional protein [258]. Nevertheless, they are involved in a wide variety of cellular processes and control gene expression patterns, which are critical in disease progression, including cancer [259]. miRNAs are located in regions of the genomes that are aberrant in cancers [260]; further, miRNA expression patterns are important diagnostic indicators of patient survival [261, 262]. miRNAs exert their enzymatic activity by direct binding to target mRNAs and to inhibit gene expression via translational inhibition and/or mRNA degradation [259] (Chapter 1, Figure 4). However, recent reports have indicated that miRNAs may also positively regulate gene expression [128-130].

In Chapter 4, we demonstrated that miR-494 mediates cell death response induced upon drug treatment in HEY ovarian cancer cells. Interestingly, miR-494 is located at chr14:101,495,971-chr14:101,496,051, within the 14q32 cluster [131]. The functional effect of

miR-494 has been investigated in a number of cancer types, implicating it in a variety of cancer-related responses such as EMT [263], senescence [135, 264], cell cycle arrest [25], and

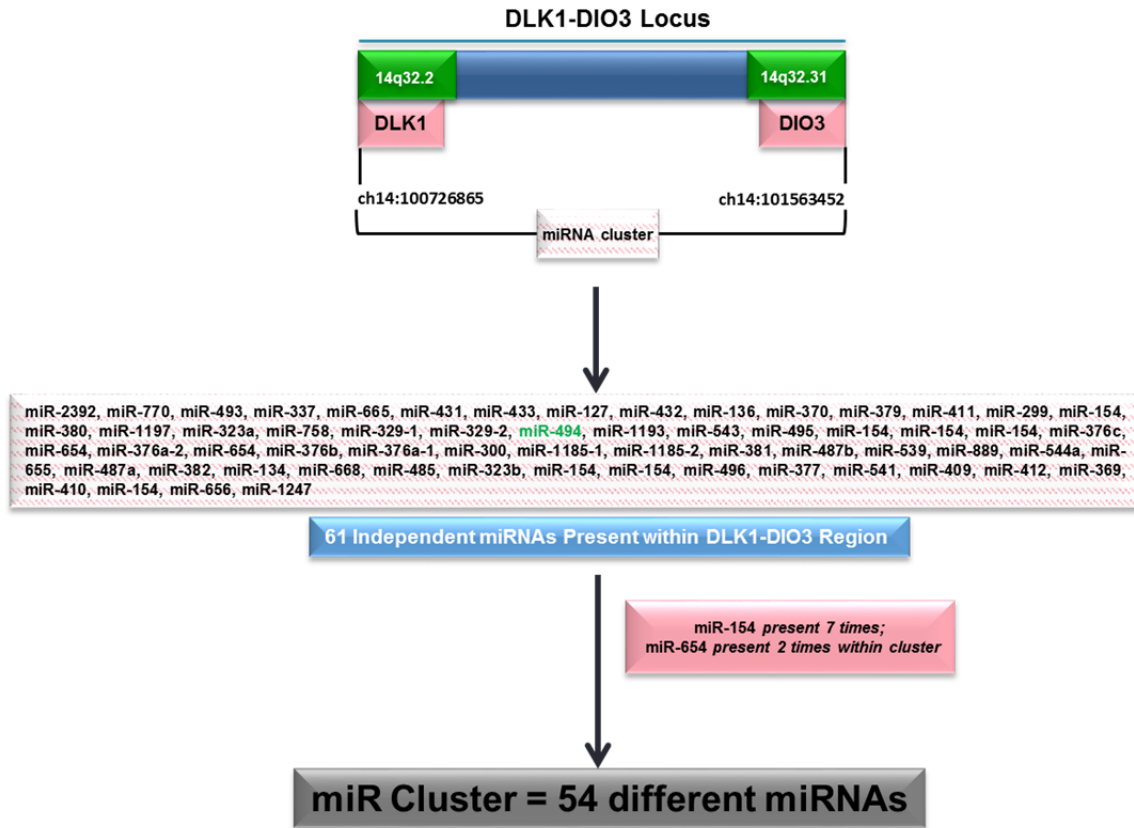


**Figure 22: The DLK1-DIO3 genomic cluster harbors a set of 54 miRNAs**

Schematic representation of the DLK1-DIO3 miRNA cluster at the 14q32 chromosomal locus, spanning ch14:100726865 to ch14:101563452. (\*Figure created by Punashi Dutta)

apoptosis [24]. Interestingly, miR-494 is associated with both oncogenic and tumor suppressive functions. For example, miR-494 targets PTEN, inhibiting apoptosis [251], down-regulates pro-apoptotic BIM in non-small cell lung carcinoma [142], and enhances glioma cell invasion by stabilizing EGFR [237]. Additionally, miR-494 targets and inhibits the gene expression of several invasion-suppressing miRNAs in hepatocellular cancer [146] and elicits oncogenic functions in colorectal cancer [145]. On the contrary, the tumor suppressive properties of miR-494 include attenuation of cell proliferation and induction of senescence in lung cancer cells [248], induction

of cell cycle arrest in cholangiocarcinoma cells [25], and targeting c-KIT [24] and c-myc [249] to impede gastrointestinal tumor proliferation. Further, miR-494 suppresses breast [265], cervical, and oral [136] cancer progression. In addition, miR-494 also elicits functional responses in other diseases like neurodegeneration [266] and cystic fibrosis [267, 268]. Collectively, these studies indicate that a particular miRNA elicits different functional activity depending on the disease type. Table 1 presented in Chapter 1 summarizes all the targets of miR-494 that have been identified thus far. Although miR-494 targets and functions have been identified in other cancer cell types, nothing is yet known about miR-494 in renal cancer biology. Thus, we hypothesize that miR-494 expression reduces renal cell survival.

In this chapter, we attempt to elucidate the functional outcomes elicited by the exogenous expression of miR-494 mimic in renal cells. We demonstrate that miR-494 reduces renal cancer cell survival, a response accompanied by increased LC3B (both mRNA and protein), cleaved PARP, and apoptosis. We identified LC3B as a novel possible miR-494 target via luciferase assay. Expression of miR-494 in 769-P renal cancer cells led to increased lipid droplets (LDs) and reduced total cellular cholesterol amounts. This accumulation in LDs was mediated via LC3B. miR-494 expressing cells exhibit disorganized mitochondrial structural pattern, which is associated with reduced PINK1 protein levels and altered Drp1 subcellular localization.

## **Results**

### miR-494 modulates the protein levels of LC3B and cleaved PARP in normal and renal cancer cells

Since miR-494 is located within the frequently deleted 14q region [23] [45] and considering previously published reports of the cell death and tumor suppressive responses elicited by miR-494 in cancers (as stated above), we assessed the functional outcomes upon miR-494 mimic transfection in renal cells. We transfected immortalized normal kidney tubule

HK-2 cells [269] as well as three renal cancer cell lines (769-P, 786-O, and A-498) with negative control or miR-494 mimic and examined changes in cellular morphology ninety-six hours post miR-494 transfection (a similar time point used for miRNA studies in Chapter 4). Light microscopic images showed a noticeable reduction in cell density and appearance of large cytoplasmic vacuoles in HK-2 and 769-P cells expressing miR-494 (Figure 23A). No distinct morphological changes were observed in A-498 cells, although 786-O cells demonstrated a disorganized pattern. Since autophagy and apoptotic pathways mediate cellular death responses [270], we next tested the protein levels of LC3B (an autophagic marker) and cleaved PARP (an apoptotic marker) in miR-494 expressing cells as compared to control.

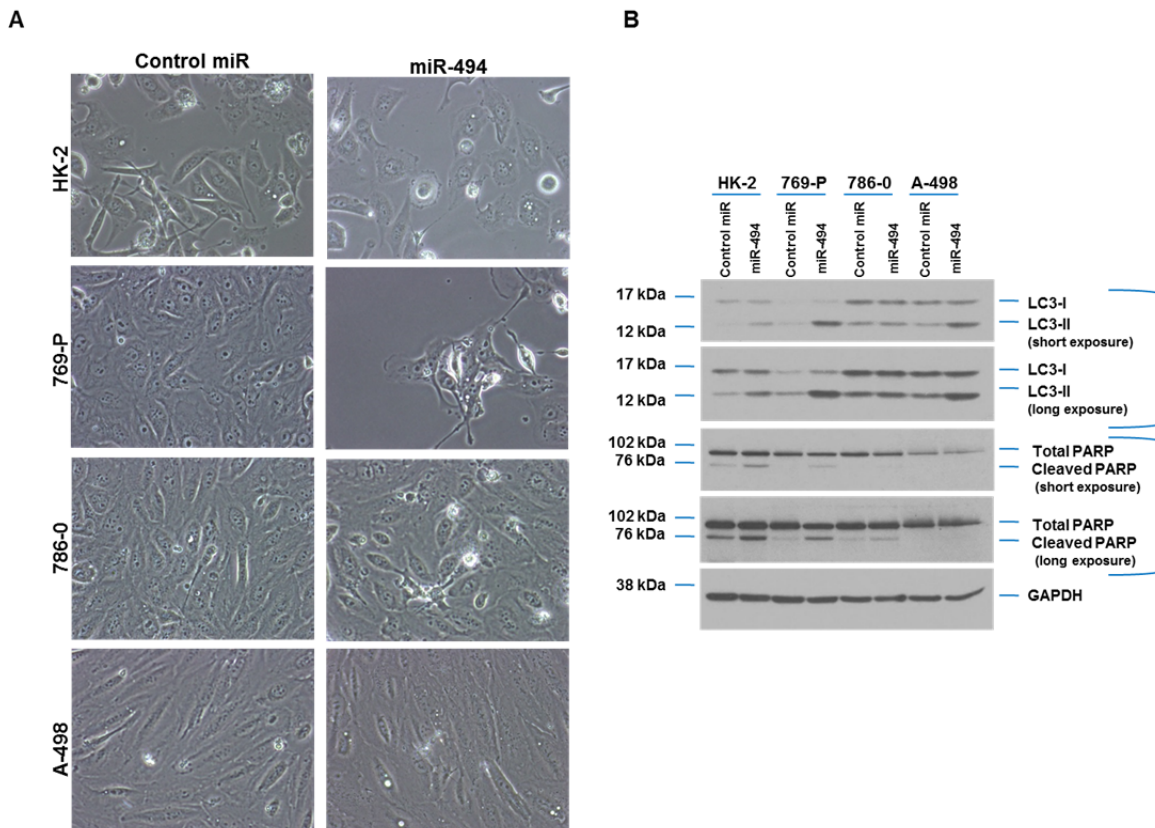


**Figure 23: miR-494 modulates cell death in renal cancer cells (\*Continued on next page)**

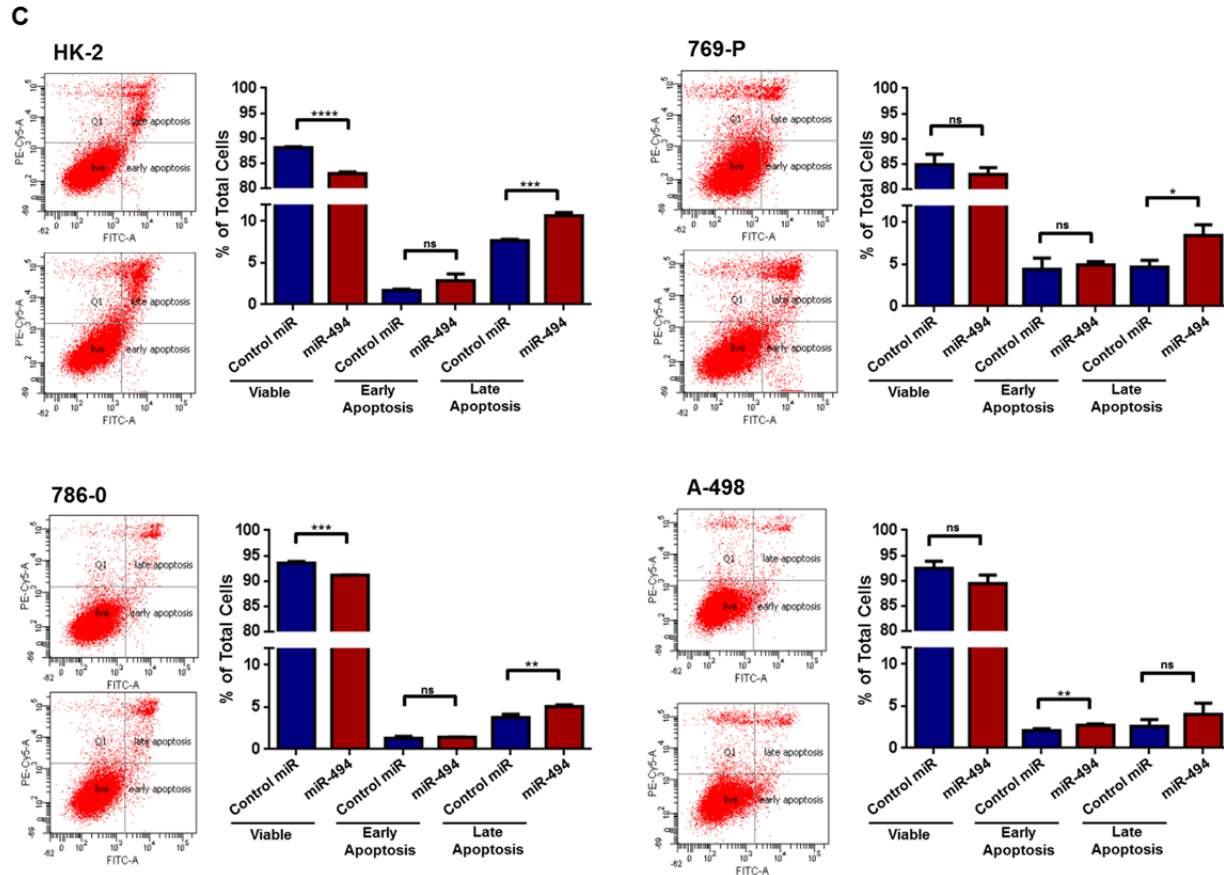


**Figure 23: miR-494 modulates cell death in renal cancer cells**

(A) Bright field light microscopic images of HK-2, 769-P, 786-O, and A-498 cells captured 96 hours post-transfection with negative control miR or miR-494 mimic (200 pmol). (B) HK-2, 769-P, 786-O, and A498 cells were transfected with negative control or miR-494 mimic. Protein lysates were collected 96 hours post-transfection and samples run on a 10% SDS-PAGE gel. Western blotting analyses were performed using the specified antibodies as shown. The data shown is representative of three different experiments. (C) HK-2, 769-P, 786-O, and A498 cells were treated as (A). Ninety-six hours post-transfection, both adherent and floating cells were collected and processed, as indicated in the materials and methods section. Cells were further stained with annexin V-FITC and PI followed by flow cytometric analysis. Raw data plots are and the percentage of viable, early apoptotic, and late apoptotic/necrotic cells are presented. The data shown is compiled from three different experiments.



As shown in Figure 23B, we observed an increase in LC3B in HK-2, 769-P, and A-498 cells. Cleaved PARP levels increased with miR-494 expression in HK-2, 769-P, and 786-O cells. Further, in order to determine whether cell death response was mediated by apoptosis, we performed annexin V/PI staining in these cells. miR-494 expression induced a significant

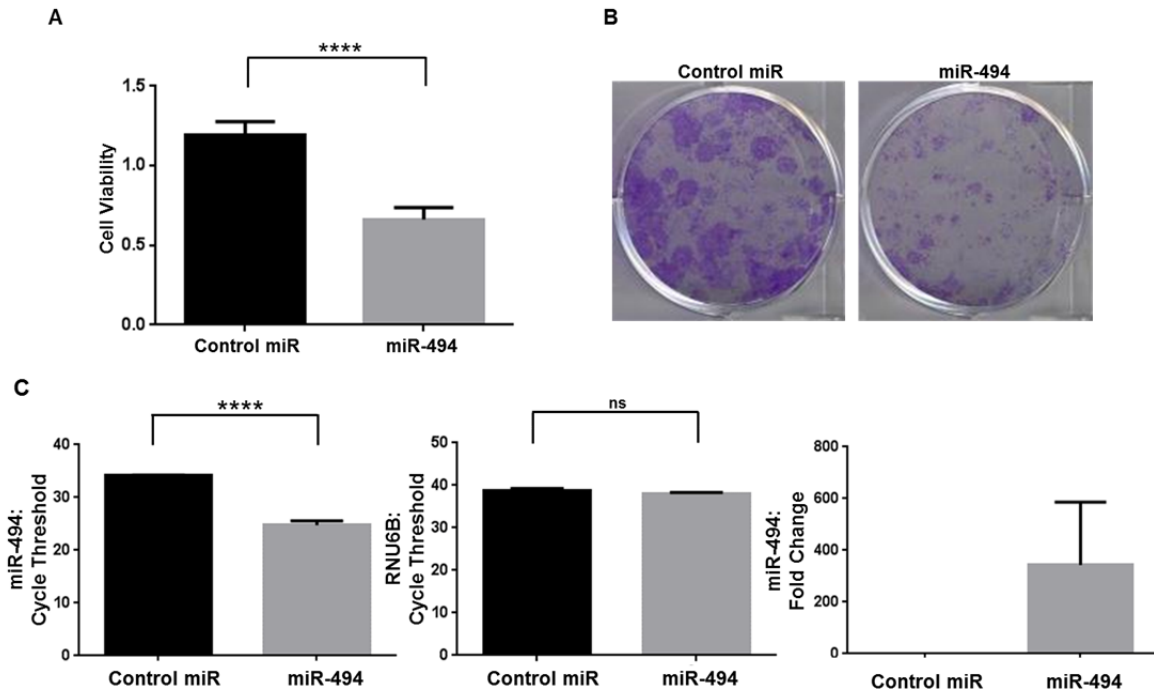


**Figure 24: miR-494 reduces 769-P viability and colony forming ability**

(A) 769-P cells expressing miR-494 or control miR were re-seeded in 96 well plate 24 hour post-mimic transfection. These cell were assessed for changes in cell viability by crystal violet staining, 96 hours post-mimic transfection. The data shown is derived from two different experiments. (B) 769-P cells expressing miR-494 or control miR, grown for 2 weeks at low density (5,000 cells initial seeding/well), were stained with crystal violet. The data shown is representative of two different experiments. (C) Control or miR-494 mimic transfected 769-P cells were processed for miRNA isolation 96 hours post-transfection. miR-494 levels were quantified by real-time PCR using the correlative method and RNU6B was used as the endogenous control. Cycle threshold ( $C_T$ ) value and RNA-fold changes are presented. The data shown is compiled from three different experiments.

increase in late apoptotic cell numbers in HK-2, 769-P, and 786-O cells (Figure 23C). Since we observed changes in both LC3B and cleaved PARP protein levels with miR-494 expression in 769-P cells, we also tested changes in cell viability using crystal violet staining in these cells. As indicated in Figure 24A, we noticed a significant decrease in cell viability with miR-494. Next, we performed a colony formation assay which assesses the ability of cells to form colonies in culture. For this purpose, miR-494 mimic transfected 769-P cells were plated at a low density of 5000 cells/well of a six-well plate. After carefully monitoring the cells over a period of 2 weeks, we stained them with crystal violet. We noticed an attenuation in the colony formation ability of the cells transfected with the miR-494 mimic, as depicted in the Figure 24B. We also quantified miR-494 levels upon mimic transfection via real-time PCR analysis and found these to be within the physiological limit of endogenously expressed miRNAs [271] (Figure 24C). These experiments suggest that miR-494 elicits tumor suppressive responses in renal cells.

miR-494 antagomir and Ago2 siRNA-mediated knockdown reverse the induction of LC3B-I/II and cleaved PARP protein levels in 769-P renal cancer cells upon miR-494 mimic transfection

In order to ensure that the functional response elicited by miR-494 (increase in LC3B and cleaved PARP protein levels) occurred via the miRNA pathway, we transfected 769-P cells with different miR-494 mimic/antagomir combinations. These included (1) control mimic, (2) miR-494 mimic, (3) control antagomir, (4) miR-494 antagomir, (5) control mimic and control antagomir, (6) control mimic and miR-494 antagomir, (7) control antagomir and miR-494 mimic, and (8) miR-494 mimic and miR-494 antagomir. Light microscopy images obtained 96 hours post-transfection indicated that transfection with miR-494 antagomir reversed the effect on cell

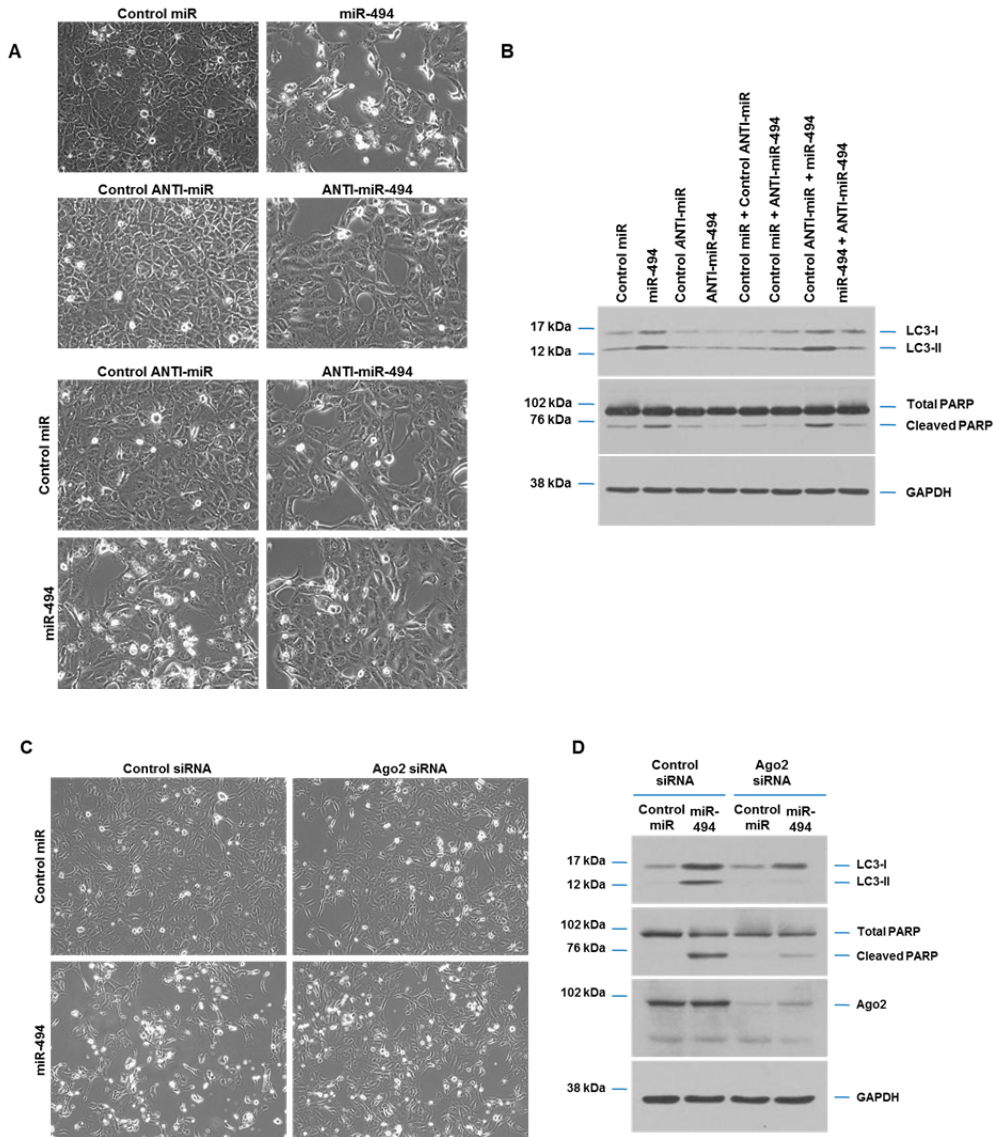


**Figure 25: Validation of miR-494-mediated cellular responses**

(A) Light microscopic images of 769-P cells transfected with negative control or miR-494 mimic/antagomir at 96 hours post-transfection is presented. (B) 769-P cells were transfected as stated above in (A). Protein lysates were collected 96 hours post-transfection and samples run on a 10% SDS-PAGE gel. Western blotting analyses were performed using the specified antibodies as shown. The data shown is representative of three different experiments. (C) Control or Ago2 siRNA transfected 769-P cells were transfected with negative control or miR-494 mimic. Light microscope images were captured at 96 hours post-transfection and representative images are presented. (D) 769-P cells were treated as described above in (C). Protein lysates were collected 96 hours post-transfection and samples run on a 10% SDS-PAGE gel. Western blotting analyses were performed using the specified antibodies as shown. The data shown is representative of three different experiments.

density that was observed with miR-494 mimic (Figure 25A). The miR-494 antagomir also inhibited the increase in LC3B and cleaved PARP protein levels observed with miR-494 mimic expression (Figure 25B). In addition, we also performed siRNA-mediated knockdown of Ago2. The miR-494 mimic (that we have utilized for overexpressing miR-494 for our studies herein) is the mature miRNA form which requires the activity of endogenous Ago2 in order to bind to the target mRNA. Therefore, in order to determine whether knockdown of endogenous Ago2 can affect the activity of the mimic, we performed siRNA-mediated knockdown of Ago2 and then transfected the cells with the miR-494 mimic. As shown in Figure 25C and 25D, we did not observe changes in LC3B and cleaved PARP upon miR-494 mimic transfection in the presence of Ago2 siRNA compared to control siRNA. Collectively, these studies indicate that changes in LC3B and cleaved PARP protein occurred via a miRNA-dependent mechanism.

#### miR-494-mediated apoptotic induction occurs in the absence of change in protein levels of pro-caspases or nuclear localization of AIF

Apoptosis is a type of programmed cell death mechanism that primarily involves the activation of the caspase family of proteases [162]. However, caspase-independent apoptosis is also an established phenomena which is mediated by the movement of apoptosis-inducing factor (AIF) from the mitochondria into the nucleus [272]. We next investigated the mechanism of apoptotic cell death elicited following miR-494 transfection. Therefore, we transfected 769-P cells with miR-494 mimic along with the negative control mimic to determine the protein levels of both initiator (pro-caspase 2, 8, and 9) and executioner (pro-caspase 3) pro-caspases [273] via western blotting analyses. Since our group has previously shown that As<sub>2</sub>O<sub>3</sub> induces a caspase-dependent apoptotic cell death in normal ovarian T80 cells, we utilized this cell line treated with increasing doses of As<sub>2</sub>O<sub>3</sub> as our positive control [15]. As shown in Figure 26A, we observed a decrease in pro-caspase 2, 3, 8, and 9 with increasing doses of As<sub>2</sub>O<sub>3</sub> in T80 cells; however, this was not observed in miR-494 expressing 769-P cells. Furthermore, AIF did not nuclear

localize in miR-494 expressing cells, as determined by immunofluorescence staining of AIF (Figure 26B). These results indicate that apoptotic cell death elicited by miR-494 is not dependent on either the change in protein levels of caspases or the nuclear localization of AIF.

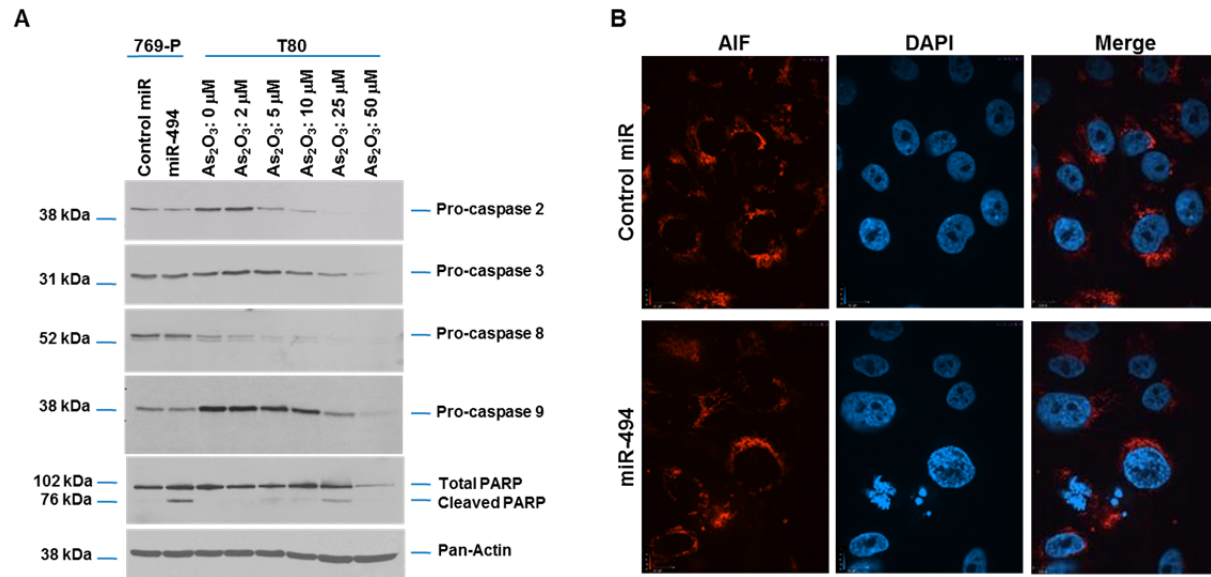


**Figure 26: Mechanism of miR-494-induced apoptosis**

(A) T80 cells were treated with 2, 5, 10, 25, and 50 μM As<sub>2</sub>O<sub>3</sub> for 18 hours and protein lysates were collected. 769-P cells were transfected with control or miR-494 mimic and protein lysates were harvested 96 hours post-transfection. All the samples were run on a 10% SDS-PAGE gel and western blotting analysis was performed using the specified antibodies. The data shown is representative of two different experiments. (B) Control or miR-494 mimic transfected 769-P cells were re-seeded at 150,000 cells/well on glass coverslips. Cells were stained with AIF primary antibody overnight at 96 hours post-transfection and further stained with goat anti-rabbit Alexa Fluor-546 secondary antibody. Coverslips were then mounted on slides using DAPI mounting media. Confocal imaging was performed and representative images from three different experiments are shown.

miR-494 reduces Bcl-2 protein levels and knockdown of Bcl-2 mimics effects elicited by miR-494 expression

Since we observed changes in LC3B protein levels with miR-494 expression and LC3B is an important autophagic marker, we next sought to identify putative miR-494 autophagy target genes. We initially performed an *in silico* analysis of autophagy-related genes listed in

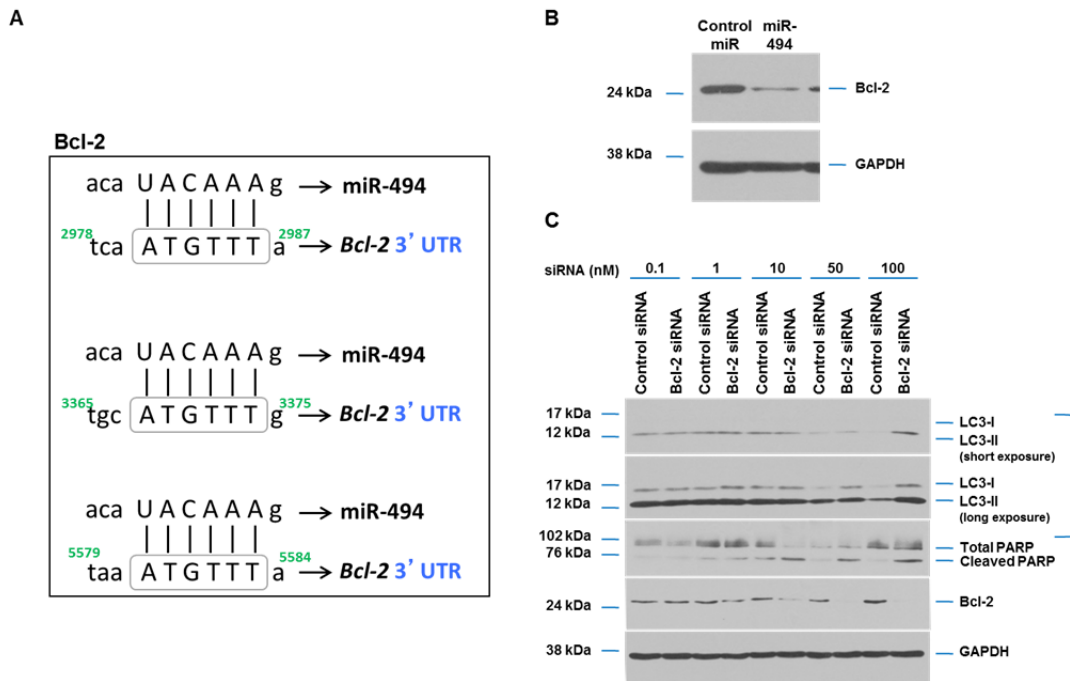


**Figure 27: miR-494 reduces Bcl-2 protein levels**

(A) A diagram depicting the 3 imperfect miR-494 binding sites at the 3'UTR of *Bcl-2* is shown. (B) 769-P cells were transfected with negative control or miR-494 mimic and protein lysates were harvested 96 hours post-transfection. Samples were run on a 10% SDS-PAGE gel and western blotting analyses were performed using the specified antibodies. The data shown is representative of three different experiments. (C) 769-P cells were seeded at 750,000 cells/well. Following overnight adherence, cells were transfected with control or Bcl-2 siRNA. Twenty-four hours post the first round of transfection, cells were transfected again with the siRNA and protein lysates collected 48 hours post the second transfection. Samples were run on a 10% SDS-PAGE gel and western blotting analysis was performed using the specified antibodies. The data shown is representative of three different experiments.

the Human Autophagy Database (HAD) [185] using TargetScanHuman. One of the hits obtained from this analysis was Bcl-2, a negative regulator of both autophagy and apoptotic pathways [274]. The 3'UTR of *Bcl-2* harbors three different imperfect miR-494 binding sites (Figure 27A). Since our western blot results demonstrated an increase in the protein levels of both autophagic and apoptotic markers (LC3B and cleaved PARP, respectively), we wondered whether Bcl-2 protein levels were altered upon miR-494 expression. As indicated in Figure 27B, there was a marked reduction in Bcl-2 protein levels upon miR-494 mimic transfection. Next, we assessed functional responses in 769-P cells upon knockdown of *Bcl-2* via siRNA-mediated strategy. A similar increase in LC3B and cleaved PARP upon *Bcl-2* siRNA was observed similar to miR-494 transfection (Figure 27C). We next attempted to investigate the effect of Bcl-2 knockdown on the increase in LC3B and cleaved PARP observed in miR-494 expressing 769-P cells. For this purpose, we co-transfected 769-P cells with *Bcl-2* siRNA and miR-494 mimic, followed by western blotting analyses for LC3B and cleaved PARP. Unfortunately, the western blotting data indicated an absence of changes in Bcl-2 protein levels in cells transfected with both control siRNA and miR-494 mimic (results not shown), which was in contrast to what was observed with miR-494 mimic transfection alone (Figure 27B). Therefore, since our prior observation that miR-494 mimic reduced Bcl-2 protein levels was not reproduced when the cells were also transfected with control siRNA in addition to miR-494, we could not interpret the results. Hence, these experimental problems that were encountered made it difficult to derive conclusive data on the combinatorial effect of *Bcl-2* siRNA and miR-494 mimic expression in 769-P cells. We next performed luciferase assay measurements to determine whether miR-494 reduces the expression of Bcl-2. For this purpose, we transfected a normal cell line with a luciferase plasmid harboring the *Bcl-2* 3'UTR downstream of the firefly luciferase gene along with miR-494 mimic. The plasmid also harbored a renilla luciferase gene for determining transfection efficiency. No difference was observed in the relative luminescence values with

miR-494 mimic, compared to control (results not shown), suggesting that Bcl-2 may be an indirect target of miR-494.

### Investigation of miR-494 targets via RT<sup>2</sup>-PCR arrays identify LC3B as a potential target

In our search for miR-494 targets, we next analyzed autophagy and apoptosis pathway focused RT<sup>2</sup>-PCR arrays to identify potential targets. These arrays identified an increase in

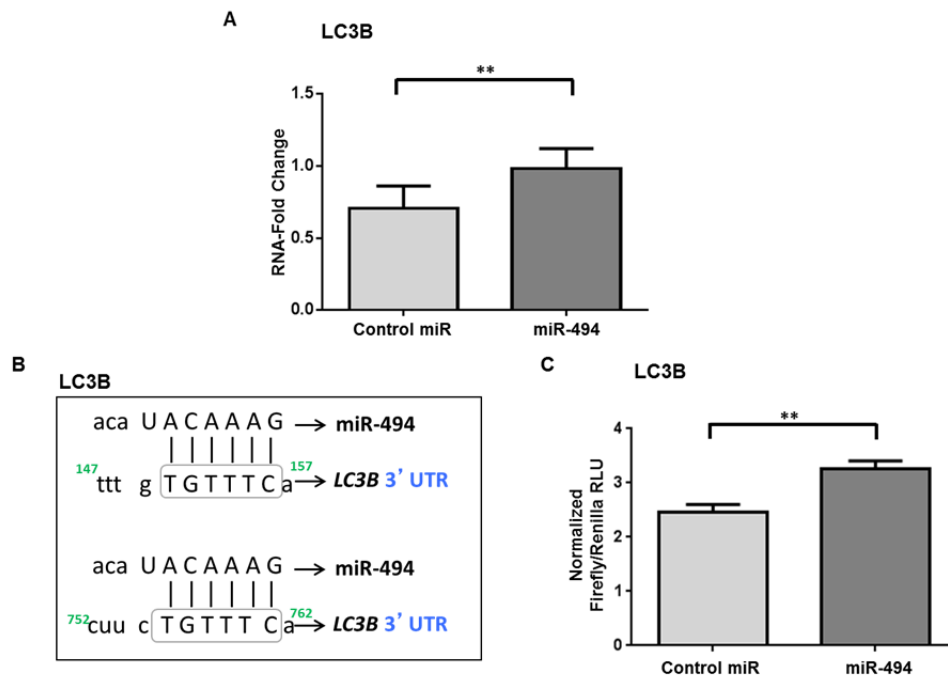


**Figure 28: LC3B, a potential direct target of miR-494**

(A) Control or miR-494 mimic transfected 769-P cells were processed for miRNA isolation 96 hours post-transfection. *LC3B* mRNA levels were quantified by real-time PCR using the correlative method and  $\beta$ -actin was used as the endogenous control. RNA-fold changes are presented. The data shown is compiled from three different experiments. (B) A diagram depicting the 2 imperfect miR-494 binding sites at the 3'UTR of *LC3B* is shown. (C) T80 cells were transfected with *pEZX-MT01* luciferase plasmid harboring *LC3B* 3'UTR downstream of the luciferase gene with control or miR-494 mimic. Cells were processed for luciferase assay and luminescence readings captured 24 hours post-transfection (as described in Chapter 2). The data shown is compiled from three different experiments.

*LC3B* with miR-494 expression (results not shown). We validated the increase in *LC3B* mRNA levels in miR-494-expressing cells by performing real-time PCR analysis using FAM-labelled TaqMan probes/primers and noted a fold increase of 1.39 (Figure 28A). Interestingly, *LC3B* was



also identified as one of the targets of miR-494 in the above mentioned *in silico* analysis (using HAD). A schematic representation of the miR-494 binding sites (2 imperfect sites) within the 3'UTR of *LC3B* is shown in Figure 28B. Also, as indicated above, we observed an increase in LC3B protein levels with miR-494 expression (Figure 23B). Since there have been reports indicating that miRNAs can also up-regulate the expression of target genes [128-130] and induce translational up-regulation via direct binding at 3'UTR sites [275], we next assessed whether miR-494 binds to the 3'UTR of *LC3B*. For this purpose, we performed a luciferase assay, as described above for Bcl-2. As shown in Figure 28C, we observed a significant decrease in the relative light units with miR-494 expression, relative to control transfected cells, indicating that LC3B may be a potential target of miR-494. Additional studies involving 3'UTR mutations in the miR-494 binding site will need to be performed in order to confirm LC3B as a direct target of miR-494.

Increase in LC3B mRNA and protein levels upon miR-494 transfection occur in the absence of autophagic flux changes

Since elevated LC3B levels may suggest increased autophagic flux [276], we next wanted to identify changes in autophagic flux upon miR-494 expression. We initially assessed

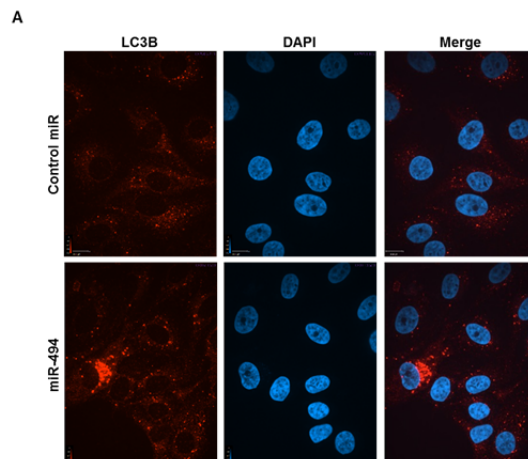


**Figure 29: miR-494 expressing cells exhibit increased LC3B punctae without changes in autophagic flux (\*Continued on next page)**

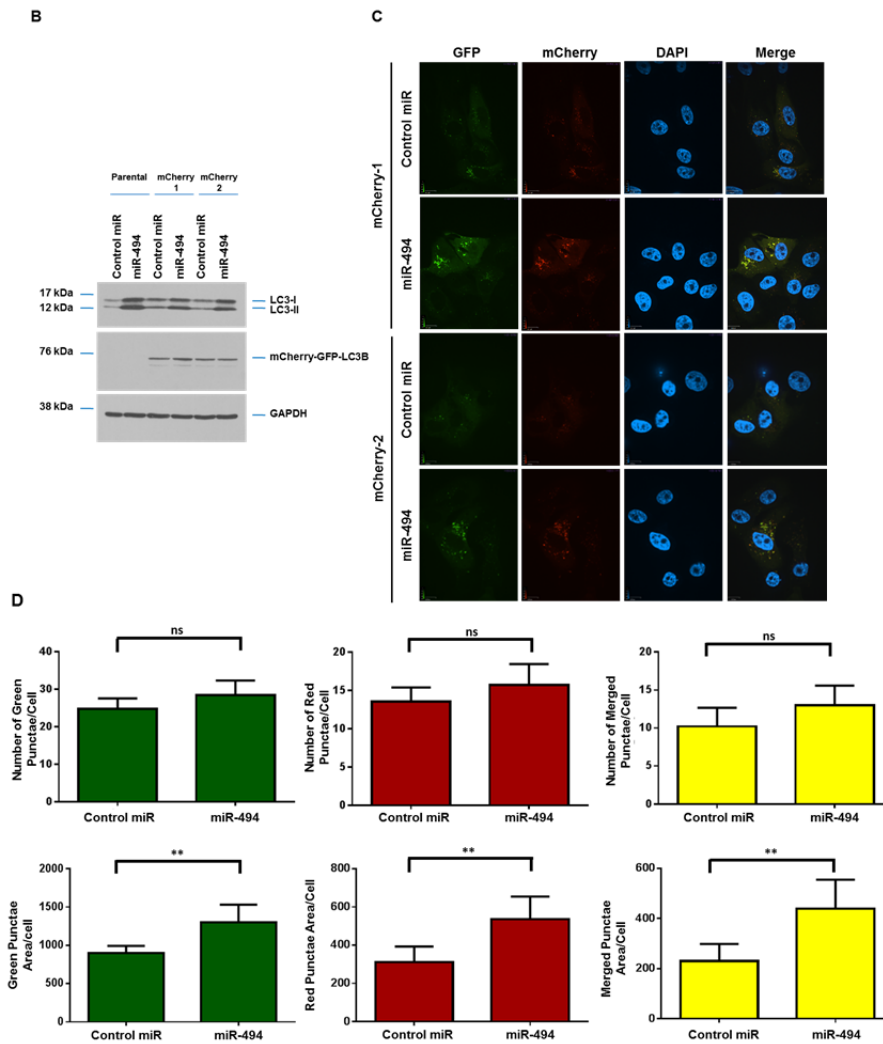


**Figure 29: miR-494 expressing cells exhibit increased LC3B punctae without changes in autophagic flux**

(A) Control or miR-494 mimic transfected 769-P cells were re-seeded at 150,000 cells/well on glass coverslips. Cells were stained with LC3B primary antibody overnight at 96 hours post-transfection and further stained with goat anti-rabbit Alexa Fluor-546 secondary antibody. Coverslips were then mounted on slides using DAPI mounting media. Confocal imaging was performed and data shown is representative of two different experiments. (B) 769-P cells stably expressing mCherry-GFP-LC3B fusion protein were transfected with negative control or miR-494 mimic. Protein lysates were harvested 96 hours post-transfection. Samples were run on a 10% SDS-PAGE gel and western blotting analysis was performed using the specified antibodies. The data shown is representative of three different experiments. (C) 769-P cells stably expressing mCherry-GFP-LC3B fusion protein were transfected with negative control or miR-494 mimic. Twenty-four hours post-transfection, cells were re-seeded at 150,000 cells/well on glass coverslips. Ninety-six hours post-transfection, coverslips were mounted on slides using DAPI mounting media. Confocal imaging analysis was performed and representative images are presented. The data shown is representative of three different experiments. (D) Confocal imaging data from (C) was quantified using the Image J macro analysis. Number of punctae and number of punctae area/cell for green, red, and merged punctae is presented.

endogenous LC3B staining in miR-494-transfected cells. As indicated in Figure 29A, an increase in both the number and intensity of LC3B punctae was observed in miR-494 expressing cells, relative to control. In order to determine changes in autophagic flux, we performed immunofluorescence analysis, using the pH-sensor mCherry-GFP-LC3B fusion protein, developed by Hundeshagen and group [277]. The GFP-tag in this protein is acid-sensitive and loses its green fluorescence when the autophagosome fuses with the lysosome, in contrast to the mCherry tag (red fluorescence) which is acid-insensitive [277]. This strategy distinguishes the lysosomes from the autophagosomes and hence determines autophagic turnover [277]. Therefore, we established retroviral stable 769-P cells overexpressing mCherry-GFP-LC3B fusion protein and validated the protein levels via western blotting analysis in the absence or presence of miR-494 mimic transfection (Figure 29B). As shown in Figure 29C and 29D, there was no change in autophagic flux with miR-494 expression, relative to control. We evaluated the data obtained from this analysis by confocal analysis and further quantified using Image J macro analysis program. However, both confocal imaging and quantitative analysis indicated an increase in punctae area, suggesting an increase in autophagosome size.

#### miR-494 expression leads to accumulation of LDs, an event mediated via LC3B

In order to examine cellular changes upon miR-494 expression, we performed TEM analysis in control and miR-494 expressing cells. Interestingly, we observed an increase in the number of LDs in miR-494 expressing cells (Figure 30A). Additionally, there was also an increase in cholesterol clefts and multilamellar bodies. We next performed staining of neutral lipids (using green LipidTOX stain) in cells transfected with negative control or miR-494 mimic in order to assess change in LDs size/number. Both the number and size of LDs increased significantly with miR-494 (Figure 30B and 30C).

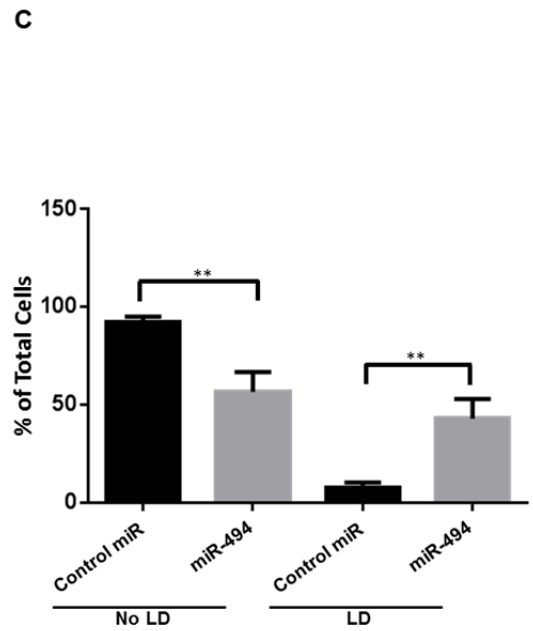
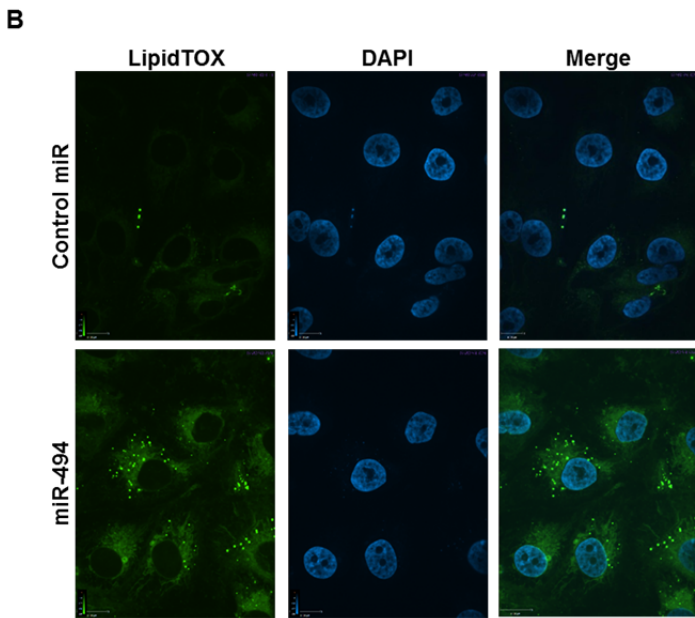
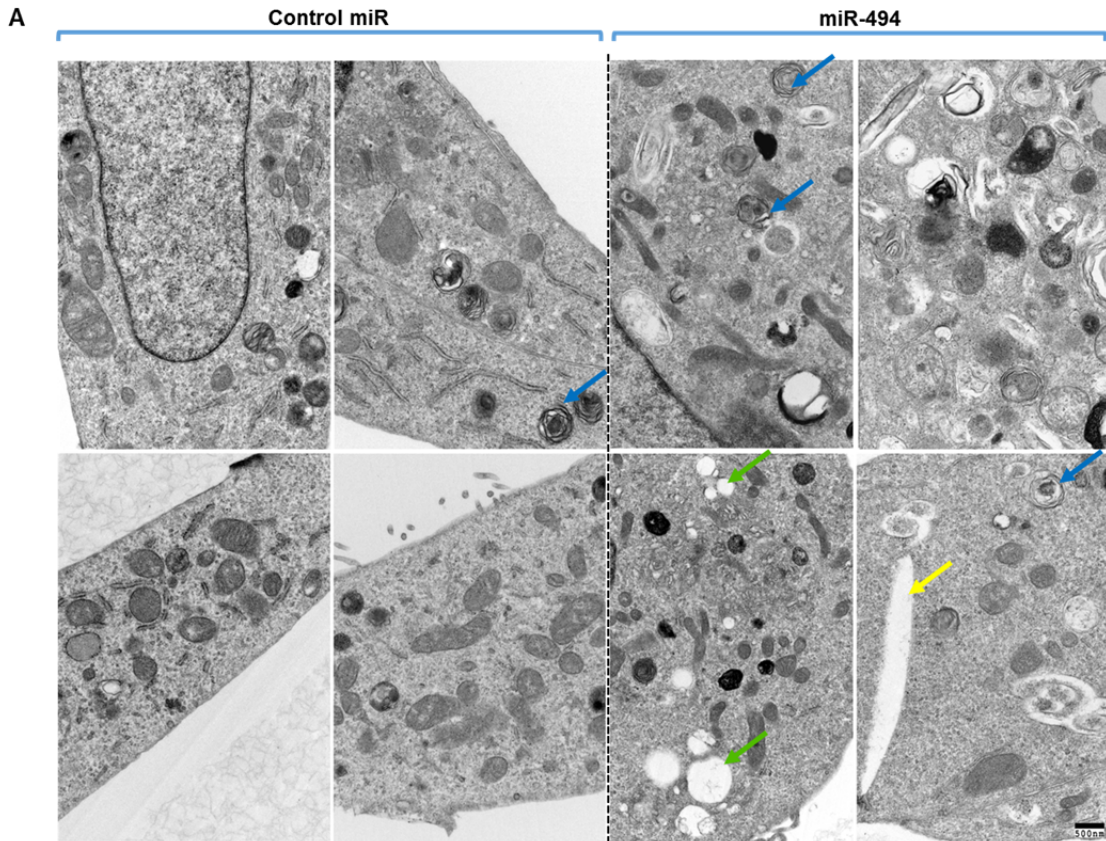


**Figure 30: Accumulation of LDs in miR-494 expressing cells occurs in an LC3B-dependent mechanism (\*Continued on next page)**

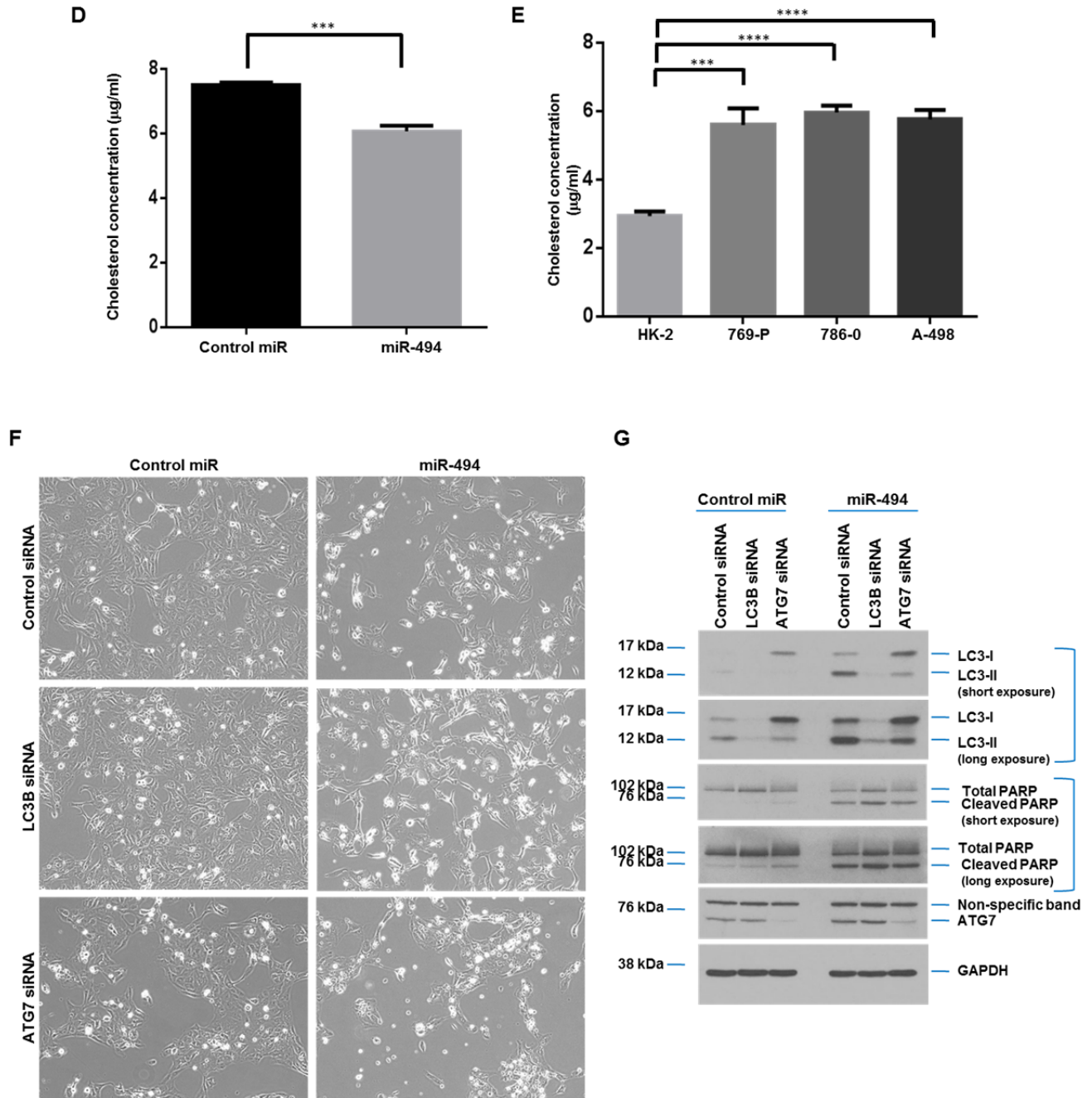
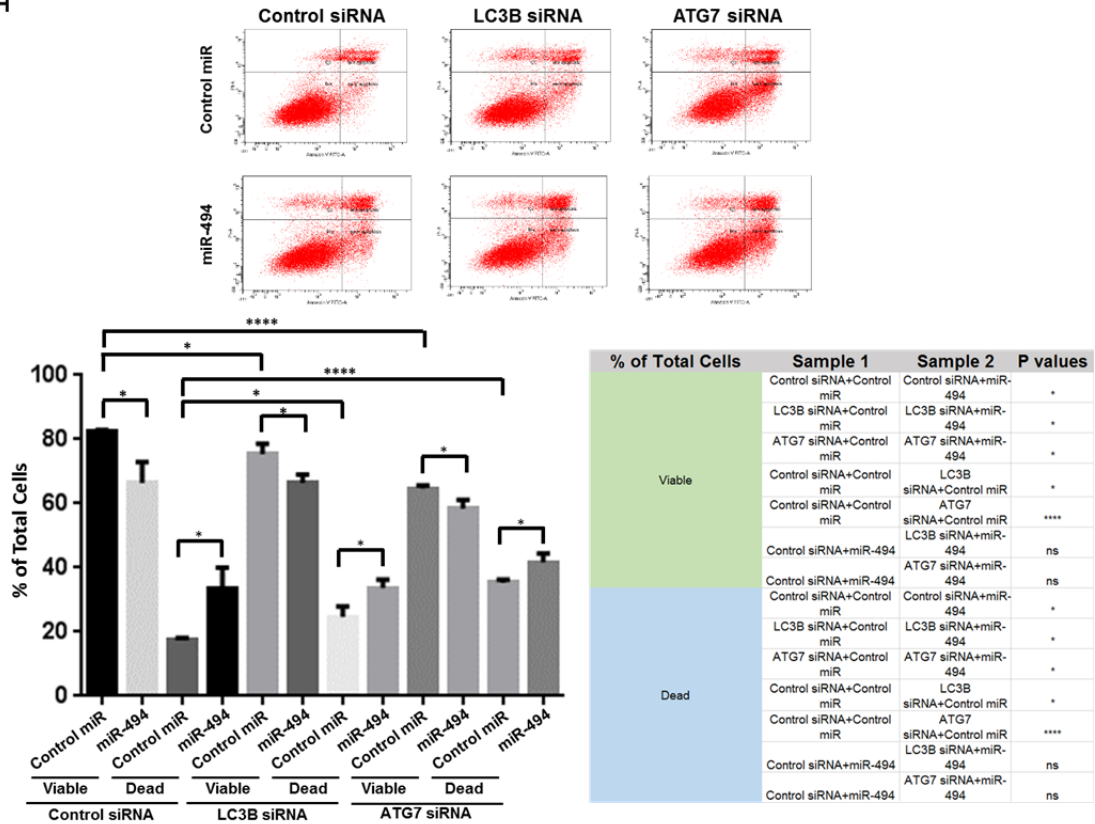


**Figure 30: Accumulation of LDs in miR-494 expressing cells occurs in an LC3B-dependent mechanism (\*Continued on next page)**

H



I

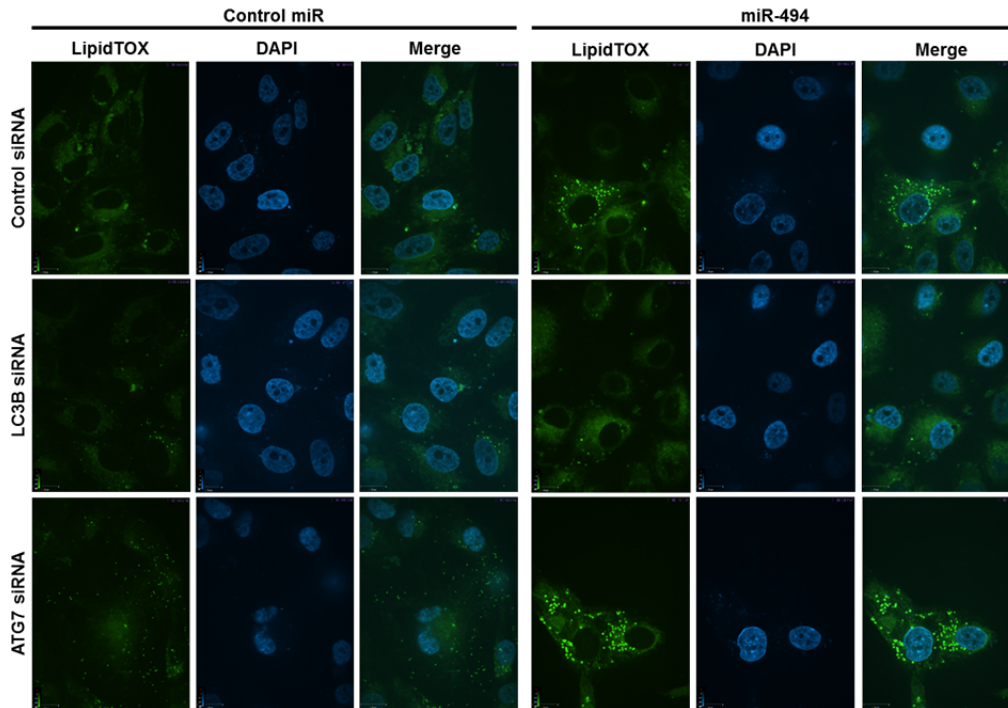
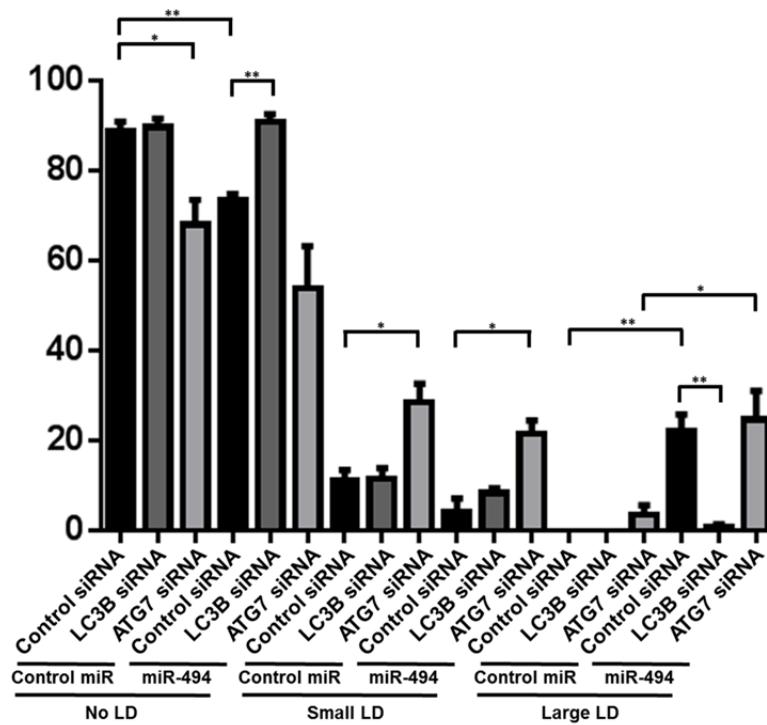


Figure 30: Accumulation of LDs in miR-494 expressing cells occurs in an LC3B-dependent mechanism (\*Continued on next page)

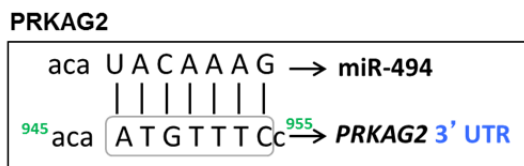
J



K

Lipid droplet status	Sample 1	Sample 2	P values
No LD	Control siRNA+Control miR	LC3B siRNA+Control miR	ns
	Control siRNA+Control miR	ATG7 siRNA+Control miR	*
	Control siRNA+miR-494	LC3B siRNA+miR-494	**
	Control siRNA+miR-494	ATG7 siRNA+miR-494	ns
	Control siRNA+Control miR	Control siRNA+miR-494	**
	LC3B siRNA+Control miR	LC3B siRNA+miR-494	ns
	ATG7 siRNA+Control miR	ATG7 siRNA+miR-494	ns
	Control siRNA+Control miR	LC3B siRNA+Control miR	ns
	Control siRNA+Control miR	ATG7 siRNA+Control miR	*
	Control siRNA+miR-494	LC3B siRNA+miR-494	ns
Small LD	Control siRNA+miR-494	ATG7 siRNA+miR-494	*
	Control siRNA+Control miR	Control siRNA+miR-494	ns
	LC3B siRNA+Control miR	LC3B siRNA+miR-494	ns
	ATG7 siRNA+Control miR	ATG7 siRNA+miR-494	ns
	Control siRNA+Control miR	LC3B siRNA+Control miR	NA
	Control siRNA+Control miR	ATG7 siRNA+Control miR	ns
	Control siRNA+miR-494	LC3B siRNA+miR-494	**
	Control siRNA+miR-494	ATG7 siRNA+miR-494	ns
	Control siRNA+Control miR	Control siRNA+miR-494	**
	LC3B siRNA+Control miR	LC3B siRNA+miR-494	ns
Large LD	ATG7 siRNA+Control miR	ATG7 siRNA+miR-494	*
	Control siRNA+Control miR	LC3B siRNA+Control miR	ns
	Control siRNA+Control miR	ATG7 siRNA+Control miR	ns
	Control siRNA+miR-494	LC3B siRNA+miR-494	**
	Control siRNA+miR-494	ATG7 siRNA+miR-494	ns
	Control siRNA+Control miR	Control siRNA+miR-494	**
LC3B siRNA+Control miR	LC3B siRNA+miR-494	ns	
ATG7 siRNA+Control miR	ATG7 siRNA+miR-494	*	

L



M

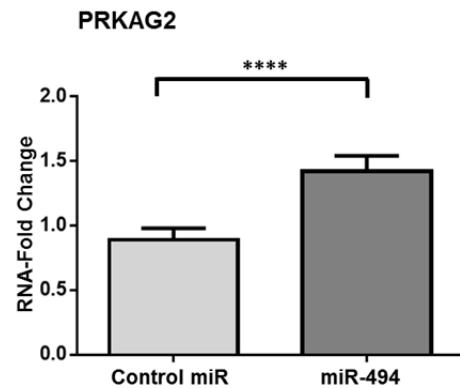


Figure 30: Accumulation of LDs in miR-494 expressing cells occurs in an LC3B-dependent mechanism (\*Continued on next page)

### Figure 30: Accumulation of LDs in miR-494 expressing cells occurs in an LC3B-dependent mechanism

(A) Transmission electron micrographs of 769-P cells transfected with negative control or miR-494 mimic. Green arrows indicate LDs, blue arrows indicate multilamellar bodies, and yellow arrows indicate cholesterol clefts. (B) Control or miR-494 mimic transfected 769-P cells were re-seed at 150,000 cells/well on glass coverslips. Ninety-six hours post-transfection cells were stained with green neutral lipid stain (LipidTOX). Coverslips were then mounted on slides using DAPI mounting media. Confocal imaging was performed and data shown is representative of three different experiments. (C) The data as shown in (B) was quantified and is presented in a graphical manner, compiled from three different experiments. (D) Protein lysates were collected from control or miR-494 mimic transfected 769-P cells and were then processed as described in Chapter 2 for cholesterol measurement. The data shown is compiled from three different experiments. (E) Protein lysates were collected from control transfected HK-2, 769-P, 786-O, and A-498 cells and were then processed as described in Chapter 2 for cholesterol measurement. The data shown is compiled from three different experiments. (F) 769-P cells transfected with control, *LC3B*, or *ATG7* siRNA were re-seeded at 250,000 cells/well. Twenty-four hours post re-seeding, cells were transfected with negative control or miR-494 mimic. Representative light microscopic pictures are presented from three different experiments. (G) Cells were processed as described in (F). Protein samples collected 96 hours post-transfection were run on a 10% SDS-PAGE gel and western blotting analyses were performed using the specified antibodies. The data shown is representative of three different experiments. (H) Cells were transfected as stated in (F). Ninety-six hours post-transfection, both adherent and floating cells were collected and processed, as indicated in Chapter 2. Cells were further stained with annexin V-FITC and PI followed by flow cytometry. Raw data plots (upper panel), and the percentage of viable, early apoptotic, and late apoptotic/necrotic cells are presented (bottom left panel). A table summarizing all the p-values is presented (bottom right panel). The data shown is compiled from three different experiments. (I) 769-P cells transfected with control, *LC3B*, or *ATG7* siRNA were re-seeded at 250,000 cells/well on glass coverslips. Twenty-four hours post re-seeding cells were transfected with negative control or miR-494 mimic. Ninety-six hours post-transfection cells were stained with green neutral lipid stain (LipidTOX). Coverslips were then mounted on slides using DAPI mounting media. Confocal imaging was performed and representative images from three different experiments are shown. (J) Graphical representation of data as presented in (I). (K) A table showing p-values for the graph presented in (J). (L) A diagram depicting perfect miR-494 binding site at the 3'UTR of *PRKAG2*. (M) Control or miR-494 mimic transfected 769-P cells were processed for miRNA isolation 96 hours post-transfection. *PRKAG2* mRNA levels were quantified by real-time PCR using the correlative method and  $\beta$ -actin was used as the endogenous control. RNA-fold changes compiled from three different experiments are presented.

We also measured total cholesterol content in 769-P cells transfected with control or miR-494 mimic. Surprisingly, in contrast to the TEM results, we observed a decrease in cholesterol content with miR-494 (Figure 30D). This reduction in cholesterol levels was similar to the effect of certain chemotherapeutic agents that reduce intracellular cholesterol and sensitize cancer



cells to cell death response [278]. Furthermore, we noted that the total cellular cholesterol levels were elevated in renal cancer cells compared to the normal immortalized HK-2 cells (Figure 30E). Collectively, these results suggest that miR-494 expression can mediate metabolic changes which may contribute to the observed reduced cellular viability in 769-P renal cancer cells. We next investigated the mechanism of LD accumulation and thus used siRNA-mediated knockdown strategy against LC3B and ATG7 since both these proteins associate with outer LD membrane [279]. Additionally, depletion of ATG7 also induces LD accumulation in *ATG7*<sup>-/-</sup> mouse model [280]. Captured light micrographs (Figure 30F) showed that *ATG7* knockdown markedly reduced cell numbers compared to control siRNA. The expression of miR-494 in *ATG7* knockdown cells appeared to further decrease cell numbers. We next assessed changes in LC3B and cleaved PARP levels upon knockdown of *LC3B* and *ATG7*. As demonstrated in Figure 30G, we observed an altered ratio of LC3B-I/II with *ATG7* siRNA. miR-494 expression led to an increase in cleaved PARP in control, *LC3B*, and *ATG7* siRNA treated cells. However, annexin V/PI staining did not demonstrate a large change in apoptotic cell death in miR-494 expressing cells with *LC3B* or *ATG7* knockdown as compared to control siRNA (Figure 30H). These results indicate that the contribution of ATG7 and LC3B to the miR-494-mediated cell death response is negligible.

LipidTOX staining indicated an increase in LDs with *ATG7* siRNA, which further increased with miR-494 transfection (Figure 30I, 30J, and 30K). miR-494 transfection along with *LC3B* siRNA led to a significant reduction in LDs, as compared to control siRNA. These studies indicate that miR-494 mediated LD accumulation is LC3B-dependent and ATG7-independent. Next, in order to investigate whether miR-494 was involved in the regulation of genes associated with lipid metabolism, we performed another pathway focused RT<sup>2</sup>-PCR array for lipoprotein signaling and cholesterol metabolism. We identified an increase in the expression of the gamma subunit of AMPK (*PRKAG2*) (results not shown). *PRKAG2* harbors a perfect miR-494 binding site in its 3'UTR (Figure 30L). We validated the increase in *PRKAG2* mRNA levels

in miR-494-expressing cells by performing real-time PCR analysis using FAM-labelled TaqMan probes and primers (Figure 30M). We also attempted to determine the protein changes in PRKAG2 upon miR-494 expression; however, the antibody failed to detect a band at the appropriate molecular weight (results not shown).

#### Mitochondrial structural organization is altered upon miR-494 expression in 769-P cells

The TEM analysis also demonstrated an increased number of electron dense regions in the mitochondria in cells expressing miR-494. These electron dense regions represent calcium accumulation which may indicate mitochondrial injury or degradation [281] (Figure 31A). In order to examine mitochondrial structural changes with miR-494, we performed immunofluorescence staining with cytochrome c, a mitochondrial protein marker which is located in the mitochondrial intermembrane space [282]. Additionally, we also co-stained for LC3B in order to assess their co-localization pattern. Not only did we observe an increase in LC3B punctae (as seen previously in Figure 29A), we also noted that the staining pattern of cytochrome c was disorganized in miR-494 expressing cells compared to control (Figure 30B). Data quantification was performed by grouping the images captured based on mitochondrial structural patterns into four categories (Figure 30C). These categories included (1) tubular, (2) tubular shortened, (3) tubular shortened fragmented, and (4) fragmented mitochondria. We observed a greater percentage of miR-494 expressing cells in the category 3 or 4 (tubular shortened fragmented or fragmented mitochondria).

Mitochondria structural patterns are regulated by fission and fusion processes [283]. Proteins such as Parkin and PTEN-induced putative kinase 1 (PINK1) play critical roles in maintaining mitochondrial structural dynamics [284]. Dynamin-related protein 1 (Drp1) is another critical mitochondrial fragmentation associated protein [283]. In order to further our understanding of mitochondrial structural alterations, we next examined the protein levels of these mitochondrial proteins reported to be associated with mitochondrial fragmentation.

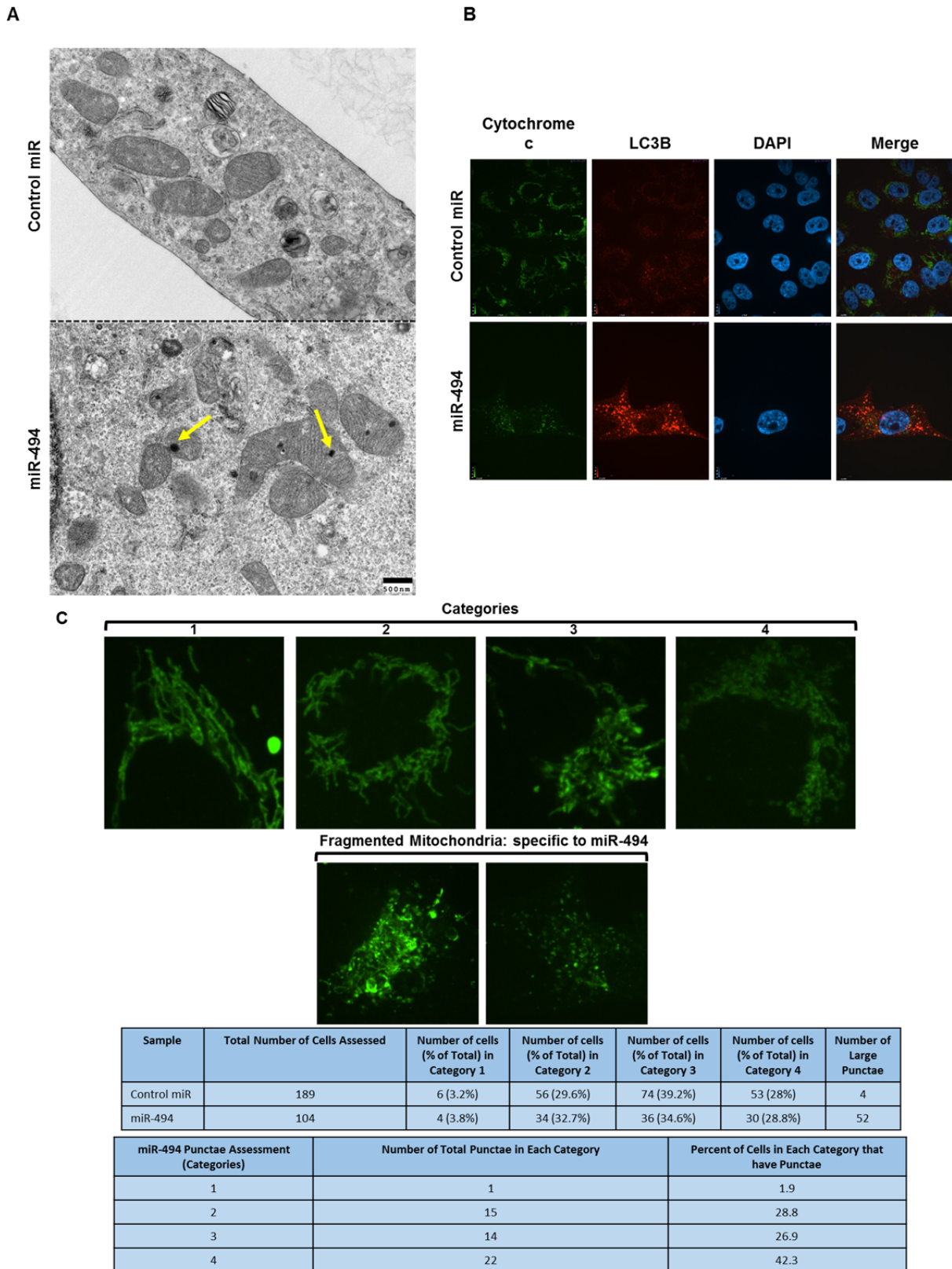


**Figure 31: miR-494 induces disorganized structural mitochondrial patterns (\*Continued on next page)**

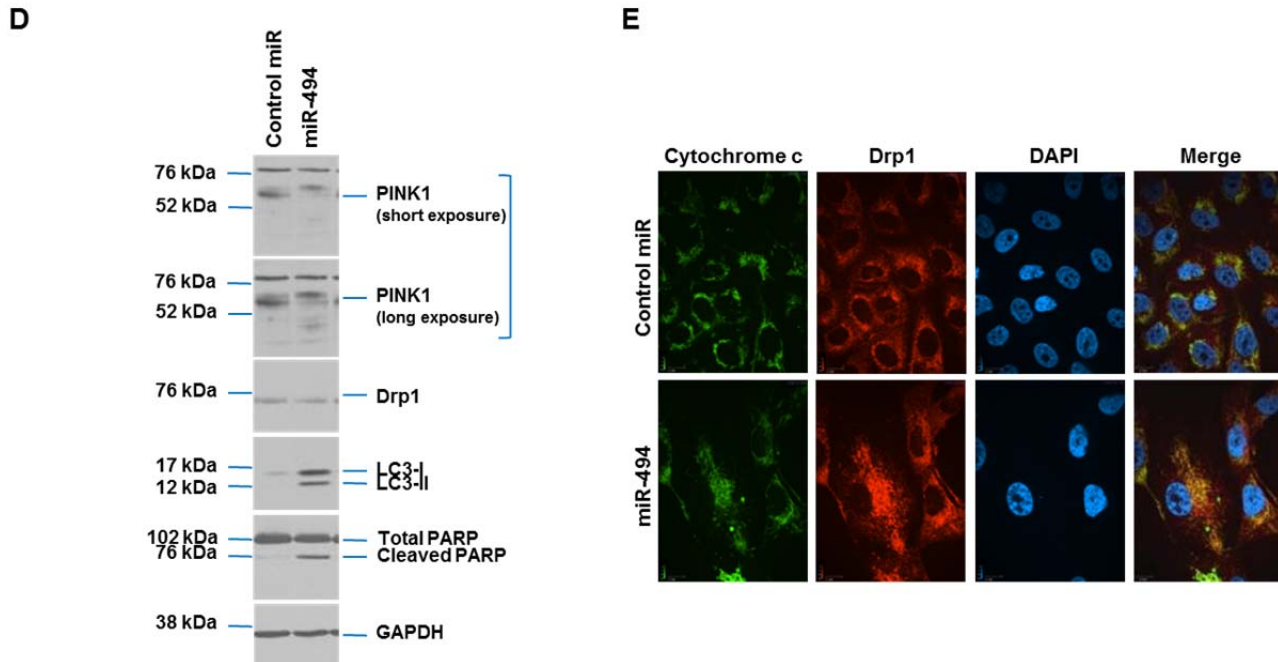


**Figure 31: miR-494 induces disorganized structural mitochondrial patterns**

(A) TEMs of 769-P cells transfected with negative control or miR-494 mimic. Yellow arrows indicate electron dense regions in the mitochondria. (B) Control or miR-494 mimic transfected 769-P cells were re-seeded at 150,000 cells/well on glass coverslips. Cells were stained with LC3B primary antibody overnight at 96 hours post-transfection and further stained with goat anti-rabbit Alexa Fluor-546 secondary antibody. On the same day, cells were then stained with cytochrome c primary antibody overnight. The next day goat anti-mouse Alexa Fluor-488 was applied. Coverslips were then mounted on slides using DAPI mounting media. Confocal imaging was performed and data shown is representative of three different experiments. (C) Representative images captured via confocal microscope demonstrating the different mitochondrial structural patterns (as stated in the text). A table showing the number of cells assessed, the designated category, and punctae number is presented. (D) 769-P cells were transfected with negative control or miR-494 mimic and protein lysates were harvested 96 hours post-transfection. All the samples were run on a 10% SDS-PAGE gel and western blotting analyses were performed using the specified antibodies. The data shown is representative of three different experiments. (E) Control or miR-494 mimic transfected 769-P cells were re-seeded at 150,000 cells/well on glass coverslips. Cells were stained with Drp1 primary antibody overnight at 96 hours post-transfection and further stained with goat anti-rabbit Alexa Fluor-546 secondary antibody. On the same day, cells were then stained with cytochrome c primary antibody overnight. The next day goat anti-mouse Alexa Fluor-488 was applied. Coverslips were then mounted on slides using DAPI mounting media. Confocal imaging was performed and data shown is representative of three different experiments.

As shown in the western blotting analyses in Figure 31D, we observed a decrease in PINK1 protein levels but no change in Drp1. Reduced PINK1 protein has been previously reported to contribute to mitochondrial fragmentation (mediated by Drp1) and oxidative stress-induced mitophagy [285, 286]. Therefore, we next examined subcellular localization of Drp1 via immunofluorescence analysis upon co-staining with both Drp1 and cytochrome c. As shown in Figure 31E, increased Drp1 co-localization with cytochrome c was observed in miR-494 expressing cells. Further, we also assessed mitochondrial superoxide levels in miR-494 expressing cells using the MitoSOX assay; however, no difference was observed (results not shown). Collectively, these experimental outcomes may suggest that increased mitochondrial disorganization/fragmentation upon miR-494 transfection may be due to PINK1 loss and altered Drp1 localization.

## Discussion

Clear cell renal carcinoma is the most common form of kidney cancer and is characterized by the loss of the VHL tumor suppressor gene, located at 3p25 [287]. The loss of this region is related to increased risk of renal cancer and poor patient outcome [23, 287, 288]. The additional loss of chromosome 14q along with 3p deletions leads to increased aggressiveness of this cancer [23]. miRNAs are frequently found in such genomic regions; indeed, the 14q region harbors one of the largest miRNA clusters in the human genome [119]. The role of these miRNAs in cancer biology is unclear. miRNAs regulate key cellular processes and many are associated with reduced cellular growth. miR-494 in other cancer cell types has also been shown to be associated with reduced cell viability [138, 248, 289], although a detailed mechanism has yet to be elucidated. In this chapter, we show that miR-494 leads to reduction in cell growth in normal and renal cancer cells. miR-494 failed to elicit these effects in the presence of Ago2 siRNA or transfection with anti-miR-494 leading to a reversal in miR-494-mediated changes, indicating that our experimental outcomes were miRNA-dependent. As

demonstrated in Figure 32, miR-494 increased LC3B mRNA and protein levels. LC3B may be a potential miR-494 target as indicated by the luciferase assay and miRNAs have been reported to enhance target gene expression [128-130]. miR-494 expression also led to increased cleaved PARP and apoptosis. miR-494 expressing cells exhibited increased LC3B punctae and mitochondrial disorganization. The accumulation of LDs in miR-494 expressing cells was mediated by LC3B. Small LDs that increased with the knockdown of ATG7 occurred independently of miR-494.

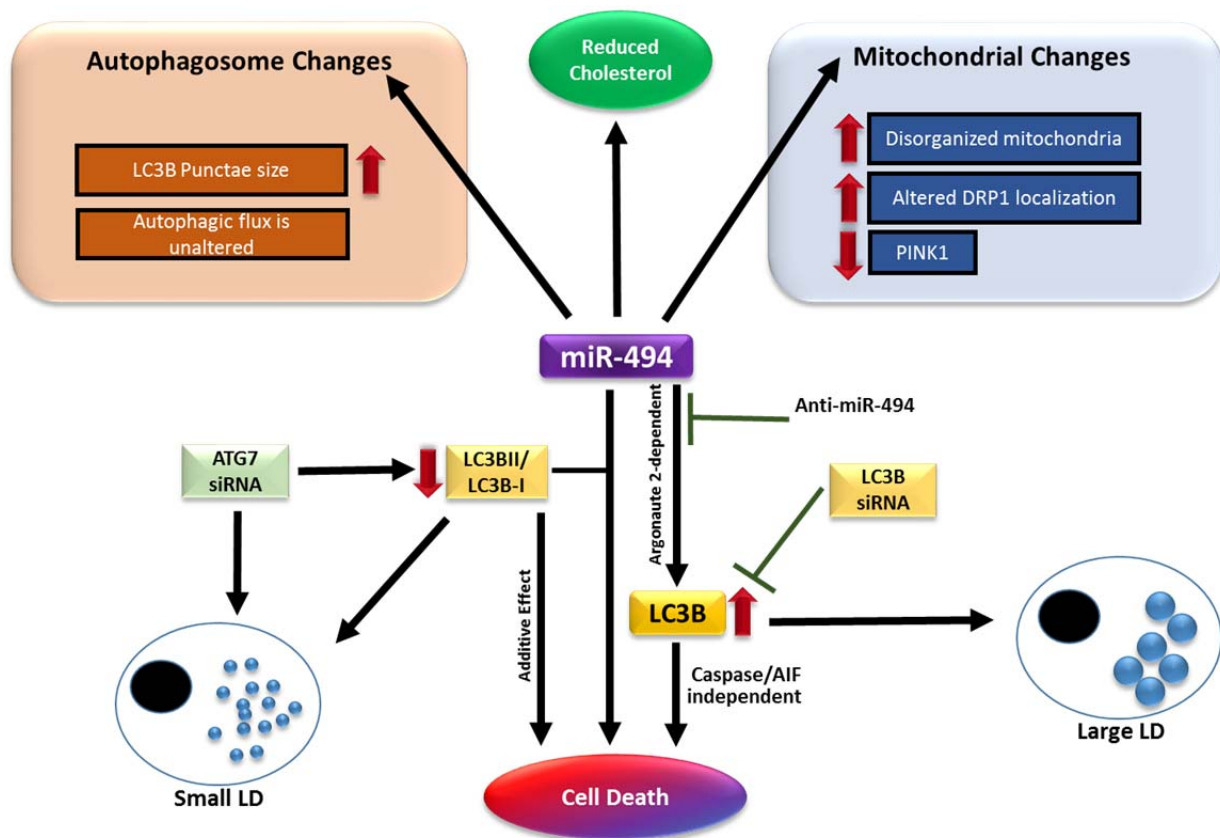


**Figure 32: Schematic of miR-494 functional responses in 769-P renal cancer cells**

miR-494 expression leads to accumulation of LDs, which is mediated by LC3B; however, ATG7 induces small LDs formation, independently of miR-494. miR-494 expression also leads to reduced cholesterol levels and increased mitochondrial structural disorganization. These cellular changes are accompanied by reduced growth and increase in cell death. (\*Figure created by Punashi Dutta)

In order to delineate the cell death mechanism mediated by miR-494, we investigated mitochondrial changes since these are critical in the intrinsic apoptotic pathway. However, we did not witness any change in pro-caspase levels via western analysis or the movement of AIF to the nucleus, an event which occurs in caspase-independent cell death. Cell death upon miR-494 expression occurred with a reduction in PINK1 protein levels (a kinase involved in mitochondrial fission/fusion effects) and altered subcellular localization of Drp1 (a protein associated with mitochondrial fission). The loss of PINK1 has been previously reported to enhance Drp1 recruitment to mitochondria and induce mitochondrial fission, along with increase in oxidative stress and mitophagy [285, 286]. Although, the mitochondrial superoxide levels were found to be unaltered in miR-494 expressing cells, we observed increased LC3B punctae, associated with disorganized mitochondria.

Kidney cancer exhibits metabolic dysfunction including increase in LDs which are composed of triglycerides and cholesterol esters [290]. These LDs have also been found to be increased upon chemotherapeutic treatments such as with simvastatin [291]. Simvastatin is a chemotherapeutic drug that induces apoptosis and there have been reports showing that apoptosis is accompanied by mitochondrial loss of function and increased LD formation [292]. Interestingly, from our studies shown in Figure 30, we noted an increased accumulation of LDs, which was associated with reduced cell survival and increase in late apoptotic cell numbers. Along with changes in cleaved PARP levels and cell death, miR-494 also increased LC3B levels (mRNA and protein). Indeed, as shown in Figure 29A, we saw an increase in endogenous LC3B levels in the parental 769-P cells upon miR-494 expression in the absence of change in autophagic flux. Autophagy is involved in the turnover of lipids, a process referred to as lipophagy [293] and autophagic proteins have major roles in LD biogenesis [279]. Previous studies have demonstrated both ATG7 and LC3B to be associated with LDs [279]. ATG7 is critical in the conjugation of LC3-I to LC3-II; however, since the formation of LDs can occur in an ATG7-independent mechanism since LC3B is known to be localized to LDs both in its

conjugated and non-conjugated form. Therefore, ATG7 is dispensable for this event [294], as also observed in our studies (Figure 30). Consistent with our observation regarding the increase in small LDs with *ATG7* siRNA, *ATG7* knockout mouse model has also been reported to lead to increased LDs [280]. LDs are dynamic organelles and it has been previously reported that the presence of certain proteins at the LD-LD contact site can mediate LD growth by directional transfer of lipids from a smaller to a larger LD [295]. Our findings as reported in this chapter show an increase in LDs upon miR-494 expression, a process that is LC3B dependent and is associated with reduced renal cancer cell survival.

Furthermore, AMPK mediates lipid synthesis by decreasing malonyl-CoA [296] and we observed a significant increase in PRKAG2 (gamma subunit of AMPK) mRNA levels upon miR-494 expression. The increase in LC3B and PRKAG2 upon miR-494 expression implicates the role of miRNAs in positively regulating gene expression, as also reported in other studies [128, 129]. Although we noted the presence of cholesterol clefts in miR-494 expressing cells via TEMs, similar in nature to that reported for atherosclerosis [297]; miR-494 expressing cells exhibited reduced total cellular cholesterol levels. Indeed, the cholesterol disrupting agents such as lovastatin can lead to improved sensitivity to chemotherapeutic agents [278, 298, 299] in cancer cell lines. Our observation that cholesterol levels were increased in our renal cancer cell lines supports this notion that increased cholesterol levels can confer resistance to chemotherapeutic agents and in the present study towards miR-494.

Certain miRNAs have been known to regulate lipid metabolism, via targeting important genes in the pathway. these include miR-33, miR-122, miR-378 and miR-125 [300]. miR-33 is located in the intronic region of *SREBF-2*, a critical regulator of genes involved in cholesterol synthesis [300]. Of interest, certain miRNAs at the 14q locus have also been reported to regulate lipid biogenesis. These include miR-370 [300], miR-376a [301], miR-379 [302] and miR-410 [303]. We propose that miR-494 may be involved in modulating the expression of genes involved in lipid biogenesis altering the turnover of lipids and thus leading to their



accumulation. It will be worthwhile to assess the combinatorial effect of miRNAs at 14q32 locus, in mediating cell death in renal cancers.

### **Acknowledgments**

I extend my sincere gratitude to my mentor, Dr. Meera Nanjundan for her constant guidance, motivation, and support throughout the working of this chapter. I would like to thank Edward Haller, M.S. (Lab Manager, Electron Microscopy Core Lab, Department of Integrative Biology, University of South Florida, Tampa, FL) for the TEM analyses, and Karoly Szekeres, Ph.D. (Scientific Researcher, College of Medicine, Flow cytometry core, University of South Florida, Tampa, FL) for his assistance with flow cytometric analyses.

I would also like to thank Daniel J. Shiwarski, B.S. (University of Pittsburgh), Ruben K. Dagda Ph.D. (University of Nevada School of Medicine, Reno), and Charleen T. Chu M.D., Ph.D. (Pathology Department, University of Pittsburgh) for the development of Image J macro program, utilized for autophagic flux measurements.

## Chapter 6

### Future Directions and Significance of the Study

#### Overview of the Major Findings

Genomic alterations contribute to the development of cancers [11]. Therefore, characterizing specific genes located within these altered chromosomal regions and their associated functions are important in understanding cancer biology. This dissertation focuses on the contribution of specific genes located at the 3q26.2 [1, 2] (EVI1 and SnoN) and 14q32 [23] (miR-494) loci to ovarian and renal cancer pathophysiology, respectively. As presented in Chapter 3, we demonstrated that the knockdown of EVI1 splice variants altered the mRNA and protein levels of certain EMT markers in ovarian and breast cancer cells [14]. We also showed that the migratory potential of these cells was altered upon knockdown of specific EVI1 splice forms. When we measured the expression of miR-200 a/b/c (critical regulators of EMT), we identified that their levels were unchanged in the siME (reduces the expression of MDS1/EVI1 and EVI1<sup>Del190-515</sup>) knockdown cells relative to control siRNA treated cells [14]. When we overexpressed specific EVI1 splice forms, we noted changes in Cyclin E1 expression [14]. In Chapter 4, we focused on another gene located within the 3q26.2 region, SnoN/SkiL. We previously reported that the EGFR and PI3K/AKT pathway contributes to induction of SnoN/SkiL upon drug treatment [17]. In this dissertation, we assessed the contribution of miRNAs in the regulation of SnoN expression upon As<sub>2</sub>O<sub>3</sub> treatment in HEY ovarian cancer cells. We performed *in silico* analysis using several bioinformatics programs and identified a subset of

miRNAs (including miR-494) that could potentially bind to the 3'UTR of *SnoN*. We also identified that miR-494 sensitized HEY cells to As<sub>2</sub>O<sub>3</sub> treatment.

Kroeger and colleagues identified that loss of 14q chromosomal region (which harbors 54 miRNAs) correlates with a worsened patient outcome in clear cell renal carcinoma [23]; however, the method which was employed (cytogenetic analyses) would not be able to determine the exact bases deleted in this region. There are other methods that will allow one to delineate the exact locus deleted giving a clear picture of which genes are altered. However, there are reports that alterations at the 14q32 locus are associated with disease pathogenesis [253, 304]. In Chapter 5, we specifically focused on the contribution of miR-494 (one of the miRNAs located within this cluster) in renal cancer pathophysiology. Several of the so far identified miR-494 targets are associated with reduced cell survival [26, 136-138, 248, 249, 252]; however, the role of miR-494 in renal cancer is presently unknown. In our TCGA analysis, we determined that the expression of miR-494 was reduced in kidney renal clear cell carcinoma (KIRC) samples relative to control specimens (data not shown). We demonstrated that expression of miR-494 in 769-P renal cancer cells reduced cellular viability by partially inducing apoptosis which occurred in a caspase- and AIF-independent manner. We also delineated the involvement of specific autophagic mediators, such as LC3B and ATG7, in miR-494 mediated responses. miR-494 increased both LC3B mRNA and protein levels. Additionally, miR-494 expression altered the structure of the mitochondria and also induced the formation of LDs. The increase in LDs upon miR-494 expression was mediated by LC3B, which could potentially be a direct target of miR-494 (assessed via a luciferase-based assay whereby co-transfection of control or miR-494 mimic was performed with a plasmid harboring the 3'UTR of *LC3B* downstream of the luciferase gene).

## **Chapters 3 and 4: Limitations of the Studies**

In Chapter 3 involving overexpression or knockdown studies of EVI1 splice variants, we acknowledge challenges in data interpretation. Each cell line (with the exception of OVCAR8 cells which contains a deletion at the 3q26.2 locus as determined by aCGH [2]) has a certain baseline expression of specific EVI1 splice variants. By altering expression of one form via overexpression, the ratios of the endogenous specific splice forms are thus altered. Also, since the knockdown is not specific to one splice variant, it is difficult to attribute the altered functional effects to a specific splice variant. For example, siME reduces both MDS1/EVI1 and the EVI1<sup>Del190-515</sup> forms; however, this leads to an increase in the wild type EVI1 form relative to the other splice forms.

In Chapter 4, we identified that miR-494 could sensitize HEY ovarian cancer cells and modulate SnoN/SkiL expression in the presence of As<sub>2</sub>O<sub>3</sub> treatment. As<sub>2</sub>O<sub>3</sub> is used in hematological malignancies as an important chemotherapeutic agent that has been FDA-approved [221]. However, there is little success in its use as a chemotherapeutic agent in solid cancers due to the increased dosage which may lead to toxic effects [305]. Nevertheless, the mechanism underlying SnoN induction upon treatment with drugs is of importance because platinum-based drugs such as cisplatin also induce SnoN (results not shown). This mechanism of SnoN up-regulation needs to be further investigated.

## **Chapter 5: Potential Mechanisms Underlying Altered Mitochondrial Organization and Accumulation of LDs with miR-494 Expression**

### miR-494 expression increases LC3B levels: implications in lipid metabolism

LDs are cellular organelles composed of triacylglycerol and cholesterol esters, primarily involved in the storage of lipids [306]. As presented in Figure 30 and 29, we observed an increase in LDs and LC3B punctae size in miR-494 expressing cells in the absence of changes

in autophagic flux. Since LC3B localizes to LDs [279], we attempted to determine whether LC3B also localized to LDs under our experimental conditions (i.e. miR-494 expression in 769-P cells). To address this question, we performed co-staining using the LC3B antibody with a neutral lipid dye (LipidTOX). Using our LC3B antibody (rabbit polyclonal) which requires methanol fixation followed by LipidTOX staining, our results indicated that methanol fixation alters lipid structure as previously reported [307]. Indeed, the use of  $-20^{\circ}\text{C}$  temperature-methanol or acetone fixation removes phospholipids from the LD membrane and promotes fusion of LDs [307].

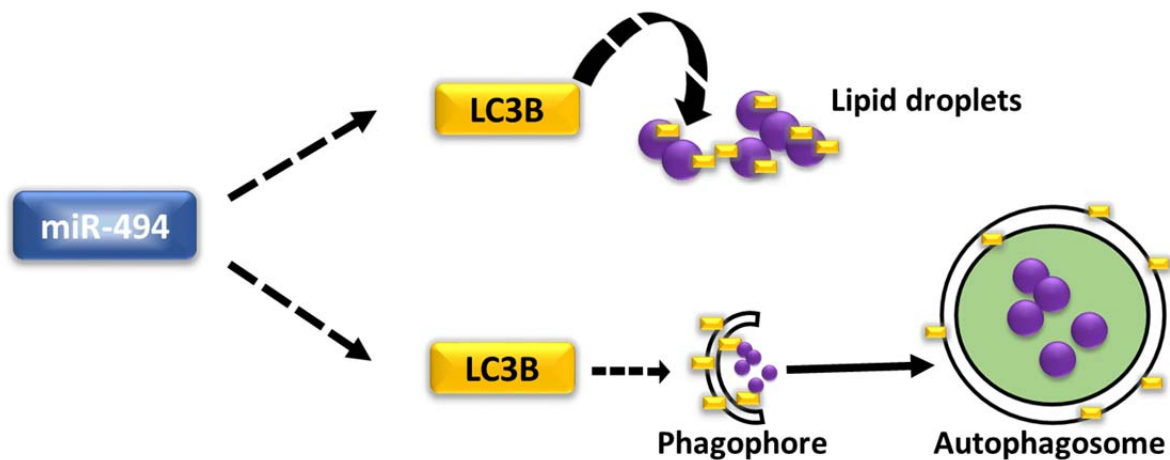


**Figure 33: miR-494 leads to increased LC3B levels - implications in lipid metabolism**

miR-494 expression increases LC3B punctae accompanied with an increase in LC3B protein and mRNA levels. We propose that these LC3B punctae may associate with LD membranes or the autophagosome membranes engulfing LDs, or both. (\*Figure created by Punashi Dutta)

Formaldehyde is the suggested fixation method which preserves the structure of the LDs [307]. Therefore, it was not technically possible to address our experimental question with the presently available tools. We suggest that an antibody against LC3B which requires formaldehyde fixation (which presently does not exist) would allow co-staining with LipidTOX. The outcome of this experiment once tools become available may indicate that LC3B may localize to both the LD membrane and the autophagosomal membrane, following miR-494 expression. This is schematically depicted in Figure 33; we hypothesize that LC3B localizes to

LDs and/or to the autophagosome membrane, leading to the engulfment and clearance of LDs via autophagy (lipophagy) [293]. We propose that this could be assessed by TEM using immunogold-labelled LC3B antibody. The outcome of this study would provide information with regard to the co-localization of LC3B with LDs and/or autophagosomes. This information will be important to connect our observations between LC3B levels, autophagosome size, and LD numbers in miR-494 expressing cells.

### Contribution of miR-494 in lipid metabolism

It is well known that both saturated and unsaturated fatty acids such as palmitate (16:0) and oleate (18:1cis<sup>9</sup>) alter autophagic responses [308]. In Chapter 5, we demonstrate that miR-494 increases LD numbers, (which store fatty acids in the form of triacylglycerol) [306] and LC3B levels (an important mediator of autophagy) [309]. To determine whether miR-494 expression alters the levels of saturated/unsaturated fatty acids which may in turn modulate autophagic and/or other cellular responses, we propose that one could assess the fatty acid (and other lipid) profile in miR-494 expressing cells. To address this question, one could perform lipidomic [310] studies involving GC-MS (Gas Chromatography-Mass Spectrometry). In order to identify miR-494 targets in the lipid metabolism pathway [311], we performed *in silico* analysis using TargetScan; we identified a subset of genes that harbored miR-494 binding sites (Table 6). One such potential target included PPAP2C (phosphatidic acid phosphatase type 2C), which is involved in *de novo* synthesis of phospholipids and glycerolipids [312]. Its family member, PPAP2A, has been reported to be significantly up-regulated upon simvastatin treatment, a cholesterol depleting agent, which leads to the formation of LDs coincident with an apoptotic response [291]. In this regard, we propose that studies could be performed to investigate whether PPAP2C is altered upon treatment with miR-494 but also cholesterol depleting drugs. We also performed RT<sup>2</sup>-PCR pathway focused array for genes involved in lipoprotein signaling as well as cholesterol metabolism and found that the gamma catalytic subunit of AMPK

(PRKAG2) was significantly up-regulated upon miR-494 expression (results not shown). AMPK mediates lipid synthesis by decreasing malonyl-CoA levels; it is an enzyme that maintains balance between fatty acid  $\beta$ -oxidation and lipogenesis [296]. Regrettably, we could not validate changes in its protein levels upon miR-494 expression. In order to further identify miR-494 targets which may promote accumulation of LDs, we propose that other pathway focused RT<sup>2</sup>-PCR arrays such as the fatty acid metabolism array could be employed. Dysregulated cholesterol biosynthesis is implicated in clear cell renal carcinoma [313]. Indeed, cholesterol levels in cells expressing miR-494 were reduced. One drawback of the amplex red cholesterol assay that we employed to measure cholesterol content is that it measures total cell cholesterol content instead of that specific to LDs which contains triacylglycerol and cholesterol esters [306]. Therefore, to measure triacylglycerol and cholesterol esters amounts specifically associated with the LD core, we would need to purify the LD enriched fraction from control and miR-494 expressing cells and then measure cholesterol levels.

#### Involvement of miR-494 in mitochondrial dynamics and mitophagy

Mitochondria are dynamic organelles that are constantly undergoing fission and fusion events [314]. Specific proteins have been so far identified to be involved in these important processes. The PINK1/Parkin pathway is essential in the maintenance of mitochondrial integrity [315] and the loss of PINK1 inhibits Drp1-dependent mitochondrial fission, promoting mitophagy (an autophagic process which clears damaged mitochondria) [286] [285]. In addition, autophagy proteins, ATG7 and LC3B, are involved in mitochondrial fragmentation [285]. As reported in Chapter 5, we observed distinct changes (either protein levels/intracellular

**Table 6: A summary of a subset of genes involved in lipid metabolism harboring miR-494 binding sites**

Gene Abbreviation	Gene Name	Type of Binding (perfect/imperfect)	Number of Sites
ACACa	Acetyl-CoA Carboxylase Alpha	perfect	1
ACACb	Acetyl-CoA Carboxylase Beta	perfect	1
AGPAT3	1-acylglycerol-3-phosphate O-acyltransferase 3	perfect/imperfect	1/1
AGPAT4	1-acylglycerol-3-phosphate O-acyltransferase 4	imperfect	1
AGPAT5	1-acylglycerol-3-phosphate O-acyltransferase 5	perfect	1
AGPAT6	1-acylglycerol-3-phosphate O-acyltransferase 6	imperfect	1
AMACR	alpha-methylacyl-CoA racemase	perfect	1
ASAH1	N-acylsphingosine amidohydrolase (acid ceramidase) 1	imperfect	1
B4GALT6	UDP-Gal:betaGlcNAc beta 1,4- galactosyltransferase, polypeptide 6	perfect/imperfect	2/1
BDH1	3-hydroxybutyrate dehydrogenase, type 1	perfect	1
CHPT1	choline phosphotransferase 1	imperfect	1
CH25H	cholesterol 25-hydroxylase	perfect	2
CYP4F3	cytochrome P450, family 4, subfamily F, polypeptide 3	imperfect	1
CYP3A4	cytochrome P450, family 3, subfamily A, polypeptide 4	perfect	1
DHCR24	24-dehydrocholesterol reductase	perfect	1
ENPP1	ectonucleotide pyrophosphatase/phosphodiesterase 1	perfect/imperfect	1/2
ENPP5	ectonucleotide pyrophosphatase/phosphodiesterase 5 (putative)	imperfect	1
GPD2	glycerol-3-phosphate dehydrogenase 2 (mitochondrial)	perfect/imperfect	1/1
LCLAT1	lysocardiolipin acyltransferase 1	perfect/imperfect	1/1
MOGAT2	monoacylglycerol O-acyltransferase 2	perfect	1
PCYT1A	phosphate cytidylyltransferase 1, choline, alpha	imperfect	1
PPAP2C	phosphatidic acid phosphatase type 2C	imperfect	1
SGMS1	sphingomyelin synthase 1	perfect/imperfect	1/1
SGPL1	sphingosine-1-phosphate lyase 1	perfect	1
SRD5A1	steroid-5-alpha-reductase, alpha polypeptide 1 (3-oxo-5 alpha-steroid delta 4-dehydrogenase alpha 1)	imperfect	1
UGT1A4	UDP glucuronosyltransferase 1 family, polypeptide A4	perfect	1
UGT2A1	UDP glucuronosyltransferase 2 family, polypeptide A1, complex locus	perfect	1
UGT1A3	UDP glucuronosyltransferase 1 family, polypeptide A3	perfect	1
UGT1A6	UDP glucuronosyltransferase 1 family, polypeptide A6	perfect	1
UGT1A9	UDP glucuronosyltransferase 1 family, polypeptide A9	perfect	1
UGT2B17	UDP glucuronosyltransferase 2 family, polypeptide B17	perfect	1
UGT8	UDP glycosyltransferase 8	perfect	1



localization) in several of these above-described proteins, involved in mediating mitochondrial changes. Indeed, in miR-494 expressing cells, we observed reduced PINK1 protein, increased LC3B mRNA and protein, and altered subcellular localization of Drp1. We propose that it would be important to understand how miR-494 modulates changes in these key proteins to better understand the contribution of miR-494 in altering mitochondrial dynamics and the mitophagy pathway. Although we identified LC3B as a target of miR-494 (through a 3'-UTR luciferase-based assay), it is likely that the other proteins (Drp1, Parkin, and PINK1) are regulated in an indirect manner since there were no miR-494 binding sites in the 3'UTR of PINK1, Parkin, or Drp1 via TargetScan. We propose that miR-494 may modulate expression of an upstream gene in the mitochondrial/mitophagy pathway which would indirectly affect PINK1 and Drp1. For example, NF $\kappa$ B signaling has been reported to induce PINK1 expression [316]; although miR-494 induces expression of inflammatory cytokines in an NF- $\kappa$ B-dependent manner, it has yet to be shown whether miR-494 modulates upstream signaling leading to activation of NF- $\kappa$ B [317]. PINK1 recently is reported to regulate cell cycle progression and promote cell survival [318]; thus, it would be worthwhile to determine whether miR-494 alters cell cycle progression since we observed reduced PINK1 levels which is accompanied by reduced cellular growth.

#### Accumulation of LDs in miR-494 expressing cells: mitochondrial involvement

During starvation, cytoplasmic lipases hydrolyzes LDs to glycerol (which is converted to glucose by the liver) and fatty acids [319]. These fatty acids are substrates for  $\beta$ -oxidation leading to the formation of acetyl CoA, which is used in the Krebs cycle; these steps occur in the mitochondrial compartment [319]. Evidence implicates mitochondrial dysfunction or induction of apoptosis leads to inhibition of mitochondrial  $\beta$ -oxidation resulting in re-direction of the fatty acids to LDs which then accumulate [292] [320] [321] [322]. Recent studies by Rambold and colleagues implicate both the autophagy and lipolysis pathways in the trafficking

of fatty acids in starved cells [320]. Further, inhibition of mitochondrial fusion redirected fatty acids back to the LDs [320]. Indeed, in Chapter 5, we demonstrated that miR-494 increased LDs, accompanied by mitochondrial structural disorganization, reduced cell survival, and increased apoptotic cells. In order to determine whether miR-494 alters the rate of  $\beta$ -oxidation, we propose to measure mitochondrial oxygen consumption rate (mtOCR) in miR-494 expressing cells.

Since we observed accumulation of fragmented mitochondria, we propose that miR-494 may modulate targets that are involved in mitochondrial fusion (which is needed for transfer of fatty acids from LDs to mitochondria). Indeed, the 3'-UTR of mitofusin-1 (Mfn1) and mitofusin-2 (Mfn2) (major proteins involved in mitochondrial fusion [323]) contain miR-494 binding sites.

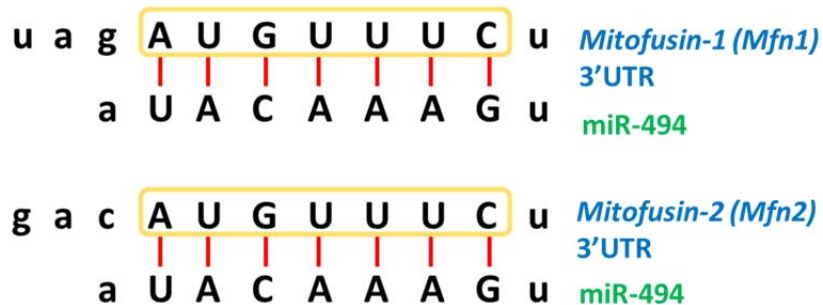


**Figure 34: Mfn1/Mfn2 - potential targets of miR-494**

Schematic showing the perfect complementarity of miR-494 binding sites within the 3'UTRs of Mfn1 and Mfn2. (\*Figure created by Punashi Dutta)

As depicted in Figure 34, there are perfect miR-494 binding sites in the 3'UTR of both *Mfn1* and *Mfn2*. We hypothesize that miR-494 could modulate mitochondrial fusion by directly regulating the gene expression of Mfn1 and Mfn2. Since we observed increased Drp1 localization to mitochondria in miR-494 expressing cells (suggestive of increased mitochondrial fission), we propose that miR-494 expressing cells have reduced rates of mitochondrial fusion

which may then lead to increased numbers of fragmented mitochondria. Increased mitochondrial fragmentation is associated with increased apoptosis [324] [325-327] and/or mitophagy [285]. Figure 35 depicts a proposed model for the miR-494-mediated mitochondrial dynamic changes.

Increase in reactive oxygen species are major causes of oxidative stress-induced mitochondrial dysfunction and damage [328]. Although we did not observe any changes in mitochondrial superoxide levels in miR-494 expressing cells compared to control cells, there may be changes in other reactive oxygen species (ROS) such as hydrogen peroxide and hydroxyl radical [329], which may be worthwhile investigating.

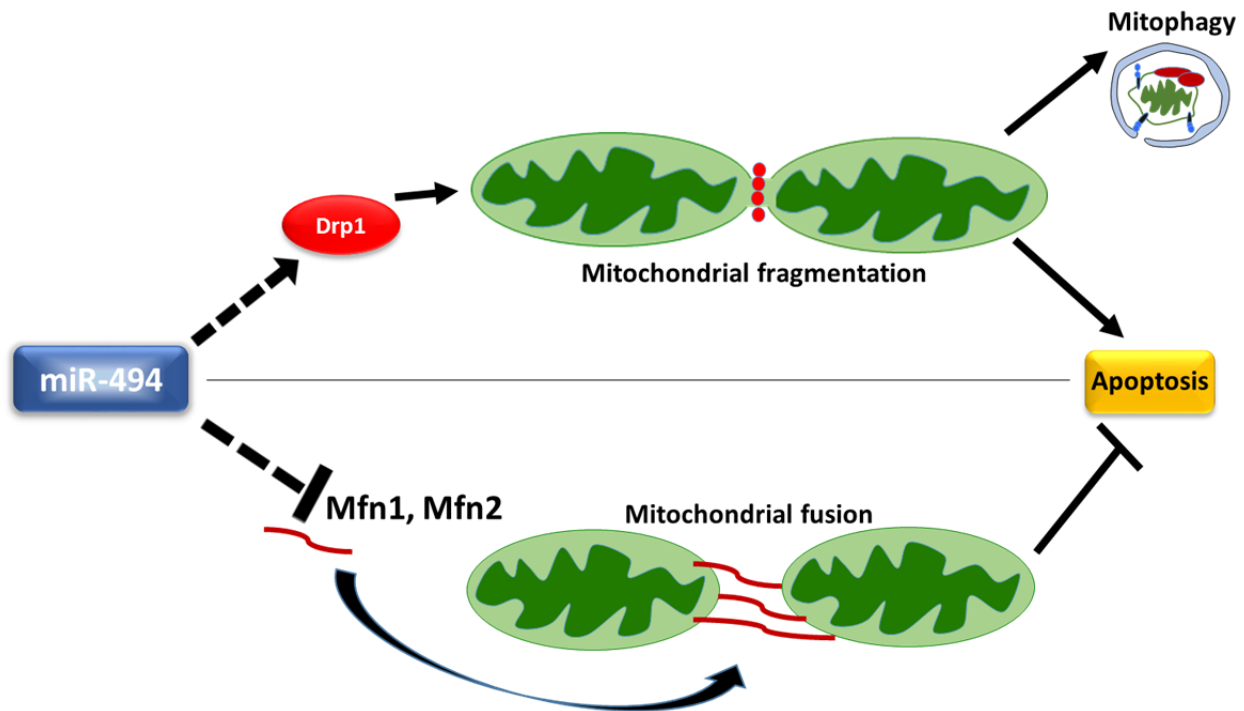


**Figure 35: Potential contribution of miR-494 to the mitochondrial fission/fusion events**

We propose that miR-494 expression induces the localization of Drp1 to mitochondrial fission sites, leading to mitochondrial fragmentation, mitophagy, and apoptosis. Additionally, we propose that miR-494 targets Mfn1/2 and thus inhibits mitochondrial fusion, leading to apoptosis. (\*Figure created by Punashi Dutta)

## Cross-talk between miR-494 and the pro-survival Bcl-2 molecule

Although we observed a reduction in Bcl-2 protein levels in miR-494 expressing cells via western blotting analyses (Chapter 5), 3'-UTR luciferase assays failed to demonstrate Bcl-2 as a direct target of miR-494. However, this suggests an inverse association between Bcl-2 and miR-494. Interestingly, Bcl-2 opposes BNIP1-mediated Drp1 recruitment to mitochondrial fission sites [330] (Figure 36A). Since we observed reduced Bcl-2 protein and increased recruitment of Drp1 to mitochondria in miR-494 expressing cells, we hypothesize that the presence of Bcl-2 may antagonize Drp-1 recruitment to mitochondrial fission sites; this would lead to increased mitochondrial fusion.

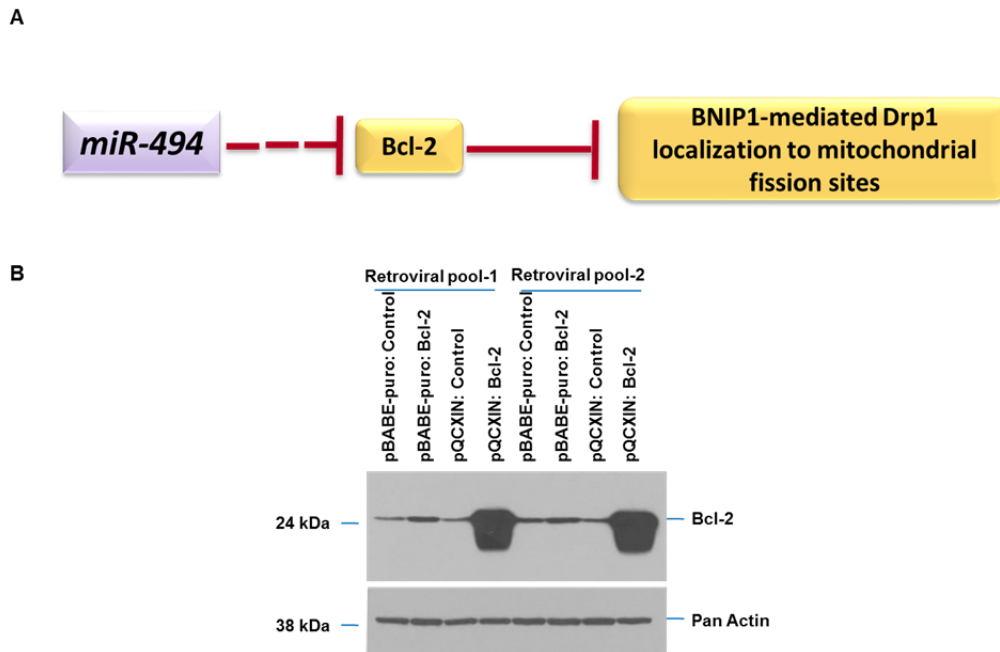


**Figure 36: Potential cross-talk between Bcl-2 and miR-494**

(A) Schematic of our proposed hypothesis whereby miR-494 reduces Bcl-2 protein which is reported to inhibit Drp-1 mediated mitochondrial fission. The cumulative effect of this pathway would then lead to increase mitochondrial fission in miR-494 expressing cells via Drp1. (\*Figure created by Punashi Dutta). (B) Parental 769-P cells stably expressing pBABE-puro-Bcl-2 or mCherry-GFP-LC3B 769-P cells stably expressing pQCXIN-Bcl-2 were seeded at 250,000 cells/well. Protein lysates were harvested 48 hours post-seeding. Samples were run on a 10% SDS-PAGE gel and western blotting analyses were performed using the specified antibodies.

We have begun to address this hypothesis by generating Bcl-2 overexpressing 769-P parental and mCherry-GFP-LC3B stable cell lines (Figure 36B). We propose to perform rescue experiments by expressing miR-494 in these Bcl-2 overexpressing stable cell lines; we would then assess changes in LD formation, Drp1 recruitment to mitochondria, modulation of autophagosome size, and cell death responses. If the reduction in Bcl-2 levels is required for the observed miR-494 cellular changes, we expect that Bcl-2 would antagonize the cellular responses mediated by miR-494.

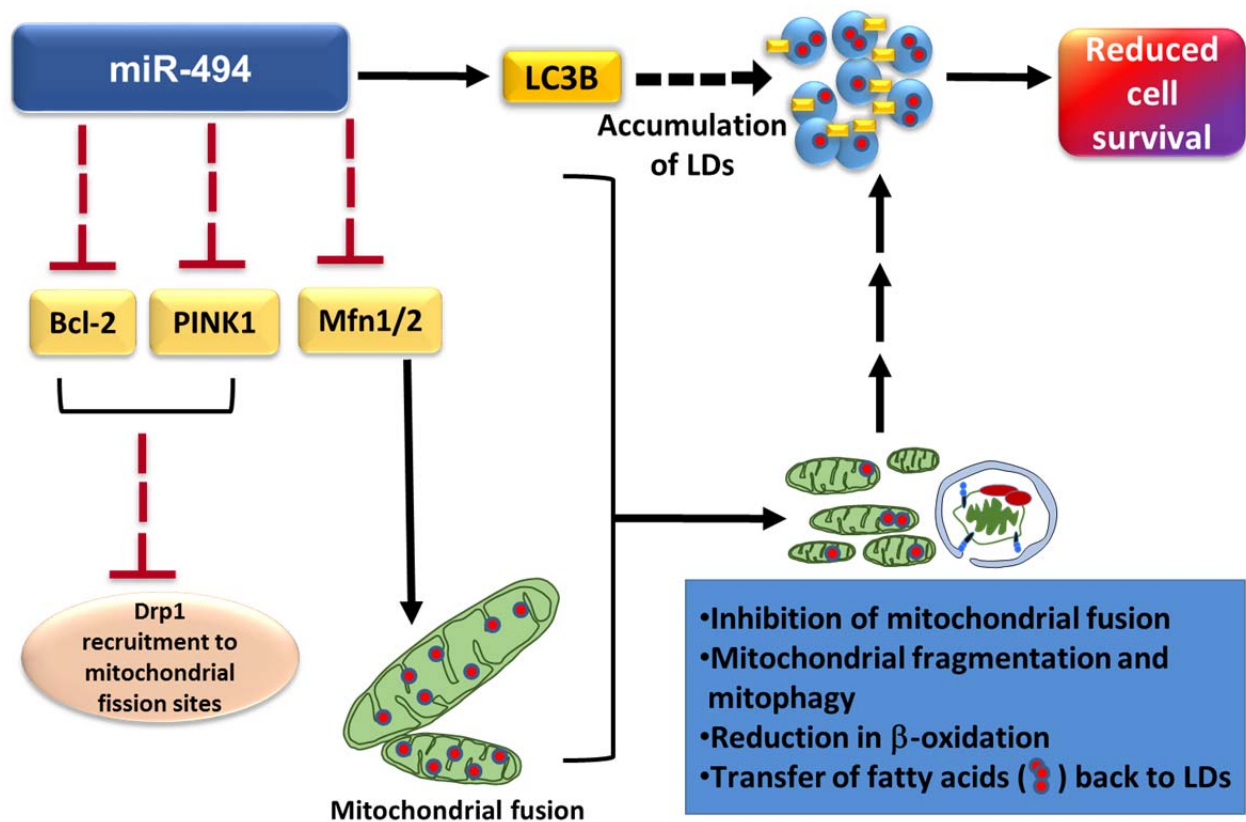


Figure 37: Overall model of proposed cellular effects mediating the cell death response elicited by miR-494 (\*Continued on next page)

### **Figure 37: Overall model of proposed cellular effects mediating the cell death response elicited by miR-494**

The model as presented summarizes our findings and links these to published reports in order to better understand the potential effects of miR-494 in lipid metabolism and mitochondrial dynamics. We propose that miR-494 targets Bcl-2, PINK-1, and Mfn1/2 thus increasing Drp-1 mediated mitochondrial fission. We have shown herein, that miR-494 increases LC3B expression. We propose that LC3B localizes to LDs. Collectively, these effects lead to inhibition of mitochondrial fusion, transfer of fatty acids back to the mitochondria, reduction in  $\beta$ -oxidation, and reduced cellular survival. (\*Figure created by Punashi Dutta)

A schematic of our model depicting all the key proteins involved in miR-494-mediated responses is shown in Figure 37. We propose that miR-494 increases LC3B mRNA and protein levels, leading to increased co-localization of LC3B to LDs. miR-494 also reduces Bcl-2 and PINK1 protein levels and both these proteins antagonize the movement of Drp1 to mitochondrial fission sites, which inhibit mitochondrial fragmentation and mitophagy [285, 286, 330]. Since we identified miR-494 perfect match binding sites in the 3'UTR of both Mitofusin-1/2 via an *in silico* approach, a reduction in mitofusin expression may thus lead to increased Drp1 localization to mitochondria. This would next lead to fragmented mitochondria which would be deficient in  $\beta$ -oxidation, causing an efflux of fatty acids from mitochondria to the LDs which would subsequently lead to an over-accumulation of LDs and thus, cell death.

### **Contribution of the miRNA Cluster at 14q32 in Renal Cancer Pathophysiology**

A study conducted by Laddha and colleagues analyzed the expression of the 14q32 genomic cluster miRNAs across various cancers and found 61% of these to be down-regulated in renal cancer [304]. Several miRNAs at 14q32 regulate autophagic mediators. These include miR-379 which targets LAMP-2A [331], miR-376a and miR-376b which target ATG4C and beclin-1 [332, 333], and miR-410 which targets AMPK $\alpha$  [334]. Additionally, several other miRNAs at 14q32 regulate genes in the lipid biosynthesis pathway including miR-370 [300], miR-376a [301], miR-379 [302], and miR-410 [303]. However, the detailed role of this miRNA

cluster in renal cancer biology is presently unclear. Therefore, it would be worthwhile to investigate the contribution of the other miRNAs present at the 14q32 locus in autophagy and/or altered lipid metabolism.

A custom-design screen using a 96-well plate format in which each well contain a miRNA mimic (54 wells in total) could be designed for this purpose. By reverse transfection in parental 769-P cells, the formation of LDs would be assessed using LipidTOX green neutral lipid stain. This would be analyzed either manually or using an INCell Analyzer, if available. In a similar procedure, 769-P renal cancer cells stably overexpressing mCherry-GFP-LC3 would allow assessment of red/green punctae to identify changes in autophagic flux and autophagosome size. Additionally, a MTT survival assay using the above custom-designed screen and parental 769-P renal cancer cells could be performed to assess changes in cell viability. The positive hits that are identified via this screening strategy would then be assessed in *in vitro* experiments (using mimic and/or antagomirs). Since genes harboring neighboring loci on the chromosome may co-operatively regulate common cellular processes [335], we speculate that expression of a combination of a subset of these miRNAs in renal cancer cells may induce robust cellular changes including cell growth and viability.

### **Renal Cancer Specimens: Cellular Changes with Altered miR-494 Expression**

TCGA analysis demonstrated that miR-494 levels were reduced by 32% in KIRC samples compared to normal (results not shown). To follow-up on this observation, we propose to assess changes in patient survival and chemotherapeutic responsiveness in panel of normal and renal cancer patient specimens with high/low expression of miR-494. It would also be worthwhile to assess fatty acid/phospholipid levels and mitochondrial dynamics across different stages of renal cancers. Additionally, using a real-time PCR and western analysis approaches, changes in mRNA and protein of autophagy markers in KIRC samples (compared to normal) across different stages of kidney cancer could be assessed. From kidney tumor specimens,

miR-494 levels and Bcl-2, PINK1, LC3B, Mfn1/2 mRNA, and protein levels can be assessed. Immunohistochemical analysis of cytochrome c, Drp1, and LC3B could be performed on the tissue specimens. Additionally, lipidomic studies and fatty acid measurements could also be performed on these specimens. The resultant data could also then be correlated to patient clinical variables.

### **Renal Cancer Mouse Models: Effects of miR-494 on Tumor Growth**

To determine whether miR-494 alters *in vivo* tumor growth, we propose two different orthotopic cancer xenograft mouse studies as shown in Figure 7. For the purpose of the first study, stable cell lines overexpressing control (vector backbone) or miR-494 would be established. These cells will then be injected under the kidney capsule directly into the proximal kidney tubule of athymic nude mice, as shown in Figure 38. After the tumors are established, they would be excised from the mice and assessed for size/volume and histological features. Immunohistochemical analyses of the tumor sections will be performed to assess morphological changes including dysfunctional mitochondria and accumulation of LDs. TEM analysis will allow us to determine whether there is an alterations in LD formation. Using these specimens, we will also measure changes in mitochondrial  $\beta$ -oxidation.

In the second study, we will establish the tumor by subcutaneously injecting cancer cells into the athymic nude mice (Figure 38). After the establishment of the tumor, we would inject miR-494 mimic via an intratumoral injection into the mice. In order for the miRNA gene delivery strategies to be successful, it is of importance that certain hurdles such as their instability *in vivo*, inappropriate distribution, or off-target effects are overcome [336]. A recent study has suggested that the use of lipid-based vesicles, Stable Nucleic Acid Lipid Particles (SNALPs), as a tool for encapsulated delivery of miRNA mimic for *in vivo* studies may ease the miRNA mimic



1

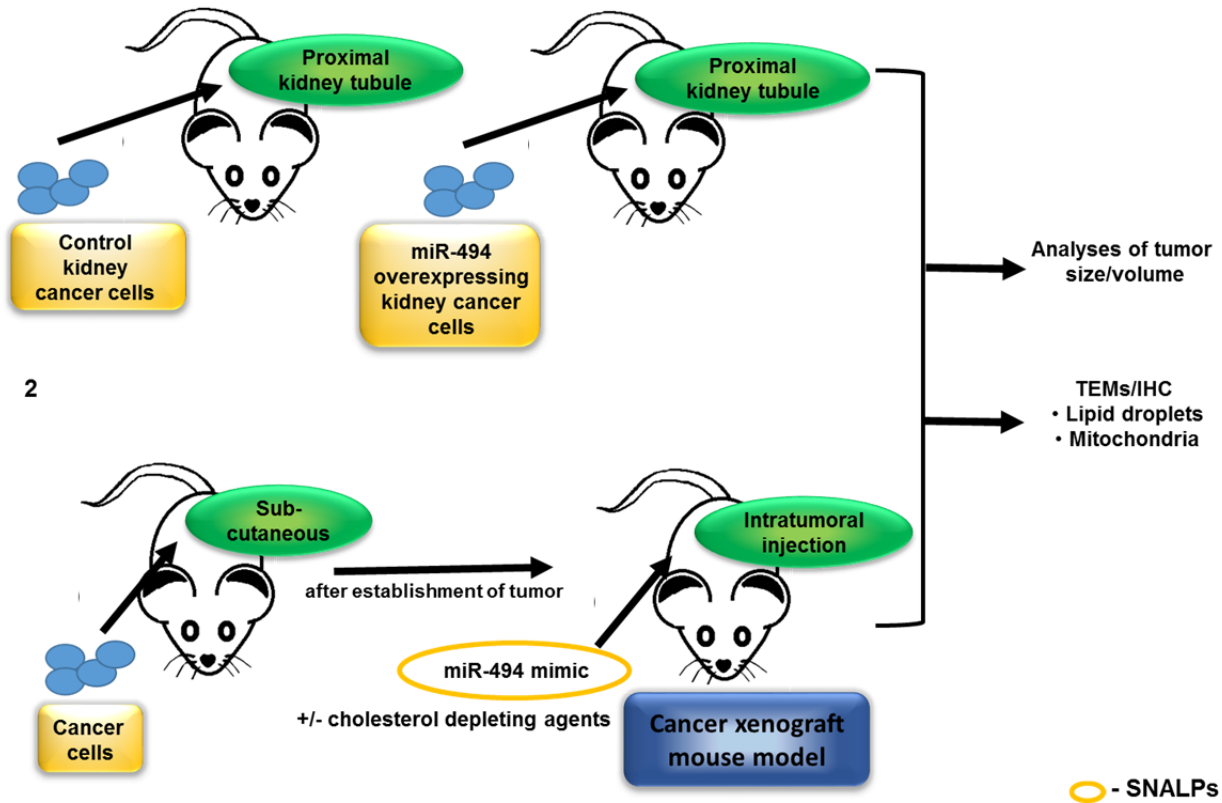


**Figure 38: Proposed experimental outline to investigate the effects of miR-494 on tumor growth in mouse model**

Two different mouse models are proposed in the figure. In the first mouse study, miR-494 expressing retroviral stable cell lines would be established and then injected into the proximal kidney tubule of an athymic nude mouse. After establishment and excision of the tumor following appropriate time period, analyses would be performed as indicated. In the second mouse study, cancer cells would be injected subcutaneously into the mice. After the establishment of the tumor, miR-494 mimic would be injected intratumorally into the mice using SNALPs. This study would be performed with or without the use of cholesterol depleting agents. Further analyses would be performed as indicated in the figure. (\*Figure created by Punashi Dutta)

delivery [337]. This strategy for miRNA mimic delivery could be utilized for the above study. Similar analytical strategy will be employed as described in the first study.

As mentioned earlier, depletion of cholesterol activates the apoptotic response in cells; certainly, inhibitors that block cholesterol biosynthesis can induce apoptosis [278, 298, 299]. HMG CoA-reductase (an important enzyme involved in cholesterol biosynthesis) inhibitors such

as lovastatin and simvastatin reduce cholesterol levels and induce apoptosis [338] [291]. Since renal cancer is a metabolic disease [41] with altered lipid metabolism, and cholesterol accumulation plays an important role in the disease progression [313], it would also be worthwhile to analyze the effect of these drugs along with miR-494 mimic in renal cancer cells to determine whether the addition of mimic can further strengthen the cell death response. Once we gain more insight into the outcome of this combinatorial regime in *in vitro* studies, these studies could then be applied *in vivo*, using a kidney cancer xenograft mouse model, as described above.

Since miR-494 has not yet been studied in terms of organismal development, there is no information regarding whether this non-coding RNA is essential for survival or development of mice. There has not been any report as yet involving study with a miR-494 transgenic or knockout mouse model. It is presently unknown if such mice would be embryonically lethal or not. Therefore, we would generate a miR-494 whole-body transgenic and knockout mouse model and if these mice fail to live, we would then generate a tissue-specific mouse model for the kidney by using the kidney proximal tubule-specific type 1  $\gamma$ -glutamyltranspeptidase promoter to drive the overexpression/knockdown [339]. The miR-494 knockout mouse model can be crossed with the PIK3CA mutant mouse (which has increased propensity to develop cancer); such mice will then be injected with adenoviral CRE recombinase harboring PIK3CA mutation [340] (renal cancer exhibit mutations at the 3q region [43]) and the tumor progression will be assessed.

## **Acknowledgments**

I would like to acknowledge the contribution of my mentor, Dr. Meera Nanjundan for the cloning Bcl-2 into *pBABE-puro* and *pQCXIN* plasmids. I would like to kindly thank Dr. Meera Nanjundan for her valuable guidance and inputs in the discussion herein. I acknowledge the contribution of undergraduate students, Gautam-Krishna Koipallil and Joseph Raffel for their

assistance in performing the *in silico* analysis for assessing miR-494 binding sites in the 3'UTR of genes involved in the lipid biogenesis pathway.

## References

1. Nanjundan, M., et al., *Overexpression of SnoN/SkiL, amplified at the 3q26.2 locus, in ovarian cancers: a role in ovarian pathogenesis*. Mol Oncol, 2008. **2**(2): p. 164-81.
2. Nanjundan, M., et al., *Amplification of MDS1/EVI1 and EVI1, located in the 3q26.2 amplicon, is associated with favorable patient prognosis in ovarian cancer*. Cancer Res, 2007. **67**(7): p. 3074-84.
3. Jazaeri, A.A., et al., *Evaluation of EVI1 and EVI1s (Delta324) as potential therapeutic targets in ovarian cancer*. Gynecol Oncol, 2010. **118**(2): p. 189-95.
4. Fears, S., et al., *Intergenic splicing of MDS1 and EVI1 occurs in normal tissues as well as in myeloid leukemia and produces a new member of the PR domain family*. Proc Natl Acad Sci U S A, 1996. **93**(4): p. 1642-7.
5. Wullschleger, S., R. Loewith, and M.N. Hall, *TOR signaling in growth and metabolism*. Cell, 2006. **124**(3): p. 471-84.
6. Kalluri, R. and R.A. Weinberg, *The basics of epithelial-mesenchymal transition*. J Clin Invest, 2009. **119**(6): p. 1420-8.
7. Finnegan, E.F. and A.E. Pasquinelli, *MicroRNA biogenesis: regulating the regulators*. Crit Rev Biochem Mol Biol, 2013. **48**(1): p. 51-68.
8. Levine, B. and G. Kroemer, *Autophagy in the pathogenesis of disease*. Cell, 2008. **132**(1): p. 27-42.
9. Pattingre, S., et al., *Bcl-2 antiapoptotic proteins inhibit Beclin 1-dependent autophagy*. Cell, 2005. **122**(6): p. 927-39.
10. Glick, D., S. Barth, and K.F. Macleod, *Autophagy: cellular and molecular mechanisms*. J Pathol, 2010. **221**(1): p. 3-12.
11. Beroukhi, R., et al., *The landscape of somatic copy-number alteration across human cancers*. Nature, 2010. **463**(7283): p. 899-905.
12. Etemadmoghadam, D., et al., *Integrated genome-wide DNA copy number and expression analysis identifies distinct mechanisms of primary chemoresistance in ovarian carcinomas*. Clin Cancer Res, 2009. **15**(4): p. 1417-27.
13. Cancer Genome Atlas Research, N., *Integrated genomic analyses of ovarian carcinoma*. Nature, 2011. **474**(7353): p. 609-15.
14. Dutta, P., et al., *EVI1 splice variants modulate functional responses in ovarian cancer cells*. Mol Oncol, 2013. **7**(3): p. 647-68.
15. Smith, D.M., et al., *Arsenic trioxide induces a beclin-1-independent autophagic pathway via modulation of SnoN/SkiL expression in ovarian carcinoma cells*. Cell Death Differ, 2010. **17**(12): p. 1867-81.
16. Cai, J., et al., *The role of the PTEN/PI3K/Akt pathway on prognosis in epithelial ovarian cancer: a meta-analysis*. Oncologist, 2014. **19**(5): p. 528-35.

17. Kodigepalli, K.M., et al., *SnoN/SkiL expression is modulated via arsenic trioxide-induced activation of the PI3K/AKT pathway in ovarian cancer cells*. FEBS Lett, 2013. **587**(1): p. 5-16.
18. Deheuninck, J. and K. Luo, *Ski and SnoN, potent negative regulators of TGF-beta signaling*. Cell Res, 2009. **19**(1): p. 47-57.
19. Levati, L., et al., *MicroRNA-155 targets the SKI gene in human melanoma cell lines*. Pigment Cell Melanoma Res, 2011. **24**(3): p. 538-50.
20. Teichler, S., et al., *MicroRNA29a regulates the expression of the nuclear oncogene Ski*. Blood, 2011. **118**(7): p. 1899-902.
21. Jiang, H., et al., *Next generation sequencing analysis of miRNAs: MiR-127-3p inhibits glioblastoma proliferation and activates TGF-beta signaling by targeting SKI*. OMICS, 2014. **18**(3): p. 196-206.
22. Li, J., et al., *MiR-21 inhibits c-Ski signaling to promote the proliferation of rat vascular smooth muscle cells*. Cell Signal, 2014. **26**(4): p. 724-9.
23. Kroeger, N., et al., *Deletions of chromosomes 3p and 14q molecularly subclassify clear cell renal cell carcinoma*. Cancer, 2013. **119**(8): p. 1547-54.
24. Kim, W.K., et al., *MicroRNA-494 downregulates KIT and inhibits gastrointestinal stromal tumor cell proliferation*. Clinical cancer research : an official journal of the American Association for Cancer Research, 2011. **17**(24): p. 7584-94.
25. Yamanaka, S., et al., *Coordinated effects of microRNA-494 induce G(2)/M arrest in human cholangiocarcinoma*. Cell Cycle, 2012. **11**(14): p. 2729-38.
26. Zhang, R., et al., *Upregulation of miR-494 Inhibits Cell Growth and Invasion and Induces Cell Apoptosis by Targeting Cleft Lip and Palate Transmembrane 1-Like in Esophageal Squamous Cell Carcinoma*. Dig Dis Sci, 2014.
27. Rauh-Hain, J.A., et al., *Ovarian cancer screening and early detection in the general population*. Rev Obstet Gynecol, 2011. **4**(1): p. 15-21.
28. Vaughan, S., et al., *Rethinking ovarian cancer: recommendations for improving outcomes*. Nat Rev Cancer, 2011. **11**(10): p. 719-25.
29. Prat, J., *Ovarian carcinomas: five distinct diseases with different origins, genetic alterations, and clinicopathological features*. Virchows Arch, 2012. **460**(3): p. 237-49.
30. Kim, A., et al., *Therapeutic strategies in epithelial ovarian cancer*. J Exp Clin Cancer Res, 2012. **31**: p. 14.
31. Dasari, S. and P.B. Tchounwou, *Cisplatin in cancer therapy: molecular mechanisms of action*. Eur J Pharmacol, 2014. **740**: p. 364-78.
32. Monk, B.J., et al., *Antiangiogenic agents as a maintenance strategy for advanced epithelial ovarian cancer*. Crit Rev Oncol Hematol, 2013. **86**(2): p. 161-75.
33. Lawrie, T.A., et al., *Pegylated liposomal doxorubicin for first-line treatment of epithelial ovarian cancer*. Cochrane Database Syst Rev, 2013. **10**: p. CD010482.
34. Liu, J.F., P.A. Konstantinopoulos, and U.A. Matulonis, *PARP inhibitors in ovarian cancer: current status and future promise*. Gynecol Oncol, 2014. **133**(2): p. 362-9.
35. Foley, O.W., J.A. Rauh-Hain, and M.G. del Carmen, *Recurrent epithelial ovarian cancer: an update on treatment*. Oncology (Williston Park), 2013. **27**(4): p. 288-94, 298.
36. Voduc, K.D., et al., *Breast cancer subtypes and the risk of local and regional relapse*. J Clin Oncol, 2010. **28**(10): p. 1684-91.
37. Fan, C., et al., *Concordance among gene-expression-based predictors for breast cancer*. N Engl J Med, 2006. **355**(6): p. 560-9.

38. Onitilo, A.A., et al., *Breast cancer subtypes based on ER/PR and Her2 expression: comparison of clinicopathologic features and survival*. Clin Med Res, 2009. **7**(1-2): p. 4-13.
39. Higgins, M.J. and J. Baselga, *Targeted therapies for breast cancer*. J Clin Invest, 2011. **121**(10): p. 3797-803.
40. Oostendorp, L.J., et al., *Efficacy and safety of palliative chemotherapy for patients with advanced breast cancer pretreated with anthracyclines and taxanes: a systematic review*. Lancet Oncol, 2011. **12**(11): p. 1053-61.
41. Linehan, W.M., R. Srinivasan, and L.S. Schmidt, *The genetic basis of kidney cancer: a metabolic disease*. Nat Rev Urol, 2010. **7**(5): p. 277-85.
42. Linehan, W.M., M.M. Walther, and B. Zbar, *The genetic basis of cancer of the kidney*. J Urol, 2003. **170**(6 Pt 1): p. 2163-72.
43. Cancer Genome Atlas Research, N., *Comprehensive molecular characterization of clear cell renal cell carcinoma*. Nature, 2013. **499**(7456): p. 43-9.
44. Cowey, C.L. and W.K. Rathmell, *VHL gene mutations in renal cell carcinoma: role as a biomarker of disease outcome and drug efficacy*. Curr Oncol Rep, 2009. **11**(2): p. 94-101.
45. Shen, C., et al., *Genetic and functional studies implicate HIF1alpha as a 14q kidney cancer suppressor gene*. Cancer Discov, 2011. **1**(3): p. 222-35.
46. Lee-Ying, R., R. Lester, and D. Heng, *Current management and future perspectives of metastatic renal cell carcinoma*. Int J Urol, 2014. **21**(9): p. 847-55.
47. Negrini, S., V.G. Gorgoulis, and T.D. Halazonetis, *Genomic instability--an evolving hallmark of cancer*. Nat Rev Mol Cell Biol, 2010. **11**(3): p. 220-8.
48. Michels, E., et al., *Detection of DNA copy number alterations in cancer by array comparative genomic hybridization*. Genet Med, 2007. **9**(9): p. 574-84.
49. Micci, F., et al., *Genomic profile of ovarian carcinomas*. BMC Cancer, 2014. **14**: p. 315.
50. Lim, D. and E. Oliva, *Precursors and pathogenesis of ovarian carcinoma*. Pathology, 2013. **45**(3): p. 229-42.
51. Martins, F.C., et al., *Combined image and genomic analysis of high-grade serous ovarian cancer reveals PTEN loss as a common driver event and prognostic classifier*. Genome Biol, 2014. **15**(12): p. 526.
52. Campeau, P.M., W.D. Foulkes, and M.D. Tischkowitz, *Hereditary breast cancer: new genetic developments, new therapeutic avenues*. Hum Genet, 2008. **124**(1): p. 31-42.
53. Cancer Genome Atlas, N., *Comprehensive molecular portraits of human breast tumours*. Nature, 2012. **490**(7418): p. 61-70.
54. Li, L., et al., *SQSTM1 is a pathogenic target of 5q copy number gains in kidney cancer*. Cancer Cell, 2013. **24**(6): p. 738-50.
55. Weber-Mangal, S., et al., *Breast cancer in young women (< or = 35 years): Genomic aberrations detected by comparative genomic hybridization*. Int J Cancer, 2003. **107**(4): p. 583-92.
56. Wessels, L.F., et al., *Molecular classification of breast carcinomas by comparative genomic hybridization: a specific somatic genetic profile for BRCA1 tumors*. Cancer Res, 2002. **62**(23): p. 7110-7.
57. Goyama, S. and M. Kurokawa, *Pathogenetic significance of ecotropic viral integration site-1 in hematological malignancies*. Cancer Sci, 2009. **100**(6): p. 990-5.

58. Jolkowska, J. and M. Witt, *The EVI-1 gene--its role in pathogenesis of human leukemias*. Leuk Res, 2000. **24**(7): p. 553-8.
59. Alzuhherri, H., et al., *Conservation and expression of a novel alternatively spliced Evi1 exon*. Gene, 2006. **384**: p. 154-62.
60. Perkins, A.S. and J.H. Kim, *Zinc fingers 1-7 of EVI1 fail to bind to the GATA motif by itself but require the core site GACAAGATA for binding*. J Biol Chem, 1996. **271**(2): p. 1104-10.
61. Yuasa, H., et al., *Oncogenic transcription factor Evi1 regulates hematopoietic stem cell proliferation through GATA-2 expression*. EMBO J, 2005. **24**(11): p. 1976-87.
62. Kurokawa, M., et al., *The oncoprotein Evi-1 represses TGF-beta signalling by inhibiting Smad3*. Nature, 1998. **394**(6688): p. 92-6.
63. Alliston, T., et al., *Repression of bone morphogenetic protein and activin-inducible transcription by Evi-1*. J Biol Chem, 2005. **280**(25): p. 24227-37.
64. Kurokawa, M., et al., *The evi-1 oncoprotein inhibits c-Jun N-terminal kinase and prevents stress-induced cell death*. EMBO J, 2000. **19**(12): p. 2958-68.
65. Kilbey, A. and C. Bartholomew, *Evi-1 ZF1 DNA binding activity and a second distinct transcriptional repressor region are both required for optimal transformation of Rat1 fibroblasts*. Oncogene, 1998. **16**(17): p. 2287-91.
66. Derunes, C., et al., *Characterization of the PR domain of RIZ1 histone methyltransferase*. Biochem Biophys Res Commun, 2005. **333**(3): p. 925-34.
67. Bordereaux, D., et al., *Alternative splicing of the Evi-1 zinc finger gene generates mRNAs which differ by the number of zinc finger motifs*. Oncogene, 1990. **5**(6): p. 925-7.
68. Morishita, K., et al., *Unique expression of the human Evi-1 gene in an endometrial carcinoma cell line: sequence of cDNAs and structure of alternatively spliced transcripts*. Oncogene, 1990. **5**(7): p. 963-71.
69. Aytekin, M., et al., *Regulation of the expression of the oncogene EVI1 through the use of alternative mRNA 5'-ends*. Gene, 2005. **356**: p. 160-8.
70. Izutsu, K., et al., *The corepressor CtBP interacts with Evi-1 to repress transforming growth factor beta signaling*. Blood, 2001. **97**(9): p. 2815-22.
71. Sato, T., et al., *Evi-1 promotes para-aortic splanchnopleural hematopoiesis through up-regulation of GATA-2 and repression of TGF-b signaling*. Cancer Sci, 2008. **99**(7): p. 1407-13.
72. Chi, Y., et al., *EVI1 promotes cell proliferation by interacting with BRG1 and blocking the repression of BRG1 on E2F1 activity*. J Biol Chem, 2003. **278**(50): p. 49806-11.
73. Tanaka, T., et al., *Evi-1 raises AP-1 activity and stimulates c-fos promoter transactivation with dependence on the second zinc finger domain*. J Biol Chem, 1994. **269**(39): p. 24020-6.
74. Senyuk, V., et al., *Repression of RUNX1 activity by EVI1: a new role of EVI1 in leukemogenesis*. Cancer Res, 2007. **67**(12): p. 5658-66.
75. Cattaneo, F. and G. Nucifora, *EVI1 recruits the histone methyltransferase SUV39H1 for transcription repression*. J Cell Biochem, 2008. **105**(2): p. 344-52.
76. Spensberger, D. and R. Delwel, *A novel interaction between the proto-oncogene Evi1 and histone methyltransferases, SUV39H1 and G9a*. FEBS Lett, 2008. **582**(18): p. 2761-7.

77. Vinatzer, U., et al., *The leukaemia-associated transcription factors EVI-1 and MDS1/EVI1 repress transcription and interact with histone deacetylase*. Br J Haematol, 2001. **114**(3): p. 566-73.
78. Chakraborty, S., et al., *Interaction of EVI1 with cAMP-responsive element-binding protein-binding protein (CBP) and p300/CBP-associated factor (P/CAF) results in reversible acetylation of EVI1 and in co-localization in nuclear speckles*. J Biol Chem, 2001. **276**(48): p. 44936-43.
79. Shimahara, A., et al., *Acetylation of lysine 564 adjacent to the C-terminal binding protein-binding motif in EVI1 is crucial for transcriptional activation of GATA2*. J Biol Chem, 2010. **285**(22): p. 16967-77.
80. Senyuk, V., et al., *The oncoprotein EVI1 and the DNA methyltransferase Dnmt3 cooperate in binding and de novo methylation of target DNA*. PLoS One, 2011. **6**(6): p. e20793.
81. Pradhan, A.K., et al., *EVI1 up-regulates the stress responsive gene SIRT1 which triggers deacetylation and degradation of EVI1*. Biochim Biophys Acta, 2011. **1809**(4-6): p. 269-75.
82. Yoshimi, A., et al., *Evi1 represses PTEN expression and activates PI3K/AKT/mTOR via interactions with polycomb proteins*. Blood, 2011. **117**(13): p. 3617-28.
83. Brooks, D.J., et al., *Expression of the zinc finger gene EVI-1 in ovarian and other cancers*. Br J Cancer, 1996. **74**(10): p. 1518-25.
84. Sunde, J.S., et al., *Expression profiling identifies altered expression of genes that contribute to the inhibition of transforming growth factor-beta signaling in ovarian cancer*. Cancer Res, 2006. **66**(17): p. 8404-12.
85. Wimmer, K., et al., *Comparative expression analysis of the antagonistic transcription factors EVI1 and MDS1-EVI1 in murine tissues and during in vitro hematopoietic differentiation*. Biochem Biophys Res Commun, 1998. **252**(3): p. 691-6.
86. Senyuk, V., et al., *The leukemia-associated transcription repressor AML1/MDS1/EVI1 requires CtBP to induce abnormal growth and differentiation of murine hematopoietic cells*. Oncogene, 2002. **21**(20): p. 3232-40.
87. Cuenco, G.M. and R. Ren, *Both AML1 and EVI1 oncogenic components are required for the cooperation of AML1/MDS1/EVI1 with BCR/ABL in the induction of acute myelogenous leukemia in mice*. Oncogene, 2004. **23**(2): p. 569-79.
88. Bard-Chapeau, E.A., et al., *EVI1 oncoprotein interacts with a large and complex network of proteins and integrates signals through protein phosphorylation*. Proc Natl Acad Sci U S A, 2013. **110**(31): p. E2885-94.
89. Liu, Y., et al., *Evi1 is a survival factor which conveys resistance to both TGFbeta- and taxol-mediated cell death via PI3K/AKT*. Oncogene, 2006. **25**(25): p. 3565-75.
90. Deng, X., et al., *Overexpression of Evi-1 oncoprotein represses TGF-beta signaling in colorectal cancer*. Mol Carcinog, 2013. **52**(4): p. 255-64.
91. Zhu, Q., S. Pearson-White, and K. Luo, *Requirement for the SnoN oncoprotein in transforming growth factor beta-induced oncogenic transformation of fibroblast cells*. Mol Cell Biol, 2005. **25**(24): p. 10731-44.
92. Stroschein, S.L., et al., *Negative feedback regulation of TGF-beta signaling by the SnoN oncoprotein*. Science, 1999. **286**(5440): p. 771-4.



93. Nomura, T., et al., *Ski is a component of the histone deacetylase complex required for transcriptional repression by Mad and thyroid hormone receptor*. Genes Dev, 1999. **13**(4): p. 412-23.
94. Karagianni, P. and J. Wong, *HDAC3: taking the SMRT-N-CoRrect road to repression*. Oncogene, 2007. **26**(37): p. 5439-49.
95. He, J., et al., *The transforming activity of Ski and SnoN is dependent on their ability to repress the activity of Smad proteins*. J Biol Chem, 2003. **278**(33): p. 30540-7.
96. Zhang, F., et al., *Ski-related novel protein N (SnoN), a negative controller of transforming growth factor-beta signaling, is a prognostic marker in estrogen receptor-positive breast carcinomas*. Cancer Res, 2003. **63**(16): p. 5005-10.
97. Poser, I., et al., *Characterization of Sno expression in malignant melanoma*. Int J Oncol, 2005. **26**(5): p. 1411-7.
98. Imoto, I., et al., *SNO is a probable target for gene amplification at 3q26 in squamous-cell carcinomas of the esophagus*. Biochem Biophys Res Commun, 2001. **286**(3): p. 559-65.
99. Buess, M., et al., *Amplification of SKI is a prognostic marker in early colorectal cancer*. Neoplasia, 2004. **6**(3): p. 207-12.
100. Ritter, M., et al., *Inhibition of retinoic acid receptor signaling by Ski in acute myeloid leukemia*. Leukemia, 2006. **20**(3): p. 437-43.
101. Zhu, Q., et al., *Dual role of SnoN in mammalian tumorigenesis*. Mol Cell Biol, 2007. **27**(1): p. 324-39.
102. Le Scolan, E., et al., *Transforming growth factor-beta suppresses the ability of Ski to inhibit tumor metastasis by inducing its degradation*. Cancer Res, 2008. **68**(9): p. 3277-85.
103. Krakowski, A.R., et al., *Cytoplasmic SnoN in normal tissues and nonmalignant cells antagonizes TGF-beta signaling by sequestration of the Smad proteins*. Proc Natl Acad Sci U S A, 2005. **102**(35): p. 12437-42.
104. Bonni, S., et al., *TGF-beta induces assembly of a Smad2-Smurf2 ubiquitin ligase complex that targets SnoN for degradation*. Nat Cell Biol, 2001. **3**(6): p. 587-95.
105. Wan, Y., X. Liu, and M.W. Kirschner, *The anaphase-promoting complex mediates TGF-beta signaling by targeting SnoN for destruction*. Mol Cell, 2001. **8**(5): p. 1027-39.
106. Kajino, T., et al., *TAK1 MAPK kinase kinases mediates transforming growth factor-beta signaling by targeting SnoN oncoprotein for degradation*. J Biol Chem, 2007. **282**(13): p. 9475-81.
107. Mitsumori, K., et al., *Chromosome 14q LOH in localized clear cell renal cell carcinoma*. J Pathol, 2002. **198**(1): p. 110-4.
108. Toma, M.I., et al., *Loss of heterozygosity and copy number abnormality in clear cell renal cell carcinoma discovered by high-density affymetrix 10K single nucleotide polymorphism mapping array*. Neoplasia, 2008. **10**(7): p. 634-42.
109. Klatte, T., et al., *Cytogenetic profile predicts prognosis of patients with clear cell renal cell carcinoma*. J Clin Oncol, 2009. **27**(5): p. 746-53.
110. Kohn, L., et al., *Specific Genomic Aberrations Predict Survival, But Low Mutation Rate in Cancer Hot Spots, in Clear Cell Renal Cell Carcinoma*. Appl Immunohistochem Mol Morphol, 2014.
111. Chin, K., et al., *Genomic and transcriptional aberrations linked to breast cancer pathophysiology*. Cancer Cell, 2006. **10**(6): p. 529-41.

112. Al-Mulla, F., et al., *Metastatic recurrence of early-stage colorectal cancer is linked to loss of heterozygosity on chromosomes 4 and 14q*. J Clin Pathol, 2006. **59**(6): p. 624-30.
113. De Angelis, P.M., et al., *Prognostic significance of recurrent chromosomal aberrations detected by comparative genomic hybridization in sporadic colorectal cancer*. Int J Colorectal Dis, 2001. **16**(1): p. 38-45.
114. Al-Mulla, F., et al., *Genetic profiling of stage I and II colorectal cancer may predict metastatic relapse*. Mod Pathol, 2006. **19**(5): p. 648-58.
115. Bandera, C.A., et al., *Deletion mapping of two potential chromosome 14 tumor suppressor gene loci in ovarian carcinoma*. Cancer Res, 1997. **57**(3): p. 513-5.
116. Yang, J., et al., *Genetic aberrations of gastrointestinal stromal tumors*. Cancer, 2008. **113**(7): p. 1532-43.
117. Zhang, L., et al., *Genomic and epigenetic alterations deregulate microRNA expression in human epithelial ovarian cancer*. Proc Natl Acad Sci U S A, 2008. **105**(19): p. 7004-9.
118. Saito, Y., et al., *Specific activation of microRNA-127 with downregulation of the proto-oncogene BCL6 by chromatin-modifying drugs in human cancer cells*. Cancer Cell, 2006. **9**(6): p. 435-43.
119. Benetatos, L., et al., *The microRNAs within the DLK1-DIO3 genomic region: involvement in disease pathogenesis*. Cellular and molecular life sciences : CMLS, 2013. **70**(5): p. 795-814.
120. Juan, D., et al., *Identification of a microRNA panel for clear-cell kidney cancer*. Urology, 2010. **75**(4): p. 835-41.
121. Jansson, M.D. and A.H. Lund, *MicroRNA and cancer*. Mol Oncol, 2012. **6**(6): p. 590-610.
122. Lee, R.C., R.L. Feinbaum, and V. Ambros, *The C. elegans heterochronic gene lin-4 encodes small RNAs with antisense complementarity to lin-14*. Cell, 1993. **75**(5): p. 843-54.
123. Calin, G.A., et al., *Frequent deletions and down-regulation of micro- RNA genes miR15 and miR16 at 13q14 in chronic lymphocytic leukemia*. Proc Natl Acad Sci U S A, 2002. **99**(24): p. 15524-9.
124. Ling, H., M. Fabbri, and G.A. Calin, *MicroRNAs and other non-coding RNAs as targets for anticancer drug development*. Nat Rev Drug Discov, 2013. **12**(11): p. 847-65.
125. Valinezhad Orang, A., R. Safaralizadeh, and M. Kazemzadeh-Bavili, *Mechanisms of miRNA-Mediated Gene Regulation from Common Downregulation to mRNA-Specific Upregulation*. Int J Genomics, 2014. **2014**: p. 970607.
126. Ha, M. and V.N. Kim, *Regulation of microRNA biogenesis*. Nat Rev Mol Cell Biol, 2014. **15**(8): p. 509-24.
127. Hayes, J., P.P. Peruzzi, and S. Lawler, *MicroRNAs in cancer: biomarkers, functions and therapy*. Trends Mol Med, 2014. **20**(8): p. 460-9.
128. Dharap, A., et al., *MicroRNA miR-324-3p induces promoter-mediated expression of RelA gene*. PLoS One, 2013. **8**(11): p. e79467.
129. Huang, V., et al., *Upregulation of Cyclin B1 by miRNA and its implications in cancer*. Nucleic Acids Res, 2012. **40**(4): p. 1695-707.
130. Vasudevan, S., *Posttranscriptional upregulation by microRNAs*. Wiley Interdiscip Rev RNA, 2012. **3**(3): p. 311-30.

131. Kent, W.J., et al., *The human genome browser at UCSC*. Genome Res, 2002. **12**(6): p. 996-1006.
132. Wang, X., et al., *MicroRNA-494 targeting both proapoptotic and antiapoptotic proteins protects against ischemia/reperfusion-induced cardiac injury*. Circulation, 2010. **122**(13): p. 1308-18.
133. Esquela-Kerscher, A. and F.J. Slack, *Oncomirs - microRNAs with a role in cancer*. Nat Rev Cancer, 2006. **6**(4): p. 259-69.
134. Yang, H., et al., *MicroRNA expression profiling in human ovarian cancer: miR-214 induces cell survival and cisplatin resistance by targeting PTEN*. Cancer Res, 2008. **68**(2): p. 425-33.
135. Ohdaira, H., et al., *MicroRNA-494 suppresses cell proliferation and induces senescence in A549 lung cancer cells*. Cell proliferation, 2012. **45**(1): p. 32-8.
136. Liborio-Kimura, T.N., H.M. Jung, and E.K. Chan, *miR-494 represses HOXA10 expression and inhibits cell proliferation in oral cancer*. Oral Oncol, 2015. **51**(2): p. 151-7.
137. Shen, P.F., et al., *MicroRNA-494-3p targets CXCR4 to suppress the proliferation, invasion, and migration of prostate cancer*. Prostate, 2014. **74**(7): p. 756-67.
138. Oлару, A.V., et al., *MicroRNA down-regulated in human cholangiocarcinoma control cell cycle through multiple targets involved in the G1/S checkpoint*. Hepatology, 2011. **54**(6): p. 2089-98.
139. Zhou, R.P., et al., *Cinobufacin suppresses cell proliferation via miR-494 in BGC- 823 gastric cancer cells*. Asian Pac J Cancer Prev, 2014. **15**(3): p. 1241-5.
140. Duan, H.F., et al., *Functional elucidation of miR-494 in the tumorigenesis of nasopharyngeal carcinoma*. Tumour Biol, 2015.
141. Sun, H.B., et al., *miR494 is an independent prognostic factor and promotes cell migration and invasion in colorectal cancer by directly targeting PTEN*. Int J Oncol, 2014. **45**(6): p. 2486-94.
142. Romano, G., et al., *MiR-494 is regulated by ERK1/2 and modulates TRAIL-induced apoptosis in non-small-cell lung cancer through BIM down-regulation*. Proc Natl Acad Sci U S A, 2012. **109**(41): p. 16570-5.
143. Liu, L., et al., *Overexpressed miR-494 down-regulates PTEN gene expression in cells transformed by anti-benzo(a)pyrene-trans-7,8-dihydrodiol-9,10-epoxide*. Life Sci, 2010. **86**(5-6): p. 192-8.
144. Liu, Y., et al., *MicroRNA-494 is required for the accumulation and functions of tumor-expanded myeloid-derived suppressor cells via targeting of PTEN*. J Immunol, 2012. **188**(11): p. 5500-10.
145. Lim, L., et al., *MicroRNA-494 within an oncogenic microRNA megacluster regulates G1/S transition in liver tumorigenesis through suppression of mutated in colorectal cancer*. Hepatology, 2014. **59**(1): p. 202-15.
146. Chuang, K.H., et al., *MiR-494 is A Master Epigenetic Regulator of Multiple Invasion-Suppressor MicroRNAs via Targeting TET1 in Invasive Human HCC Tumors*. Hepatology, 2015.
147. Elliott, R.L. and G.C. Blobe, *Role of transforming growth factor Beta in human cancer*. J Clin Oncol, 2005. **23**(9): p. 2078-93.
148. Shi, Y. and J. Massague, *Mechanisms of TGF-beta signaling from cell membrane to the nucleus*. Cell, 2003. **113**(6): p. 685-700.
149. Massague, J., *TGFbeta in Cancer*. Cell, 2008. **134**(2): p. 215-30.

150. Raffoul, F., C. Campla, and M. Nanjundan, *SnoN/SkiL, a TGFbeta signaling mediator: a participant in autophagy induced by arsenic trioxide*. *Autophagy*, 2010. **6**(7): p. 955-7.
151. Cheng, J.C., N. Auersperg, and P.C. Leung, *TGF-beta induces serous borderline ovarian tumor cell invasion by activating EMT but triggers apoptosis in low-grade serous ovarian carcinoma cells*. *PLoS One*, 2012. **7**(8): p. e42436.
152. Micalizzi, D.S., S.M. Farabaugh, and H.L. Ford, *Epithelial-mesenchymal transition in cancer: parallels between normal development and tumor progression*. *J Mammary Gland Biol Neoplasia*, 2010. **15**(2): p. 117-34.
153. Brabletz, T., *EMT and MET in metastasis: where are the cancer stem cells?* *Cancer Cell*, 2012. **22**(6): p. 699-701.
154. Yilmaz, M. and G. Christofori, *EMT, the cytoskeleton, and cancer cell invasion*. *Cancer Metastasis Rev*, 2009. **28**(1-2): p. 15-33.
155. Valentijn, A.J., N. Zouq, and A.P. Gilmore, *Anoikis*. *Biochem Soc Trans*, 2004. **32**(Pt3): p. 421-5.
156. Korpala, M., et al., *The miR-200 family inhibits epithelial-mesenchymal transition and cancer cell migration by direct targeting of E-cadherin transcriptional repressors ZEB1 and ZEB2*. *J Biol Chem*, 2008. **283**(22): p. 14910-4.
157. Kodigepalli, K.M., et al., *Phospholipid Scramblase 1, an interferon-regulated gene located at 3q23, is regulated by SnoN/SkiL in ovarian cancer cells*. *Mol Cancer*, 2013. **12**: p. 32.
158. Hanahan, D. and R.A. Weinberg, *The hallmarks of cancer*. *Cell*, 2000. **100**(1): p. 57-70.
159. Jaattela, M., *Multiple cell death pathways as regulators of tumour initiation and progression*. *Oncogene*, 2004. **23**(16): p. 2746-56.
160. Galluzzi, L., et al., *Molecular definitions of cell death subroutines: recommendations of the Nomenclature Committee on Cell Death 2012*. *Cell Death Differ*, 2012. **19**(1): p. 107-20.
161. Dixon, S.J., et al., *Ferroptosis: an iron-dependent form of nonapoptotic cell death*. *Cell*, 2012. **149**(5): p. 1060-72.
162. Elmore, S., *Apoptosis: a review of programmed cell death*. *Toxicol Pathol*, 2007. **35**(4): p. 495-516.
163. Fernald, K. and M. Kurokawa, *Evading apoptosis in cancer*. *Trends Cell Biol*, 2013. **23**(12): p. 620-33.
164. Ouyang, L., et al., *Programmed cell death pathways in cancer: a review of apoptosis, autophagy and programmed necrosis*. *Cell Prolif*, 2012. **45**(6): p. 487-98.
165. Narita, M., et al., *Bax interacts with the permeability transition pore to induce permeability transition and cytochrome c release in isolated mitochondria*. *Proc Natl Acad Sci U S A*, 1998. **95**(25): p. 14681-6.
166. Tsujimoto, Y., *Role of Bcl-2 family proteins in apoptosis: apoptosomes or mitochondria?* *Genes Cells*, 1998. **3**(11): p. 697-707.
167. Liu, B., et al., *Autophagic pathways as new targets for cancer drug development*. *Acta Pharmacol Sin*, 2010. **31**(9): p. 1154-64.
168. Tsukada, M. and Y. Ohsumi, *Isolation and characterization of autophagy-defective mutants of Saccharomyces cerevisiae*. *FEBS Lett*, 1993. **333**(1-2): p. 169-74.

169. Reggiori, F. and D.J. Klionsky, *Autophagy in the eukaryotic cell*. Eukaryot Cell, 2002. **1**(1): p. 11-21.
170. Eskelinen, E.L., *New insights into the mechanisms of macroautophagy in mammalian cells*. Int Rev Cell Mol Biol, 2008. **266**: p. 207-47.
171. Kim, J., et al., *AMPK and mTOR regulate autophagy through direct phosphorylation of Ulk1*. Nat Cell Biol, 2011. **13**(2): p. 132-41.
172. Kihara, A., et al., *Two distinct Vps34 phosphatidylinositol 3-kinase complexes function in autophagy and carboxypeptidase Y sorting in Saccharomyces cerevisiae*. J Cell Biol, 2001. **152**(3): p. 519-30.
173. Mizushima, N., et al., *A protein conjugation system essential for autophagy*. Nature, 1998. **395**(6700): p. 395-8.
174. Shintani, T., et al., *Apg10p, a novel protein-conjugating enzyme essential for autophagy in yeast*. EMBO J, 1999. **18**(19): p. 5234-41.
175. Ichimura, Y., et al., *A ubiquitin-like system mediates protein lipidation*. Nature, 2000. **408**(6811): p. 488-92.
176. Kirisako, T., et al., *The reversible modification regulates the membrane-binding state of Apg8/Aut7 essential for autophagy and the cytoplasm to vacuole targeting pathway*. J Cell Biol, 2000. **151**(2): p. 263-76.
177. Rosenfeldt, M.T. and K.M. Ryan, *The multiple roles of autophagy in cancer*. Carcinogenesis, 2011. **32**(7): p. 955-63.
178. Eisenberg-Lerner, A., et al., *Life and death partners: apoptosis, autophagy and the cross-talk between them*. Cell Death Differ, 2009. **16**(7): p. 966-75.
179. Fantin, V.R. and P. Leder, *F16, a mitochondriotoxic compound, triggers apoptosis or necrosis depending on the genetic background of the target carcinoma cell*. Cancer Res, 2004. **64**(1): p. 329-36.
180. N'Diaye, E.N., et al., *PLIC proteins or ubiquilins regulate autophagy-dependent cell survival during nutrient starvation*. EMBO Rep, 2009. **10**(2): p. 173-9.
181. Lee, I.H., et al., *A role for the NAD-dependent deacetylase Sirt1 in the regulation of autophagy*. Proc Natl Acad Sci U S A, 2008. **105**(9): p. 3374-9.
182. Dagda, R.K., et al., *Mitochondrially localized ERK2 regulates mitophagy and autophagic cell stress: implications for Parkinson's disease*. Autophagy, 2008. **4**(6): p. 770-82.
183. Nanjundan, M., et al., *Proteomic profiling identifies pathways dysregulated in non-small cell lung cancer and an inverse association of AMPK and adhesion pathways with recurrence*. J Thorac Oncol, 2010. **5**(12): p. 1894-904.
184. Bauckman, K.A., et al., *Iron modulates cell survival in a Ras- and MAPK-dependent manner in ovarian cells*. Cell Death Dis, 2013. **4**: p. e592.
185. Moussay, E., et al., *The acquisition of resistance to TNFalpha in breast cancer cells is associated with constitutive activation of autophagy as revealed by a transcriptome analysis using a custom microarray*. Autophagy, 2011. **7**(7): p. 760-70.
186. Perkins, A.S., et al., *Patterns of Evi-1 expression in embryonic and adult tissues suggest that Evi-1 plays an important regulatory role in mouse development*. Development, 1991. **111**(2): p. 479-87.
187. Rimann, I. and A. Hajnal, *Regulation of anchor cell invasion and uterine cell fates by the egl-43 Evi-1 proto-oncogene in Caenorhabditis elegans*. Dev Biol, 2007. **308**(1): p. 187-95.

188. Garriga, G., C. Guenther, and H.R. Horvitz, *Migrations of the Caenorhabditis elegans HSNs are regulated by egl-43, a gene encoding two zinc finger proteins*. Genes Dev, 1993. **7**(11): p. 2097-109.
189. Hwang, B.J., A.D. Meruelo, and P.W. Sternberg, *C. elegans EVI1 proto-oncogene, EGL-43, is necessary for Notch-mediated cell fate specification and regulates cell invasion*. Development, 2007. **134**(4): p. 669-79.
190. Bard-Chapeau, E.A., et al., *Ecotopic viral integration site 1 (EVI1) regulates multiple cellular processes important for cancer and is a synergistic partner for FOS protein in invasive tumors*. Proc Natl Acad Sci U S A, 2012. **109**(6): p. 2168-73.
191. Vleminckx, K. and R. Kemler, *Cadherins and tissue formation: integrating adhesion and signaling*. Bioessays, 1999. **21**(3): p. 211-20.
192. Peinado, H., et al., *Snail mediates E-cadherin repression by the recruitment of the Sin3A/histone deacetylase 1 (HDAC1)/HDAC2 complex*. Mol Cell Biol, 2004. **24**(1): p. 306-19.
193. Bolos, V., et al., *The transcription factor Slug represses E-cadherin expression and induces epithelial to mesenchymal transitions: a comparison with Snail and E47 repressors*. J Cell Sci, 2003. **116**(Pt 3): p. 499-511.
194. Vesuna, F., et al., *Twist is a transcriptional repressor of E-cadherin gene expression in breast cancer*. Biochem Biophys Res Commun, 2008. **367**(2): p. 235-41.
195. Alexander, N.R., et al., *N-cadherin gene expression in prostate carcinoma is modulated by integrin-dependent nuclear translocation of Twist1*. Cancer Res, 2006. **66**(7): p. 3365-9.
196. Sanchez-Tillo, E., et al., *ZEB1 represses E-cadherin and induces an EMT by recruiting the SWI/SNF chromatin-remodeling protein BRG1*. Oncogene, 2010. **29**(24): p. 3490-500.
197. Hirai, H., *The transcription factor Evi-1*. Int J Biochem Cell Biol, 1999. **31**(12): p. 1367-71.
198. Bullock, M.D., et al., *MicroRNAs: critical regulators of epithelial to mesenchymal (EMT) and mesenchymal to epithelial transition (MET) in cancer progression*. Biol Cell, 2012. **104**(1): p. 3-12.
199. Korpala, M. and Y. Kang, *The emerging role of miR-200 family of microRNAs in epithelial-mesenchymal transition and cancer metastasis*. RNA Biol, 2008. **5**(3): p. 115-9.
200. Gao, J.S., et al., *The Evi1, microRNA-143, K-Ras axis in colon cancer*. FEBS Lett, 2011. **585**(4): p. 693-9.
201. Vazquez, I., et al., *Silencing of hsa-miR-124 by EVI1 in cell lines and patients with acute myeloid leukemia*. Proc Natl Acad Sci U S A, 2010. **107**(44): p. E167-8; author reply E169-70.
202. Tanaka, M., et al., *EVI1 oncogene promotes KRAS pathway through suppression of microRNA-96 in pancreatic carcinogenesis*. Oncogene, 2014. **33**(19): p. 2454-63.
203. De Weer, A., et al., *EVI1-mediated down regulation of MIR449A is essential for the survival of EVI1 positive leukaemic cells*. Br J Haematol, 2011. **154**(3): p. 337-48.
204. Yamada, S.D., R.L. Baldwin, and B.Y. Karlan, *Ovarian carcinoma cell cultures are resistant to TGF-beta1-mediated growth inhibition despite expression of functional receptors*. Gynecol Oncol, 1999. **75**(1): p. 72-7.

205. Donnellan, R. and R. Chetty, *Cyclin E in human cancers*. FASEB J, 1999. **13**(8): p. 773-80.
206. Wingate, H., et al., *The low molecular weight (LMW) isoforms of cyclin E deregulate the cell cycle of mammary epithelial cells*. Cell Cycle, 2003. **2**(5): p. 461-6.
207. Akli, S. and K. Keyomarsi, *Low-molecular-weight cyclin E: the missing link between biology and clinical outcome*. Breast Cancer Res, 2004. **6**(5): p. 188-91.
208. Prislei, S., et al., *MiR-200c and HuR in ovarian cancer*. BMC Cancer, 2013. **13**: p. 72.
209. Ward, A.J. and T.A. Cooper, *The pathobiology of splicing*. J Pathol, 2010. **220**(2): p. 152-63.
210. Naro, C. and C. Sette, *Phosphorylation-mediated regulation of alternative splicing in cancer*. Int J Cell Biol, 2013. **2013**: p. 151839.
211. Patel, N.A., et al., *Molecular and genetic studies imply Akt-mediated signaling promotes protein kinase Cbeta11 alternative splicing via phosphorylation of serine/arginine-rich splicing factor SRp40*. J Biol Chem, 2005. **280**(14): p. 14302-9.
212. Pelisch, F., et al., *Cross-talk between signaling pathways regulates alternative splicing: a novel role for JNK*. J Biol Chem, 2005. **280**(27): p. 25461-9.
213. Hung, M.C. and W. Link, *Protein localization in disease and therapy*. J Cell Sci, 2011. **124**(Pt 20): p. 3381-92.
214. Nanjundan, M., et al., *Amplification of MDS1/EVI1 and EVI1, located in the 3q26.2 amplicon, is associated with favorable patient prognosis in ovarian cancer*. Cancer research, 2007. **67**(7): p. 3074-84.
215. Nanjundan, M., et al., *Overexpression of SnoN/SkiL, amplified at the 3q26.2 locus, in ovarian cancers: a role in ovarian pathogenesis*. Molecular oncology, 2008. **2**(2): p. 164-81.
216. Chen, L., et al., *Integrative network analysis to identify aberrant pathway networks in ovarian cancer*. Pac Symp Biocomput, 2012: p. 31-42.
217. Hennessy, B.T., et al., *Ovarian cancer: linking genomics to new target discovery and molecular markers--the way ahead*. Adv Exp Med Biol, 2008. **617**: p. 23-40.
218. Fukuchi, M., et al., *Increased expression of c-Ski as a co-repressor in transforming growth factor-beta signaling correlates with progression of esophageal squamous cell carcinoma*. Int J Cancer, 2004. **108**(6): p. 818-24.
219. Reed, J.A., et al., *SKI pathways inducing progression of human melanoma*. Cancer Metastasis Rev, 2005. **24**(2): p. 265-72.
220. Hu, W., et al., *Anomalies of the TGF-beta postreceptor signaling pathway in ovarian cancer cell lines*. Anticancer Res, 2000. **20**(2A): p. 729-33.
221. Zhang, T.D., et al., *Arsenic trioxide, a therapeutic agent for APL*. Oncogene, 2001. **20**(49): p. 7146-53.
222. Bornstein, J., et al., *Arsenic Trioxide inhibits the growth of human ovarian carcinoma cell line*. Gynecol Oncol, 2005. **99**(3): p. 726-9.
223. Kong, B., et al., *Arsenic trioxide induces apoptosis in cisplatin-sensitive and -resistant ovarian cancer cell lines*. Int J Gynecol Cancer, 2005. **15**(5): p. 872-7.
224. Uslu, R., et al., *Arsenic trioxide-mediated cytotoxicity and apoptosis in prostate and ovarian carcinoma cell lines*. Clin Cancer Res, 2000. **6**(12): p. 4957-64.
225. Kabeya, Y., et al., *LC3, a mammalian homologue of yeast Apg8p, is localized in autophagosome membranes after processing*. EMBO J, 2000. **19**(21): p. 5720-8.

226. Lytle, J.R., T.A. Yario, and J.A. Steitz, *Target mRNAs are repressed as efficiently by microRNA-binding sites in the 5' UTR as in the 3' UTR*. Proc Natl Acad Sci U S A, 2007. **104**(23): p. 9667-72.
227. Brummer, A. and J. Hausser, *MicroRNA binding sites in the coding region of mRNAs: extending the repertoire of post-transcriptional gene regulation*. Bioessays, 2014. **36**(6): p. 617-26.
228. Nomura, N., et al., *Isolation of human cDNA clones of ski and the ski-related gene, sno*. Nucleic Acids Res, 1989. **17**(14): p. 5489-500.
229. Harazono, Y., et al., *miR-655 Is an EMT-suppressive microRNA targeting ZEB1 and TGFBR2*. PLoS One, 2013. **8**(5): p. e62757.
230. Macfarlane, L.A. and P.R. Murphy, *MicroRNA: Biogenesis, Function and Role in Cancer*. Curr Genomics, 2010. **11**(7): p. 537-61.
231. Boulares, A.H., et al., *Role of poly(ADP-ribose) polymerase (PARP) cleavage in apoptosis. Caspase 3-resistant PARP mutant increases rates of apoptosis in transfected cells*. J Biol Chem, 1999. **274**(33): p. 22932-40.
232. Rand, T.A., et al., *Biochemical identification of Argonaute 2 as the sole protein required for RNA-induced silencing complex activity*. Proc Natl Acad Sci U S A, 2004. **101**(40): p. 14385-9.
233. Ghaffari, S.H., et al., *Alteration in miRNA gene expression pattern in acute promyelocytic leukemia cell induced by arsenic trioxide: a possible mechanism to explain arsenic multi-target action*. Tumour biology : the journal of the International Society for Oncodevelopmental Biology and Medicine, 2012. **33**(1): p. 157-72.
234. Liang, H., et al., *MicroRNAs contribute to promyelocyte apoptosis in As2O3-treated APL cells*. Cellular physiology and biochemistry : international journal of experimental cellular physiology, biochemistry, and pharmacology, 2013. **32**(6): p. 1818-29.
235. Chai, J., et al., *MicroRNA-494 sensitizes colon cancer cells to fluorouracil through regulation of DPYD*. IUBMB Life, 2015. **67**(3): p. 191-201.
236. Sun, G., et al., *Over-expression of microRNA-494 up-regulates hypoxia-inducible factor-1 alpha expression via PI3K/Akt pathway and protects against hypoxia-induced apoptosis*. J Biomed Sci, 2013. **20**: p. 100.
237. Kwak, S.Y., et al., *Ionizing radiation-inducible miR-494 promotes glioma cell invasion through EGFR stabilization by targeting p190B rhoGAP*. Biochim Biophys Acta, 2014. **1843**(3): p. 508-16.
238. Melo, S.A. and M. Esteller, *Dysregulation of microRNAs in cancer: playing with fire*. FEBS Lett, 2011. **585**(13): p. 2087-99.
239. Wang, W., et al., *MicroRNA-497 inhibition of ovarian cancer cell migration and invasion through targeting of SMAD specific E3 ubiquitin protein ligase 1*. Biochemical and biophysical research communications, 2014.
240. Kim, Y.W., et al., *Differential microRNA expression signatures and cell type-specific association with Taxol resistance in ovarian cancer cells*. Drug design, development and therapy, 2014. **8**: p. 293-314.
241. Delfino, K.R. and S.L. Rodriguez-Zas, *Transcription factor-microRNA-target gene networks associated with ovarian cancer survival and recurrence*. PLoS One, 2013. **8**(3): p. e58608.



242. Flavin, R.J., et al., *Potentially important microRNA cluster on chromosome 17p13.1 in primary peritoneal carcinoma*. Modern pathology : an official journal of the United States and Canadian Academy of Pathology, Inc, 2009. **22**(2): p. 197-205.
243. Park, Y.T., et al., *MicroRNAs overexpressed in ovarian ALDH1-positive cells are associated with chemoresistance*. Journal of ovarian research, 2013. **6**(1): p. 18.
244. De Cecco, L., et al., *Increased sensitivity to chemotherapy induced by CpG-ODN treatment is mediated by microRNA modulation*. PLoS One, 2013. **8**(3): p. e58849.
245. Shih, K.K., et al., *A microRNA survival signature (MiSS) for advanced ovarian cancer*. Gynecologic oncology, 2011. **121**(3): p. 444-50.
246. Kim, Y.W., et al., *Differential microRNA expression signatures and cell type-specific association with Taxol resistance in ovarian cancer cells*. Drug Des Devel Ther, 2014. **8**: p. 293-314.
247. Titone, R., et al., *Epigenetic control of autophagy by microRNAs in ovarian cancer*. Biomed Res Int, 2014. **2014**: p. 343542.
248. Ohdaira, H., et al., *MicroRNA-494 suppresses cell proliferation and induces senescence in A549 lung cancer cells*. Cell Prolif, 2012. **45**(1): p. 32-8.
249. He, W., et al., *miR-494 acts as an anti-oncogene in gastric carcinoma by targeting c-myc*. J Gastroenterol Hepatol, 2014. **29**(7): p. 1427-34.
250. Wang, T., et al., *MicroRNA-494 inhibition protects nucleus pulposus cells from TNF-alpha-induced apoptosis by targeting JunD*. Biochimie, 2015.
251. Li, X.T., et al., *miR-494-3p Regulates Cellular Proliferation, Invasion, Migration, and Apoptosis by PTEN/AKT Signaling in Human Glioblastoma Cells*. Cell Mol Neurobiol, 2015.
252. Bai, Y., et al., *Overexpression of secretagogin inhibits cell apoptosis and induces chemoresistance in small cell lung cancer under the regulation of miR-494*. Oncotarget, 2014. **5**(17): p. 7760-75.
253. Benetatos, L., et al., *The microRNAs within the DLK1-DIO3 genomic region: involvement in disease pathogenesis*. Cell Mol Life Sci, 2013. **70**(5): p. 795-814.
254. Chang, W.Y., et al., *Novel suppressor loci on chromosome 14q in primary bladder cancer*. Cancer Res, 1995. **55**(15): p. 3246-9.
255. Young, J., et al., *Frequent loss of heterozygosity on chromosome 14 occurs in advanced colorectal carcinomas*. Oncogene, 1993. **8**(3): p. 671-5.
256. Fujino, T., et al., *Allelotype of endometrial carcinoma*. Cancer Res, 1994. **54**(16): p. 4294-8.
257. Suzuki, T., et al., *Frequent loss of heterozygosity on chromosome 14q in neuroblastoma*. Cancer Res, 1989. **49**(5): p. 1095-8.
258. Holley, C.L. and V.K. Topkara, *An introduction to small non-coding RNAs: miRNA and snoRNA*. Cardiovasc Drugs Ther, 2011. **25**(2): p. 151-9.
259. Garzon, R., G.A. Calin, and C.M. Croce, *MicroRNAs in Cancer*. Annu Rev Med, 2009. **60**: p. 167-79.
260. Zhang, L., et al., *Genomic and epigenetic alterations deregulate microRNA expression in human epithelial ovarian cancer*. Proceedings of the National Academy of Sciences of the United States of America, 2008. **105**(19): p. 7004-9.
261. Zhang, L., et al., *microRNAs exhibit high frequency genomic alterations in human cancer*. Proceedings of the National Academy of Sciences of the United States of America, 2006. **103**(24): p. 9136-41.

262. Croce, C.M., *Causes and consequences of microRNA dysregulation in cancer*. Nature reviews. Genetics, 2009. **10**(10): p. 704-14.
263. Haga, C.L. and D.G. Phinney, *MicroRNAs in the imprinted DLK1-DIO3 region repress the epithelial-to-mesenchymal transition by targeting the TWIST1 protein signaling network*. The Journal of biological chemistry, 2012. **287**(51): p. 42695-707.
264. Comegna, M., et al., *Identification of miR-494 direct targets involved in senescence of human diploid fibroblasts*. FASEB journal : official publication of the Federation of American Societies for Experimental Biology, 2014.
265. Song, L., et al., *miR-494 suppresses the progression of breast cancer in vitro by targeting CXCR4 through the Wnt/beta-catenin signaling pathway*. Oncol Rep, 2015.
266. Xiong, R., et al., *MicroRNA-494 reduces DJ-1 expression and exacerbates neurodegeneration*. Neurobiol Aging, 2014. **35**(3): p. 705-14.
267. Megiorni, F., et al., *Synergistic post-transcriptional regulation of the Cystic Fibrosis Transmembrane conductance Regulator (CFTR) by miR-101 and miR-494 specific binding*. PLoS One, 2011. **6**(10): p. e26601.
268. Oglesby, I.K., et al., *Regulation of cystic fibrosis transmembrane conductance regulator by microRNA-145, -223, and -494 is altered in DeltaF508 cystic fibrosis airway epithelium*. J Immunol, 2013. **190**(7): p. 3354-62.
269. Ryan, M.J., et al., *HK-2: an immortalized proximal tubule epithelial cell line from normal adult human kidney*. Kidney Int, 1994. **45**(1): p. 48-57.
270. Bursch, W., et al., *Programmed cell death (PCD). Apoptosis, autophagic PCD, or others?* Ann N Y Acad Sci, 2000. **926**: p. 1-12.
271. Qureshi, R. and A. Sacan, *A novel method for the normalization of microRNA RT-PCR data*. BMC Med Genomics, 2013. **6 Suppl 1**: p. S14.
272. Cande, C., et al., *Apoptosis-inducing factor (AIF): caspase-independent after all*. Cell Death Differ, 2004. **11**(6): p. 591-5.
273. McIlwain, D.R., T. Berger, and T.W. Mak, *Caspase functions in cell death and disease*. Cold Spring Harb Perspect Biol, 2013. **5**(4): p. a008656.
274. Zhou, F., Y. Yang, and D. Xing, *Bcl-2 and Bcl-xL play important roles in the crosstalk between autophagy and apoptosis*. FEBS J, 2011. **278**(3): p. 403-13.
275. Vasudevan, S., Y. Tong, and J.A. Steitz, *Switching from repression to activation: microRNAs can up-regulate translation*. Science, 2007. **318**(5858): p. 1931-4.
276. Mizushima, N. and T. Yoshimori, *How to interpret LC3 immunoblotting*. Autophagy, 2007. **3**(6): p. 542-5.
277. Hansen, T.E. and T. Johansen, *Following autophagy step by step*. BMC Biol, 2011. **9**: p. 39.
278. Liu, Y., et al., *Lovastatin enhances adenovirus-mediated TRAIL induced apoptosis by depleting cholesterol of lipid rafts and affecting CAR and death receptor expression of prostate cancer cells*. Oncotarget, 2014.
279. Shibata, M., et al., *The MAP1-LC3 conjugation system is involved in lipid droplet formation*. Biochem Biophys Res Commun, 2009. **382**(2): p. 419-23.
280. Guo, J.Y., et al., *Autophagy suppresses progression of K-ras-induced lung tumors to oncocytomas and maintains lipid homeostasis*. Genes Dev, 2013. **27**(13): p. 1447-61.
281. Solenski, N.J., et al., *Ultrastructural changes of neuronal mitochondria after transient and permanent cerebral ischemia*. Stroke, 2002. **33**(3): p. 816-24.

282. Munoz-Pinedo, C., et al., *Different mitochondrial intermembrane space proteins are released during apoptosis in a manner that is coordinately initiated but can vary in duration*. Proc Natl Acad Sci U S A, 2006. **103**(31): p. 11573-8.
283. van der Bliek, A.M., Q. Shen, and S. Kawajiri, *Mechanisms of mitochondrial fission and fusion*. Cold Spring Harb Perspect Biol, 2013. **5**(6).
284. Yu, W., et al., *The PINK1/Parkin pathway regulates mitochondrial dynamics and function in mammalian hippocampal and dopaminergic neurons*. Hum Mol Genet, 2011. **20**(16): p. 3227-40.
285. Dagda, R.K., et al., *Loss of PINK1 function promotes mitophagy through effects on oxidative stress and mitochondrial fission*. J Biol Chem, 2009. **284**(20): p. 13843-55.
286. Lutz, A.K., et al., *Loss of parkin or PINK1 function increases Drp1-dependent mitochondrial fragmentation*. J Biol Chem, 2009. **284**(34): p. 22938-51.
287. Shen, C., et al., *Genetic and functional studies implicate HIF1alpha as a 14q kidney cancer suppressor gene*. Cancer discovery, 2011. **1**(3): p. 222-35.
288. Shen, C. and W.G. Kaelin, Jr., *The VHL/HIF axis in clear cell renal carcinoma*. Seminars in cancer biology, 2013. **23**(1): p. 18-25.
289. Chen, S., et al., *MicroRNA-494 inhibits the growth and angiogenesis-regulating potential of mesenchymal stem cells*. FEBS Lett, 2015. **589**(6): p. 710-717.
290. Pinthus, J.H., et al., *Metabolic features of clear-cell renal cell carcinoma: mechanisms and clinical implications*. Can Urol Assoc J, 2011. **5**(4): p. 274-82.
291. Gbelcova, H., et al., *The effect of simvastatin on lipid droplets accumulation in human embryonic kidney cells and pancreatic cancer cells*. Lipids Health Dis, 2013. **12**: p. 126.
292. Boren, J. and K.M. Brindle, *Apoptosis-induced mitochondrial dysfunction causes cytoplasmic lipid droplet formation*. Cell Death Differ, 2012. **19**(9): p. 1561-70.
293. Weidberg, H., E. Shvets, and Z. Elazar, *Lipophagy: selective catabolism designed for lipids*. Dev Cell, 2009. **16**(5): p. 628-30.
294. Singh, R. and A.M. Cuervo, *Lipophagy: connecting autophagy and lipid metabolism*. Int J Cell Biol, 2012. **2012**: p. 282041.
295. Gong, J., et al., *Fsp27 promotes lipid droplet growth by lipid exchange and transfer at lipid droplet contact sites*. J Cell Biol, 2011. **195**(6): p. 953-63.
296. Gwinn, D.M., et al., *AMPK phosphorylation of raptor mediates a metabolic checkpoint*. Mol Cell, 2008. **30**(2): p. 214-26.
297. Guyton, J.R. and K.F. Klemp, *Transitional features in human atherosclerosis. Intimal thickening, cholesterol clefts, and cell loss in human aortic fatty streaks*. Am J Pathol, 1993. **143**(5): p. 1444-57.
298. Gniadecki, R., *Depletion of membrane cholesterol causes ligand-independent activation of Fas and apoptosis*. Biochem Biophys Res Commun, 2004. **320**(1): p. 165-9.
299. Li, Y.C., et al., *Elevated levels of cholesterol-rich lipid rafts in cancer cells are correlated with apoptosis sensitivity induced by cholesterol-depleting agents*. Am J Pathol, 2006. **168**(4): p. 1107-18; quiz 1404-5.
300. Fernandez-Hernando, C., et al., *MicroRNAs in lipid metabolism*. Curr Opin Lipidol, 2011. **22**(2): p. 86-92.
301. Pescador, N., et al., *Serum circulating microRNA profiling for identification of potential type 2 diabetes and obesity biomarkers*. PLoS One, 2013. **8**(10): p. e77251.

302. de Guia, R.M., et al., *microRNA-379 couples glucocorticoid hormones to dysfunctional lipid homeostasis*. EMBO J, 2015. **34**(3): p. 344-60.
303. Richardson, K., et al., *Gain-of-function lipoprotein lipase variant rs13702 modulates lipid traits through disruption of a microRNA-410 seed site*. Am J Hum Genet, 2013. **92**(1): p. 5-14.
304. Laddha, S.V., et al., *Genome-wide analysis reveals downregulation of miR-379/miR-656 cluster in human cancers*. Biol Direct, 2013. **8**: p. 10.
305. Ahn, R.W., et al., *A novel nanoparticulate formulation of arsenic trioxide with enhanced therapeutic efficacy in a murine model of breast cancer*. Clin Cancer Res, 2010. **16**(14): p. 3607-17.
306. Guo, Y., et al., *Lipid droplets at a glance*. J Cell Sci, 2009. **122**(Pt 6): p. 749-52.
307. DiDonato, D. and D.L. Brasaemle, *Fixation methods for the study of lipid droplets by immunofluorescence microscopy*. J Histochem Cytochem, 2003. **51**(6): p. 773-80.
308. Niso-Santano, M., et al., *Unsaturated fatty acids induce non-canonical autophagy*. EMBO J, 2015.
309. Tanida, I., T. Ueno, and E. Kominami, *LC3 and Autophagy*. Methods Mol Biol, 2008. **445**: p. 77-88.
310. Wenk, M.R., *The emerging field of lipidomics*. Nat Rev Drug Discov, 2005. **4**(7): p. 594-610.
311. Zhang, Y., et al., *Comparative genomics and functional study of lipid metabolic genes in Caenorhabditis elegans*. BMC Genomics, 2013. **14**: p. 164.
312. Kanoh, H., M. Kai, and I. Wada, *Molecular characterization of the type 2 phosphatidic acid phosphatase*. Chem Phys Lipids, 1999. **98**(1-2): p. 119-26.
313. Drabkin, H.A. and R.M. Gemmill, *Cholesterol and the development of clear-cell renal carcinoma*. Curr Opin Pharmacol, 2012. **12**(6): p. 742-50.
314. Archer, S.L., *Mitochondrial fission and fusion in human diseases*. N Engl J Med, 2014. **370**(11): p. 1074.
315. Poole, A.C., et al., *The PINK1/Parkin pathway regulates mitochondrial morphology*. Proc Natl Acad Sci U S A, 2008. **105**(5): p. 1638-43.
316. Duan, X., et al., *Upregulation of human PINK1 gene expression by NFkappaB signalling*. Mol Brain, 2014. **7**: p. 57.
317. Lan, Y.F., et al., *MicroRNA-494 reduces ATF3 expression and promotes AKI*. J Am Soc Nephrol, 2012. **23**(12): p. 2012-23.
318. O'Flanagan, C.H., et al., *The Parkinson's gene PINK1 regulates cell cycle progression and promotes cancer-associated phenotypes*. Oncogene, 2015. **34**(11): p. 1363-74.
319. Finn, P.F. and J.F. Dice, *Proteolytic and lipolytic responses to starvation*. Nutrition, 2006. **22**(7-8): p. 830-44.
320. Rambold, A.S., S. Cohen, and J. Lippincott-Schwartz, *Fatty Acid Trafficking in Starved Cells: Regulation by Lipid Droplet Lipolysis, Autophagy, and Mitochondrial Fusion Dynamics*. Dev Cell, 2015.
321. Santos, C.R. and A. Schulze, *Lipid metabolism in cancer*. FEBS J, 2012. **279**(15): p. 2610-23.
322. Lee, S.J., et al., *Mitochondrial dysfunction induces formation of lipid droplets as a generalized response to stress*. Oxid Med Cell Longev, 2013. **2013**: p. 327167.
323. Ranieri, M., et al., *Mitochondrial fusion proteins and human diseases*. Neurol Res Int, 2013. **2013**: p. 293893.

324. Suen, D.F., K.L. Norris, and R.J. Youle, *Mitochondrial dynamics and apoptosis*. Genes Dev, 2008. **22**(12): p. 1577-90.
325. Duarte, F.V., C.M. Palmeira, and A.P. Rolo, *The Role of microRNAs in Mitochondria: Small Players Acting Wide*. Genes (Basel), 2014. **5**(4): p. 865-86.
326. Pyakurel, A., et al., *Extracellular Regulated Kinase Phosphorylates Mitofusin 1 to Control Mitochondrial Morphology and Apoptosis*. Mol Cell, 2015.
327. Youle, R.J. and M. Karbowski, *Mitochondrial fission in apoptosis*. Nat Rev Mol Cell Biol, 2005. **6**(8): p. 657-63.
328. Cui, H., Y. Kong, and H. Zhang, *Oxidative stress, mitochondrial dysfunction, and aging*. J Signal Transduct, 2012. **2012**: p. 646354.
329. Sullivan, L.B. and N.S. Chandel, *Mitochondrial reactive oxygen species and cancer*. Cancer Metab, 2014. **2**: p. 17.
330. Ryu, S.W., et al., *Endoplasmic reticulum-specific BH3-only protein BNIP1 induces mitochondrial fragmentation in a Bcl-2- and Drp1-dependent manner*. J Cell Physiol, 2012. **227**(8): p. 3027-35.
331. Alvarez-Erviti, L., et al., *Influence of microRNA deregulation on chaperone-mediated autophagy and alpha-synuclein pathology in Parkinson's disease*. Cell Death Dis, 2013. **4**: p. e545.
332. Korkmaz, G., et al., *miR-376b controls starvation and mTOR inhibition-related autophagy by targeting ATG4C and BECN1*. Autophagy, 2012. **8**(2): p. 165-76.
333. Korkmaz, G., et al., *MIR376A is a regulator of starvation-induced autophagy*. PLoS One, 2013. **8**(12): p. e82556.
334. Potts, M.B., et al., *Using functional signature ontology (FUSION) to identify mechanisms of action for natural products*. Sci Signal, 2013. **6**(297): p. ra90.
335. Glazko, G.V. and A.R. Mushegian, *Detection of evolutionarily stable fragments of cellular pathways by hierarchical clustering of phyletic patterns*. Genome Biol, 2004. **5**(5): p. R32.
336. Zhang, Y., Z. Wang, and R.A. Gemeinhart, *Progress in microRNA delivery*. J Control Release, 2013. **172**(3): p. 962-74.
337. Di Martino, M.T., et al., *In vivo activity of miR-34a mimics delivered by stable nucleic acid lipid particles (SNALPs) against multiple myeloma*. PLoS One, 2014. **9**(2): p. e90005.
338. Iimura, O., et al., *HMG-CoA reductase inhibitors induce apoptosis in mouse proximal tubular cells in primary culture*. Kidney Int, 1997. **52**(4): p. 962-72.
339. Fu, L., et al., *Generation of a mouse model of Von Hippel-Lindau kidney disease leading to renal cancers by expression of a constitutively active mutant of HIF1alpha*. Cancer Res, 2011. **71**(21): p. 6848-56.
340. Kinross, K.M., et al., *An activating Pik3ca mutation coupled with Pten loss is sufficient to initiate ovarian tumorigenesis in mice*. J Clin Invest, 2012. **122**(2): p. 553-7.

## Appendices

### Appendix A: Copyright Permissions

**From:** Rights and Permissions (ELS)  
**Sent:** 17 April 2015 10:34  
**To:** Meesters, Olaf (ELS-AMS)  
**Subject:** PLEASE READ - IMPORTANT INFORMATION ON OBTAINING PERMISSION

Thank you for your email. If you are requesting to re-use content from any publication found on <http://www.ScienceDirect.com>, Elsevier requires that you follow the directions below to obtain permission.

Please understand that Elsevier will **not** reply to your permission request if the publication you wish to use content from is available on ScienceDirect.

#### **IF THE CONTENT YOU WISH TO USE IS AVAILABLE ON SCIEDIRECT, PLEASE FOLLOW THESE INSTRUCTIONS:**

- Locate the publication containing your desired content on <http://www.sciencedirect.com/science/jrnllallbooks>
- Click on the article/chapter name to access the abstract
- Below the author details, click "Get Rights and Content"
- The Rightslink request page will then be launched (please disable your pop-up blocker)
- Select the way you would like to reuse the content
- Create a Rightslink account if you haven't done so already
- Accept the terms and conditions and you're done

Please note that certain requests may require review before a license to reuse is available; should this occur, you will be emailed to accept or decline the fee and/or terms of the license as set by Elsevier's Global Rights Department upon review.

For questions about using the Rightslink service, please contact Customer Support via phone - US [877/622-5543](tel:8776225543) (toll free) or [978/777-9929](tel:9787779929) 8:00 am – 6:00 pm Eastern Time, or email [customercare@copyright.com](mailto:customercare@copyright.com).

#### **IF THE CONTENT YOU WISH TO USE IS NOT AVAILABLE ON SCIEDIRECT OR YOU HAVE SUBMITTED A QUESTION/QUERY, PLEASE NOTE THE FOLLOWING:**

- The Elsevier Global Rights team will review your request/email and respond within 15 working days unless you have specified a more immediate deadline.
- You should not reply to this automated response. Should you need to follow up on your request please ensure you attach it to any correspondence.
- Please verify that the content you wish to use is not available online before awaiting a response to your email.

For general questions about obtaining permission, please contact the Permissions Helpdesk at [permissionshelpdesk@elsevier.com](mailto:permissionshelpdesk@elsevier.com) or US [800/523-4069 x 3808](tel:8005234069) (toll free).

Kind regards,

Global Rights Department  
Tel: [+44 \(0\)1865 843830](tel:+4401865843830) (UK) or [+ 1 215 239 3804](tel:+12152393804) (US)  
Email: [permissions@elsevier.com](mailto:permissions@elsevier.com)

\*\*\*\*\*

From: Punashi Dutta [<mailto:punashidutta@mail.usf.edu>]  
Sent: 16. april 2015 14:31  
To: Molecular Oncology  
Subject: Requesting permission to use published content in doctoral dissertation

Dear Editor,

I am a doctoral candidate from the University of South Florida, Tampa FL. USA. I am currently writing my doctoral dissertation and would like to rewrite and include data/content from one of the articles that was published in Molecular Oncology Journal on June 7,2013. I am the primary author on this article.

In this regard, I am writing to you to request your permission to rewrite the article entitled 'EV11 splice variants modulate functional responses in ovarian cancer cells' Mol Oncol. 2013 Jun;7(3):647-68. doi: 10.1016/j.molonc.2013.02.008. Epub 2013 Mar 5..

I would greatly appreciate your help and thank you in advance for your valuable time.

Sincerely,  
Punashi Dutta  
Doctoral candidate, Department of CMMB,  
University of South Florida, Tampa. FL. USA

Dear Punashi Dutta

Thank you for your email.

Please note that as one of the Authors of this article, you retain the right to include the journal article, in full or in part, in a thesis or dissertation. You do not require permission to do so.

For full details of your rights as a Journal Author, please visit: <http://www.elsevier.com/wps/find/authorsview.authors/copyright#whatrights>

Your retained rights allow you to submit your article in electronic format and to post this Elsevier article online if it is embedded within your thesis. You are also permitted to post your Author Accepted Manuscript online; however posting of the final published article is prohibited.

Please refer to Elsevier's Posting Policy for further information: <http://www.elsevier.com/wps/find/authors.authors/postingpolicy>

Feel free to contact me if you have any queries.

Regards

Lakshmi Priya

Global Rights Department

Elsevier

(A division of Reed Elsevier India Pvt. Ltd.)

International Tech Park | Crest – 12<sup>th</sup> Floor | Taramani Road | Taramani | Chennai 600 113 | India

Tel: [+91 44 42994660](tel:+914442994660) | Fax: [+91 44 42994701](tel:+914442994701)

E-mail: [l.shridhar@elsevier.com](mailto:l.shridhar@elsevier.com) | url: [www.elsevier.com](http://www.elsevier.com)

**Subject:** Requesting permission to use published content in doctoral dissertation

Dear Editor,

I am a doctoral candidate from the University of South Florida, Tampa FL. USA. I am currently writing my doctoral dissertation and would like to rewrite and include data/content from one of the articles that was published in Molecular Oncology Journal on June 7,2013. I am the primary author on this article.

In this regard, I am writing to you to request your permission to rewrite the article entitled '**EV11 splice variants modulate functional responses in ovarian cancer cells**' Mol. Oncol. 2013 Jun;7(3):647-68. doi: 10.1016/j.molonc.2013.02.008. Epub 2013 Mar 5..

I would greatly appreciate your help and thank you in advance for your valuable time.

Sincerely,

Punashi Dutta

Doctoral candidate, Department of CMMB,  
University of South Florida, Tampa. FL. USA

**ELSEVIER**  
**TERMS AND CONDITIONS**

May 15, 2015

**LICENSE**



---

---

This is a License Agreement between Punashi Dutta ("You") and Elsevier ("Elsevier") provided by Copyright Clearance Center ("CCC"). The license consists of your order details, the terms and conditions provided by Elsevier, and the payment terms and conditions.

**All payments must be made in full to CCC. For payment instructions, please see information listed at the bottom of this form.**

Supplier	Elsevier The Boulevard, Langford Kidlington, Oxford, OX5 1GB, UK	Limited Lane
Registered Company Number	1982084	
Customer name	Punashi Dutta	
Customer address	4103 Monticello Gardens place, Apt 202D TAMPA, FL 33613	
License number	3621500051984	
License date	May 03, 2015	
Licensed content publisher	Elsevier	
Licensed content publication	Molecular Oncology	
Licensed content title	EVI1 splice variants modulate functional responses in ovarian cancer cells	
Licensed content author	None	
Licensed content date	June 2013	
Licensed content volume number	7	
Licensed content issue number	3	
Number of pages	22	
Start Page	647	
End Page	668	
Type of Use	reuse in a thesis/dissertation	
Portion	full article	
Format	both print and electronic	
Are you the author of this Elsevier article?	Yes	
Will you be translating?	No	
Title of your thesis/dissertation	Genomic aberrations at the 3q and 14q loci:	

Investigation of key players in ovarian and renal cancer biology

Expected completion date	Jun 2015
Estimated size (number of pages)	125
Elsevier VAT number	GB 494 6272 12
Permissions price	0.00 USD
VAT/Local Sales Tax	0.00 USD / 0.00 GBP
Total	0.00 USD

[Terms and Conditions](#)

## INTRODUCTION

1. The publisher for this copyrighted material is Elsevier. By clicking "accept" in connection with completing this licensing transaction, you agree that the following terms and conditions apply to this transaction (along with the Billing and Payment terms and conditions established by Copyright Clearance Center, Inc. ("CCC"), at the time that you opened your Rightslink account and that are available at any time at <http://myaccount.copyright.com>).

## GENERAL TERMS

2. Elsevier hereby grants you permission to reproduce the aforementioned material subject to the terms and conditions indicated.

3. Acknowledgement: If any part of the material to be used (for example, figures) has appeared in our publication with credit or acknowledgement to another source, permission must also be sought from that source. If such permission is not obtained then that material may not be included in your publication/copies. Suitable acknowledgement to the source must be made, either as a footnote or in a reference list at the end of your publication, as follows:

"Reprinted from Publication title, Vol /edition number, Author(s), Title of article / title of chapter, Pages No., Copyright (Year), with permission from Elsevier [OR APPLICABLE SOCIETY COPYRIGHT OWNER]." Also Lancet special credit - "Reprinted from The Lancet, Vol. number, Author(s), Title of article, Pages No., Copyright (Year), with permission from Elsevier."

4. Reproduction of this material is confined to the purpose and/or media for which permission is hereby given.

5. Altering/Modifying Material: Not Permitted. However figures and illustrations may be altered/adapted minimally to serve your work. Any other abbreviations, additions, deletions and/or any other alterations shall be made only with prior written authorization of Elsevier Ltd. (Please contact Elsevier at [permissions@elsevier.com](mailto:permissions@elsevier.com))

6. If the permission fee for the requested use of our material is waived in this instance, please be advised that your future requests for Elsevier materials may attract a fee.

7. Reservation of Rights: Publisher reserves all rights not specifically granted in the combination of (i) the license details provided by you and accepted in the course of this licensing transaction, (ii) these terms and conditions and (iii) CCC's Billing and Payment terms and conditions.

8. License Contingent Upon Payment: While you may exercise the rights licensed immediately upon issuance of the license at the end of the licensing process for the transaction, provided that you have disclosed complete and accurate details of your proposed use, no license is finally effective unless and until full payment is received from you (either by publisher or by CCC) as provided in CCC's Billing and Payment terms and conditions. If full payment is not received on a timely basis, then any license preliminarily granted shall be deemed automatically revoked and shall be void as if never granted. Further, in the event that you breach any of these terms and conditions or any of CCC's Billing and Payment terms and conditions, the license is automatically revoked and shall be void as if never granted. Use of materials as described in a revoked license, as well as any use of the materials beyond the scope of an unrevoked license, may constitute copyright infringement and publisher reserves the right to take any and all action to protect its copyright in the materials.

9. Warranties: Publisher makes no representations or warranties with respect to the licensed material.

10. Indemnity: You hereby indemnify and agree to hold harmless publisher and CCC, and their respective officers, directors, employees and agents, from and against any and all claims arising out of your use of the licensed material other than as specifically authorized pursuant to this license.

11. No Transfer of License: This license is personal to you and may not be sublicensed, assigned, or transferred by you to any other person without publisher's written permission.

12. No Amendment Except in Writing: This license may not be amended except in a writing signed by both parties (or, in the case of publisher, by CCC on publisher's behalf).

13. Objection to Contrary Terms: Publisher hereby objects to any terms contained in any purchase order, acknowledgment, check endorsement or other writing prepared by you, which terms are inconsistent with these terms and conditions or CCC's Billing and Payment terms and conditions. These terms and conditions, together with CCC's Billing and Payment terms and conditions (which are incorporated herein), comprise the entire agreement between you and publisher (and CCC) concerning this licensing transaction. In the event of any conflict between your obligations established by these terms and conditions and those established by CCC's Billing and Payment terms and conditions, these terms and conditions shall control.

14. Revocation: Elsevier or Copyright Clearance Center may deny the permissions described in this License at their sole discretion, for any reason or no reason, with a full

refund payable to you. Notice of such denial will be made using the contact information provided by you. Failure to receive such notice will not alter or invalidate the denial. In no event will Elsevier or Copyright Clearance Center be responsible or liable for any costs, expenses or damage incurred by you as a result of a denial of your permission request, other than a refund of the amount(s) paid by you to Elsevier and/or Copyright Clearance Center for denied permissions.

## LIMITED LICENSE

The following terms and conditions apply only to specific license types:

**15. Translation:** This permission is granted for non-exclusive world **English** rights only unless your license was granted for translation rights. If you licensed translation rights you may only translate this content into the languages you requested. A professional translator must perform all translations and reproduce the content word for word preserving the integrity of the article. If this license is to re-use 1 or 2 figures then permission is granted for non-exclusive world rights in all languages.

**16. Posting licensed content on any Website:** The following terms and conditions apply as follows: Licensing material from an Elsevier journal: All content posted to the web site must maintain the copyright information line on the bottom of each image; A hyper-text must be included to the Homepage of the journal from which you are licensing at <http://www.sciencedirect.com/science/journal/xxxxx> or the Elsevier homepage for books at <http://www.elsevier.com>; Central Storage: This license does not include permission for a scanned version of the material to be stored in a central repository such as that provided by Heron/XanEdu.

Licensing material from an Elsevier book: A hyper-text link must be included to the Elsevier homepage at <http://www.elsevier.com>. All content posted to the web site must maintain the copyright information line on the bottom of each image.

**Posting licensed content on Electronic reserve:** In addition to the above the following clauses are applicable: The web site must be password-protected and made available only to bona fide students registered on a relevant course. This permission is granted for 1 year only. You may obtain a new license for future website posting.

**17. For journal authors:** the following clauses are applicable in addition to the above:

### Preprints:

A preprint is an author's own write-up of research results and analysis, it has not been peer-reviewed, nor has it had any other value added to it by a publisher (such as formatting, copyright, technical enhancement etc.).

Authors can share their preprints anywhere at any time. Preprints should not be added to or enhanced in any way in order to appear more like, or to substitute for, the final versions of articles however authors can update their preprints on arXiv or RePEc with

their Accepted Author Manuscript (see below).

If accepted for publication, we encourage authors to link from the preprint to their formal publication via its DOI. Millions of researchers have access to the formal publications on ScienceDirect, and so links will help users to find, access, cite and use the best available version. Please note that Cell Press, The Lancet and some society-owned have different preprint policies. Information on these policies is available on the journal homepage.

**Accepted Author Manuscripts:** An accepted author manuscript is the manuscript of an article that has been accepted for publication and which typically includes author-incorporated changes suggested during submission, peer review and editor-author communications.

Authors can share their accepted author manuscript:

- immediately
  - via their non-commercial person homepage or blog
  - by updating a preprint in arXiv or RePEc with the accepted manuscript
  - via their research institute or institutional repository for internal institutional uses or as part of an invitation-only research collaboration work-group
  - directly by providing copies to their students or to research collaborators for their personal use
  - for private scholarly sharing as part of an invitation-only work group on commercial sites with which Elsevier has an agreement
- after the embargo period
  - via non-commercial hosting platforms such as their institutional repository
  - via commercial sites with which Elsevier has an agreement

In all cases accepted manuscripts should:

- link to the formal publication via its DOI
- bear a CC-BY-NC-ND license - this is easy to do
- if aggregated with other manuscripts, for example in a repository or other site, be shared in alignment with our hosting policy not be added to or enhanced in any way to appear more like, or to substitute for, the published journal article.

**Published journal article (JPA):** A published journal article (PJA) is the definitive final record of published research that appears or will appear in the journal and embodies all value-adding publishing activities including peer review co-ordination, copy-editing, formatting, (if relevant) pagination and online enrichment.

Policies for sharing publishing journal articles differ for subscription and gold open access articles:

**Subscription Articles:** If you are an author, please share a link to your article rather than the full-text. Millions of researchers have access to the formal publications on

ScienceDirect, and so links will help your users to find, access, cite, and use the best available version.

Theses and dissertations which contain embedded PJAs as part of the formal submission can be posted publicly by the awarding institution with DOI links back to the formal publications on ScienceDirect.

If you are affiliated with a library that subscribes to ScienceDirect you have additional private sharing rights for others' research accessed under that agreement. This includes use for classroom teaching and internal training at the institution (including use in course packs and courseware programs), and inclusion of the article for grant funding purposes.

**Gold Open Access Articles:** May be shared according to the author-selected end-user license and should contain a [CrossMark logo](#), the end user license, and a DOI link to the formal publication on ScienceDirect.

Please refer to Elsevier's [posting policy](#) for further information.

**18. For book authors** the following clauses are applicable in addition to the above: Authors are permitted to place a brief summary of their work online only. You are not allowed to download and post the published electronic version of your chapter, nor may you scan the printed edition to create an electronic version. **Posting to a repository:** Authors are permitted to post a summary of their chapter only in their institution's repository.

**19. Thesis/Dissertation:** If your license is for use in a thesis/dissertation your thesis may be submitted to your institution in either print or electronic form. Should your thesis be published commercially, please reapply for permission. These requirements include permission for the Library and Archives of Canada to supply single copies, on demand, of the complete thesis and include permission for Proquest/UMI to supply single copies, on demand, of the complete thesis. Should your thesis be published commercially, please reapply for permission. Theses and dissertations which contain embedded PJAs as part of the formal submission can be posted publicly by the awarding institution with DOI links back to the formal publications on ScienceDirect.

### **Elsevier Open Access Terms and Conditions**

You can publish open access with Elsevier in hundreds of open access journals or in nearly 2000 established subscription journals that support open access publishing. Permitted third party re-use of these open access articles is defined by the author's choice of Creative Commons user license. See our [open access license policy](#) for more information.

### **Terms & Conditions applicable to all Open Access articles published with Elsevier:**

Any reuse of the article must not represent the author as endorsing the adaptation of the article nor should the article be modified in such a way as to damage the author's honour

or reputation. If any changes have been made, such changes must be clearly indicated.

The author(s) must be appropriately credited and we ask that you include the end user license and a DOI link to the formal publication on ScienceDirect.

If any part of the material to be used (for example, figures) has appeared in our publication with credit or acknowledgement to another source it is the responsibility of the user to ensure their reuse complies with the terms and conditions determined by the rights holder.

#### **Additional Terms & Conditions applicable to each Creative Commons user license:**

**CC BY:** The CC-BY license allows users to copy, to create extracts, abstracts and new works from the Article, to alter and revise the Article and to make commercial use of the Article (including reuse and/or resale of the Article by commercial entities), provided the user gives appropriate credit (with a link to the formal publication through the relevant DOI), provides a link to the license, indicates if changes were made and the licensor is not represented as endorsing the use made of the work. The full details of the license are available at <http://creativecommons.org/licenses/by/4.0>.

**CC BY NC SA:** The CC BY-NC-SA license allows users to copy, to create extracts, abstracts and new works from the Article, to alter and revise the Article, provided this is not done for commercial purposes, and that the user gives appropriate credit (with a link to the formal publication through the relevant DOI), provides a link to the license, indicates if changes were made and the licensor is not represented as endorsing the use made of the work. Further, any new works must be made available on the same conditions. The full details of the license are available at <http://creativecommons.org/licenses/by-nc-sa/4.0>.

**CC BY NC ND:** The CC BY-NC-ND license allows users to copy and distribute the Article, provided this is not done for commercial purposes and further does not permit distribution of the Article if it is changed or edited in any way, and provided the user gives appropriate credit (with a link to the formal publication through the relevant DOI), provides a link to the license, and that the licensor is not represented as endorsing the use made of the work. The full details of the license are available at <http://creativecommons.org/licenses/by-nc-nd/4.0>. Any commercial reuse of Open Access articles published with a CC BY NC SA or CC BY NC ND license requires permission from Elsevier and will be subject to a fee.

Commercial reuse includes:

- Associating advertising with the full text of the Article
- Charging fees for document delivery or access
- Article aggregation
- Systematic distribution via e-mail lists or share buttons

Posting or linking by commercial companies for use by customers of those companies.

20. Other Conditions:

v1.7

Questions? [customercare@copyright.com](mailto:customercare@copyright.com) or +1-855-239-3415 (toll free in the US) or +1-978-646-2777.

Gratis licenses (referencing \$0 in the Total field) are free. Please retain this printable license for your reference. No payment is required.

---